Large Volume Metrology Assisted Production of Aero-structures

Wang, Zheng

Award date:
2013

Awarding institution:
University of Bath

Large Volume Metrology Assisted Production of Aero-structures

Zheng Wang

A thesis submitted for the degree of Doctor of Philosophy

University of Bath
Department of Mechanical Engineering
March 2013

Abstract

The research presented in this thesis was carried out within the Large Volume Metrology group at the University of Bath.

The main goal of the research study is to develop and demonstrate novel applications of integrated and automated metrology systems in aero-structure production, with a particular focus on the development and capability assessment of real-time metrology integration.

A survey through the relatively limited amount of literature on the state of the art of integrated and automated metrology showed some promising results.

Encouraged by the positive results, studies were undertaken showing that many of the current aero-structure production issues involving measurement and data processing can be solved through better integration and automation of metrology systems. It was partially demonstrated that the health assessment of an entire wing jig could be carried out automatically within 13 minutes, compared to the traditional manual process which could takes many days.

To better understand and quantify the capabilities and benefits of a hypothetical production system with integrated metrology, methods of mathematically simulating Metrology Assisted Assembly (MAA) systems were developed, and tested in a number of application case studies. It was shown that MAA processes can be effectively simulated using the Monte Carlo method. The case studies showed that these simulations can provide critical insight and information of the processes to the decision makers.

The practical implementations of real-time integration with metrology instruments, a key enabler of MAA, were then addressed, and software methods of interfacing directly with a number of instruments in real-time were developed and demonstrated. The potential application of real-time metrology in mobile robot navigation was also highlighted.

Finally, building upon software instrument interfaces, a prototype 3-axis machine was constructed using low cost off-the-shelf components in order to demonstrate the potentials of real-time MAA for manufacturing processes such as milling and drilling. Using a laser tracker to provide real-time error correction, it was possible to dramatically increase the positioning accuracy and repeatability of the machine. Using real-time feedback, a 50% reduction in static repeatability and 40 to 140 times reduction in static positioning errors were achieved.

List of Figures

List of Tables

List of Publications

Wang, Z.; Maropoulos, P.; Jamshidi, J.; Owen, G. and Mileham, A. (2008). *Experimental Deployment of the Indoor GPS Large Volume Metrology System in a Large Scale Production Facility*. In: Proceedings of the 3rd International Conference on Manufacturing Engineering, Kallithea of Chalkidiki, Greece, pp.827-8325.

Muelaner, J.E.; Wang, Z.; Jamshidi, J.; Maropoulos, P.; Mileham, A.R.; Hughes, E.B. and Forbes, A.B. (2008). *iGPS - An Initial Assessment Of Technical And Deployment Capability*. In: Proceedings of the 3rd International Conference on Manufacturing Engineering, Kallithea of Chalkidiki, Greece, pp.805-810.

Muelaner, J.E.; Wang, Z.; Jamshidi, J.; Maropoulos, P.G.; Mileham, A.M.; Hughes, E.B. and Forbes, A.B. (2009). *Study of the uncertainty of angle measurement for a rotary-laser automatic theodolite (R-LAT)*. Proceedings of the Institution of Mechanical Engineers, Part B: Journal of Engineering Manufacture, 223(3): pp.217-229.

Wang, Z.; Maropoulos, P.; Mastrogiacomo, L. and Franceschini, F. (2009). *Experimental testing of the dynamic tracking performance of iGPS and laser tracker*. In: Proceedings of the 9th International Conference and Exhibition on Laser Metrology, Machine Tool, CMM & Robotic Performance, Bedford, UK, pp.305-316, Euspen.

Muelaner, J.E.; Wang, Z.; Martin, O.; Jamshidi, J. and Maropoulos, P. (2010). *Verification of the Indoor GPS System, by Comparison with Calibrated Coordinates and by Angular Reference*. Journal of Intelligent Manufacturing, DOI: 10.1007/s10845-010-0488-y.

Muelaner, J.E.; Wang, Z.; Martin, O.; Jamshidi, J. and Maropoulos, P.G. (2010). *Estimation of uncertainty in three dimensional coordinate measurement by comparison with calibrated points*. Measurement Science and Technology, 21(2): pp.025106

Muelaner, J.E.; Wang, Z. and Maropoulos, G. (2010). *Concepts for and Analysis of a High accuracy and High Capacity (HAHC) Aerospace Robot*. In: Proceedings of the 21st International Computer-Aided Production Engineering Conference, Edinburgh, UK.

Muelaner, J.E.; Wang, Z.; Martin, O.; Jamshidi, J. and Maropoulos, P.G. (2010). *Verification of the indoor GPS system by comparison with points calibrated using a network of laser tracker measurements*. In: Proceedings of the 6th CIRP-Sponsored International Conference on Digital Enterprise Technology, pp.607-619, Springer Verlag.

Wang, Z.; Liang, M. and Maropoulos, P.G. (2010). *High accuracy mobile robot positioning using an external large volume metrology instrument*. In: Proceedings of the 6th CIRP-Sponsored International Conference on Digital Enterprise Technology, pp.621-630, Springer Verlag.

Wang, Z.; Liang, M. and Maropoulos, P.G. (2011). *High accuracy mobile robot positioning using external Large Volume Metrology instruments*. International Journal of Computer Integrated Manufacturing, (accepted for the publication).

Wang, Z.; Mastrogiacomo, L.; Maropoulos, P. and Franceschini, F. (2011). *Experimental Comparison of Dynamic Tracking Performance of iGPS and Laser Tracker*. International Journal of Advanced Manufacturing Technology, (accepted for the publication).

Muelaner, J.E.; Wang, Z. and Maropoulos, P.G. (2011) *Concepts for and Analysis of a High accuracy and High Capacity (HAHC) Aerospace Robot*. Proceedings of the Institution of Mechanical Engineers Part B-Journal of Engineering Manufacture, (accepted for the publication).

Wang, Z. and Maropoulos, P.G. (2011) Integrated Large Volume Metrology Assisted Machine Tool Positioning. Proceedings of the 7th International Conference on Digital Enterprise Technology. Athens, Greece. pp. 47-56.

Martin, O.; Muelaner, J.; Wang, Z.; Kayani, A.; Tomlinson, D. and Maropoulos, P.G. (2011) *Metrology enhanced tooling for aerospace (META): A live fixturing Wing Box assembly case study*. Proceedings of the 7th International Conference on Digital Enterprise Technology. Athens, Greece. pp. 83-92.

Contents

1. Introduction

1.1. Background to the Research Area

1.1.1. The Wind Energy Industry

The harnessing of the power of the wind has a long and rich history. The application of wind energy reached its peak before the advent of fossil fuel in the early twentieth century. Interest in wind power resurged during the energy crises in the 1970s, many countries poured large amounts of R&D resources into the design and construction of large wind turbines for electricity production, with very mixed results. [1]

In many industrialized countries such as the United States, the Netherlands and Germany [2, 3], the R&D efforts were led by academics and engineers from the aerospace industry, with a top down science driven development philosophy with goals of maximizing efficiency and minimizing cost. Very ambitious large test wind turbines with "optimal" structures and aerodynamics were constructed, but most of these projects proved to be uneconomical, if not complete failures. The challenges of building a larger wind turbine which can operate reliably and economically proved to be much more difficult than projected.

In Denmark [2, 3] however, without an aerospace industry, much of the early developments were conducted not by engineers but by small groups of craftsman, artisans and environmental activists, with a supporting governmental frame work. Although much less funding was available in Denmark, many successful small wind turbines were built and operated, providing valuable lessons and experience for the manufacturers and operators, and without overly ambitious projects, the Danish designs matured over time, and were much more reliable than those produced in other countries.

In recent years, the ever increasing cost of energy, the threat of global warming as well as the need for energy self-sufficiency due to geopolitical instabilities have brought renewable energies such as wind power back into

the spotlight. The UK government for example, intends to increase the level of energy generated by renewable energy sources from its current rate of 0.5% to 20% by year 2020, which is in line with the policy of reduction in CO_2 gases, this along with public interest have dramatically increased the demand for green energy.

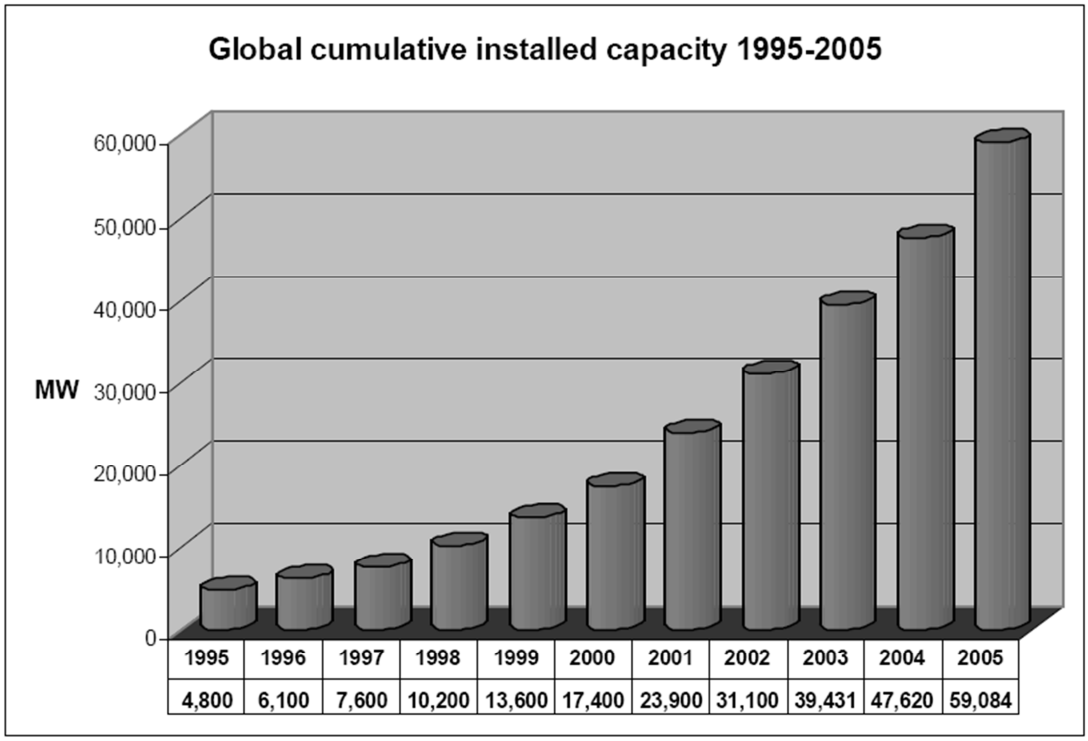

Figure 1 - Growth of wind energy [4], tenfold increase from 1995-2004

Wind energy is free of emissions and priced competitively against conventional power generation. It is also the fastest way of ramping up power generation capacity. As a result of the environmental pressures and its own advantages, the demand for wind energy globally has increased dramatically (Figure 1). This demand has led many of the wind turbine manufacturers to have presold most of their production capacity for the next 1-2 years. While the industry is expanding its production capacity, much of the wind turbine producers are still employing similar production technologies inherited from the old artisan/craftsman days, when production was mostly manual labour, and production rates were low.

As a result of the above mentioned increase in demand of their products, many wind turbine manufacturers such as Vestas Technology UK (located on the Isle of Wight), are seeking new technologies in order to modernize their production processes, and to stay at the forefront of their competitive market. In order to keep up with the ever increasing market demand, Vestas is expanding rapidly. In 2008, the company plans to increase annual production capacity by 1000 (3000 blades) turbines [5], through the construction of new manufacturing centres in China, Spain, and the United States.

In order for the wind energy industry to stay competitive, it must reduce the manufacturing cost per turbine, and increase the power generated per turbine, hence reducing the crucial dollar/KWh figure. This means the scaling up in both the diameter of the blades and the rate of production. As the diameters of the blades increase from the current 80-90m to perhaps over 120m, the present practice of constructing the a complete blade in a single mould quickly becomes unsustainable. Therefore Vestas is actively researching the concept of building “modular” blades, where blades will be assembled from interchangeable components manufactured in much smaller moulds possibly offsite. A large fraction of the cost of interchangeable components depends on the manufacturing tolerance required. Embedding metrology systems in the manufacturing and assembly processes is a possible solution to increase the quality of the product and reduce cost.

1.1.2. The Civil Aviation Industry

The demand air transport has grown steadily as the population of the world becomes more prosperous over the years (Figure 2). Despite the difficulties faced by the aviation industry after the 9/11 terrorist attacks and the recent worldwide recession, the industry is set to grow in the long term, especially in the emerging economies such as China and India, and as airlines around the globe replacing their aging fleet with newer more economical and environmentally friendly aircraft.

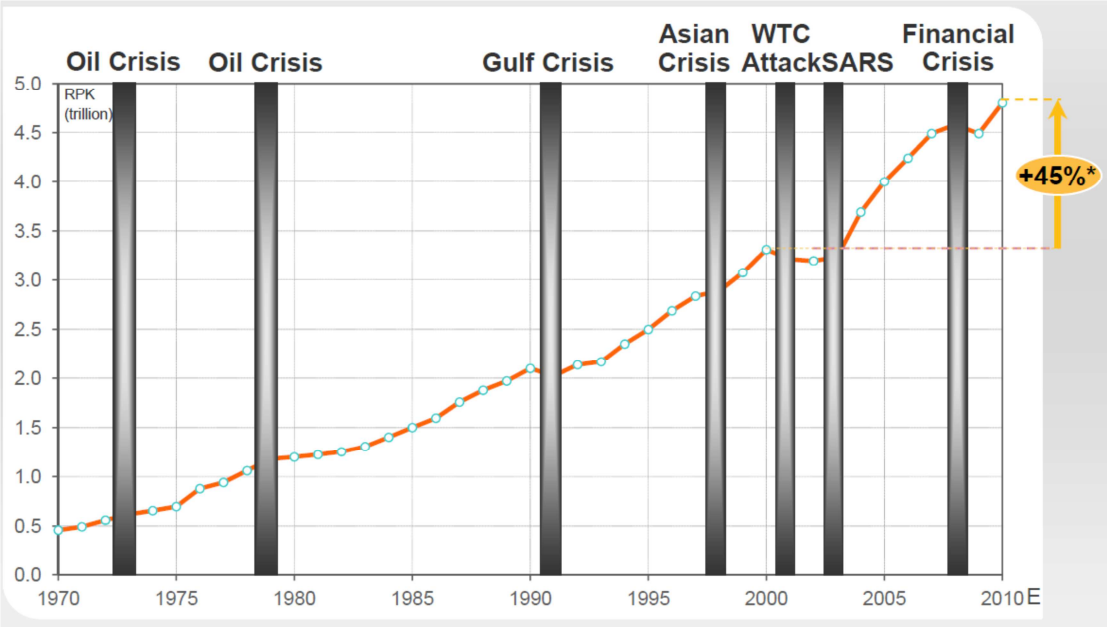

Figure 2 - World annual air traffic (Revenue Passenger Kilometre) from 1970 to 2010, with 45% increase from 2000 to 2010. [6]

Airbus has forecasted a demand for over 25800 new aircraft over the next 20 years, a market value of $3.2 trillion, at an annual growth rate of 4.8% (with

the Asia-pacific region accounting for 1/3rd of the orders), averaging 1300 airframes per year. [6]

Although the aerospace industry has much lower production rates and enjoys much more advanced manufacturing technologies compared to the wind energy industry, there are many similarities in the challenges faced by the two. Aircraft manufacturing has also evolved from small, craft operations since the beginning of the century to the complex, multinational projects of today, and faces pressures from increased customer requirements and demands for higher performance.

Despite the huge advances in the technology of aviation, the aerospace tooling systems have not changed radically from the beginning of the 20th century. A person familiar with assembly processes of the WWII bombers such as the Boeing B-17 will likely be able to recognize all the major tooling used to build the Airbus A-380, in spite of the more than 7 decade gap in time.

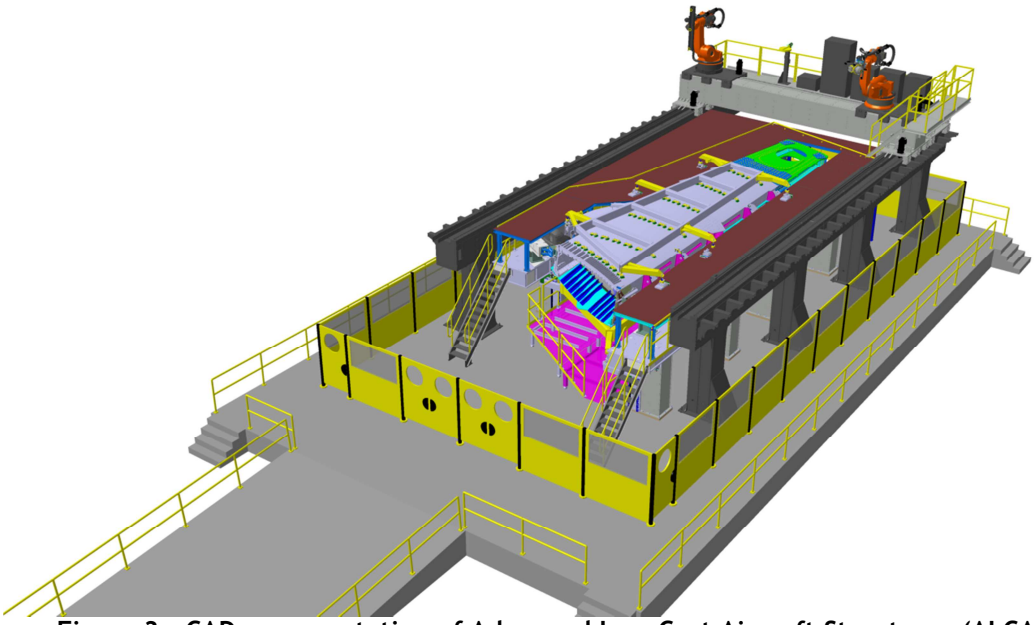

Figure 3 – CAD representation of Advanced Low Cost Aircraft Structures (ALCAS) prototype jig at Airbus Filton, a prototype demonstrating capabilities of flexible fixtures and automated assembly

The use of large and specialized jigs has played a prominent role in the history of aerospace manufacturing. Until very recently, the use of jigs has been the only way to ensure the assembly tolerances and build quality. Since it is difficult and time consuming to check the health of a jig, during which production must be halted, the quality of the jigs are assumed to be good for several months to half a year at a time. Given that the quality of the parts depends directly on the quality of the jigs, the large time gap between jig health-checks can lead to assembly and interchangeability problems. As the performance of the aircraft increased over time, so did the requirement for ever higher tolerances, putting even more demand on the quality of the tooling, further increasing their construction, commissioning

and maintenance costs, making it difficult to make design changes, ramp up production and reducing return on investment.

As a result of the draw backs of specialized tooling, aerospace companies have started to move away from the traditional jigs, and towards more flexible fixtures and potentially "jigless assembly" (Figure 3). The ability to quickly and accurately measure the positions of the fixtures using large volume metrology systems has been a key technology ensuring the quality of these flexible jigs. By integrating metrology systems directly into the jigs, it is possible to dramatically speed up the health check process, to the point of real-time monitoring.

1.1.3. Large Volume Metrology

Accurate dimensional measurements have always been a crucial and challenging part of any manufacturing process. The demand for ever increasing performance and efficiency for large engineering structures has led designers to call for ever tighter dimensional tolerances. In the case of Airbus, ±250μm over many tens of metres is often the requirement for key features on wing assemblies.

The increasing requirements have led to innovations in measurement technology, and not surprisingly, increased capabilities of measurement instruments have in turn allowed the designers to demand more accurate measurements. This development cycle has resulted in major advances over the past few decades, and continues today at a rapid pace. It is sometimes surprising to see how much the LVM technology has advanced in the past 30 years.

The term "Large Volume Metrology" or "Large Scale Metrology" is defined by M. J. Puttock in his 1978 paper [7] as:

> *That particular field of engineering dimensional metrology concerned with large engineering structures and machines and involve measurement over many metres, often in a hostile environment.*

While the nature and challenges of high-accuracy, large volume measurements have remained, the development of new instruments and sensors such as laser trackers with absolute distance measurements, digital photogrammetry systems, the indoor GPS and accompanied by the rapid advances in computing power and software algorithms have radically transformed the field. Invar tapes, theodolites, interferometers and hardware designed for specific measurement tasks (Figure 4) have largely been replaced by general purpose commercial off-the-shelf hardware and software LVM systems that are capable of direct position measurements. Modern LVM systems require less knowledgeable operators, allowing them to

be used by trained workers on the shop floor, instead of specialized measurement scientists.

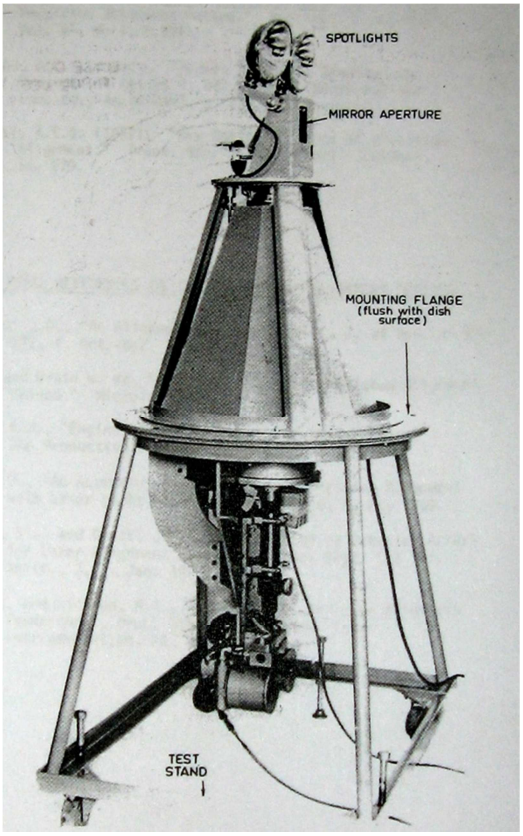

Figure 4 - An automatic theodolite circa 1962, specifically designed for measuring a radio telescope dish. It has motor actuated axes and records results on photographic film. [7]

In the recent decade, the manner in which LVM systems are being used in manufacturing is also undergoing a transition. Many aero-structure manufacturers are looking to change LVM from a separate quality assurance process occurring at the end of production to a more integrated solution where LVM systems assist production. This involves the interfacing of potentially real-time measurement data with production tooling and jigs, which may be adjusted according to measurement results. Such a system has the potential to reduce production cost and cycle time, as well as ensuring every product produced will meet specifications.

1.2. Research Area and Scope

Current aerospace assembly jigs and fixtures can have global build tolerances of below 250µm, over tens of meters. The high levels of demanded accuracy requires time consuming verification process using an assortment of Larger Volume Metrology (LVM) instruments operated by specialized personnel. This is an expensive operation that often takes hours to days to complete, during which production must be stopped. During production, the application of large volume metrology (or just metrology in

general) occurs typically at the end of assembly processes as a quality assurance step, making sure the product is within specifications.

As a result of the expensive and time consuming nature of industrial metrology as the technology is typically applied, it is therefore not surprising that metrology is often viewed negatively, as a necessary evil rather than a value adding process. This view can sometimes lead to the sentiment that metrology has no benefit other than leading to an increase of rejected parts, which are very costly, and the feeling that “No measurement, no problem”.

The research described in this thesis attempts to find solutions to the high costs and long process times typically associated with large volume metrology, and to make metrology into a “value adding” process by reviewing the state of the art and developing a Metrology Assisted Assembly (MAA) methodology to more directly integrate metrology systems into the production environment. This research study also attempts to look for novel applications of metrology technologies and mathematical algorithms, taking them from their current laboratory/research only status to a higher Technology Readiness Levels (TRL) suitable for use in production.

Implementation of a methodology of integrate and automate metrology in the manufacturing process can reduce production time, increase product quality while reducing the dependence on large and expensive jigs widely used in aero-structure manufacturing. Integration of metrology can also create new manufacturing processes that were previously unachievable, or are prohibitively expensive using traditional methods.

1.3. Research Aim

While the importance of measurement instruments in production has long been understood by manufacturers, the rapidly evolving field of metrology systems, especially in Large Volume Metrology, has only very recently opened up brand new opportunities of re-evaluating the relationship between measurement and production. It is clear that transforming metrology from a purely verification role occurring at the end of production to one that is integral during the entire process can have significant benefits.

A survey through the somewhat limited amount of literature (not surprising since details of production systems are often proprietary) on the state of the art of integrated and automated metrology shows some promising results.

As a result of the high level of interest from the aero-structure manufacturers and the positive findings in literature, the aim of this research study is to:

- Develop and demonstrate novel integrated and automated metrology systems in aero-structure production.

1.4. Research Methodology and Objectives

In order to extract the most benefit from metrology, its role in aero-structure manufacturing must change from its current use as an inspection tool, applied only after production to one of assisting production (Figure 5).

However, fully real-time measurement assisted production of aero-structures is still a distant goal, which the research presented in this thesis will attempt to bring closer to reality. While most of this research methodology focuses on the future goal, there is a large amount of room for improvement in the current metrology practices of the manufacturers. Therefore the first stage of the research methodology attempts to address these near-term production issues.

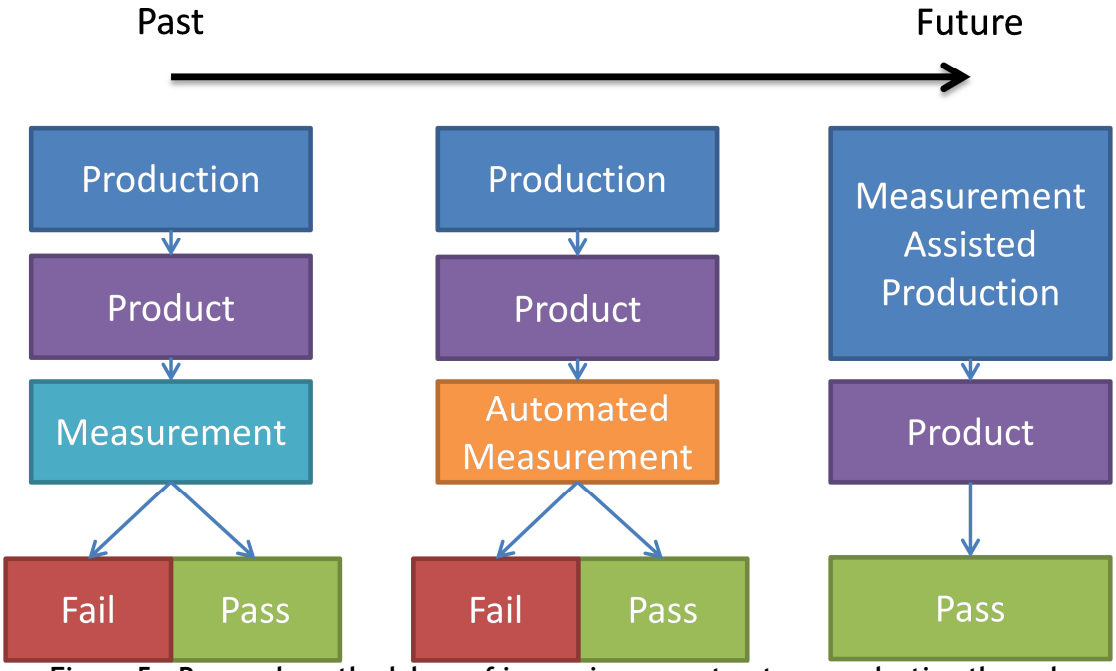

Figure 5 - Research methodology of improving aero-structure production through automation and integration.

In order to understand the current aero-structure measurement demands, a thorough understanding of the metrology systems and the manufacturing processes is required. This is achieved through onsite visits at Airbus and Vestas, extensive operational experience with the instruments, and surveys of existing literature. A number of improvements to the existing manufacturers' processes can be developed, to demonstrate the value of integrated and automated metrology in solving immediate issues in production.

After addressing the manufacturers' near-term requirements for LVM systems, the next stage of the research methodology is to show that the direct integration of LVM in the assembly process for future products can be simulated mathematically. This allows the LVM integrated assembly process to be evaluated and optimized prior to construction. The assembly simulations can also provide a sound theoretical basis illustrating potential gains from an integrated LVM system. The practical implementations of the integration must then be addressed, and software methods of interfacing directly with a number of the instruments in real-time need to be developed and demonstrated.

The final phase of the research realises the research aim by demonstrating what is possible through complete real-time metrology integration, providing a glimpse of a future production process where real-time metrology feedback can be used directly to improve the quality of the product.

In summary, the research objectives are:

1. Demonstrate the value of integrated and automated metrology in process enhancement and improvement in production environments.
2. Develop mathematical simulations of Metrology Assisted Assembly.
3. Develop and demonstrate direct software/hardware integration with LVM instruments including laser tracker and iGPS.
4. Demonstrate direct real-time control of a 3 axis positioning system assisted by a laser tracker.

1.5. Thesis Structure

This thesis is structured as follows:

Chapter 1:

Introduction of the research area and background, presents the research aims and objectives

Chapter 2:

Reviews of international standards on geometric specifications, large volume metrology instruments and uncertainties, and state of the art of metrology assisted assembly and automation

Chapter 3:

Describes a number of projects and case studies carried out to demonstrate the value of automated of metrology in solving near-term issues in production

Chapter 4:

Mathematical modelling of production processes with direct metrology integration

Chapter 5:

Develops software interfaces enabling the integration of LVM instruments. Describes the work on creating a real-time metrology assisted assembly demonstrator

Chapter 6:

Discusses and assesses the research results and presents the research conclusions and suggestions for further work

The methods and results developed in each chapter outlined here are discussed in their corresponding chapters.

2. Literature and State of the Art Review

2.1. Introduction

In this chapter, a review of the existing literature and the state of the art is presented. First, the review describes the state of the current international standards on geometric tolerancing and verification, and then a number of large volume metrology instruments are described. After which two mathematical methods of evaluating the measurement uncertainties are reviewed. Finally, the state of the art of metrology assisted assembly is examined, including the enabling technologies and examples in industry and academia.

2.2. Geometric Tolerancing and Verification

2.2.1. Geometric Product Specification

From observations on the production floor at Vestas Blades UK, and from experiences with Airbus projects, it is evident that the tolerances of the part geometry are not always very well defined, and are not properly followed in production. Thus it is likely to be beneficial to introduce a formal tolerancing scheme at the engineering design level, to better communicate the tolerancing requirements to tooling and production.

The Geometric Product Specification (GPS) aims to promote clear, concise and accurate communication of product specifications between design, manufacturing and inspection, since it is critical for the functionality, safety, reliability and interchangeability of a product, especially when the product is complex, and the design and manufacturing centres are located in different countries. GPS is specifically designed to operate in the three "worlds" of the product features, as explained in ISO 14660-1:1999 [8]:

- *The world of specification, where several representations of the future workpiece are imagined by the designer;*

- *The world of the workpiece, the physical world;*
- *The world of inspection, where a representation of a given workpiece is used through sampling of the workpiece by measuring instruments.*

…ISO 14660 defines standardized terminology for geometrical features in each world as well as standardized terminology for communicating the relationship between each world.

The application of GPS can lead to the reduction of production cost, through the proper understanding of the required tolerance by all parties, as tolerancing is frequently *"the single most important factor in determining the cost of manufacturing the product or part"* [9], and the proper understanding of uncertainties in inspection can reduce the number of out-of-spec parts being accepted and the number of correctly produced parts being rejected. Included in GPS is an international standard symbolic language for the communication of geometric tolerance in engineering, the ISO 1101 standard.

2.2.1.1. GPS ISO 1101 standard for geometric tolerancing

The ISO 1101 specifies the requirements for the geometrical tolerancing of workpieces, not only does the standard allows the designer to define the tolerances on a part, it also helps the metrologist by clearly identifying ways to measure the part. The usefulness of this standard can be demonstrated by the typical measurement of the diameter of a circle.

An example is illustrated in Figure 6 A. A simple "+/-" tolerance does not specify a method of measurement. Different results are recorded depending on whether the min, max or mean diameter is measured, and it is also unclear whether the interest is the dimension or surface profile such as roundness and run-out. Therefore it is very ambiguous and open to interpretation.

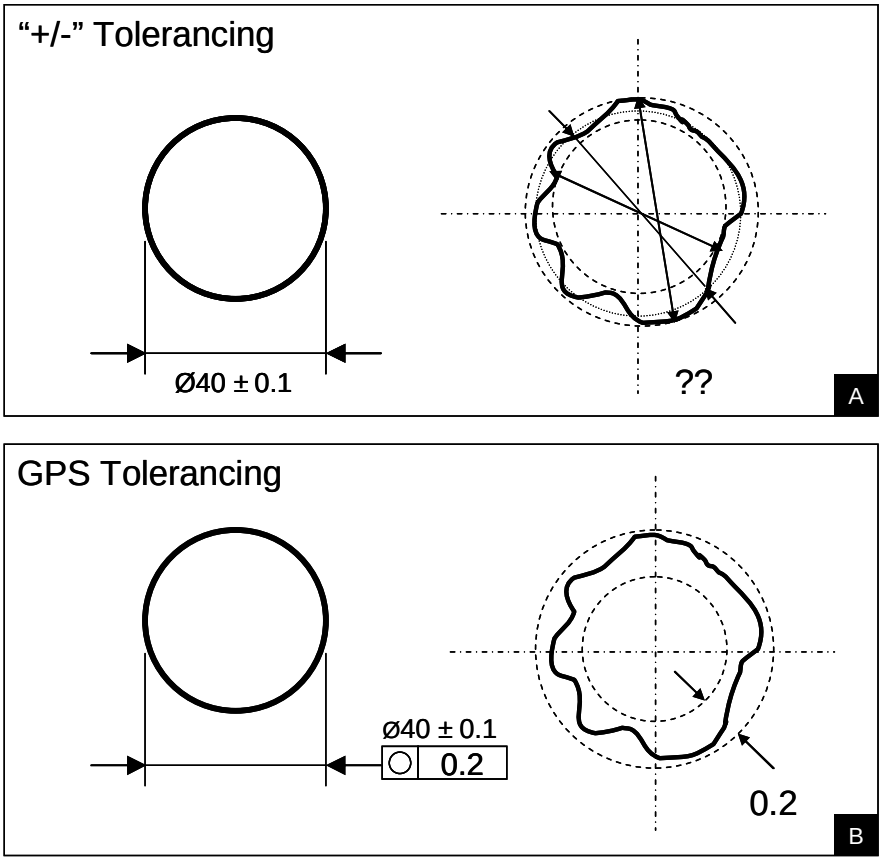

Figure 6 – A) "+/-" Tolerancing is ambiguous. B) GPS Tolerancing is much clearer.

In Figure 6 B, the geometric "Roundness" tolerance (identified by the ○ symbol) is defined on the diameter, specifying that the measured profile of the circle should lie within two concentric circles 0.2 units between each other. This not only removes any possibilities for interpretation, it also suggests methods of measurement to the metrologist: use a roundness measuring machine or a CMM [10].

2.2.1.2. Interaction between Measurement Uncertainty and Tolerances

It is a common misconception that if the measurement of a part's dimension falls within the tolerance band, the part should be declared to be within tolerance. This is however incorrect, because the assumption is that the measurement instrument has no uncertainty. [11]

Consider a part which has a dimensional tolerance specification of ±1mm. Imagine that the part is measured with an instrument with an uncertainty band, the possible interactions between the measurement, uncertainty and tolerance are shown in Figure 7.

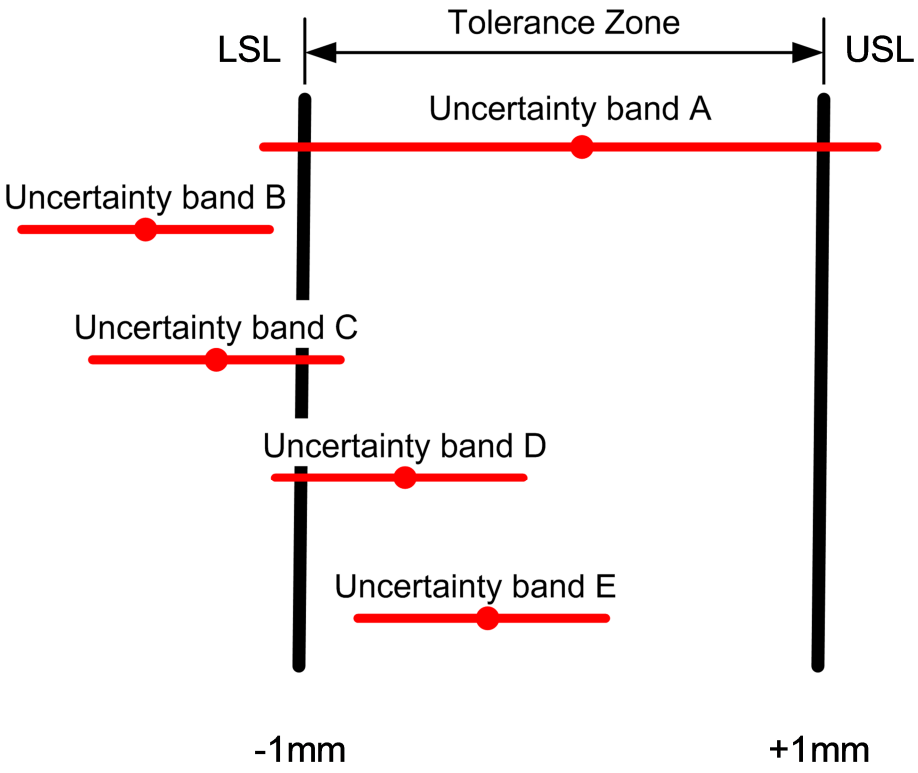

Figure 7 - Tolerance zone and uncertainty bands [12]

After the measurement, the question whether the part should be rejected or accepted needs to be answered. The correct decisions for the five possible interactions are [12]:

A. The tolerance of the part is less than the measurement uncertainty, thus the part dimension cannot be determined within the tolerance specification. A more accurate instrument with uncertainties less than ±1mm is needed.
B. The uncertainty of the instrument is less than the tolerance of the part. The reading shows the part to be sufficiently below the Lower Specification Limit (LSL) that there is no overlap between the tolerance zone and the uncertainty band. It can therefore be concluded with confidence that the part is out of tolerance, thus must be rejected.
C. The uncertainty of the instrument is less than the tolerance of the part. The reading shows the part to be out of tolerance but there is overlap between the tolerance zone and the uncertainty band. There is a slight chance that the part is in tolerance, but it must be rejected.
D. The uncertainty of the instrument is less than the tolerance of the part. The reading shows the part to be in tolerance but there is overlap between the tolerance zone and the uncertainty band. The part is probably in tolerance but it can not be stated with confidence and therefore it must be rejected.
E. The uncertainty of the instrument is less than the tolerance of the part. The reading shows the part to be sufficiently within the ±1mm tolerance that there is no overlap between the tolerance zone and the uncertainty

band. We can therefore state with confidence that the part is in tolerance. This is the only case where the part should be accepted.

2.2.1.3. GPS ISO 14253 Decision Making Rules

While the 1:10 instrument uncertainty to tolerance rule of thumb is valid in most cases, problems often arise when the supplier and the customer measure the same part with different instruments, and the results disagree. The ISO 14253 is the international standard governing the decision of conformance or non-conformance to tolerance specifications.

The ISO 14253 can be summarized in the following diagram (Figure 8):

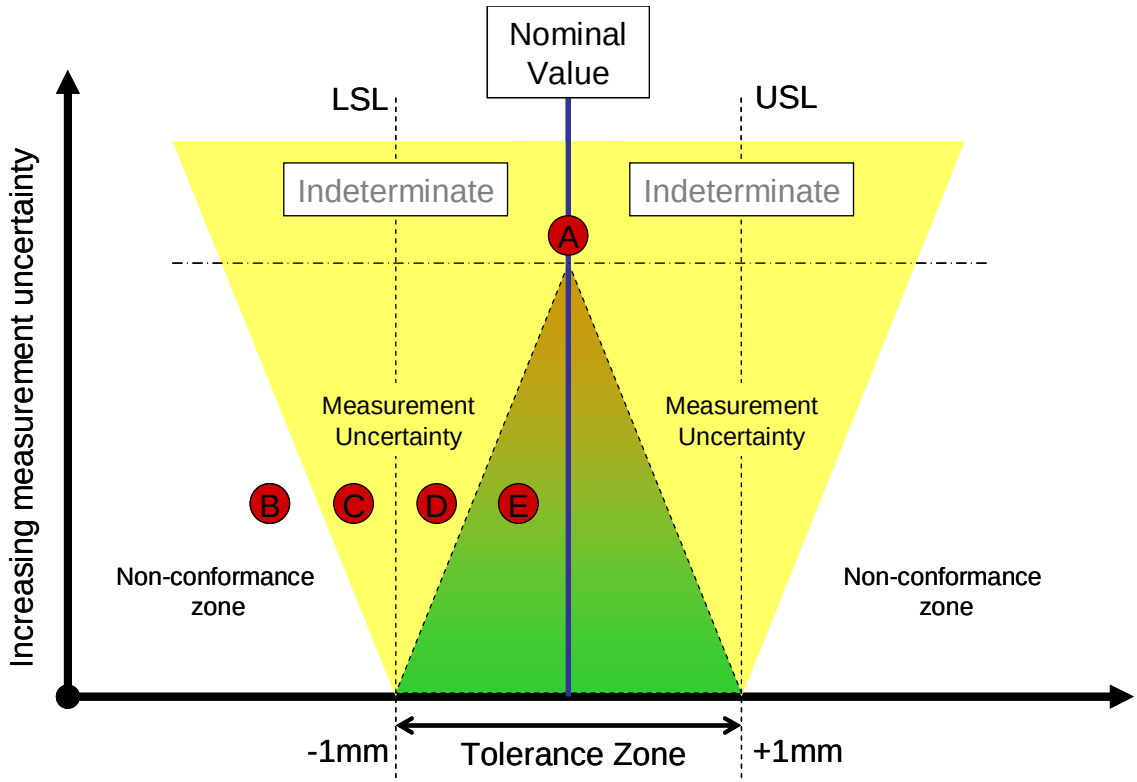

Figure 8 - The uncertainty of measurement reduces the available conformance and non-conformance zones, as per ISO 14253, with the same measurements from Figure 7 overlaid.

The supplier must prove that the part is within the tolerance zone, and if the customer wants to prove non-conformance, the customer must prove that the part is in the non-conformance zone. Thus: “When evaluating the measurement result the uncertainty is always at the disadvantage of the party with onus on proof” [13].

The practical implication of this is that for the supplier, the available tolerance zone is reduced as the uncertainty of the measurement instrument increases. The reason only measurement “E” in the previous section is the only measurement accepted to be within tolerance is further highlighted.

Therefore, when choosing a metrology instrument, it becomes important to consider the trade-offs between a cheaper instrument which must work with reduced tolerance zones, thereby increasing the likelihood of rejecting perfectly good parts, and a more accurate but more expensive instrument which is less likely to reject good parts. The fact that the more accurate instrument may often be many times the cost of the cheaper instrument makes the trade-off study even more difficult.

2.2.2. Metrology of Freeform Surfaces

Much of the manufacturing difficulties in the aerospace and wind turbine industries arise from the fact that the components are large freeform surfaces, which are difficult to manufacture to high tolerances.

A freeform surface, also known as a complex or sculpted surface, is classified in ISO 17540-1:2007 as a complex feature with no invariance degree [14]. Unlike simple features such as planes and cylinders, freeform features cannot be translated or rotated about any axis while still preserving it shape. While the ISO GPS standard allows profile tolerances on freeform surfaces, unlike straightness [15], flatness [16], cylindricity [17] and roundness [18], there is no standard for the verification of freeform surfaces. Due to the complexities of measuring such features, there is unlikely to be an international standard for inspection some time.

Fluid dynamic efficiency is one of the most common factors driving the accuracy of free form surfaces, whether is the wings on commercial aircraft, compressors blades inside a pump or the blades of a wind turbine (Figure 9). As a direct result of inaccuracies in the surfaces, gap, flush and interference problems are created at the surface interfaces. Gap and flush problems on the outside surfaces of a fluid dynamic device such as a wing are often detrimental to its performance, and inaccuracies between the surfaces and underlying structures can affect the integrity of the entire structure. Or as it is in the case of automotive panels and consumer electronics, the customer often relate the quality of the gap and flush of the exterior to the build quality of the entire product. It is therefore important to understand how these issues can be measured, verified, and reduced.

Figure 9 - A Vestas wind turbine section at University of Bath for freeform measurement testing

Accurate measurements of freeform surfaces, especially large volume features, have only recently become practical enough for use in production. There are many existing technologies for measuring free form surfaces. The detailed explanation of their working principles is outside the scope of this thesis, instead a number of applications of the measurement technologies are described in Table 1.

Table 1 - Examples of freeform surface verification applications

Measurement technology	Examples	
Photogrammetry	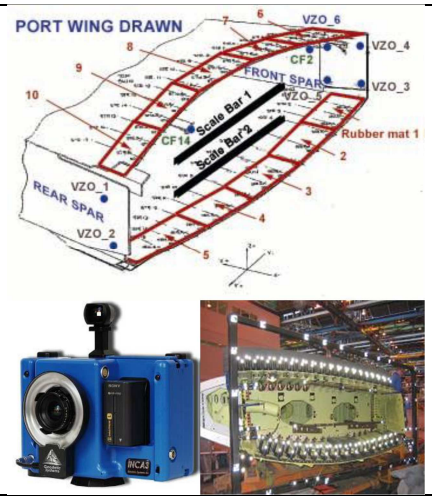	Airbus A-320 wing root geometry verification using V-Stars photogrammetry camera

Laser tracker		Mobile robot laser tracker measurement of a wind turbine blade at University of Bath
White light scanner	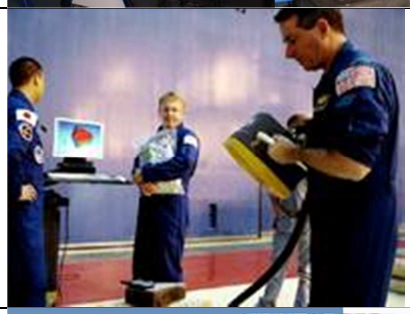	Cognitens scanner used at NASA to scan space shuttle tiles
CMM	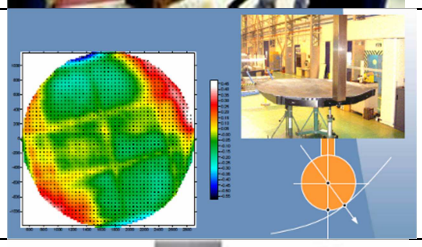	CMM measurement of an satellite antenna dish at EADS Astrium
		Renishaw Revo CMM measurement of valve seat and guide.
Laser radar		Engine nacelle geometry verification using Metris laser radar

One of the key issues in the verification of freeform surfaces is the ability to understand the instrument uncertainty. Due to the diversity of surface shapes and measurement requirements, there are a vast number of measurement instruments, some of which are listed in Table 1. There are no existing standards for testing and calibrating many instruments that are

used to in the measurements. However, National Measurement Institutes such as the National Physical Laboratory are beginning to designing artefacts that may be used for such a purpose. The NPL have developed a grid plate for verifying the accuracy of cameras (Figure 10 A) and is developing a pseudo freeform artefact for measurement instruments such as 3D laser scanners (Figure 10 B).

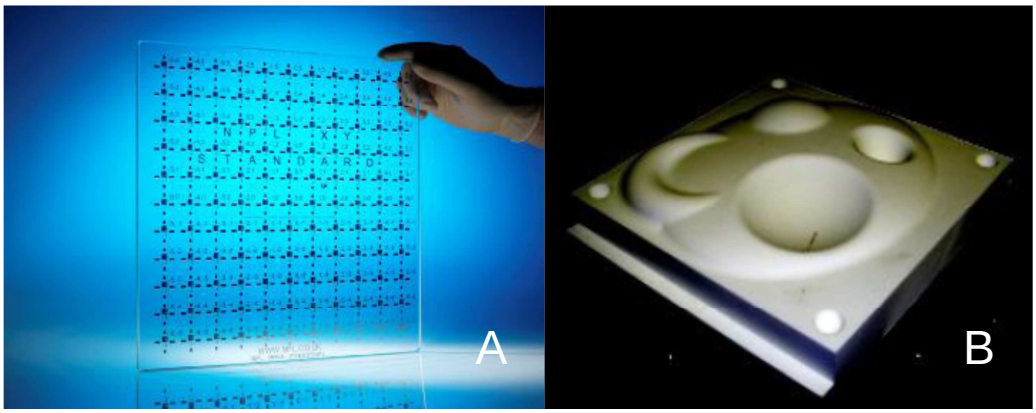

Figure 10 - A) NPL grid plate for vision systems. B) NPL Freeform artefact

The uncertainties in the surface form as it was produced, compounded by the edge trimming and the assembly processes that freeform surfaces typically are involved in, eventually manifest themselves in the gaps and steps between surfaces, and gaps or interferences between the surfaces and other components.

The assembly methods used to minimize the interface problems can be classified in three categories: build to nominal, measure and adjust, and measure for production.

- **Build to nominal**: the assembled product tolerance is met by simply making the key features of the parts as accurately as possible. Typically used for small products with features that can be accurately produced.

- **Measure and adjust**: the assembled product tolerance is met by measuring the interfaces and adjusting some of the parts' position and/or orientation to minimize interface problems. For larger parts which can be difficult and expensive to produce to tight tolerances (such as door panels in the automotive industry), the position and orientation maybe manipulated manually or automatically to minimize the overall interface problems the part is involve in [24, 25].

- **Measure assisted production**: the assembled produce tolerance is met by measuring one side of the interface and producing the other side using the measured data. For very large freeform shapes such as wings and wind turbine blades, it is very difficult and expensive to produce parts to tight tolerances. It is often more economical to

tailor parts to fit the specific physical assembly by producing parts directly using measurements from the assembly [37, 38, 39, 47].

2.3. Large Volume Metrology Instruments

The accurate measurement of large structures has always been a challenging problem, as a result of the increasing demands on the accuracy and economic production of ever-larger products, such as aircraft and wind turbines. Due to the fact that the products and requirements vary greatly between measurement projects, there is no single LVM instrument that can perform all the tasks. Rather, there is a large variety of different instruments to choose from. In fact, since the instruments can have price tags in the hundreds of thousands of US Dollars, instrument selection is a hotly researched topic in itself.

The descriptions and working principles of three of the large volume metrology instruments most frequently used in this research project are described in the rest of this chapter.

2.3.1. Laser tracker

The Laser Tracker utilises interferometry for measuring length and a pair of high resolution angle encoders to measure the horizontal and vertical angles of the laser beam. Figure 11 shows a schematic of the internal components of a typical laser tracker. In the interferometry technique a coherent laser beam of known wavelength passes through a beam-splitter. One beam is reflected back within the system while the other is aimed at a Spherical Mirror Reflector (SMR) that is a sphere with an embedded corner cubed reflector. When the two beams combine, constructive and destructive interference at the laser wavelength can be observed by the detector. The number of the bright and dark patterns is counted by the relevant electronics to calculate the distance. The SMR is used as the instrument probe, thus the laser tracker is a contact measurement system.

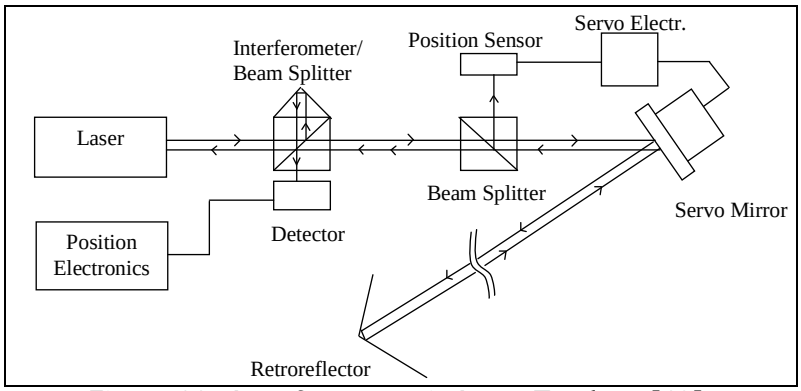

Figure 11 – Interferometry in Laser Trackers [19].

Laser trackers are considered to be one of the most reliable and well established metrology systems. An international standard exists for the system's performance evaluation [20]. Their main drawback is that the line of sight between the laser tracker head and the SMR must be maintained at all times, and only one SMR at any time can be tracked. Some laser trackers provide an Absolute Distance Measurement (ADM) system, which modulates the laser beam and detects the phase of the returned light [19]. By gradually reducing the modulation frequency, the absolute distance of the target can be determined with a high degree of accuracy. ADM enabled laser trackers are more user friendly, since when the line of sight is broken, the tracker can reconnect with the SMR without homing the SMR to the tracker's initial position, as is required for an interferometer system. The ease of use however, comes at the cost of a slight decrease in accuracy [21].

The commercial laser tracker market is dominated by three major manufacturers: the USA based Faro and Automated Precision Inc, plus Leica Geosystems based in Switzerland.

Figure 12 – Examples of latest laser trackers: A) Faro Ion, B) API Radian, C) Leica AT901

2.3.2. Photogrammetric Metrology Systems

Photogrammetry used in industrial metrology is often referred to as "Close Range Photogrammetry" or "Vision Metrology", to distinguish it from large scale Photogrammetry typically associated with the production of topological maps using aerial or satellite images.

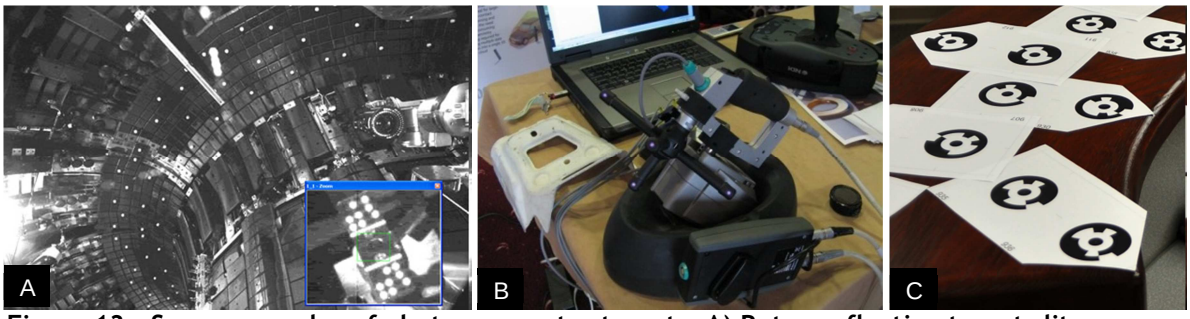

Figure 13 – Some examples of photogrammetry targets. A) Retro-reflective targets lit up by camera flash. B) Active infrared LED on NDI ScanTrack. C) Low cost printed coded paper targets.

Photogrammetry is an angle based triangulation method. Two Dimensional images of the active or passive (including normal or retro-reflective) targets are used to determine their three dimensional coordinates. This is possible because the targets on the images are related to their 3D positions through the projection of the lens.

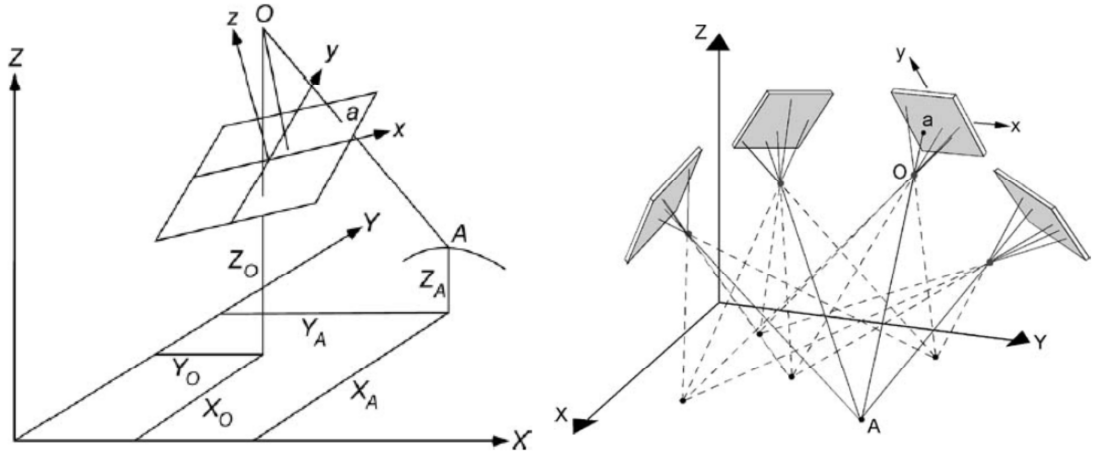

Figure 14 - Image space projection and resection [19]

Using the images, the position and orientations of the cameras and the positions of the targets can be calculated using resection and bundle adjustment. Since the images only provide the angular information, typically one or more calibrated scale bars are required to provide a distance reference.

While the principle of photogrammetry is the same, the implementation of the measurement system can be very different. Some of the most common commercial photogrammetric metrology system configurations are listed below:

Single camera offline

Single camera offline photogrammetry is currently the most commonly used configuration in industrial metrology. A single specially designed photogrammetry camera such as GSI Inca or adapted high-end consumer camera such as AICON DPA is used to take multiple photos of the parts that

needs to be measured. The images are saved to a memory card or transferred wirelessly to a computer and are processed “offline”, after the measurement is complete. The parts typically have coded and un-coded retro-reflective targets applied to them before the pictures are taken. Sometimes when a dense grid of measurements is desired, a projection system that projects bright circular spots onto the parts is used instead of the stick-on targets.

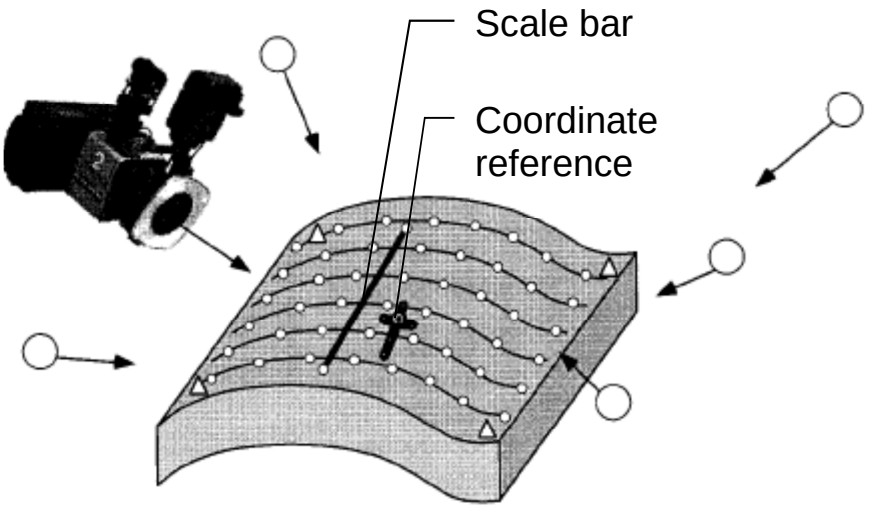

Figure 15 - Single camera taking photos from multiple directions [19]

The high quality high resolution cameras and the large number of pictures that can be taken from different position make this method the most accurate (25 - 50 µm typical). Since only a single camera carried by an operator is involved in the measurements, this method is also very flexible and scalable, allowing it to be easily applied to a large variety of different measurement jobs, from industrial equipment, aerospace components to large radio telescopes. The main draw back of this method is that the measurements need to be done manually every time, and it is very difficult to automate the measurement process. If the required number of images is high, the measurement process can also be very time consuming. Since the images are taken sequentially, any movements of the parts during the measurements can produce errors, thus this method is only applicable to static measurements.

Multiple cameras online

One way to automate a single camera offline photogrammetry system is to use multiple cameras instead of moving one camera to different positions. This has the additional benefit being able to make dynamic measurements when the cameras are synchronised. Two or more cameras all looking at the same targets can make very rapid measurements, with measurement frequencies up to thousands of times per second using high speed cameras. The images can be processed immediately on a computer (“online”), or for some high speed systems the images are processed in special processing

units attached to the cameras. This means dynamic deformations and the positions of handheld probes can be tracked in real-time or near real-time.

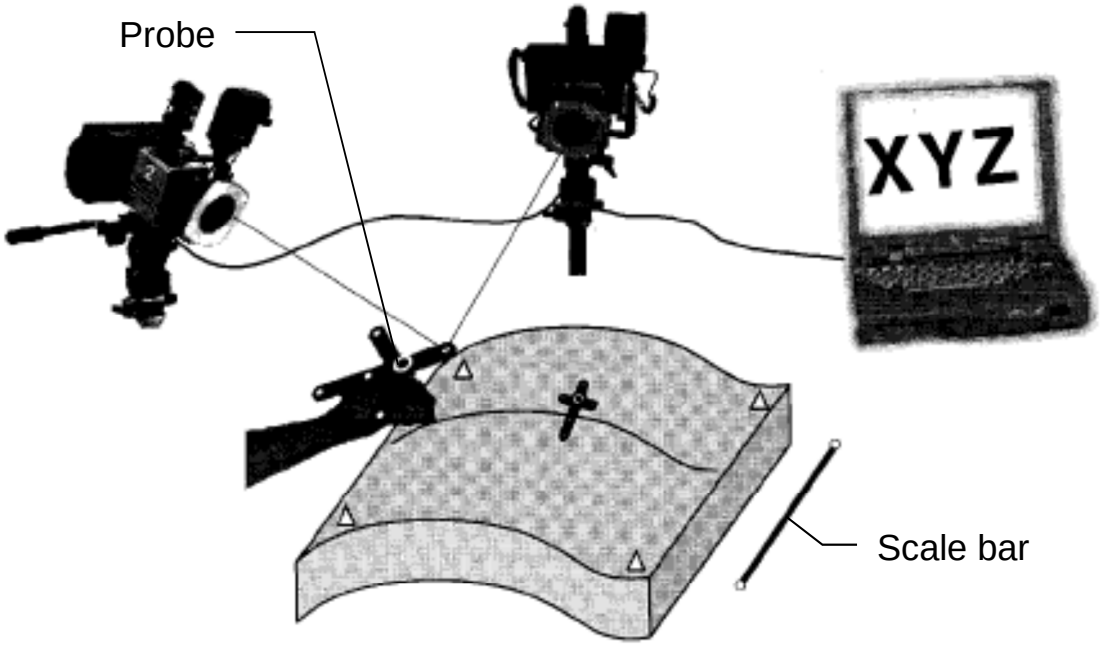

Figure 16 - Two cameras take measurements simultaneously [19]

The automated nature and the speed of the online systems can be of crucial importance for a jig health-check system. However, the typical commercial multi-camera systems have significant downsides. Perhaps the most important downside is the high cost. A single high-end photogrammetry camera is often already very expensive, making the use of multiple camera systems such as the V-STARS M8 prohibitively expensive for many measurement tasks. In addition, when compared to the typically 20 or more images taken in a single camera measurement, using only as many pictures as the number of cameras can significantly reduce the measurement accuracy. While less expensive alternatives like the Metronor DUO and AICON MoveInspect exist, because of the lower resolution cameras used, and the low number of cameras, their accuracy is also lower.

It is possible that a large number of low cost cameras may be able to achieve similar accuracies to the commercial systems that use a smaller number of higher cost cameras.

Single camera online

Figure 17 - The Metronor SOLO single camera online system

The Metronor SOLO is a single camera online system that tracks active infrared targets embedded on a measurement probe. Given that the relationships between the targets are known and are fixed, the probe acts as a scale bar and a moving measurement device at the same time, allowing positions to be measured with only a single camera. It is a low cost solution with relatively low measurement accuracy and volume.

Linear Sensors with active targets

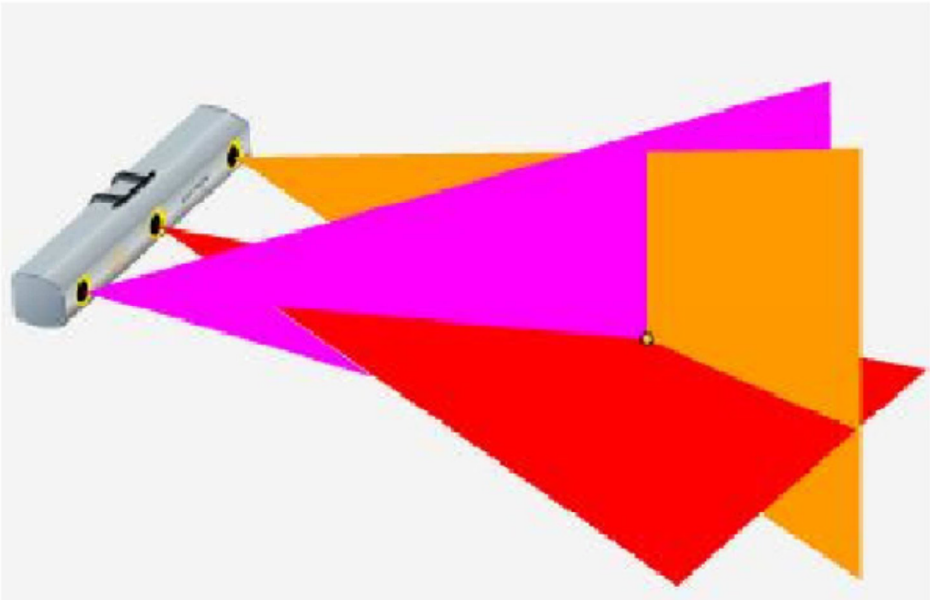

Figure 18 - Nikon K-Series linear CCD array working principle

A special case of photogrammetry technology is used in the Nikon K-Series and NDI OPTOTRAK systems. Instead of the matrix CCD or CMOS image sensors used in typical systems, three linear CCD array sensors are used to track the positions of active IR targets. Each of the linear CCD sensors provides one angle required to compute the target position. When measuring more than one target, the IR target LEDs are turned on sequentially, allowing each of the targets to be uniquely identified.

These systems are capable of dynamic measurements at very high frequency, although the measurement frequency reduces as the number of targets tracked increases. They can be fairly accurate at short ranges, but their working volumes are relatively restrictive, therefore a large number of systems may be required to cover the size of a typical aerospace jig.

2.3.3. Indoor GPS

The indoor GPS is a distributed metrology system produced by Nikon Metrology (formerly Metris) that offers a relatively lower cost alternative for measuring and tracking an unlimited number of coordinates in a large volume.

Typically, the system components of iGPS are (see Figure 19):

- At least two transmitters
- A control centre
- Wired/wireless sensors

Transmitters operate as reference points (with known position) continually generating three signals: two infrared laser fanned beams rotating in the head of the transmitter and an infrared (IR) LED strobe. Sensors are passive elements, which can be placed on the surface of the object to be measured to receive the transmitters' signals. Before starting measurements, the locations of transmitters are solved by measuring a number of points inside the working volume, and applying scaling information between the points.

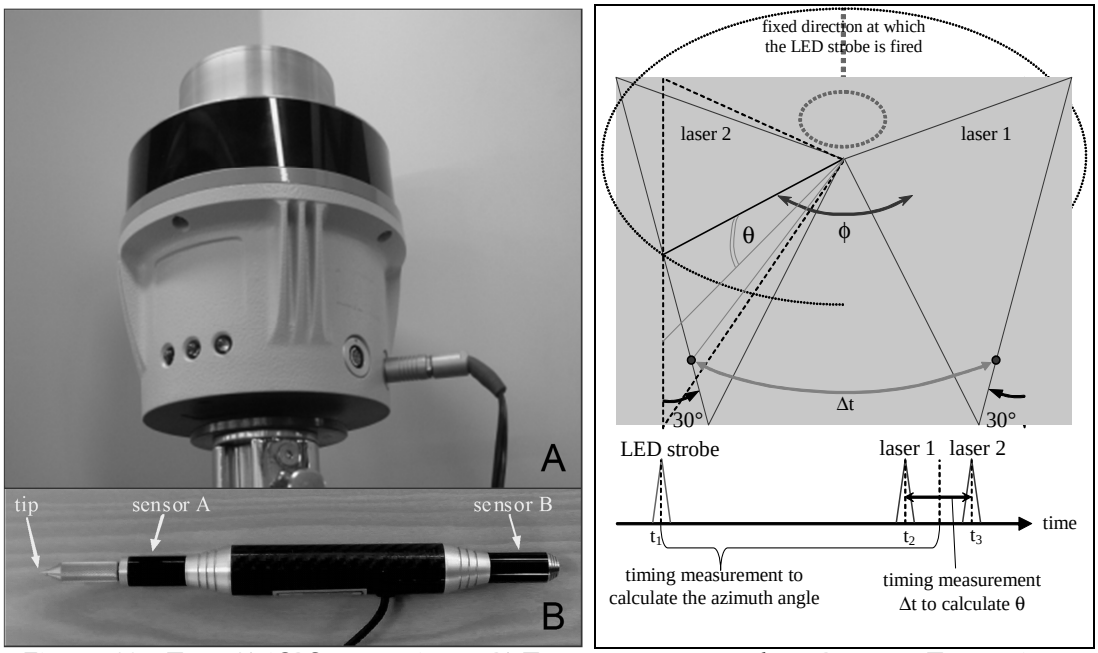

Figure 19 – Top: A) iGPS transmitter. B) Two sensor vector bar. Bottom: Transmitter laser fans and timing diagram of the signal received by the sensor [52]

During measurements, the position (x, y, and z) of each sensor is calculated. Each transmitter-sensor pair acts in the same way as a Theodolite-target pair, producing two angular measurements: the horizontal (azimuth) and the vertical (elevation) angles. Sensors can triangulate their position whenever they are located in the line-of-sight of two or more transmitters [48].

The technique used by each transmitter-receiver pair to determine the azimuth and elevation angles is as follows [48]. Each transmitter generates two rotating infrared laser beams and an infrared LED strobe. These optical signals are converted into timing pulses through the use of a photo detector. The rotation speed of the spinning head in each transmitter is set to a different value in order to differentiate between the transmitters. Additionally, the transmitter angular velocity is continuously tracked and used to convert the timing intervals into angles. As shown in the Figure 3 (bottom), the two fanned beams, radiated from the rotating head of each transmitter, are tilted with respect to the rotation axis, nominally at -30° and +30°.

The measurement of azimuth angle requires a horizontal index, which is created by firing an omni-directional LED strobe at a fixed direction in the rotation of the transmitter's head.

While the static coordinate measurement performance of the iGPS metrology system has recently been analysed in a fair amount of detail [49, 50, 51, 52, and 53], no existing literature delved into its dynamic performance. For applications such as real-time robot guidance and the analysis of parts in motion, the dynamic tracking performance of the iGPS needed to be studied.

2.4. Measurement Uncertainty

Measurement uncertainty is defined as the "parameter, associated with the result of a measurement, that characterizes the dispersion of the values that could reasonably be attributed to the measurand" in the "Evaluation of measurement data — Guide to the expression of uncertainty in measurement" (GUM) by the Joint Committee for Guide in Metrology [22]. Evaluation of the measurement uncertainty is a critical aspect of metrology, since a measurement result without an associated uncertainty is meaningless.

The uncertainty of a measurement is usually expressed in "standard uncertainties", or standard deviations. Therefore if a measurement has a standard uncertainty of 1mm, it means that the measured value is within ±1mm of the actual value of the measurand with a confidence of 68.2% if the measurement has noise that is normally distributed.

If the final result of a measurement is calculated from a number of indirect measurements, as it is often the case, the relationship between the measurements and the final result is described by a measurement model:

$$\boldsymbol{Y = f(X_1, X_2, \dots, X_N)} \qquad \textbf{Equation 1}$$

Where X_i are the measurements and Y is the final result.

A simple example of this is shown in Figure 20. The lengths of bars A and B are measured, with corresponding standard uncertainties $u(A)$ and $u(B)$, and the final result Y is the total length of bars $A + B$ which is not measured. In order to determine the uncertainty of the final result $u(Y)$, the uncertainties of A and B need to be propagated using the measurement model $Y = f(A, B) = A + B$.

There are two widely used methods of assessing and propagating the uncertainties associated with measurements: the GUM approach and the Monte Carlo approach, described in the following sections.

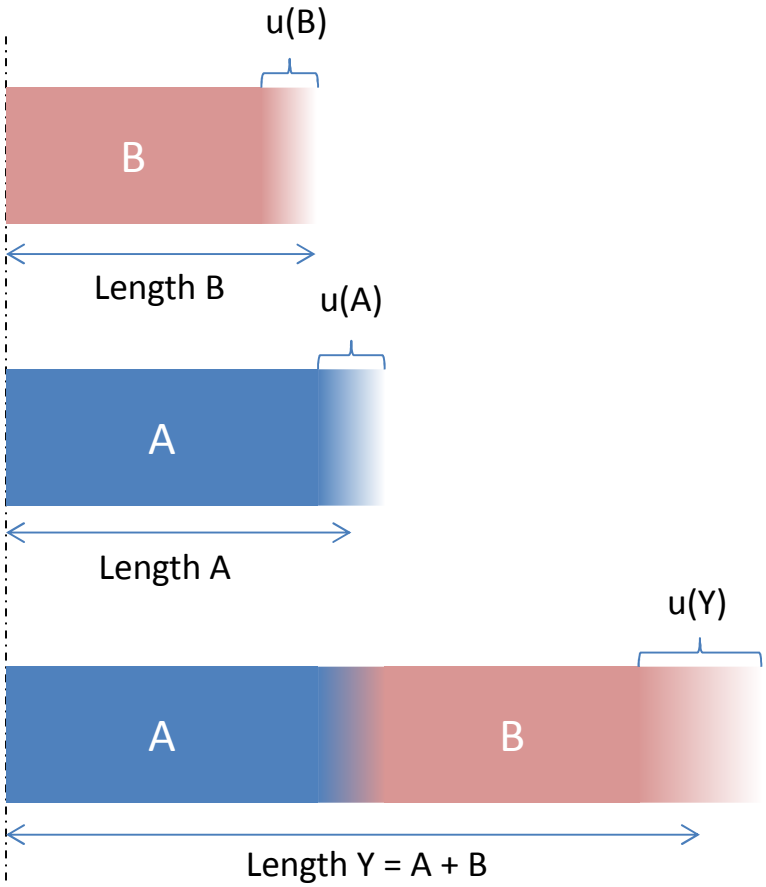

Figure 20 - Example of combined uncertainty

2.4.1. Uncertainty Propagation: GUM Approach

The GUM approach propagates the measurement uncertainties analytically, using the partial derivatives of the measurement model (Equation 1). The GUM formula for calculating the combined uncertainty $u_c(y)$ is as follows:

$$u_c(y) = \sqrt{\sum_{i=1}^{N}\left(\frac{\partial f}{\partial x_i}\right)^2 u^2(x_i) + 2\sum_{i=1}^{N-1}\sum_{j=i+1}^{N}\frac{\partial f}{\partial x_i}\frac{\partial f}{\partial x_j}u(x_i,x_j)} \qquad \textbf{Equation 2}$$

Where $u(x_i)$ are the standard uncertainties of the individual measurements, and $u(x_i, x_j)$ are the covariance of x_i and x_j.

Using Equation 2, we can find the solution to the simple example problem given previously in Figure 20. If we let $u(A)$ = 3mm, $u(B)$ = 4mm, and $u(A,B)$ = 0 because the measurement of *A* and *B* are independent of each other. We find that Equation 2 simplifies to:

$$u(Y) = \sqrt{u^2(A) + u^2(B)} = 5mm$$ **Equation 3**

Therefore the length of *Y* has a standard uncertainty of 5mm.

Advantages of the GUM approach include:

- Computationally (relatively) efficient
- Provides consistent results
- Can be solved by hand

Disadvantages of the GUM approach include:

- Simplified model assumptions (first order model, known distribution) may be completely wrong
- More difficult to implement in software
- Large covariance matrices are tedious to solve by hand

2.4.2. Uncertainty Propagation: Monte Carlo Simulation

An alternative to the GUM approach is the Monte Carlo Simulation (MCS), which is a sampling based approach. Instead of trying to propagate the uncertainties *analytically*, the measurement model is simulated *numerically* a large number of times using randomly generated values to represent the uncertainty distribution [23].

In a Monte Carlo simulation, the distributions rather than the standard uncertainties of the measurements are propagated. Therefore the result of a MCS is a distribution as well. The standard uncertainty can then be computed from the resulting distribution, and the shape of the distribution may also provide insights into the measurement model.

The example above can also be easily solved using MCS in a computational mathematics package such as MatLab.

The MatLab coded used to produce the result in Figure 21 is listed below:

```
N = 100000;
A = randn(N,1).*3;
B = randn(N,1).*4;
Y = A + B;
std(Y)
```

Here 100000 samples of A and B are generated, and put into the measurement model, generating 100000 corresponding Y values:

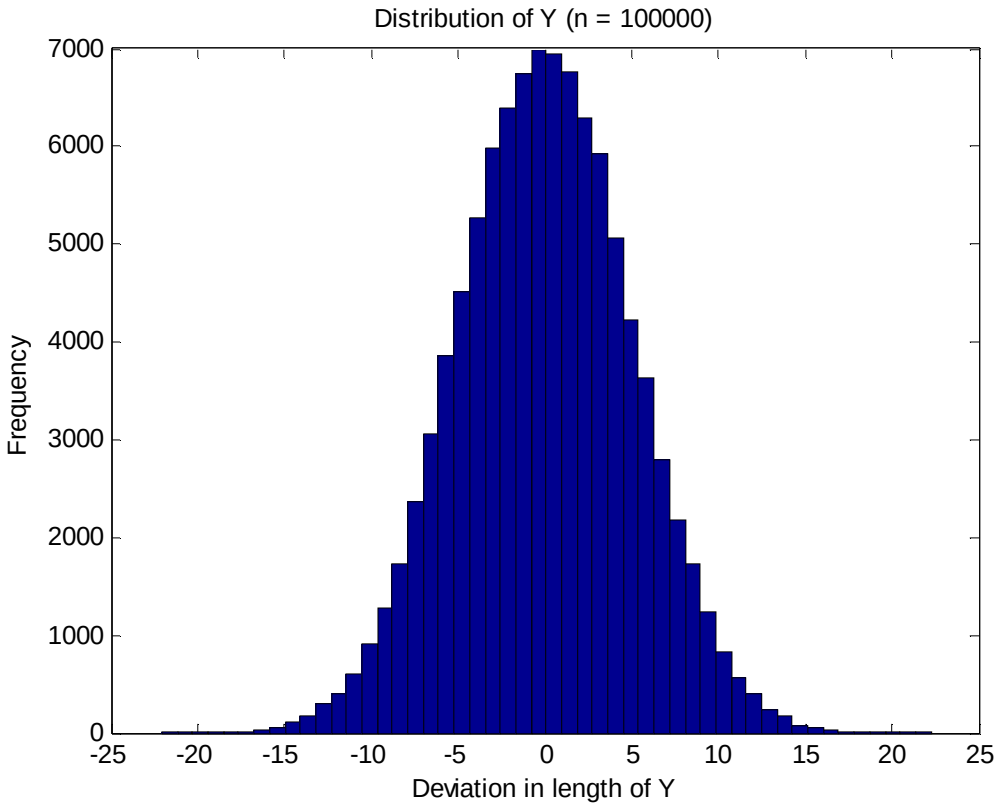

Figure 21 - MatLab MCS distribution result of example problem

The final result of u(Y) = 5.0152mm. However, the value varies slightly, depending on the choice of the random numbers. The result is also highly dependent on the number of samples used, as shown in Figure 22. While the 100000 sample simulation takes very little time for this simple example, it might be prohibitively computationally intensive for more complex problems, therefore trade-offs between simulation accuracy and may need to be considered.

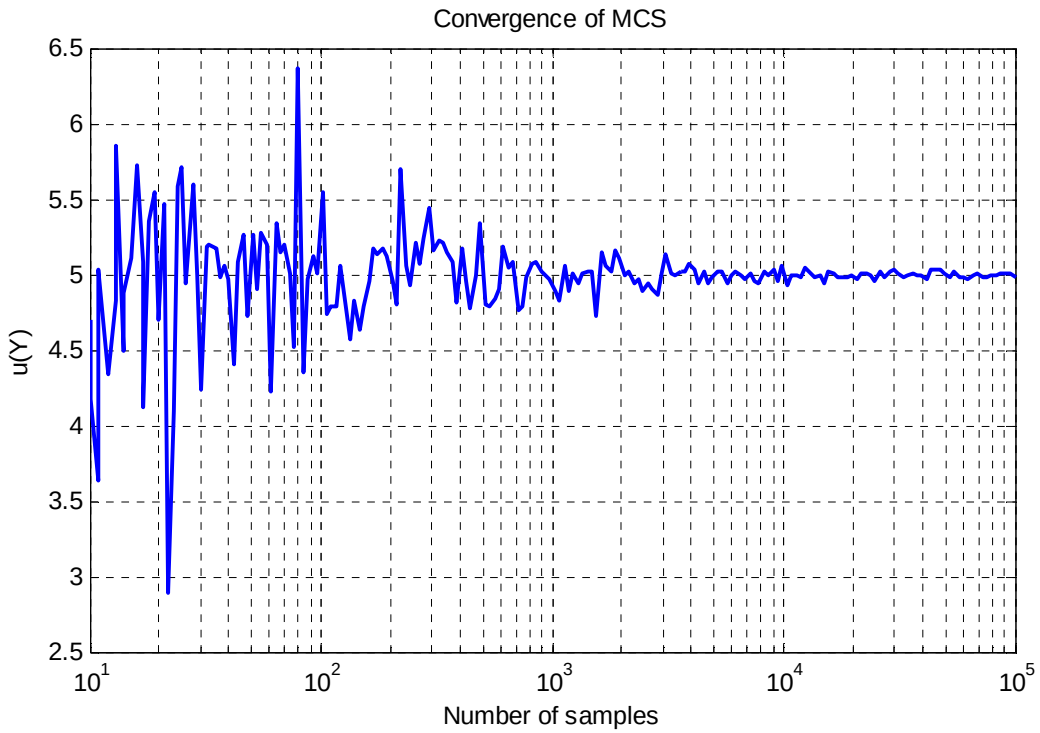

Figure 22 - MCS results depends on the number of samples used

Advantages of the MCS include:

- Easier to implement in software for large problems
- Can solve non-linear problems with non-standard distributions
- Easy to understand
- The results provide more information

Disadvantages of the MCS include:

- Computationally intensive
- Result dependent on number of samples
- Result also depends on the random numbers generated

2.5. Metrology Assisted Assembly and Automation

2.5.1. Metrology Assisted Assembly Enabling Technologies

A brief categorization of capability descriptions of some of the most frequently used systems that enables automated metrology assisted assembly are listed in this section.

2.5.1.1. Large Volume Metrology Instruments

In a MAA system, the LVM instrument provides the underlying accuracy. They can be divided in to two main types by their operating principles: spherical coordinate and triangulation. Some common systems are categorized and their capabilities summarized in Table 2.

Table 2 – Large volume metrology systems commonly used in production

Type of system	Name of system		Capability
Spherical coordinate	Laser Tracker	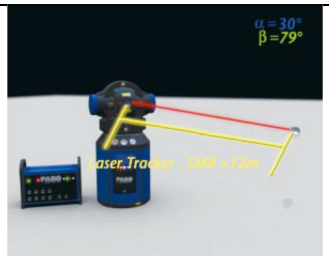	• Single point • High accuracy • Large volume • Static or Dynamic • Automation integration
	Laser Radar		• Reflector-less • Surface scanning • Mid-high accuracy • Static • Automation integration
Optical Triangulation	Theodolite Network		• Large – Very large volume • Single point • Static
	Photogrammetry		• Medium volume • Mid-high accuracy • Multipoint acquisition • 6DOF possible • Static or Dynamic • Automation integration

	Laser Line Scanners		• Med-low volume • Fast surface scanning • Automation integration • Static
	Indoor GPS	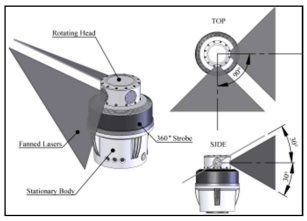	• Distributed, Large volume • 6DOF possible • Low-mid accuracy • Static

Laser trackers and photogrammetry systems are by far the most popular systems used in large volume measurements, due to their combination of accuracy, flexibility and large measurement volume. They are fairly mature technologies that are commercially available from a selection of instrument makers.

2.5.1.2. Robotic Systems

Robotic systems provide positioning capability to a MAA system. There are three main types of robotic systems based on their kinematics: serial, parallel and mobile. Some common systems are categorized and their capabilities summarized in Table 3.

Table 3 - Robotic systems commonly used in production

Category	Type of robot		Capability
Serial Robots	Cartesian	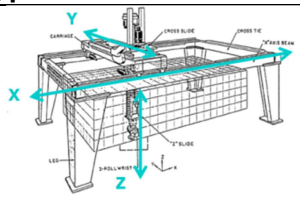	• Can be sized according to requirement • Heavy frame, high stiffness • High payload. • Low working area/size
	Articulated		• High flexibility • Relatively low cost • High working area/size • Limited payload and accuracy

Parallel Robots	Tricept	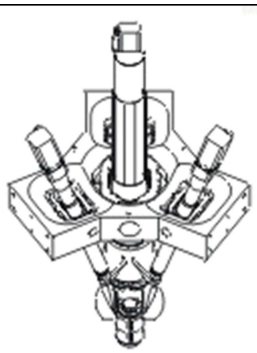	• High stiffness/weight • Less joint error build-up for high accuracy machining • Small working area
	Delta		• Low mass actuator allows fast acceleration and movement for pick and place operations
Mobile Robots	Wheel or Track	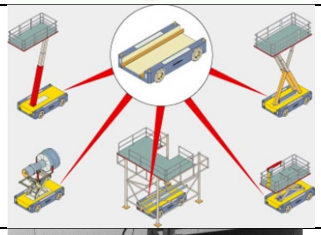	• Freedom of movement on flat surface • High load carrying ability
	Crawling	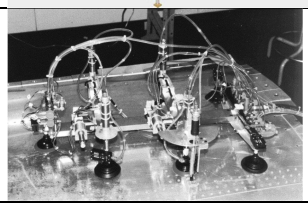	• Attachment on none-flat walls • Ability to reach difficult to access areas

Recently aero-structure manufactures have looked to relatively low cost off-the-shelf articulated robots to provide assembly automation similar to that which is commonplace in automotive manufacturing. However, since articulated robots typically have low accuracy and poor dynamics, for accurate assemblies they require external measurement system feedback. The high stiffness of parallel robots combined with external measurement systems could prove to be a flexible system for machining.

2.5.1.3. SpatialAnalyzer

While the LVM instruments and robots are the major hardware of a MAA system, software also plays a critical part in such a system, especially in the integration between the instruments and the robots.

SpatialAnalyzer (SA) is a widely used industrial standard commercial software platform that is used to control a large number of LVM instruments and sensors (Figure 23), including laser trackers, indoor GPS, portable CMM's, theodolites, laser scanners, and photogrammetry systems.

Figure 23 - Some of the metrology instruments supported by SA

One of the most important features of SA is that it provides a common interface for all of the supported instruments. This capability enables the sharing and switching of LVM equipment for a particular process without having to retrain operators. It is also uniquely capable of performing analysis on the measurement uncertainties, and fitting measurement results using the measurement uncertainties as weighting coefficients.

SA is also able to import CAD models in many other industry standard formats, as shown in Figure 24. A large number of complex analysis, alignment/transformation and reporting routines can be used on the CAD models and measurement results to perform operations such as comparing measurement to CAD nominal and GD&T checks. Measurements can be planned and plans simulated evaluated within the CAD environment.

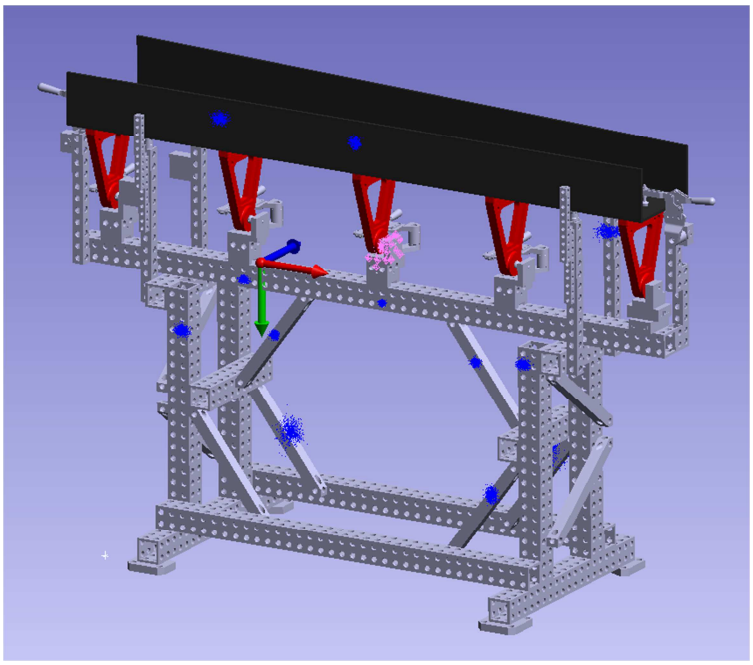

Figure 24 - Screenshot of SA showing Catia CAD Geometry fitted to photogrammetry measurements

SpatialAnalyzer's Measurement Planning (MP) scripting system allows much of the software routines to be automated, so that a complex procedure may be simplified to a single mouse click. The MP can be further enhanced using the SA Software Development Kit (SDK). The SA SDK enables advanced users to build MPs into custom user interfaces developed in main stream programming environments such as Microsoft Visual Studio.

2.5.2. Metrology Enabled Automation Examples in Aerospace Industry

While there are differences in the manufacturing technology requirements between the typical wind turbine blade and aircraft, the similarities in terms of product size and geometry leads one to believe that some technologies developed for the aerospace industry may be directly applicable to wind turbine blades production.

The commercial aircraft manufacturing industry is under ever increasing pressure to reduce the cost of assembly, arguably more so than any other industry with products of similar sizes. As a result, a large amount of research in aerospace metrology guided automation has been conducted. A number of them will be reviewed in this chapter.

2.5.2.1. The TI^2 System

The TI^2 robotic cell is a collaboration of three European automation companies. It is the result of the integration of three main systems: the

TR600 Tricept parallel kinematic robot produced by the Swedish company NEOS (Now Exechon), a Swiss Imetric photogrammetry camera, and Delmia based computer simulation software IGrip, developed by the Finnish company Tehdasmallit. It is believed to be the first photogrammetry based adaptive robotic production cell in the world, when it was delivered to Boeing's Long Beach facility in the USA for evaluation in 1996. [26, 27]

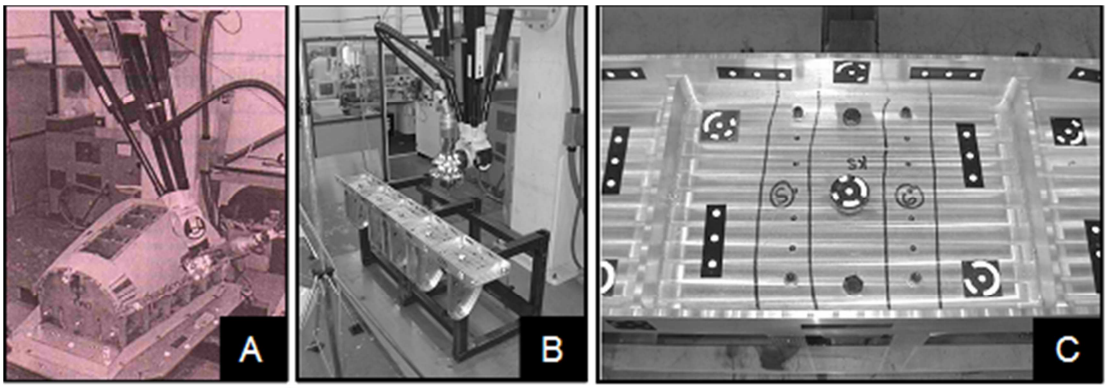

Figure 25 - The TI^2 system installed at University of Nottingham, UK. A) Drilling operation on a Lear 45 business jet forward fuselage [27]; B) Fixtureless test setup for wing rib and spar milling and drilling [28]; C) Holes drilled in spar, showing details of the photogrammetry targets [28].

In operation, two photogrammetry cameras take pictures of the targets on the work piece and the end-effector, which are used to calculate the spatial relationship between tool and the work piece. If the work piece is moved, the preloaded robot trajectory is automatically updated to take account of the deviation, thus the need for expensive specially made fixtures is avoided. [28]

The Tricept robot offers the typical benefits of a PKM, namely higher accuracy, repeatability, stiffness and flexibility, compared to typical serial robots and gantry robots. The accuracy of the TR600 is quoted at 0.20mm, while repeatablity is 0.02mm [26]. It is interesting to note that an evaluation by the University of Nottingham concluded that their system performed quite poorly, with errors of several millimeters. However, errors this large maybe due to problems in the system setup, especially the photogrammetry bundle adjustment.

The TI^2 system is currently used by Boeing and Airbus in production/production trials, enploying a variety of metrology systems as a flexible high precision machining system, the exact accuracy that is achieved by their systems is unfortunately confidential.

2.5.2.2. Kihlman Affordable Reconfigurable Tooling

Henrik Kihlman et al of Linköpings Universitet, Sweden are some of the leading researchers in the field of robotic drilling, metrology guided adaptive robotics and flexible tooling. [29]

The Affordable Reconfigurable Tooling (ART) concept developed by Kihlman et al. will be reviewed in this section. ART is an on-going research prototype system of the EU funded Automation for Drilling, Fastening, System Integration and Tooling (ADFAST) project. The goal of the ART is to replace all dedicated tooling with low cost, simple and flexible systems [32].

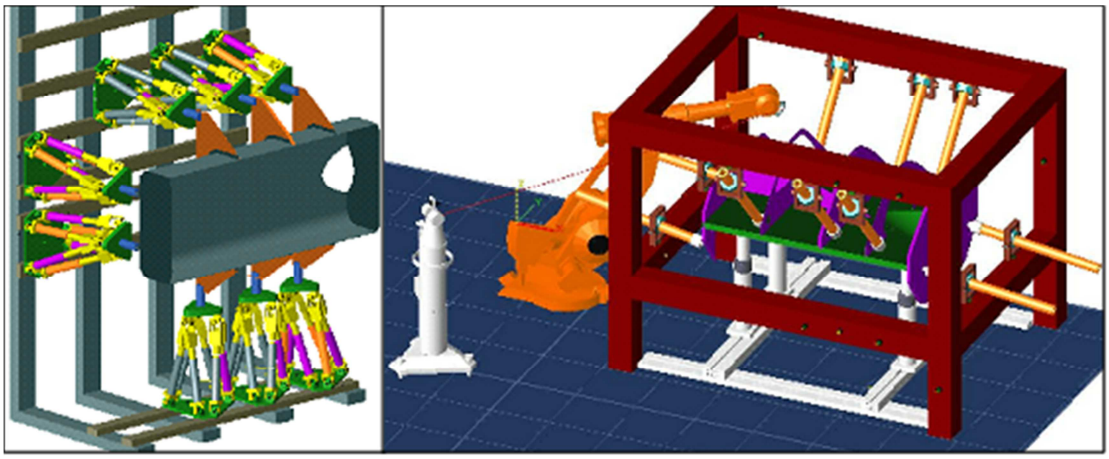

Figure 26 – ART concept designs [31]

Some of the earlier design concepts are shown in Figure 26. ART consists of a number of main modules: a reconfigurable static frame, a number of different Dynamic Modules (DM) mounted on the static frame (Figure 28), and metrology integrated robots (Figure 27 A) which are used to manipulate the DMs (Figure 27 B).

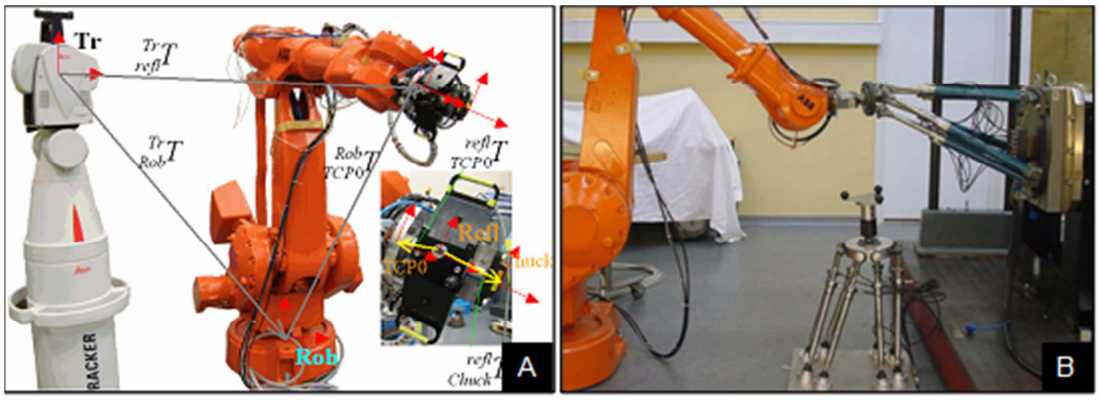

Figure 27 – A) ABB robot guided by a Leica tracker with 6DOF probe. B) Robot positioning of hexapod fixture. [30]

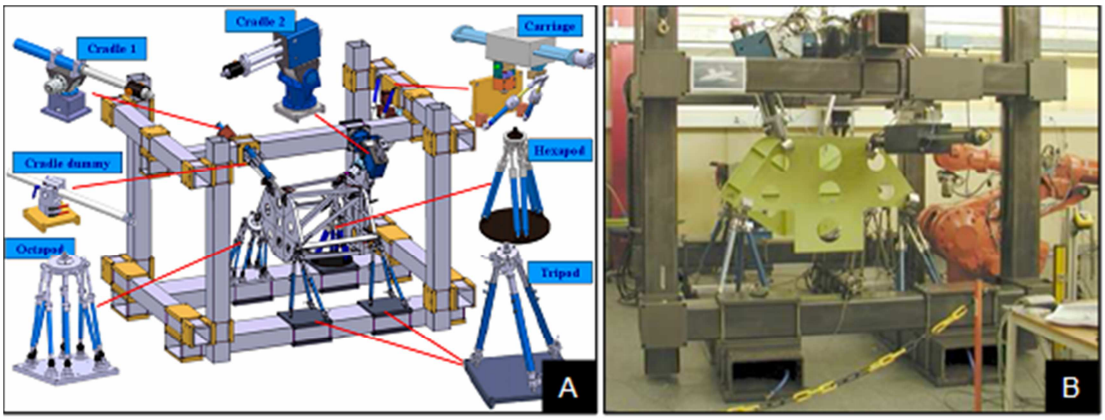

Figure 28 – The ART demonstrator at Linköpings Universitet. A) The dynamic modules in reconfigurable framework. B) Physical demonstrator. [32]

The Dynamic Modules themselves are entirely passive. When a modification to the tooling is required, the metrology guided robots are used to accurately position the modules automatically through off-line programming. The DM would then engage its hydro-mechanical locking mechanism and become rigid fixtures, at which point the robot undocks from the DM, and move to position the next one. The need for costly dedicated tooling and lengthy setup times is thereby eliminated. The results published by the group demonstrated that 50µm accuracy of the DM position can be achieved with a metrology guided robot, although some difficulties during undocking can move the DMs out of position slightly. [32, 33]

2.5.2.3. Robotic Stringer Positioning

A method of automatically aligning stringers on fuselage panels without fixtures was developed by Jayaweera et al of University of Nottingham.

In this automated assembly process, the stringer and the panel's starting positions are not precisely known. The mating part-to-part holes on the stringer are scanned with a non-contact laser scanner, as shown in Figure 29 B. The relative spatial relationships between the stringer, panel and robot are then computed using the least squares method. [34]

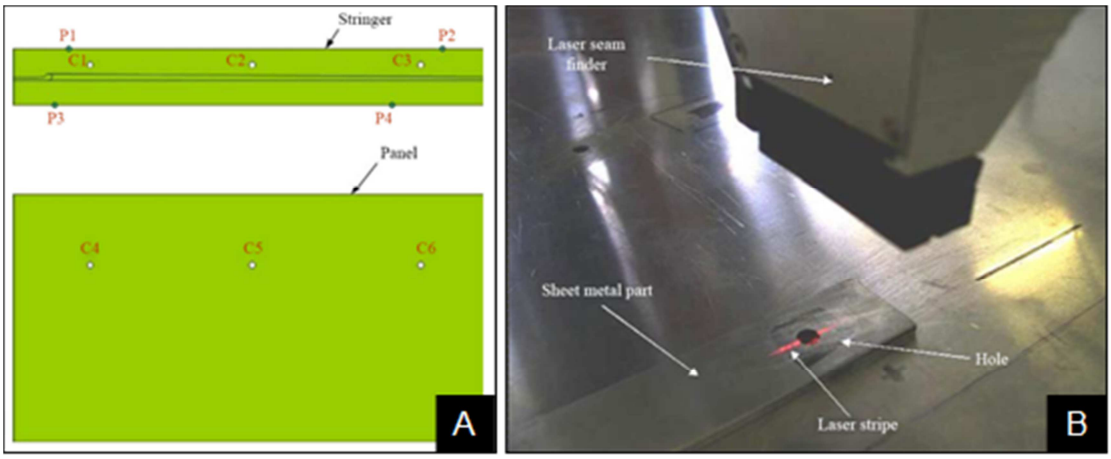

Figure 29 – A) Panel and stringer with pre-drilled holes to be aligned. [35] B) the holes are scanned with laser scanner mounted on the robot. [34]

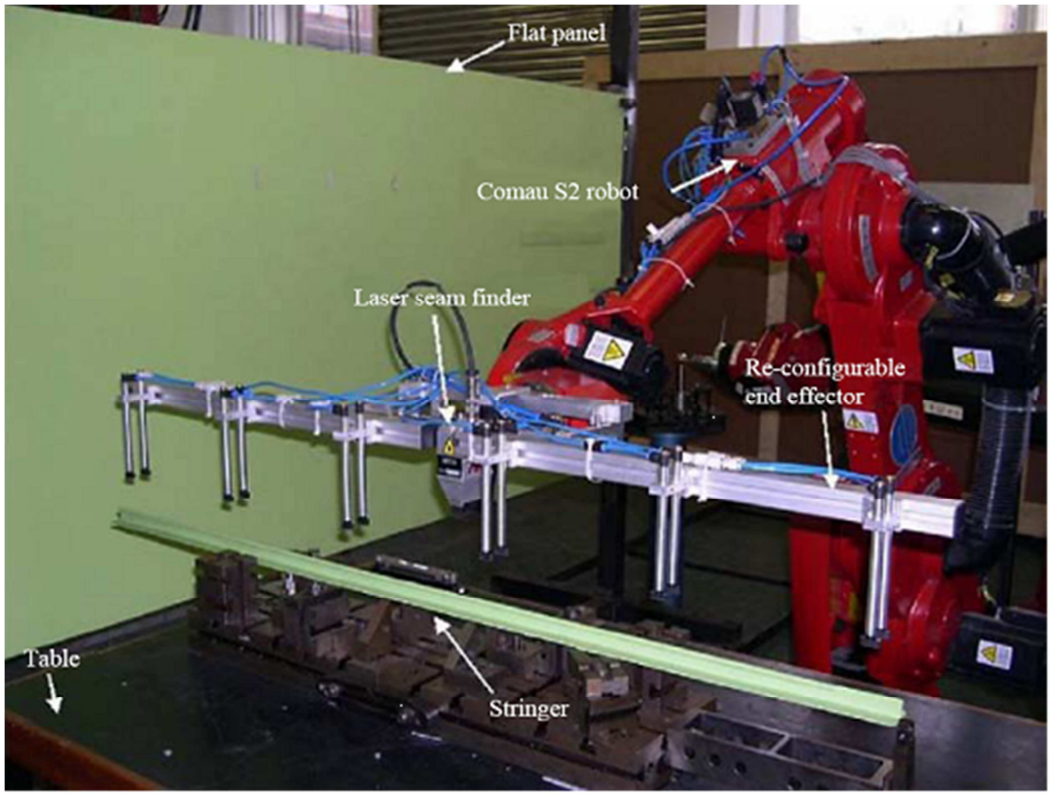

Figure 30 – Robot picks up the stringer and aligns it with panel. [36]

The robot moves to the updated pickup position and orientation (Figure 30). It picks up the stringer using its reconfigurable end-effector, and proceeds to scan the mating holes on the panel. The corrected drop-off position and orientation is then calculated, and robot moves to the corrected position and waits until the stringer is assembled.

The authors conclude that accuracy of this process can be on the order of 0.6mm, which is sufficiently below the tolerance of 1.6mm that is required. The most significant contributors of the errors are the robot repeatability and laser scanner accuracy.

2.5.2.4. Airbus Automated Wing Box Assembly/Demo Box

Airbus UK is responsible for the production of the wings of all Airbus aircraft. As a result of increased demand and market competition, investments were made to research automation methods to increase production rate, reduce production costs and improve product quality.

The major components of a typical airliner wing box are illustrated in Figure 31 A. The wing box is a very complex structure, requiring high manufacturing tolerances. Large amounts of research have been focused on automating the wing box assembly by reducing manual labour and expensive dedicated fixtures. As a part of this research, development and trials of the Automated Wing Box Assembly (AWBA) project has been conducted at Airbus UK's Broughton plant, partially funded by the Civil Aviation Research and Demonstration (CARAD) programme. [37]

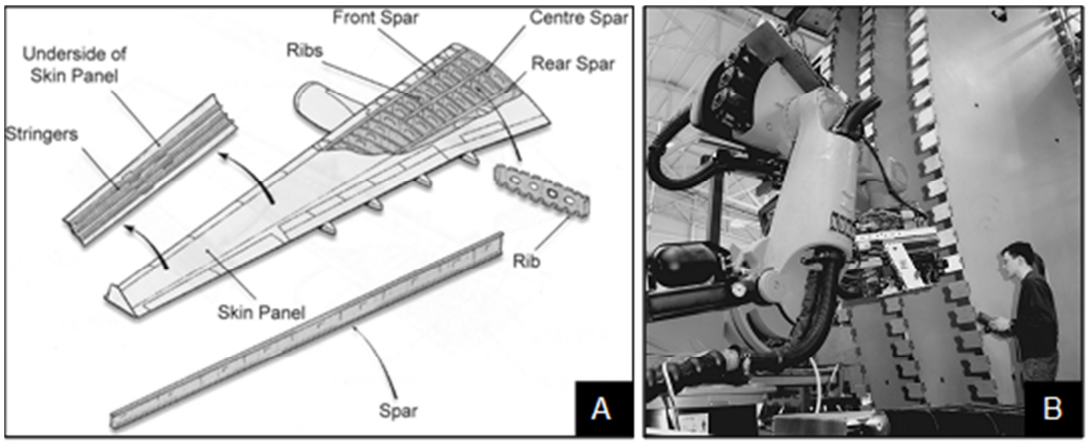

Figure 31 - A) Major components of a wing box. B) Automated Robotic drilling of rib feet. [37]

A series of AWBA trials were carried out to experiment concepts such as adaptive robotic control through metrology, robotic drilling (Figure 31 B) and machining, and auto-riveting.

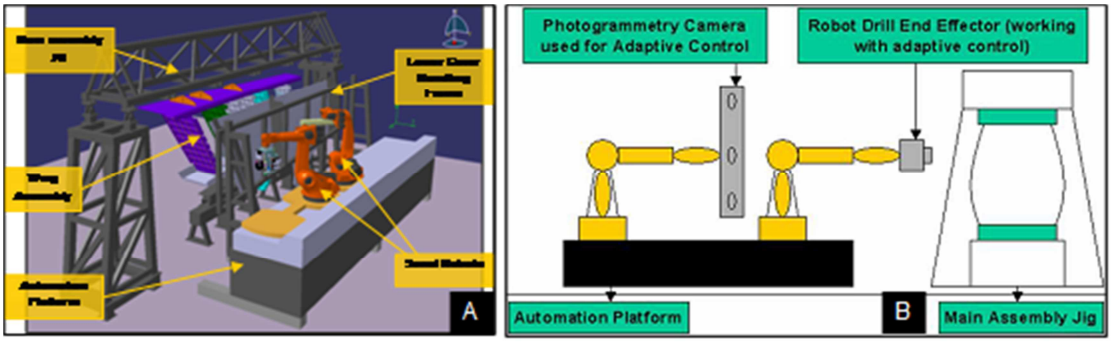

Figure 32 - Airbus A350 Demo Box concept. A) The hardware. [38] B) Metrology for adaptive control. [39]

Developed from the AWBA experience, the A350 Demo Box (DB) (Figure 32 A) was constructed to demonstrate the feasibility of amongst other things,

the ability of metrology guided robots to perform rib feet fettling and predictive shimming operations. The DB uses two robots, one carrying the end effector, the other carrying a Krypton photogrammetric camera, which provides 6 DOF position updates to the working robot. The camera is mounted on a robot in order to increase line of sight coverage in difficult robot poses. The rib feet are scanned with a laser scanner mounted on the working robot, or a separate laser radar. If a rib foot is too high, a milling path for the working robot is generated, and the robot fettles it to the correct height; if a rib foot is too short, a correctly sized shim is produced based on the scanned data. [39]

2.5.2.5. Metrology assisted production of A380 wing box struts [47]

Using a V-STARS photogrammetry system (Figure 34 C), the process of measuring the required lengths of the 143 wing box struts at Airbus Nantes was reduced from 8 hours for two operators to 1 hour 20 minutes for a single operator.

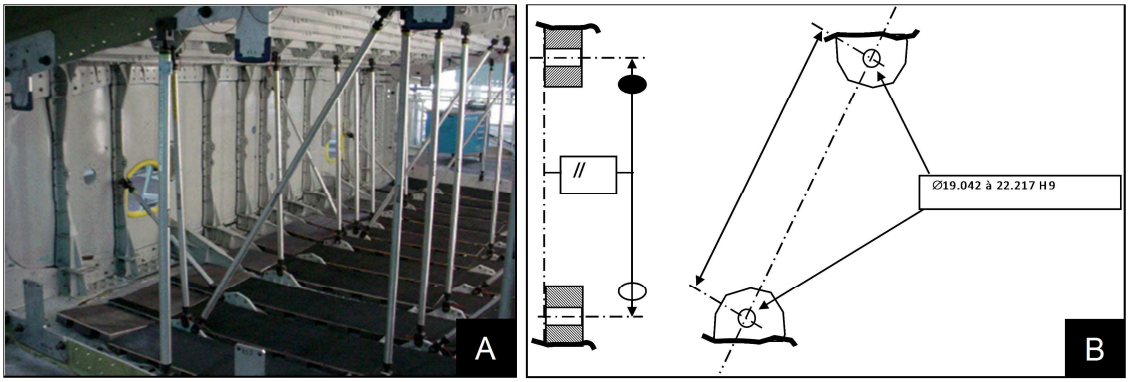

Figure 33 - A) Temporary tooling struts. B) Design specifications [47]

The A380 wing box is supported by 143 carbon fibre struts. As shown in Figure 33 A, the wing box is supported by tooling struts during construction. The carbon struts are manufactured to the lengths measured between the mounting holes, as illustrated in Figure 33 B. The 143 distances were formerly measured using specifically designed callipers one-by-one, necessitating the removal and reinstallation of the tooling struts.

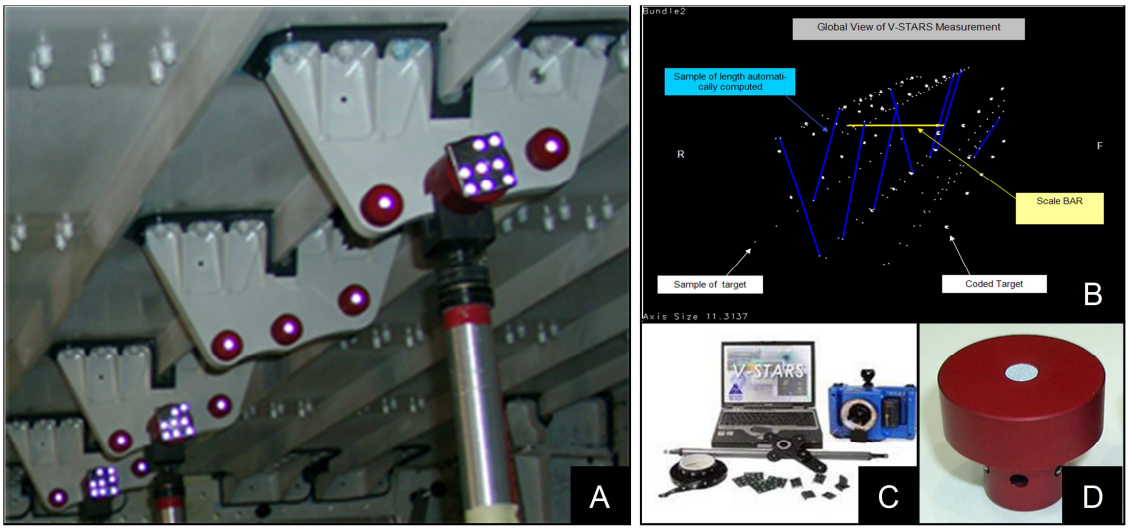

Figure 34 - A) Reflectors mounted in holes. B) Results from 50 pictures. C) The V-STARS system. D) Specially designed kinematic reflectors [47]

A new photogrammetry system was introduced, measuring a number of kinematically mounted reflector inserts (Figure 34 D), and specific reflectors that mount on top of tooling strut mountings. The operator then takes a series of 50 pictures using the photogrammetry camera, and the images are sent to a computer to be automatically processed to compute the length of the tooling struts (Figure 34 B). The installation and removal of the photogrammetry targets takes 30 minutes separately. The measured result is sent to production, where the carbon fibre struts are produced to fit the specific wing box. In trial runs, the length measurements from photogrammetry matched those from laser tracker measurement to within ±10μm.

2.6. Knowledge Gaps and Research Priorities

From the literature review, it is clear that all the major components for metrology assisted assembly are already in place. Both from the metrology instrument side and the tooling side. The key research priority should be the method of integration between the two. A number of state of the art integration examples with varying degrees of success have be described in subsection 2.5.2.

Traditionally, the measurement and tooling are separate fields handled by specialized personnel. In a future factory in which metrology will be highly integrated with tooling, the people designing such a factory must have intimate knowledge in both fields. The first part of this thesis will therefore study the value of integration automate LVM.

What are also vitally missing in the current state of the knowledge are clear quantitative theoretical analysis and experimental results that demonstrate the possible performance of MAA systems. Therefore the mathematical

modelling of MAA and the development and capability assessment of a demonstration system should be the major parts of this thesis.

3. Large Volume Metrology Data Processing Evaluation and Automation in Manufacturing

3.1. Introduction

While having metrology fully integrated into the production process is the ultimate goal, as shown in the literature and state of the art, a fully metrology assisted assembly system is complex and often has to be designed from the conception of the product, which does not solve many of the existing issues manufacturers have with metrology integration that have been highlighted during onsite visits.

This chapter describes a number of projects and case studies carried out to demonstrate the value of automating metrology and data processing in solving near to medium term issues in production.

The capabilities of modern LVM instruments have increased very quickly over the past decades, in order to get the most out of the instruments and measurement results, highly trained operators are required. There is a great deal of value in attempting to automate many of the difficult measurement processes and data processing so that unskilled operators can be quickly trained to use the systems, reducing cost, potential errors and process time.

While the instruments are already capable of meeting the manufacturers' requirements, for many people there exists a gap between having the instruments and knowing how to have the instruments produce the specific results they are after. The difficulty often lies in data processing.

Processing and understanding the measurement results is usually the most challenging and time consuming part of a measurement job. What are required are software algorithms that can automatically process the data and provide the operator the key information he/she requires in an easy to understand manner.

The manufacturers typically want to treat measurement systems as a “black box” that indicates the quality of their product, without having to have a deep understanding of their inner workings (Figure 35). The task of this “black box” is typically filled by skilled metrologists who select the instrument, perform the measurement and process the data. It is foreseeable that these types of time consuming and expensive manual processes will increasingly be replaced by automation, using a combination of existing off-the-shelf software packages and specialized software developed for specific tasks.

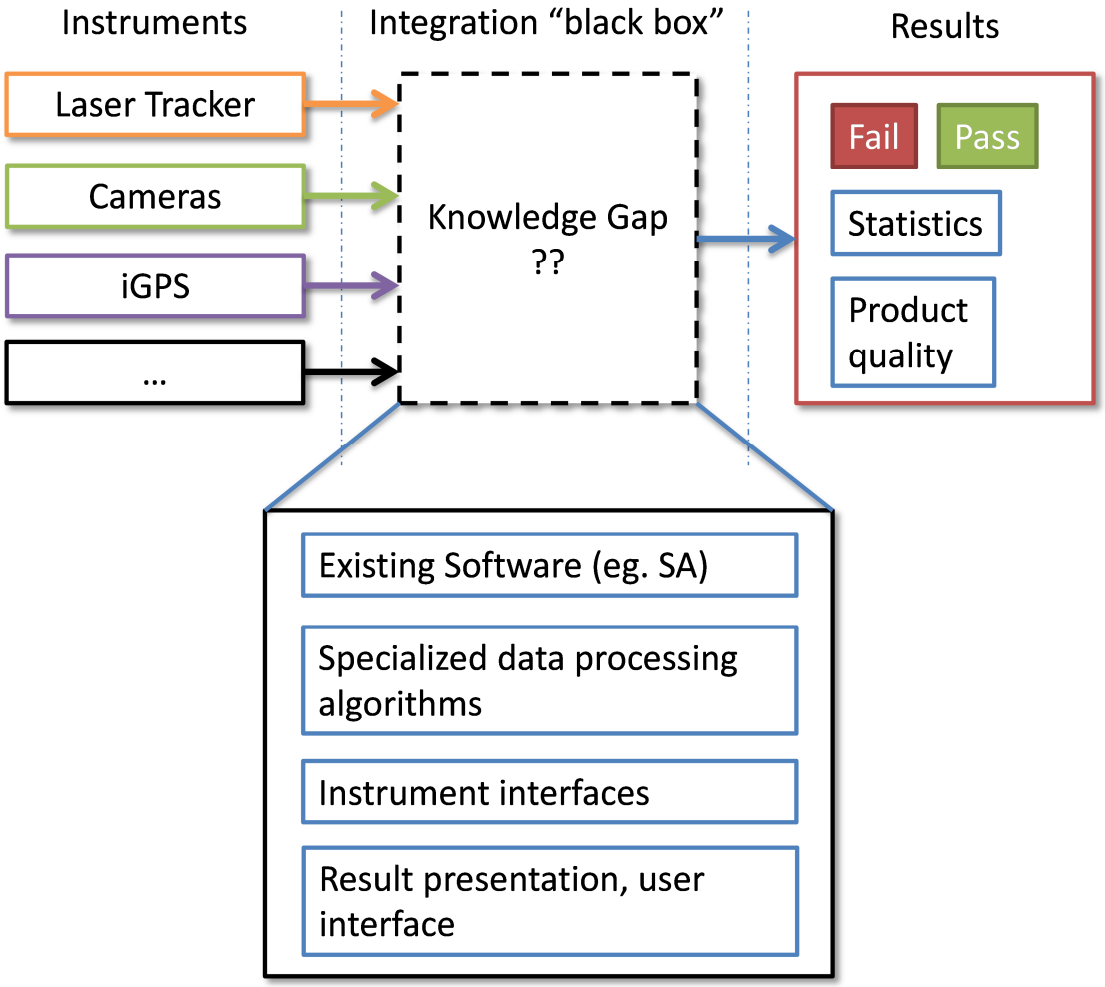

Figure 35 - The knowledge gap between measurement instruments and the results manufacturers want them to produce

Three of the metrology automation projects involving the development of bespoke software to automate data processing are described in this chapter. The first two projects involve automation of data processing and evaluation, and are completed by the author. The third one is a large scale project involving multiple people within the research group at University of Bath and at Airbus. The development of the data processing software and process simulations is done by the author, and is described in this thesis.

3.2. LVM Data Processing and Evaluation

3.2.1. Automated Positioning Repeatability Measurement of Industrial Robot

3.2.1.1. Introduction

In support of the Airbus Advanced Low-Cost Aircraft Structures (ALCAS) project, the purpose of this study is to determine the single point repeatability of a KUKA KR240 robot.

Studying the repeatability of a robot requires many thousands of measurements and generates a large amount of data which is not easy to process in existing software such as SpatialAnalyzer or Microsoft Excel. This is a good example of typical measurement problem where the data the instruments provide, i.e. the position of points, does not directly result in the key performance parameters required, which is the repeatability of the robot. Substantial processing and analysis algorithms have to be developed to solve this specific problem.

SpatialAnalyzer was used to automate the data gathering, and a MatLab script was used to automatically import and analyse the measurement results.

3.2.1.2. Experimental Procedure

The equipment and experimental setup is shown in Figure 36. The data gathering process is fully automatic, using the SA “stable point” function.

1. The Tool Centre Point (TCP) was calibrated using the laser tracker, using the centre of the Spherical Mirror Reflector (SMR) directly as the centre point of the tool
2. The KR240 robotic arm was guided through a grid of 30 points (5x3x2), each roughly 500mm apart, utilizing a series of linear moves. The layout of the points is illustrated in Figure 38.
3. At each point, the arm dwells for 6 seconds, enough time for the arm to settle and for SpatialAnalyzer (SA) software to automatically take a stable measurement averaged over 4 seconds.
4. The process is repeated over a two hour period, each complete run through 30 points took approximately 4 minutes 25 seconds, yielding 27 trials.

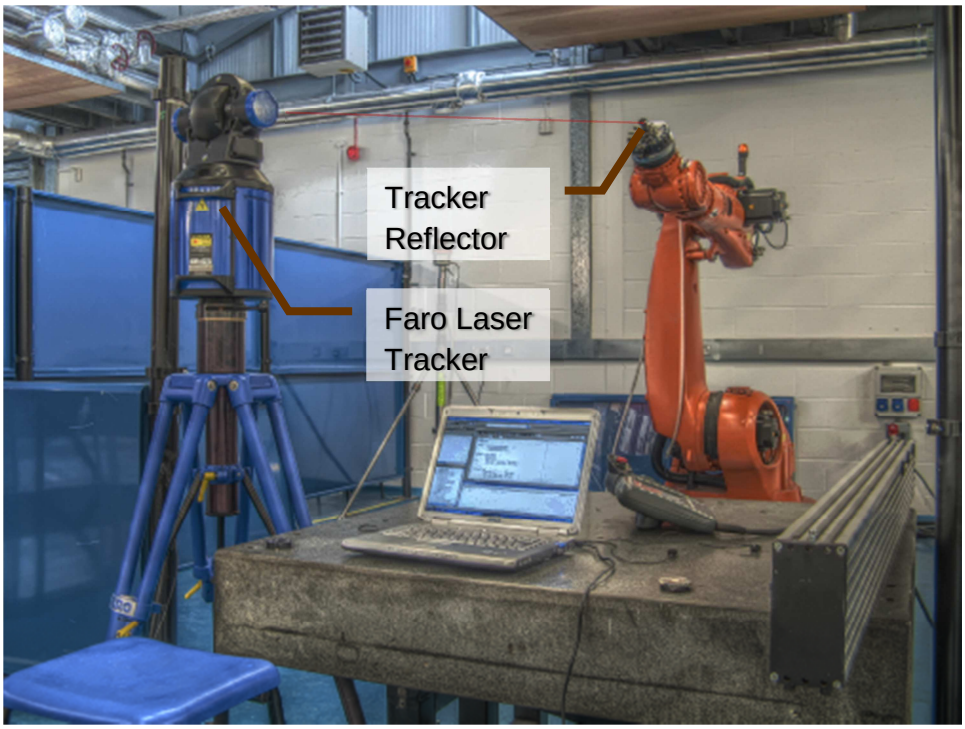

Figure 36 - Experiment setup

3.2.1.3. Automated Data Processing

The flowchart of the processing steps is shown in Figure 37.

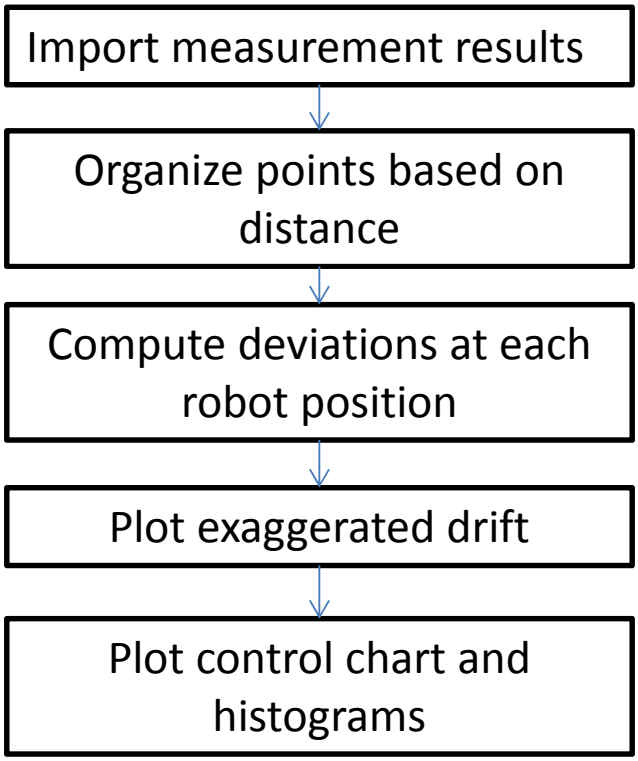

Figure 37 - High-level flowchart of the data processing MatLab script

The measurement result output from SA is a long series of 810 point coordinates. In order for the results to be meaningful, they need to be organized into groups representing the trials of each of the 30 positions. The automated processing MatLab script takes advantage of the fact that the distances between the stable robot positions are much larger than the robot repeatability to group points based on their distance to the first set of results. The grouped sets can then be processed to show drift over time.

3.2.1.4. Results and Analysis

The collected data for each of the 30 points is plotted in Figure 38, with the drift over time from the first set of measurement exaggerated 2000 times for ease of visualization. Rather than a random scatter, the general trends of the drift are clearly discernible. Qualitatively, major direction of the drift seems to be away from the robot.

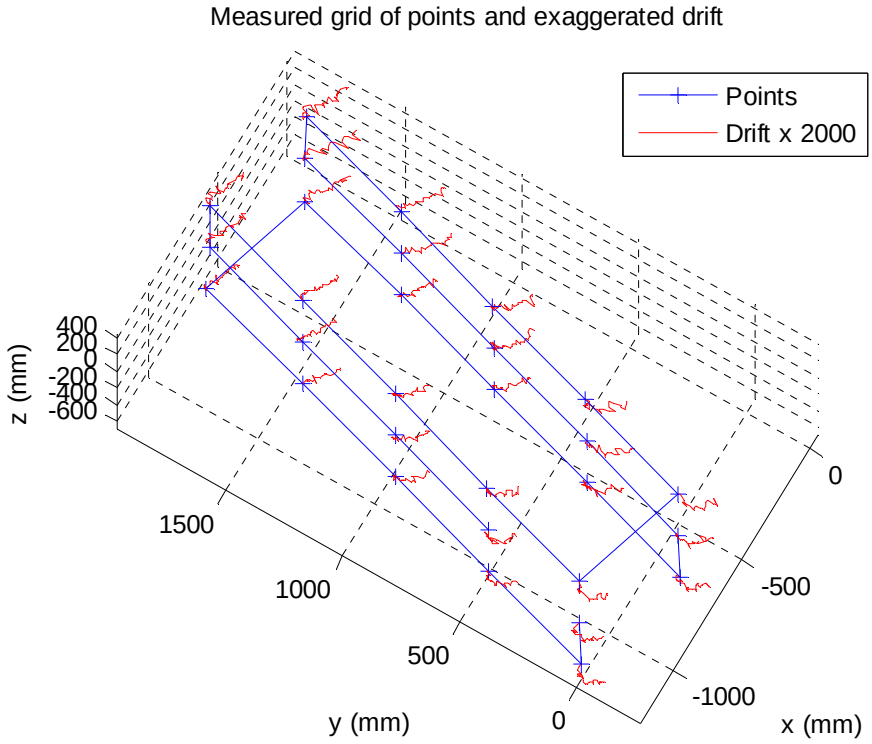

Figure 38 – Graphical view of measured points in tracker, robot trajectory and exaggerated drift

While there appears to be some general trends, the drift paths of the points are not parallel. The points further away in y-axis, being more or less directly in front of the robot, tend to drift more directly away from the robot, perhaps as due to the motors heating the arm over time, producing thermal expansion of the arm linkages. On the other hand, the points positioned close to the origin of the y-axis, being near to the edge of the robots movement envelope, have more complex drift paths, perhaps as the result of the more complex kinematics required to reach such positions.

Figure 39 is a control chart showing the x, y and z-axis drift of the 30 measured points (different coloured lines) across 27 trial runs. The largest drift over two hours is in x, 0.11mm. While this is below the manufacturer specs of ±0.12mm it is unclear whether the drifting trend will continue if the experiment was carried out over a longer period.

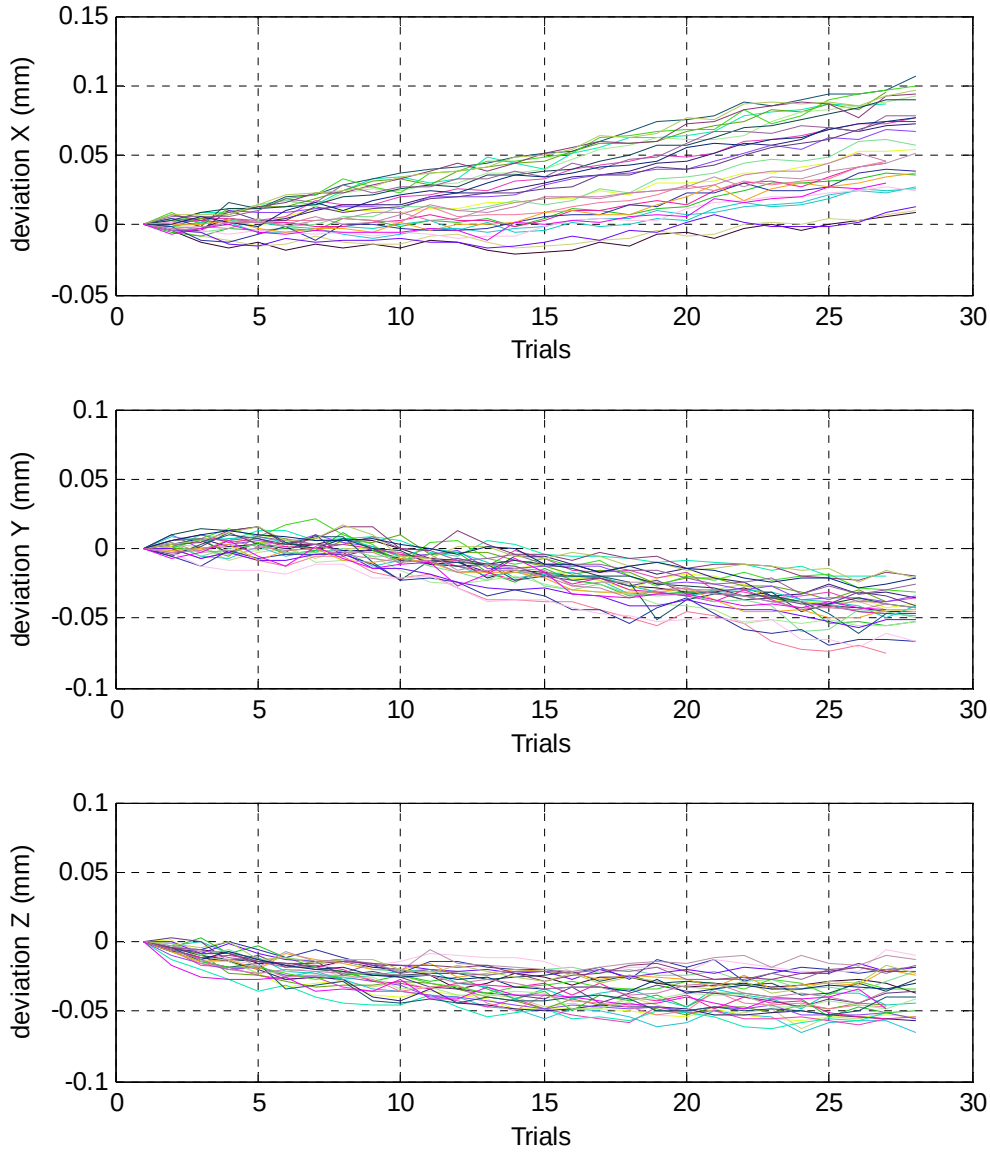

Figure 39 - Control chart of X, Y and Z drift over trial number

Measurement uncertainties and possible sources of error:

- Some part of the drift may have been caused by the SMR mount, which was fixed on the robot with thin double sided tape.

- The Faro laser tracker has a Maximum Permissible Error (MPE) of 10 – 15µm in ADM mode over the measurement range of 0.5 – 4.0m.
- Some of the points are measured with the laser hitting the SMR at very large angles.

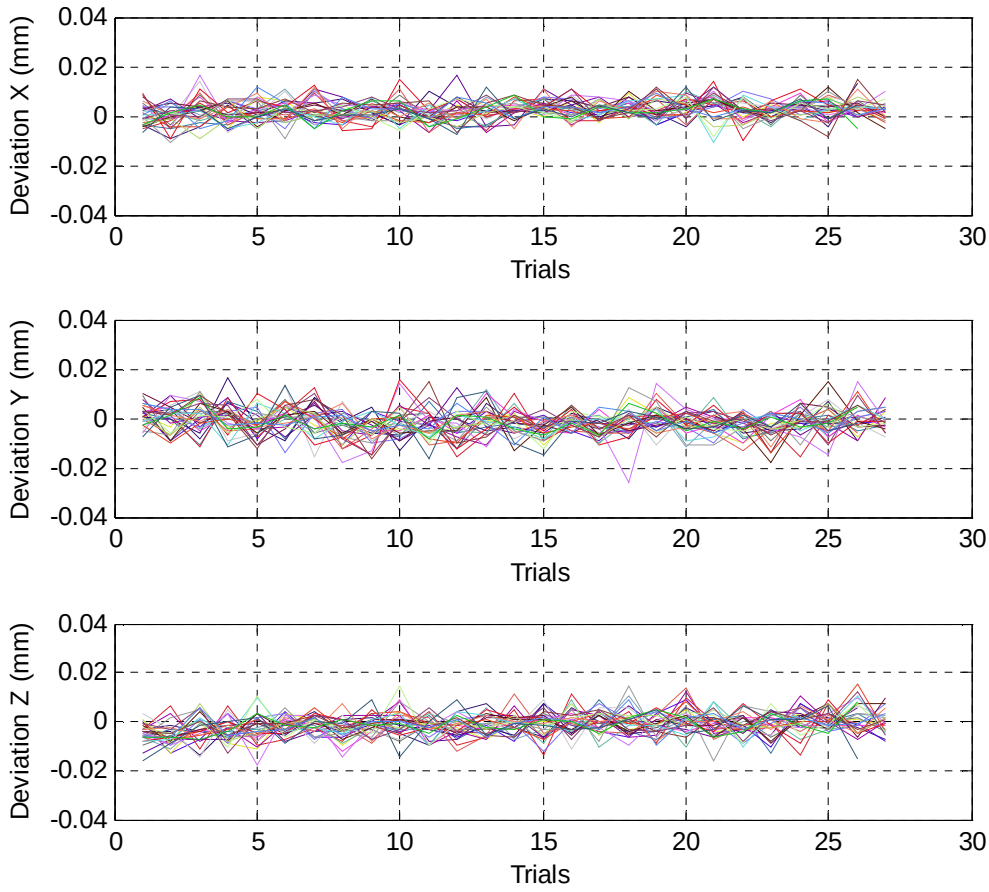

Figure 40 - Single point deviation between trials

The ALCAS project proposes to use the KR240 guided by a photogrammetry system for initial position to an accurately known point, which is then used as a basis for the subsequent fettling operations, relying on the robot repeatability alone. It is therefore interesting and more relevant to determine the short term repeatability of the robot.

Instead of the drift over the trials, the deviation of each point from its previous measurement is plotted in Figure 40. Given that each trial run took 4:25, the plot represents the repeatability of the robot over this time period.

The robot appears to perform very well over this shorter period. The majority of the data is within ±15µm. Since this is on the same order as the uncertainty of the laser tracker, the actual repeatability may be much better.

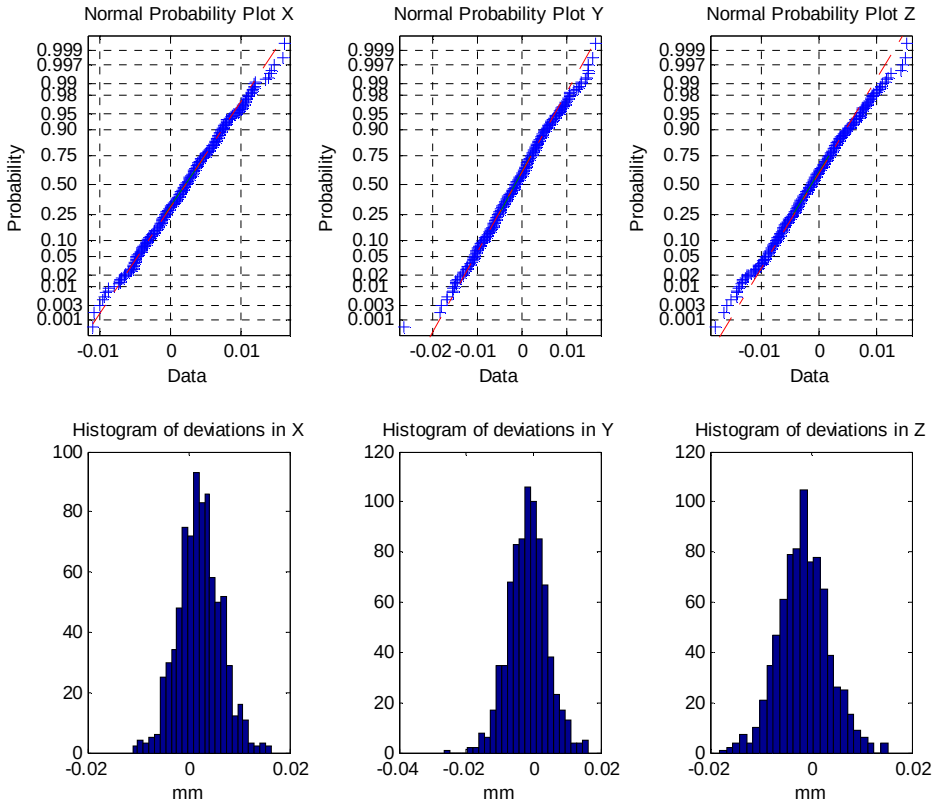

Figure 41 - Distribution of single point deviations between trials and normality test

Combining the single point deviation data from the 30 points, histograms were generated and normality test was performed on the data (Figure 41). The distributions appear to be fairly Gaussian, slightly skewed at the tails. The standard deviations of the distributions are:

X = 0.004258mm, Y = 0.005665mm, Z = 0.005005mm

At a coverage factor of 2, the short term repeatability of the KR240 is likely to be on the order of 10μm.

3.2.1.5. Conclusions

In conclusion, this study has determined that:

- The robot drift has dominant direction.
- Drift over 2 hours is 0.11μm, within KUKA specifications.
- Short term repeatability is very good, ±10μm within 4 minutes 25 seconds.

Using the software developed in this study, the point repeatability of any robot or positioning system can be quickly analysed, over any arbitrary working volume. While the algorithm not particularly complex, it performs a crucial role that cannot be easily done using commercial software. This is a

good demonstration of how even simple data processing and visualization scripts can provide value and meaning to the measurement data. The skills required to produce such scripts will be essential to metrologists as measurement becomes more and more automated and integrated.

The software in its current state requires the operator to have some familiarity with MatLab, however it can be easily made into a standalone software with an easy to use interface if required.

3.2.2. Vestas Modular Blade Flushness Measurements

3.2.2.1. Introduction

Another more complex example of measurement data processing and evaluation using bespoke algorithms is described in this section, focusing on the processing of a large amount of point cloud data and extracting the key information.

In support of the Vestas modular blade project, measurements were carried out to determine the flushness of the glue joints after the leading edge (LE) and trailing edge (TE) are assembled to the spar. The flushness tolerance necessary to meet aerodynamics performance targets is ±200μm.

It was determined that the only instrument suitable for assessing the flushness conditions and is readily available for use was the Faro CMM arm with a laser scanner attachment. However, the Faro arm with the scanner produces large amounts of data (many millions of points, 200MB per scan, 22 scans total) and it does not provide any indication of flushness directly. Therefore a MatLab software algorithm was developed to semi automatically process the scan data and convert them into plots of flushness against distance along the glue joint.

3.2.2.2. Project Details

Figure 42 - 2m prototype blade in assembly jig

The jig used to assemble the 2 metre prototype blades is shown in Figure 42. During an assembly, the LE and TE parts are loaded into the holders, a robot applies adhesive to the LE, TE and spar joints, and the TE and LE holders are then pivoted to complete the assembly.

There are four joints in total, consisting of the spar joints with the LE and TE parts for the windward (WW) and leeward (LW) sides. Figure 43 is a cross-section view of the blade, illustrating the shapes of the joints.

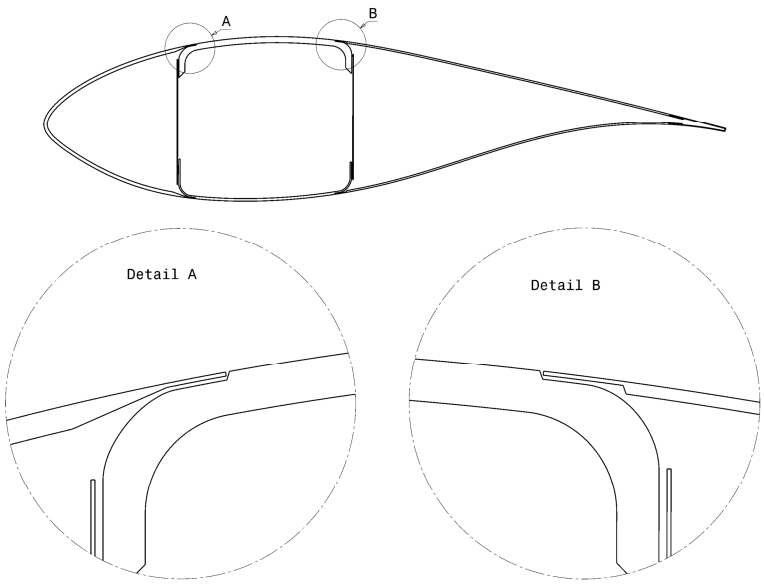

Figure 43 - Cross-section view of the component interfaces

A suction and locator system is designed to hold the edges of the LE and TE flush with the spar. Measurements of the assembled blade prototypes are carried out to establish the quality of the glue joints, and determine if this system is performing as designed.

Figure 44 - Typical glue joint

Figure 44 is a picture of one glue joint. There are a number of measurement challenges due to the size of the blade, the material, and the required accuracy. Because of the need to directly measure surface small details, and the large number of measurements required, instruments typically used for large volume measurements such as the laser tracker cannot be used. Instead, a Faro CMM arm with a laser scanner attachment was chosen as the best option.

Test scans at University of Bath using the Faro arm showed that due to the translucent nature of the fibreglass material, if it is scanned without painting the surface, very large errors can result. This is caused by sub-surface scattering, when the scanner camera picking up light scattered from under the actual surface. Therefore it is necessary to paint the surface before scanning.

Test scans of a reference part have also been conducted to determine the measurement uncertainty of the instrument and the software process used, it was found to be around 25-30μm, by measuring a reference part.

3.2.2.3. Measurement Procedure

Figure 45 (A) shows the setup of the measurement:

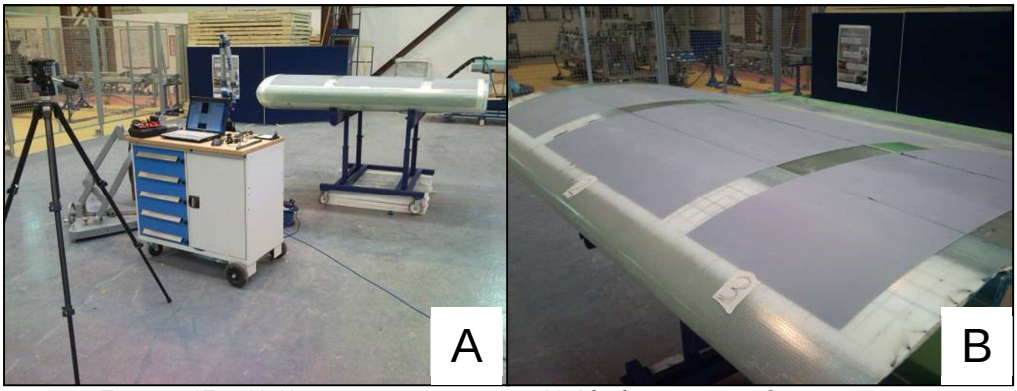

Figure 45 – A) Measurement setup, B) Blade section after painting

1. The blade sections are placed horizontally on stands, with the WW side up.
2. Protection tape is trimmed off from the glue joints, along with any large pieces of excess glue.
3. The blade sections are divided into three easily reachable parts, and are painted using a matte paint primer.
4. The Faro arm is assembled and calibrated
5. The parts are scanned using the arm and Polyworks software

3.2.2.4. Automated Data Analysis

The raw point cloud data is exported from Polyworks, and loaded into Catia (Figure 46). Two points defining a line along the centre of the glue joint, and another point on the point cloud are selected manually in Catia. The manually chosen points together with the data cloud are sent to a custom MatLab program, which then automatically determines the flushness.

In the MatLab program, the three manually chosen points are used to define a coordinate system, from which planes normal to the glue joint centre line (CL) can be created using vector cross product. These planes, created along the CL 20mm apart from each other, are used to slice the point cloud data into 20mm wide strips (Figure 47).

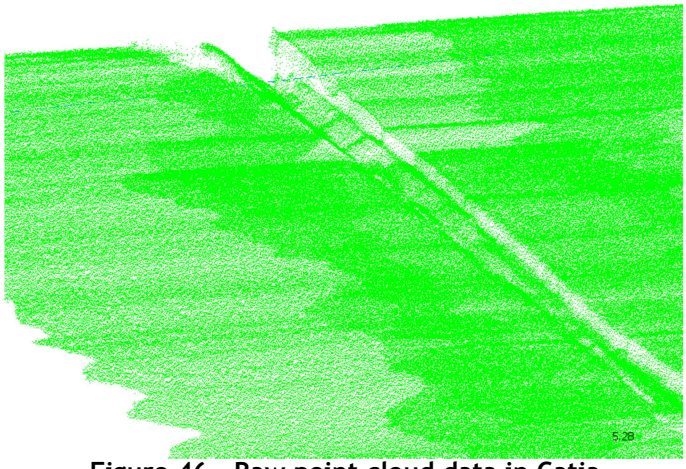
Figure 46 - Raw point cloud data in Catia

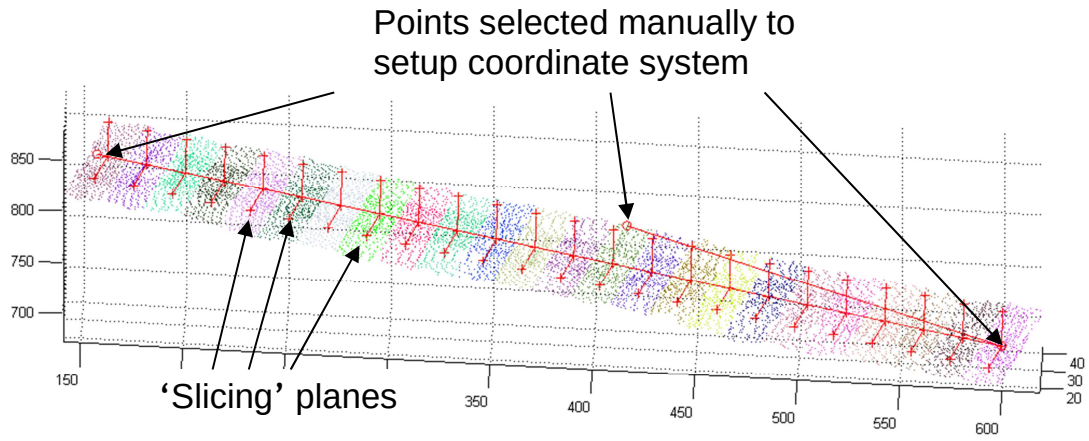

Figure 47 - Coordinate system definition and slicing of data

Each strip is then projected into its corresponding slicing plane, the result of which is a two dimensional plot of a cross-sectional view of the strip, which can be seen in Figure 48. The data very close and very far away from the centre of the joint is typically not very useful, so only points between 4mm and 25mm away from the CL (shown in blue in Figure 48) are used in the final flushness calculation.

Two straight lines are fitted to the data on either side of the CL. The varied natures of the data lead to the usage of a non-linear robust least squares fitting method, to reduce the influence of occasional outliers caused by spurious reflection.

Finally the x=0 values of the two line equations are subtracted from each other to determine the flushness.

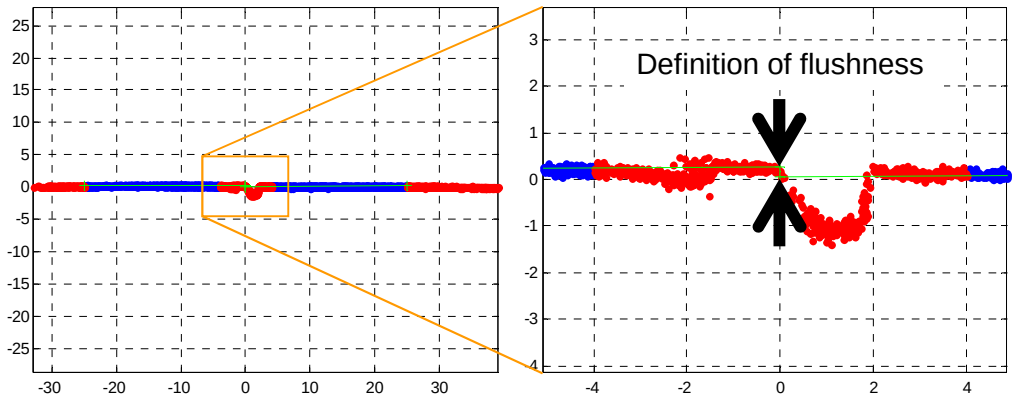

Figure 48 - An example 'strip' projected in the slicing plane, and determination of flushness using robust least squares fitted lines. Only blue points are used in the computations.

3.2.2.5. Measurement Results

Positive and negative flush are defined as shown in Figure 49. Positive flush is when the spar is higher than the LE or TE surface, and negative flush in when the spar is lower than the LE or TW surface.

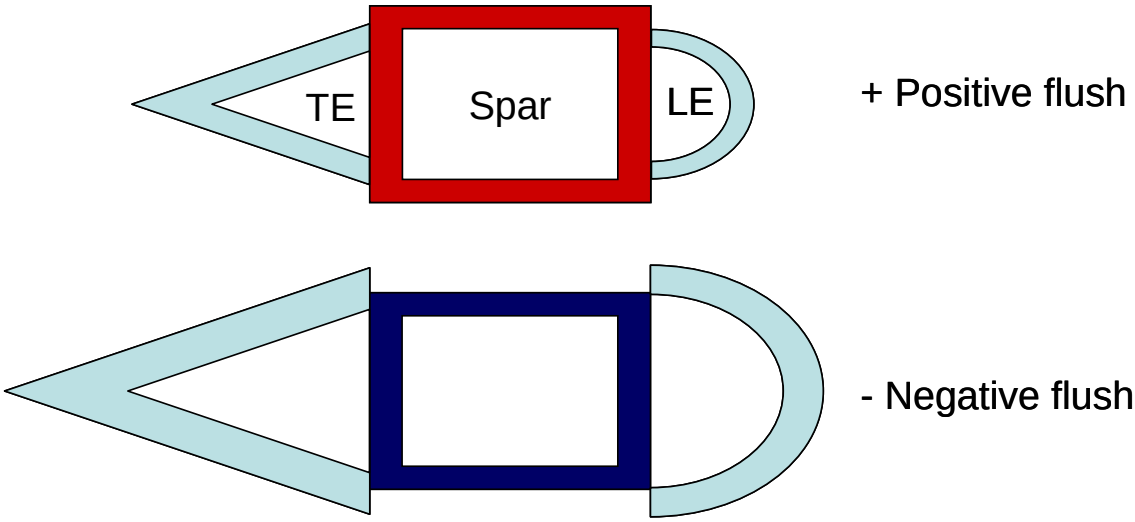

Figure 49 - Definition of positive and negative flushness

6 sections were scanned and processed in total. Sections 1 – 4 were assembled with tapes on the interfaces, so that they could be disassembled after measurements. The tape has in some cases led to glue joints becoming unstuck, resulting in very large steps. These cases were not included in the measurements, thus some parts of the blade section 1 – 4 were not measured.

Example of the flushness results output from the MatLab code for blade section 1 are plotted in Figure 50 to Figure 51. The results are plotted against the approximate distance along the blade sections, starting from the blade root direction. It can be seen that the step conditions are significantly larger than the design specifications. Keep in mind the measurement uncertainty for the instrument and software process is around 25-30µm, as mentioned in the project details.

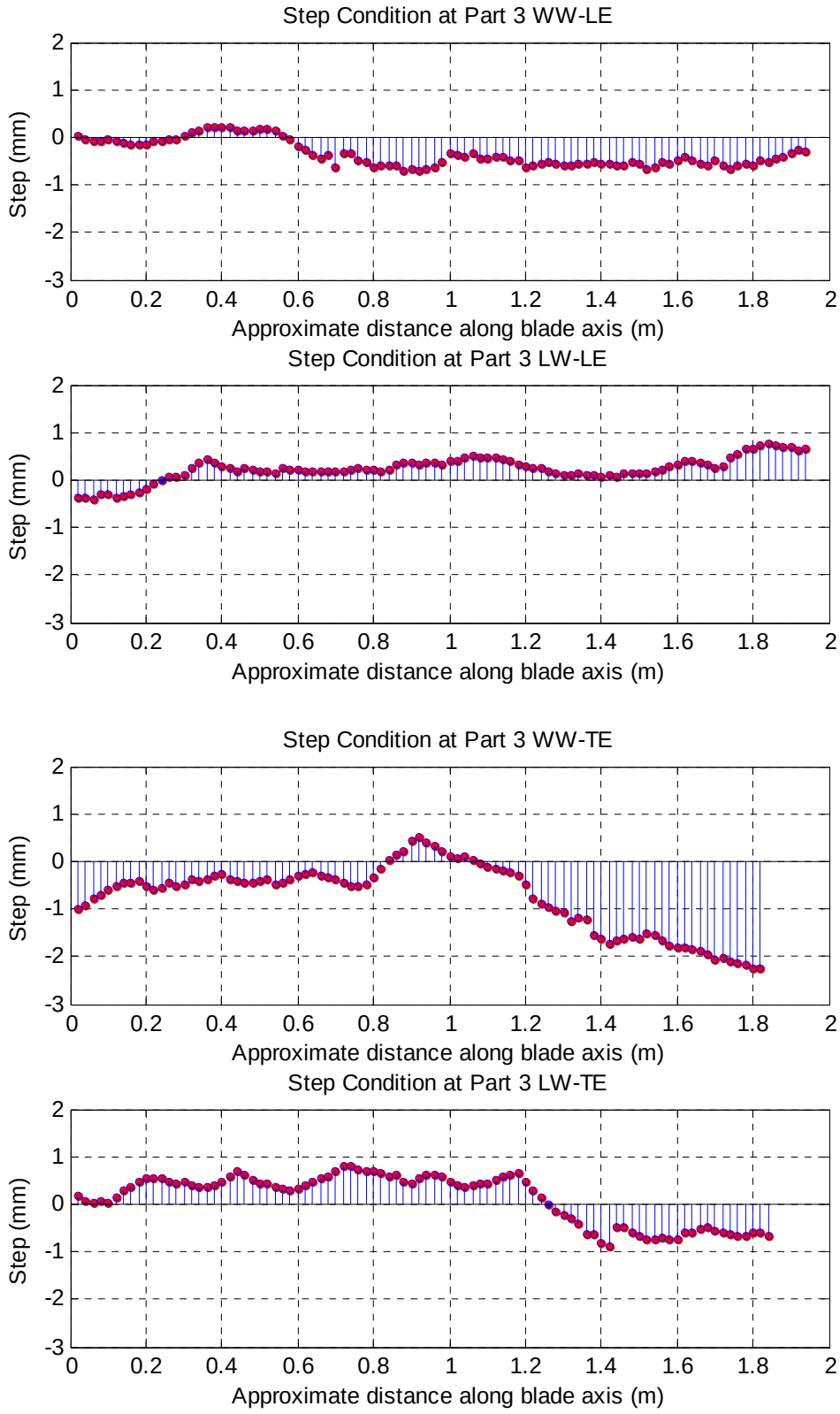

Figure 50 - Results for blade 1

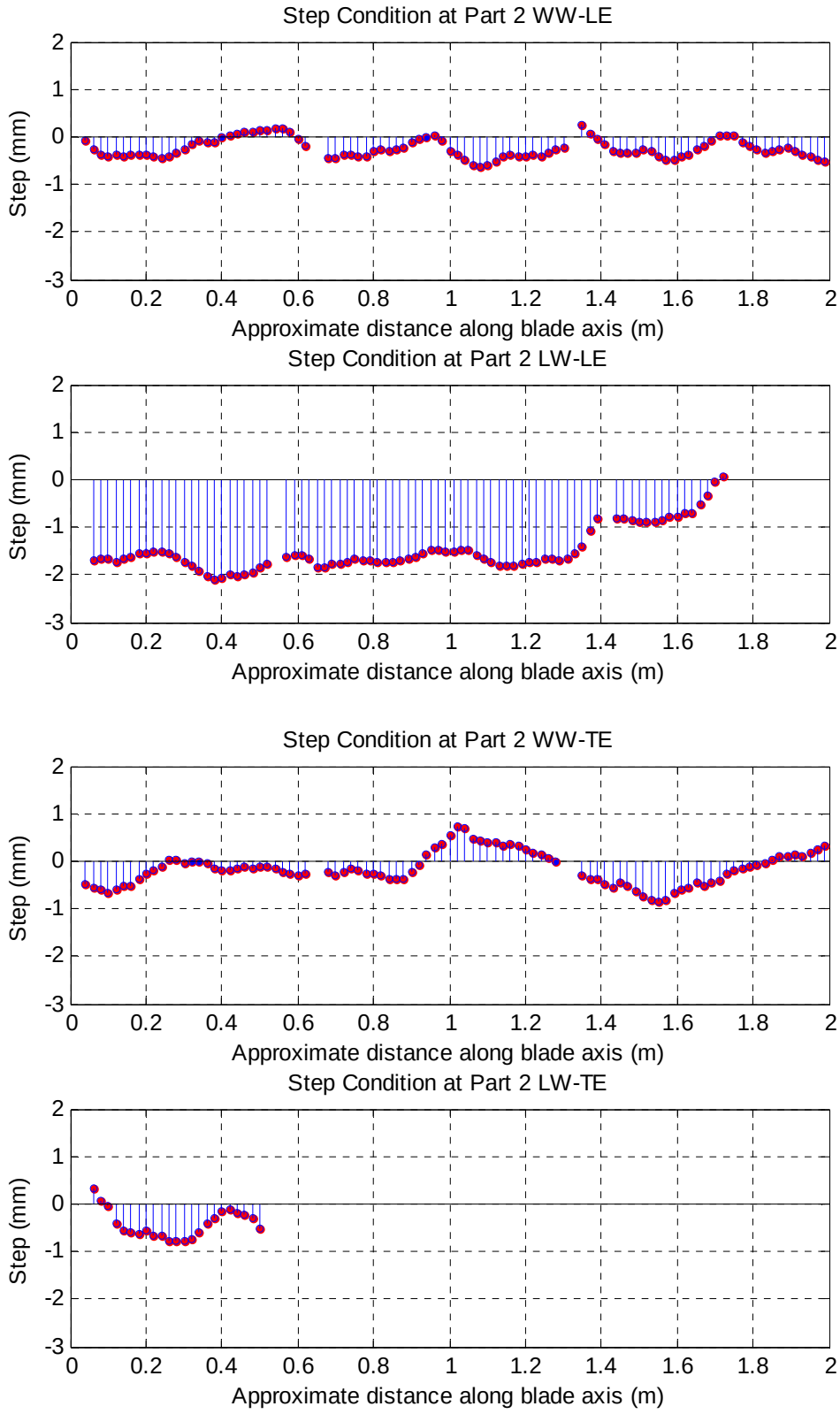

Figure 51 - Results for blade 2

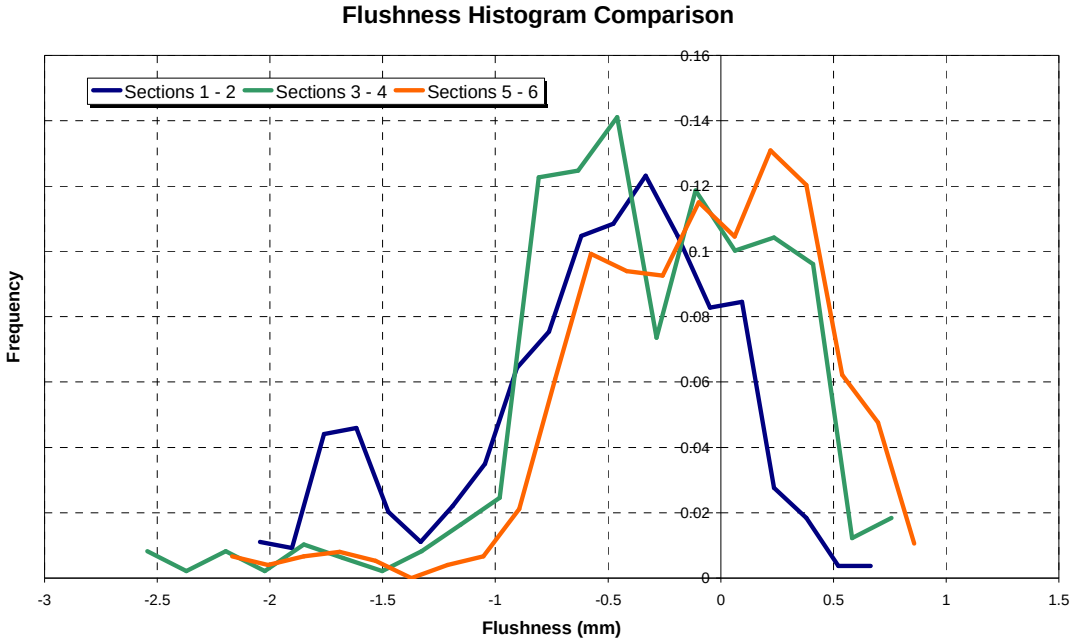

Figure 52 - Histogram of all flushness measurements

Figure 52 is a histogram summarizing all of the flushness measurements. It would appear that the bias towards negative flushness was gradually removed throughout the three assemblies.

3.2.2.6. Conclusions

The scan data processing software successfully processed all 22 scans, the results proved to be very reliable. Since this was a one-off project, the software still required some manual input, thus was not fully automatic. It was able to quickly extract key features from scan data and plot the results in a form that is easily understood by the manufacturing engineers, previously not possible using existing software. The software can also be used to analyse any scan data in general for flushness.

The measurement results show that the assembly process trialled was not able to meet the original tolerance requirements.

1. Some of the glue has de-bonded from the protective tape for sections 1 - 4, therefore no data was available. This could have been caused by the pressure from the stands the sections were resting on pressing directly on the glue joint.
2. Sections 5 – 6 were assembled without the protective tape, therefore were the only set that contained complete data.
3. Sections 5 – 6 had the best quality over all, apart from the tip end of section 5 wind-ward trailing edge. This is possibly due to lack of clamping force. Sections 1, 3 and 4 also exhibit similar issues.

4. Over the three measurements, the negative flushness biases were gradually removed, however, the final assembled prototypes clearly still do not meet the 200µm tolerance requirement.

3.3. Development of Automated Fixture Health-check (Red Amber Green Metrology)

This section describes the work on the potential integration and implementation of the concepts of bespoke data processing and visualization algorithms mentioned in the previous section for an Airbus research project on automated fixture health-check.

Aerospace assembly jigs and fixtures can have global build tolerances of sub-250µm, over tens of meters. A CAD model of Airbus Advanced Low Cost Aircraft Structures assembly system is shown in Figure 3 at the beginning of this thesis. The fixtures are generally stable structures that only require periodic checks to ensure the key interfaces are still within tolerance. However, a fixture cannot be used during the recertification process. The recertification process can take several weeks, this is dependent on the condition of the fixture and the level of work required. The level of work to correct the fixture is often *estimated*, and in many cases *over-estimated* in order to ensure the work does not run over-schedule. As Airbus increases the rate of manufacture, fixture down-time will become more critical. Reduction or elimination of the fixture downtime due to recertification is an important step in reducing manufacturing cost. Rapid fixture condition health checks are a potential interim solution to reducing production downtime from fixture recertification. An additional drawback with periodic recertification is the increased risk of non-conforming products moving to the next process step undetected, health check measurements could reduce the risk of this happening.

Rapid fixture health checks aim to automatically verify the jig condition before each assembly begins - in a short time frame, ideally within 10 minutes. These checks are measurements of key fixture interfaces, identifying gross positional/dimensional errors (approx. 100µm). In addition to verifying the fixture condition, the health check measurements can provide useful empirical information that can be used in predicting levels of recertification work and problem areas within a fixture. This could make the recertification procedure leaner as the work would be quoted and scheduled for the *actual* level of work condition of the fixture and not the *estimated* level of work.

A fixture can be compromised during the assembly process. The fixture undergoes stresses from component placement, this includes: the weight of the component or sub-assembly, residual stresses from in-fixture fastening, vibration from in-fixture material removal and accidental damage. Although

fixtures are designed to cope with these forces, unforeseen stresses and strains could cause a less robust pick-up or flag to become out of tolerance between builds. Additionally, the assembly process may require elements of the fixture to be movable; these movables are then dowelled back into nominal position when required; this process has inherent uncertainty associated with it.

During commissioning of the fixture, Enhanced Reference System (ERS) points are arbitrarily placed around the fixture. The ERS points are measured using a laser tracker network. A laser tracker network reduces the measurement uncertainty and avoids line of sight issues associated with a single laser tracker station. Due to the uncontrolled factory environment, the ERS points need to be measured with the highest achievable accuracy. Once measured, these initial ERS values are located within the jig axis system and subsequently assigned to the fixture's documentation (known as Sheet 800s). When checking a fixture, it is the pick-ups that define the Key Characteristics (KC) and Interchangeability (ICY) criteria that are of interest. The KCs ensure the functional requirements of the design, ICY criteria ensure component/ sub-assembly compatibility. These are checked by utilizing the ERS system. Conventionally, a single laser tracker will locate its relative position by measuring a sub-set of the ERS, scaling for thermal expansion, and best-fitting to the measured points by minimizing the residual fitting errors. The laser tracker is now correctly positioned within the global co-ordinate system. Each Point Of Interest (POI) - KC or ICY interface - is measured through the use of additional *facility* tooling, this tooling targets the specific POI indirectly with a defined offset. If the POI is out of tolerance it is then moved back into its nominal position.

This process requires laser tracker operators to move a Spherically Mounted Retro-reflector (SMR) target to each measurement point, this is time consuming and best carried out with two persons. This can be dangerous as it may require working at height. An advantage of the laser tracker is the ability to measure continuously and *watch* measurements when moving POI back into tolerance of the nominal position.

3.3.1. Project Background

The Red, Amber and Green (RAG) Metrology project aims to create a rapid jig health-check solution which can perform a full check in less than 10 minutes. The first RAG trials began in 2009. These initial trials explored potential measurement systems that were capable of rapid automatic measurement, these trials were performed on a small scale fixture. RAG Metrology 2009 identified photogrammetry systems as having good potential to fulfil the requirements needed for rapid fixture heath checks. The follow-on RAG 2010 trials took the technology, application and philosophy to a higher technology readiness level.

RAG 2010 explored the capability of both photogrammetric and photographic systems that is metrology specific and non-metrology specific cameras, respectively. This ensured that the measurement uncertainty was of an appropriate level. Additionally, the systems measured a fixture (ALCAS Main Assembly Jig) that was more representative of a full-scale fixture; this established times of measurement: approx. 30mins (manual process). RAG 2010 also developed a software interface to simplify health check measurements.

This project aims to build on RAG 2009 and 2010, to *progress Red, Amber and Green Metrology: Rapid Fixture Health-Checks* from the technology readiness level (TRL) 3, to TRL 4 by the end of 2011; this includes the software, measurement technology and philosophy.

3.3.2. Proposed Methodology

The software flow chart is shown in Figure 53 on the next page. The main program would be a graphical user interface (GUI) that is presented to the user, which would run the measurement, analysis and evaluation processes in the background. The RAG process will involve the measurement of the jig using a photogrammetry camera mounted on a robot, photogrammetry software that generates the target positions from the images, a SpatialAnalyzer script which performs the robust fitting and transformations of the targets to fit them to the nominal datum point and produces the deviations, and finally the logic to determine the state of the jig.

The GUI and jig health decision making processes are straight forward to program and implement; however, they are specific to the intended jig or fixture which they are deployed on. Consequently, it was decided to focus on developing the “core” processes, i.e. the transferable/generic processes at this stage of the project; this included: SpatialAnalyzer scripting/work flow and the photogrammetry process. The robotic measurement that will be simulated using the data (i.e. camera positions) generated from the manual measurements, was also explored to ascertain the feasibility of simulating hundreds of camera positions.

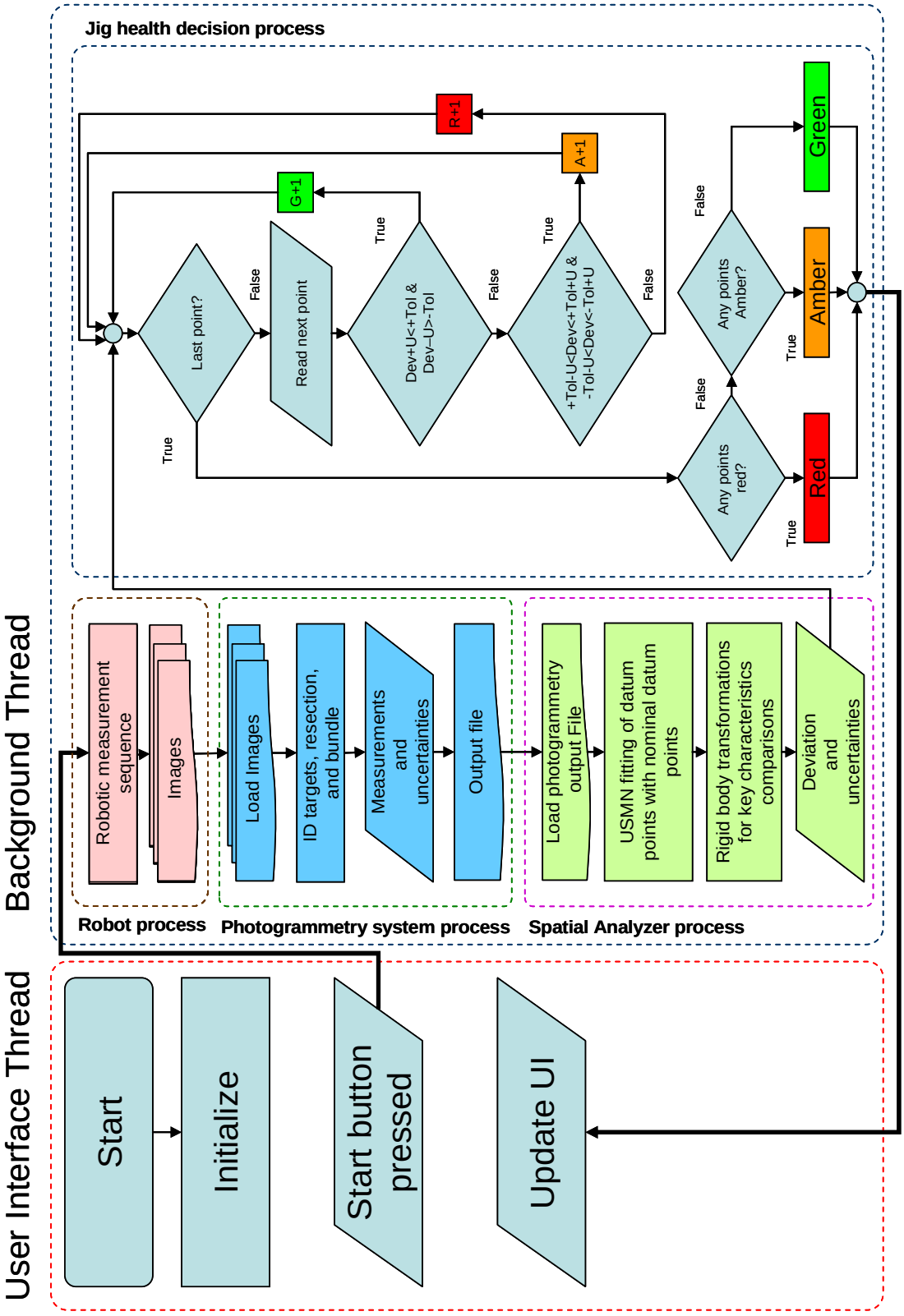

Figure 53 - The RAG Software Flowchart

A Jig Reference System (JRS) and a single Key Characteristics (KC) with its corresponding Rigid Body Transformation (RBT) have been setup on the Bath RAG demonstrator. The JRS consists of coded photogrammetry targets which are surveyed so that their positions are known with a high degree of accuracy. In the full-scale ALCAS trial, these coded targets will measured relative to the existing, traditional SMR Nest JRS points; this will maintain the appropriate axis systems. Figure 54 illustrates the points – JRS, KC and RBT – placed onto the demonstration fixture, these are level adjusted images from the AICON DPA photogrammetry surveys.

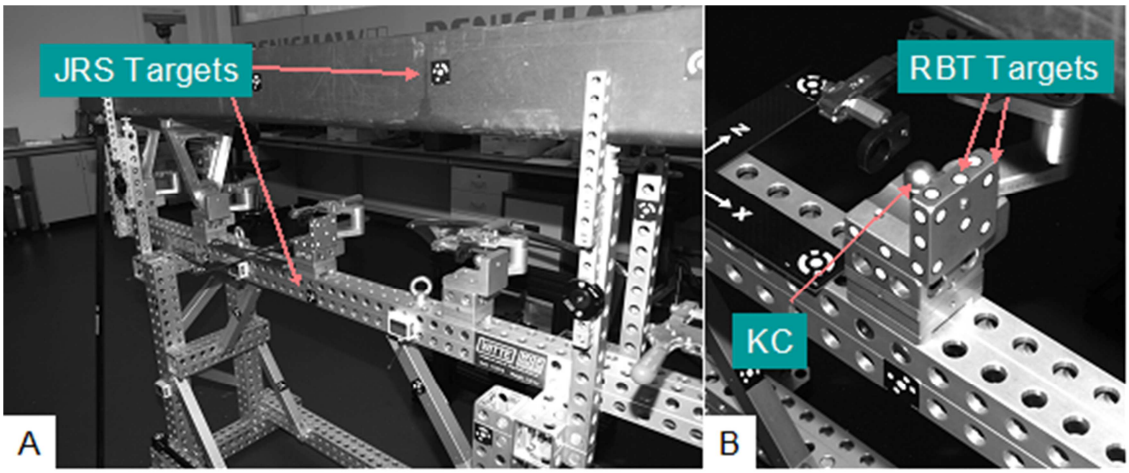

Figure 54 - Photogrammetry images of the Bath RAG demonstrator, the JRS, KC and KC's RBT points are indicated on the figure.

The KC on the demonstrator is modelled as an arbitrary point that represents the hinge bore location sphere on the University of Bath demonstrator (Figure 54B). The final ALCAS health check measurement will use KC points derived from the drawings provided by Airbus, this will be at least one point on each flag (13 KCs), but is more likely to include additional points where appropriate, e.g. two KCs on a hinge axis.

The RAG software will be used to calculate the position and measurement uncertainties of the KC by measuring the RBT targets. This will negate the need for facility tooling during a health-check measurement.

3.3.3. Description of Trialled RAG Procedure

A trial run of the proposed RAG process was carried out on the ALCAS assembly jig, the major processes are as listed below:

1. Commissioning
    a. Application of photogrammetry targets
    b. Four station laser tracker measurement of the JRS and OTP (Optical Tooling Point)

    c. Photogrammetry measurement of the jig with split bearings in JRS
    d. SA USMN of the tracker and photogrammetry measurements
    e. Establishing the RBTs in SA
2. Simulated robot photogrammetry measurement along the middle of the jig
3. Automated processing of the robot measurement images
    a. Auto-loading of images
    b. Images processing and bundling
    c. Output results
4. Analysis in SA
    a. Load robot measurement results
    b. Manual USMN/RBT process
    c. Compute deviations
    d. Report results and uncertainties
5. RAG Health decision process
    a. Load analysis results in excel
    b. Run conditional logic
    c. Report

3.3.4. Process Development

The development statuses of the key processes are illustrated in Figure 55. While the majority of the processes have been successfully demonstrated, the lack of ability to automate SA USMN prevents the development of a fully automated solution.

Each of the processes is described in detail in the following subsections.

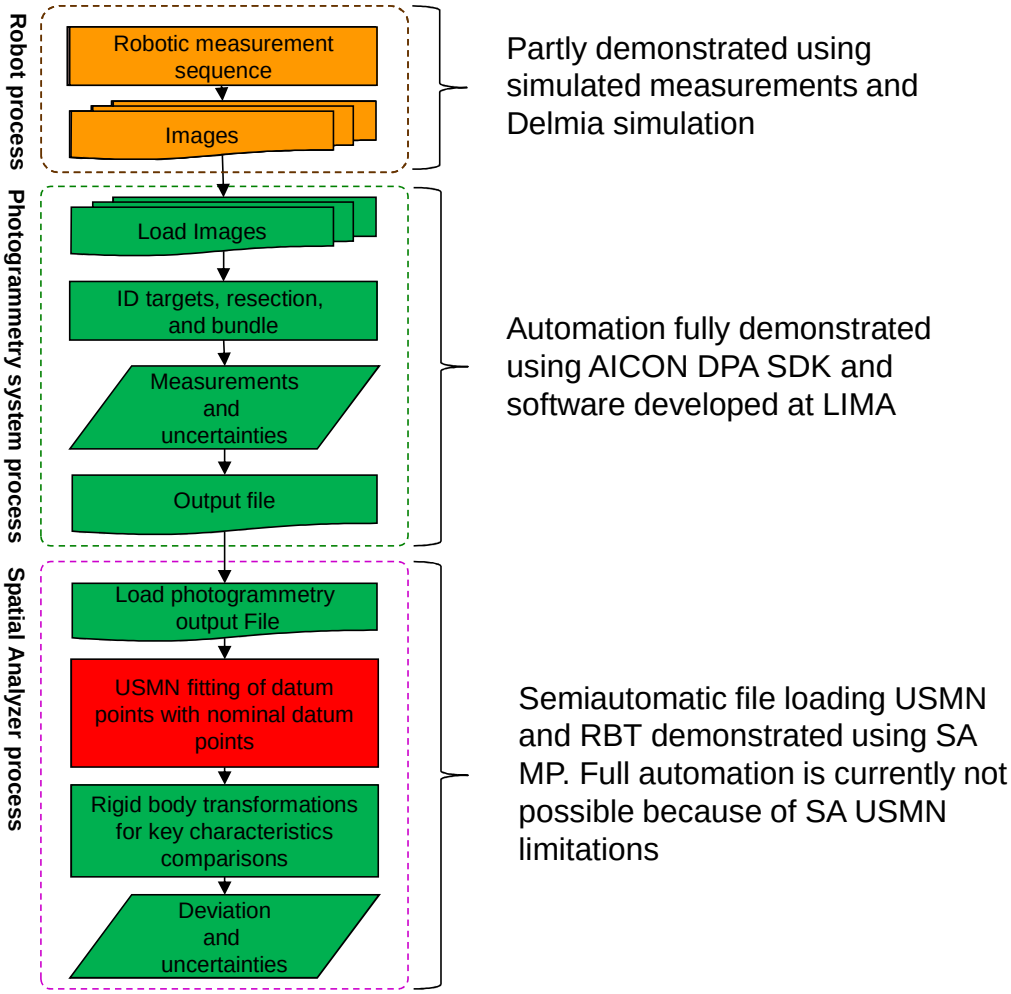

Figure 55 - Software development progress

3.3.4.1. Robot Process

In order to evaluate the feasibility and process time of the proposed robotic measurement sequence, a manual photogrammetry survey consisting of approximately 200 images of the physical jig, taking into account the possibly limited reachability of the robot, is used to mimic the robot measurement process.

The images are processed in DPA 3D Studio to solve for the camera and target positions. The camera positions from the simulated measurement from DPA 3D Studio are then imported into SpatialAnalyzer, which is used to align the camera positions to CAD. The camera positions are then imported into Delmia (Figure 56). This allows the digital simulation of an industrial robot on a linear track to reconstruct the sequence of manual measurements.

MatLab scripts are used to perform Euler – fix axis rotation transformation during the export-import processes to ensure data compatibility between the software packages.

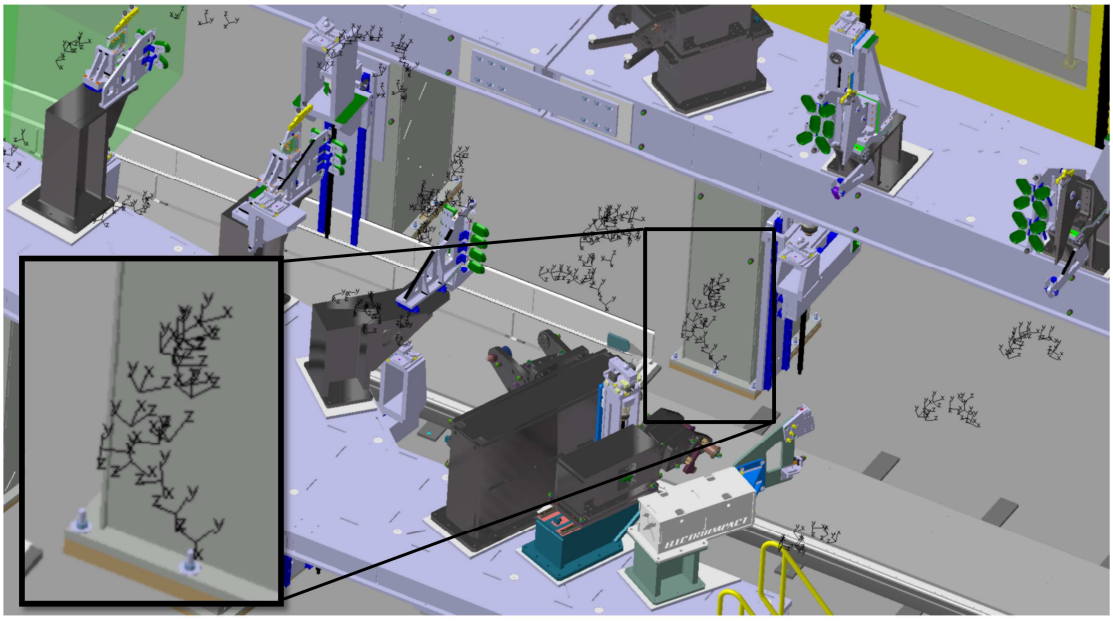

Figure 56 - Camera positions imported into Delmia as robot tag group, with a group of tags highlighted.

A robotic simulation of the photogrammetry measurement was then conducted in Delmia, as shown in Figure 57. It was determined that the measurement process will take at least 5 minutes and 12 seconds for the robot to move through the 200 TCPs without stopping. More realistically, if the robot is required to stop for 1 second at each point for the camera to take a stable picture, the process is likely to take 8 minutes and 32 seconds.

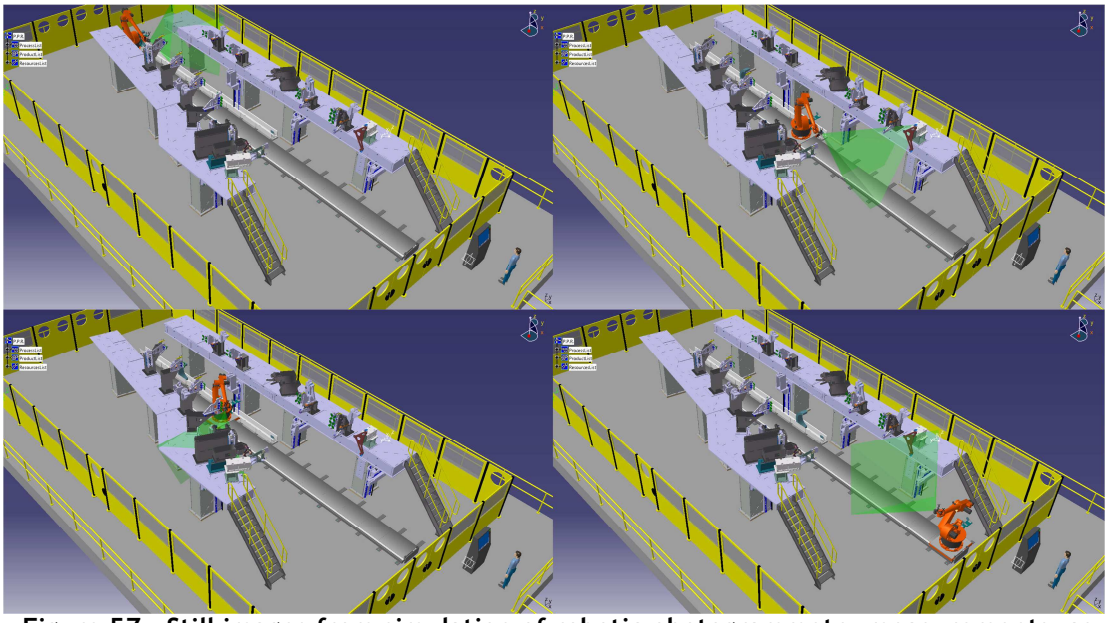

Figure 57 - Still images from simulation of robotic photogrammetry measurements, as the robot moves from one end of the jig to the other while taking pictures. The green pyramid represents the field of view of the AICON photogrammetry camera.

3.3.4.2. Photogrammetry System Process

The process of collecting the measurement images and initiating the AICON DPA bundling is now fully automated. A command line program written in Visual C++ traverses a user defined directory for jpeg images and adds them to the DPA DLL, starts the measurement, and outputs the results. The program operates without any user input (Figure 58).

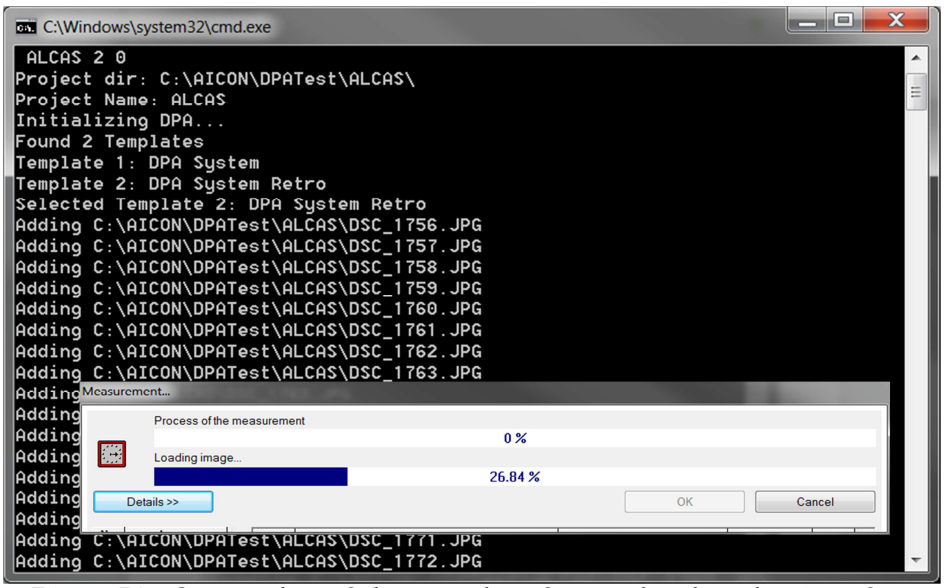

Figure 58 - Screen shot of the console software developed to interface with DPA .dll files.

This process takes approximately 5 minutes to load all the images, and an additional 1 minute and 20 seconds for the bundle adjustment. In a real process, the images loading will take place in parallel with the robotic measurement.

3.3.4.3. SpatialAnalyzer Process

The SA process loads the results from the photogrammetry process, fits the simulated robotic measurement to the results from the commissioning survey, and performs the RBTs. The deviations and measurement uncertainties are then reported (Figure 59).

While this process should be fairly straight forward to implement into a user interface using the SA SDK, several limitations of SA tools and their SDK implementation means that this part of the project is on hold awaiting updates from NRK, the developers of SA.

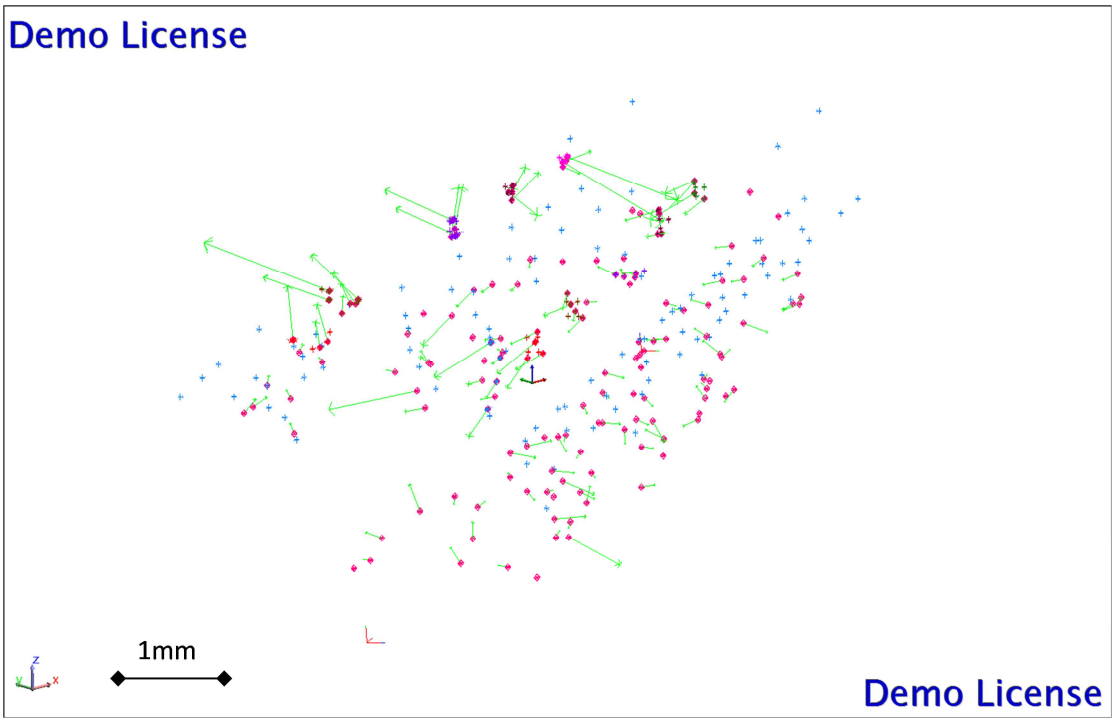

Figure 59 - USMN fit result from SA process. Blue points are the jig reference points, red points are the measured points (their sizes represent measurement uncertainties), and the green vectors are exaggerated deviations of OTP from nominal.

Current limitations of the SA process which have hindered the development of the RAG solution include:

1. Does not generate measurement uncertainty
2. Does not allow adjustment to key options such as scaling for temperature
3. Difficulty in USMN with previous USMN results (needed for RBT)
4. USMN can be very slow for large data sets

NRK is working on possible future fixes. If these limitations cannot be solved in time, it is also possible to use similar algorithms available from NPL (developed by Alistair Forbes) to perform the best fitting and RBTs.

3.3.4.4. Jig Health Decision Process

The Jig Health Decision Process is currently performed in an Excel spread sheet using conditional logic. This is a simple process that will be easily integrated into the final solution.

3.3.5. Process Timing

The estimated time-line for the RAG health check is shown in Figure 55, and a breakdown of the individual process times is listed in Table 4. The estimated total time of the health check is between 11 and 13 minutes. The

majority of the time is taken up by the 8 and a half minute robotic measurement process. The photogrammetry system can process the images in parallel with the robot process, so that during the robot move to the next camera position, the previous picture can be transferred and processed, thereby saving computation time.

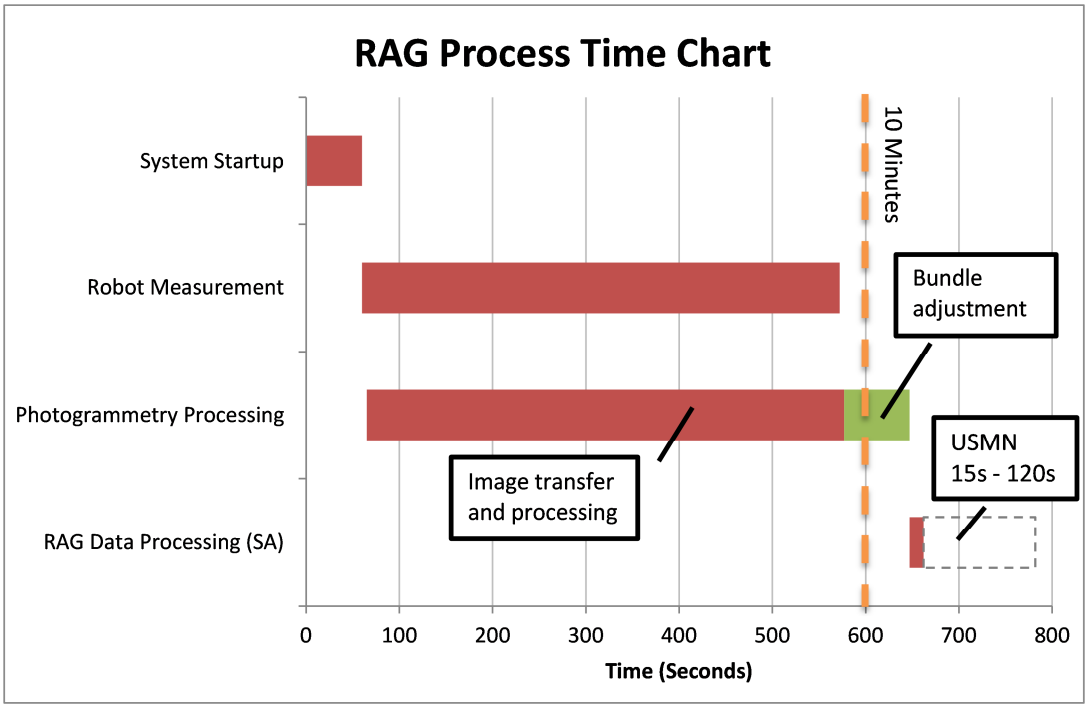

Figure 60 - Gantt chart of RAG process.

Table 4 - List of process times

Task	Time	Notes
System Start-up	01:00	Estimated start-up time of PC, robot, camera and networking equipment
Robot Measurement	08:32	312s of movement + 200 measurements at 1s per photo
Photogrammetry Processing	09:42	Must wait for robot to finish
RAG Data Processing (SA)	00:15-02:00	USMN can take different length of time depending on data quality
Total	11:00-13:00	

Due to current SA USMN limitations mentioned previously, it is difficult to determine the amount of time the process will take if it is working properly. While is it possible that the processing can be fairly short, it is more likely to be in the 60-120 second range, in order for the Monte Carlo simulation to achieve adequate convergence.

If it is absolutely necessary to keep the process below 10 minutes, there are possible ways to reduce the total time:

1. Reduce the number of camera positions

2. Reduce the amount of time the robot dwells at each camera position
3. Use a faster PC to reduce SA processing and photogrammetry bundling time
4. Reduce start-up time by leaving the PC in stand-by mode

3.3.6. Measurement Results and Analysis

3.3.6.1. Commissioning

During commission, the positions of the OTPs and JRS are measured using 4 laser tracker positions and a photogrammetry survey. The measurement results are combined in Spatial Analyzer using USMN, and fitted to the nominal CAD data.
The positions of the OTPs and their measurement uncertainties are listed in Table 5.

Table 5 - OTP positions and uncertainties from RAG commissioning measurements (all units mm)

Item	X	Y	Z	U (2σ)
OTP80910	7813.580	5296.020	114.017	0.047
OTP80910	7749.228	5402.835	105.115	0.046
OTP80910	7753.861	5395.224	-19.592	0.045
OTP80920	6422.684	4458.455	113.861	0.087
OTP80920	6358.358	4565.221	105.119	0.084
OTP80920	6362.934	4557.628	-19.570	0.087
OTP80930	2901.810	2319.056	-110.569	0.067
OTP80930	2817.264	2459.401	78.277	0.066
OTP80930	2824.618	2447.153	-121.207	0.067
OTP80930	2894.496	2331.276	88.972	0.065
OTP80940	1356.667	1388.386	-110.446	0.054
OTP80940	1349.342	1400.624	89.073	0.056
OTP80940	1272.124	1528.748	78.370	0.054
OTP80940	1279.462	1516.531	-121.147	0.053
OTP81110	7336.047	7655.336	149.832	0.095
OTP81120	5842.454	7073.348	149.798	0.044
OTP81120	5878.734	6980.389	157.001	0.040
OTP81120	5881.342	6973.686	57.269	0.039
OTP81130	4299.442	6460.261	-41.680	0.062
OTP81130	4343.075	6381.011	104.657	0.062
OTP81130	4337.904	6370.513	-4.749	0.061
OTP81130	4306.100	6473.636	97.532	0.061
OTP81312	4921.264	3266.496	-62.760	0.069
OTP81312	4921.249	3266.477	-62.750	0.066
OTP81312	4407.933	3275.562	-21.644	0.076
OTP81312	4407.902	3275.545	-21.689	0.077
OTP81511	966.266	5140.733	-520.598	0.089
OTP81512	495.236	4958.559	-622.007	0.060
OTP81711	1843.361	5537.269	-333.983	0.045
OTP81711	1740.739	6166.387	-286.864	0.098
OTP81910	120.777	973.014	414.073	0.041
OTP81910	72.288	946.070	-659.277	0.039

3.3.6.2. Jig Health Check

The final measured OTP deviations, measurement uncertainties and their RAG statuses (for 300µm tolerance) are shown in Table 6. According to these measurements, three of the tolerances are violated. Therefore the jig health is red.

Since the OTPs (apart from possibly OTP811102) didn't actually move between commissioning and the simulated robotic measurement, these deviations represent the difference between the two sets of measurement results, which for ideal measurements would be zero.

Table 6 - Jig deviations, measurement uncertainties and RAG statuses from simulated robotic measurement with ±300µm tolerance (all units mm)

Item	dX	dY	dZ	dMag	UX (2σ)	UY (2σ)	UZ (2σ)	Umag	RAG X	RAG Y	RAG Z
OTP809102	-0.132	0.054	-0.006	0.143	0.152	0.116	0.085	0.209			
OTP809103	0.223	0.266	-0.045	0.350	0.151	0.115	0.077	0.205			
OTP809104	0.339	0.290	-0.042	0.448	0.155	0.125	0.070	0.211			
OTP809202	-0.551	-0.229	-0.021	0.597	0.116	0.096	0.088	0.174			
OTP809203	-0.113	0.037	-0.006	0.119	0.113	0.097	0.065	0.163			
OTP809204	-0.157	0.028	-0.007	0.159	0.105	0.087	0.065	0.151			
OTP809301	-0.010	0.055	0.002	0.056	0.132	0.104	0.070	0.182			
OTP809303	0.119	0.114	0.015	0.165	0.142	0.129	0.075	0.206			
OTP809304	0.168	0.163	0.014	0.234	0.120	0.108	0.068	0.175			
OTP809305	-0.059	0.006	0.003	0.059	0.122	0.121	0.069	0.185			
OTP809401	0.131	0.001	0.034	0.135	0.213	0.159	0.098	0.283			
OTP809402	0.125	-0.063	0.038	0.145	0.243	0.203	0.095	0.330			
OTP809403	0.167	-0.035	0.076	0.187	0.222	0.287	0.080	0.372			
OTP809404	0.173	0.029	0.073	0.190	0.182	0.261	0.079	0.328			
OTP811102	-1.172	0.035	0.494	1.273	0.243	0.182	0.176	0.351			
OTP811202	-0.401	-0.236	0.148	0.488	0.119	0.106	0.104	0.190			
OTP811203	-0.276	-0.196	0.031	0.340	0.126	0.105	0.069	0.178			
OTP811204	-0.274	-0.070	0.023	0.284	0.115	0.091	0.069	0.162			
OTP811301	-0.156	-0.251	-0.164	0.338	0.262	0.111	0.082	0.296			
OTP811303	-0.068	-0.235	-0.182	0.305	0.193	0.203	0.090	0.294			
OTP811304	-0.125	-0.253	-0.193	0.342	0.149	0.169	0.099	0.246			
OTP811305	-0.002	-0.208	-0.176	0.273	0.327	0.146	0.087	0.369			
OTP813120	0.036	-0.048	0.003	0.060	0.065	0.117	0.074	0.153			
OTP813120B	0.036	-0.048	0.003	0.060	0.065	0.112	0.077	0.151			
OTP813121	0.049	-0.004	-0.052	0.071	0.076	0.094	0.069	0.139			
OTP813121B	0.049	-0.004	-0.052	0.071	0.072	0.095	0.067	0.137			
OTP815119	-0.125	-0.163	-0.141	0.249	0.150	0.200	0.149	0.292			
OTP815120	-0.131	-0.210	-0.037	0.250	0.148	0.144	0.114	0.236			
OTP817113	-0.069	-0.271	-0.009	0.280	0.110	0.106	0.083	0.174			
OTP817114	0.391	-0.176	-0.231	0.487	0.217	0.094	0.121	0.266			
OTP819106	0.297	-0.253	0.134	0.413	0.255	0.263	0.071	0.374			
OTP819109	-0.147	-0.216	0.157	0.305	0.263	0.253	0.077	0.373			

3.3.6.3. Analysis of Measurement Uncertainties

The final results presented in the previous section shows that the OTP deviations are quite high, as are the measurement uncertainties. If the deviations are plotted against their associated uncertainties, as shown in Figure 61, it is obvious that a greater than expected number (> 5%) of the deviations fell outside the 2 sigma confidence interval, thus cannot be explained by the instrument uncertainties. For photogrammetry measurements this likely suggests that there are errors that the instrument and software cannot account for, such as errors in scale and poor network. Since only two 1.5m scale bars were used in the 15m measurement volume, a lack of accurate scale information likely contributed to significant errors. Letting the scale float during USMN showed that the scale of the robotic measurement is off by 80µm/m.

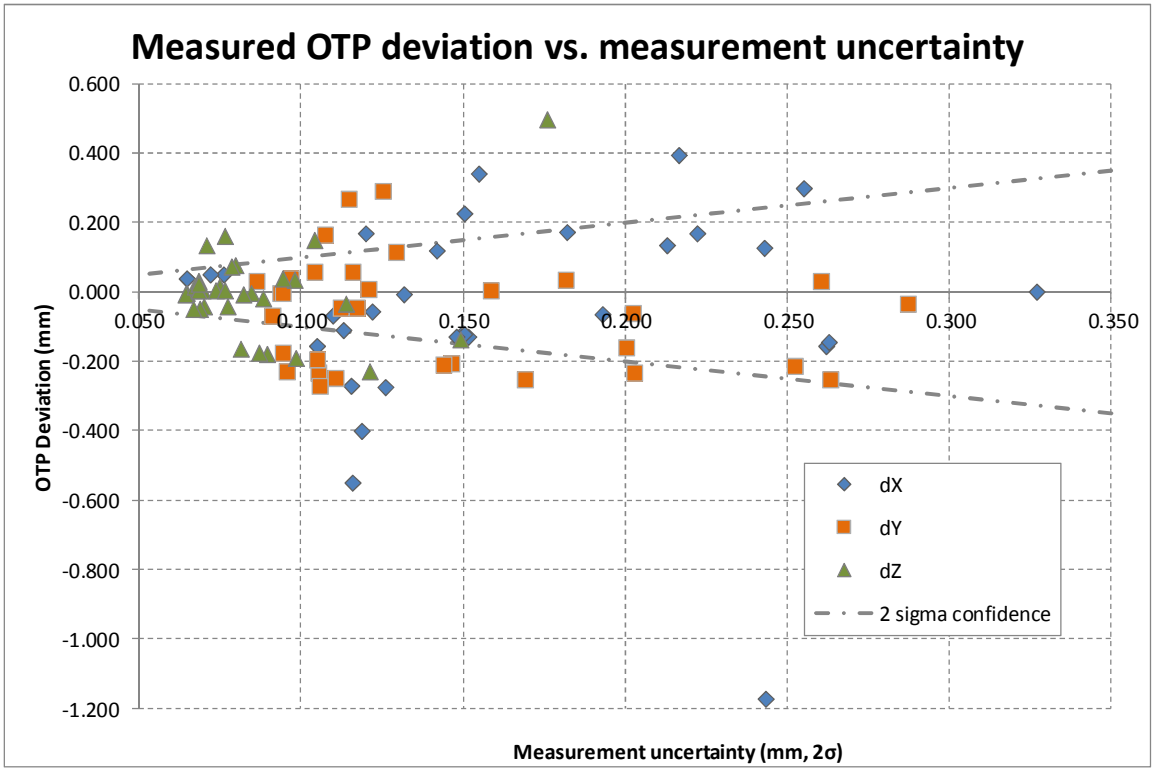

Figure 61 - A large number of measured OTP deviations are outside the 2 sigma confidence interval.

The camera positions for the measurements are also not optimal, especially for the simulated robotic measurements. The simulated robotic measurements are restricted to the centre of the jig; whereas during commissioning a much wider and less restricted network was used (Figure 62).The difference between the uncertainties for the commissioning and robotic measurements is plotted in Figure 63.

Despite the fact that more images were taken during the simulated robotic measurement compared to the commissioning stage, its suboptimal network resulted in higher median and quartile uncertainties.

In order to reduce measurement errors and uncertainties, future measurements of large structures such as the ALCAS jig will have to be more carefully planned, taking into account issues such as lines of sight, target distances from the camera, and target angles, as well as use better scale references.

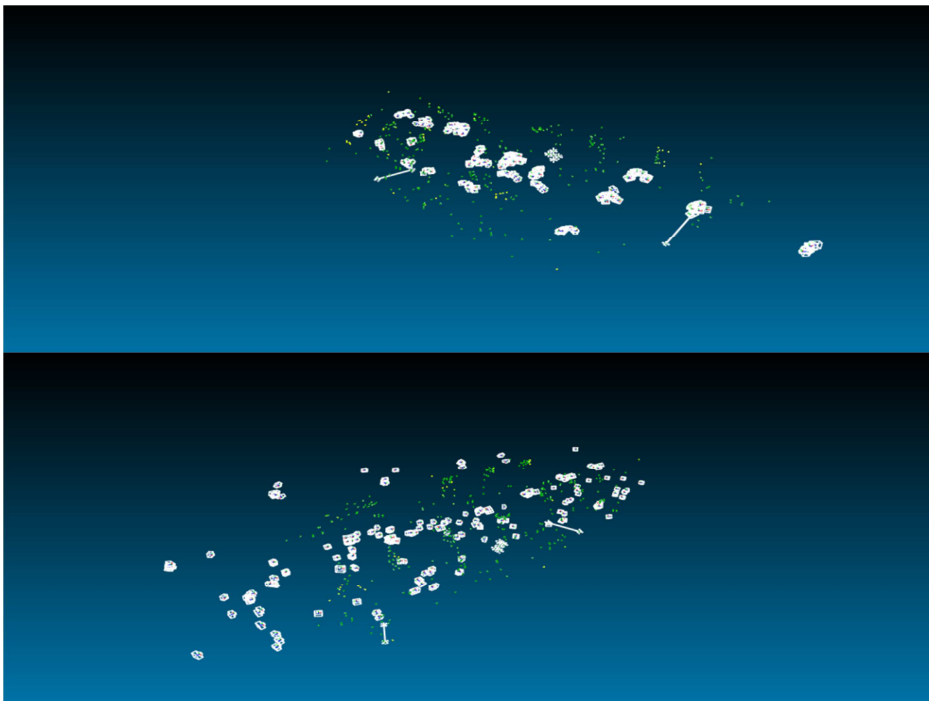

Figure 62 - Top: camera positions for simulated robot measurements. Bottom: camera positions for commissioning.

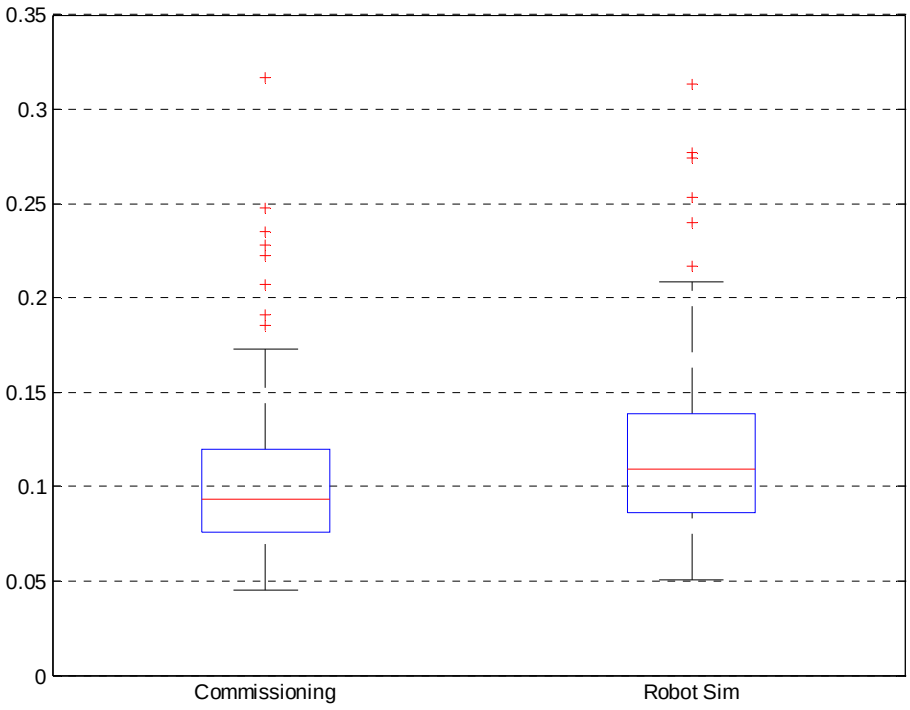

Figure 63 - Box plot of measurement uncertainty comparison between commission and simulated robot measurements (unit: mm).

3.3.7. RAG Progress and conclusions

RAG is a large project, and is still very much a work in progress. A summary of the work completed and future work is listed below.

Work completed:

1. Simulated commissioning and robotic measurement of ALCAS jig
2. Time simulation of robotic measurements
3. Software Interface with AICON DPA system for automatic photogrammetry image processing
4. RAG analysis of the measurement results

Future work required:

1. Planning, optimization of camera positions for higher accuracy photogrammetry measurement
2. Solve SA USMN problems
3. Integrate and build user interface
4. Trial of robotic measurement

This work showed that an automated fixture health-check system proposed and partly demonstrated here can potentially be completed within 13 minutes, which is vastly faster than the current manual process. All the main pieces of the technology already exist. The development of such a system is mostly an exercise in software/hardware integration, requiring the cooperation of the software/hardware developers.

3.4. Summary and Discussions

Three different application case studies of metrology data processing and automation were described in the previous sections.

In the first case study, software was used to automate the analysis of measurement data in robotic positioning repeatability, as an example of a measurement problem solved using bespoke algorithms. It allowed the point repeatability of any robot or positioning system to be quickly analysed, and is applicable over any arbitrary working volume.

In the second project, a more complex software algorithm was developed to semi automatically process the Vestas prototype wind turbine blade scan data and convert them into plots of flushness against distance along the glue joint. The scan data processing software successfully processed all 22 scans, the results proved to be very reliable. It was able to quickly extract key features from scan data and plot the results in a form that is easily understood by the manufacturing engineers, previously not possible using

existing software. The software can also be used to analyse any scan data in general for flushness.

The last project involved a rapid automatic fixture health-check of the Airbus ALCAS demonstration. Many different hardware and software processes were proposed, developed, and demonstrated to facilitate the project. This work showed that an automated fixture health-check system can potentially be completed within 13 minutes, which is vastly faster than the current manual process typically taking several days.

There exists a tremendous amount of demand from aero-structure manufacturers for metrology automation to solve near to term issues present in current production systems. While the current generation of metrology systems have the capabilities to meet the demands, the main challenges lie in system integration and data processing, as these case studies demonstrate. While these are not very difficult challenges, they do require insights into both the LVM instruments and software development, which typical manufacturers do not possess.

Since large volume measurement tasks vary greatly, LVM must be able to adapt to be effective. In the past, this “adaptation” is embodied by bespoke hardware hard tooling, and product specific measurement tools. In a future flexible production environment with reduced reliance on capital intensive large jigs and hard tooling, where the jigs and measurement instruments are more or less standardized off-the-shelf components, it is the software that must adapt.

4. Digital Modelling and Simulation of Metrology Assisted Assembly (MAA) Technology

4.1. Introduction

As more and more aero-structure manufacturers move to automate their current metrology processes, the logical next step is to *embed* or *integrate* metrology such that it is concurrent with the production processes. It is the concurrency with production that separates Metrology Assisted Assembly from automated metrology data processing discussed in chapter 3.

Before exploring the details of implementing a MAA system, it is necessary to develop methods to study how such integrated systems can work, and quantify their potential benefits.

While research efforts over the past two decades have demonstrated that process modelling is an essential technology for design evaluation and process planning [40, 41], the efforts mostly focused on the traditional industrial role of metrology as a verification stage that follows production and assembly, rather than being an integrated part of production [42-44].

In this chapter, techniques of mathematically simulating metrology assisted assembly systems that are compatible with existing assembly modelling methods are outlined, and a number of application case studies using the assembly simulation are presented. The applications include metrology assisted assembly and part-to-part interface management.

As in the previous chapter, the Airbus projects ALCAS and IntEq described in this chapter are large and involved the input from multiple people at Bath and Airbus. Included in this thesis are the mathematical modelling and simulations of MAA developed by the author for the projects.

4.2. Assembly Uncertainty Simulation Methodology

Modern aero-structures involve complex multi-station systems with large numbers of machining operations and several locating datum changes. Dimensional variability introduced at each machining operation gets transformed and causes the occurrence of new variability as the workpiece propagates through the machining system. This propagation of variability is often referred to as “Stream of Variation”.

Stream of Variation is a set of mathematical techniques used to model this propagation of variability. The refinement of these models has allowed existing control theory and multivariate statistics to be applied to solving problems in assembly quality.

In these models a single part point is defined on each component which remains in the same position on the part throughout the assembly process, similarly points can be defined to represent features. Errors due to factors such as fixture location are represented by translation and rotation of these points. The accumulated error in the part position and orientation at each assembly station can then be modelled by transforming the errors from the previous station by the errors occurring at the current station (Figure 64).

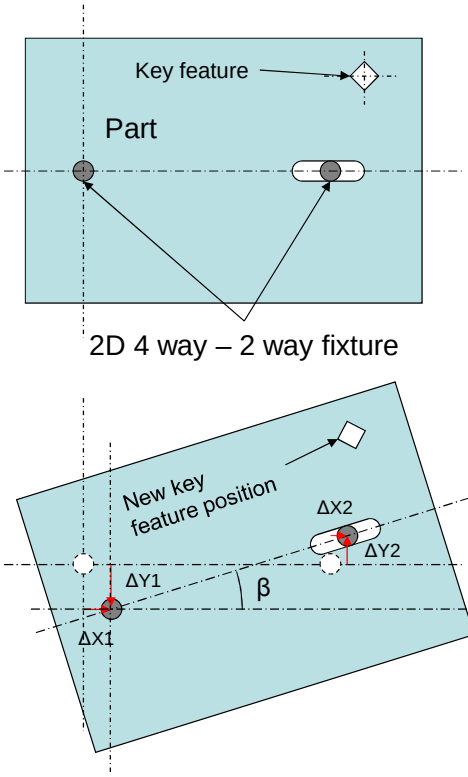

A model of the deviation of the key feature(s) as a function of the deviations in fixtures

Deviations in fixtures causes the part to move in 3DOF (2D case). R_f is the matrix that transforms fixture deviation into part deviation, and R_k is the matrix that transforms part deviation into key feature deviation.

$$\begin{bmatrix} \Delta X_p \\ \Delta Y_p \\ \Delta \beta_p \end{bmatrix} = R_f \bullet \begin{bmatrix} \Delta X1 \\ \Delta Y1 \\ \Delta X2 \\ \Delta Y2 \end{bmatrix}$$

Deviation of part

$$\begin{bmatrix} \Delta X_k \\ \Delta Y_k \\ \Delta \beta_k \end{bmatrix} = R_k \left(R_f \begin{bmatrix} \Delta X1 \\ \Delta Y1 \\ \Delta X2 \\ \Delta Y2 \end{bmatrix} \right)$$

Deviation of key feature

Figure 64 : Error in Key Feature Position and Orientation due to Fixture Errors

The stream of variation methodology allows the complex interactions between a part and a fixture or between two parts to be modelled as a simple matrix. This then allows the variation to be propagated across many such interactions to model the complete assembly process. It is important to

remember however that the actual interactions must still be modelled individually in order to obtain these simplified matrices.

The series of transformation matrices represent the degree of freedom transformations linking the position and orientation uncertainties of each assembly step to the uncertainties of the key features of the assembled product.

The uncertainty of the key features can be calculated using the partial derivative method identical to the GUM measurement uncertainty propagation formula or MCS method described in sections 2.4.1 and 2.4.2. In this research projects, the MCS method was chosen due to its ease of implementation and modification.

4.3. MAA Digital Simulation Case Studies

4.3.1. ALCAS Rib Feet Interface

Gaps between structural components are a common problem in aero-structure assembly, due to the difficulty of producing components with tight tolerances on large and flexible structures. Gaps and flushness problems are typically referred to as interface management [45].

One example of interface management issues encountered in the Airbus ALCAS project is the management of the interface between the wing ribs and the upper and lower wing skins. Figure 65 illustrates the major components of a wing box, and the key points of interest: gaps and clashes between the Inner Mould Line (IML) of the upper skin and the rib feet. Since the ribs are bonded to the wing skin using adhesives, the structural integrity of the wing is dependent on the optimal gap between the rib feet to the wing skin. If the gap is too small the adhesive will be squeezed out, and if the gap is too large it would not be able to form a strong bond.

In the ALCAS design, the IML of the wing skins, unlike the outer aerodynamic profiles, are not controlled in the production process. In order to reduce problems at the interface a MAA process was proposed: the IMLs are scanned using a vision system, and the rib feet are then fettled to dimensions extracted from the scanned data. A mathematical analysis was needed to validate the process.

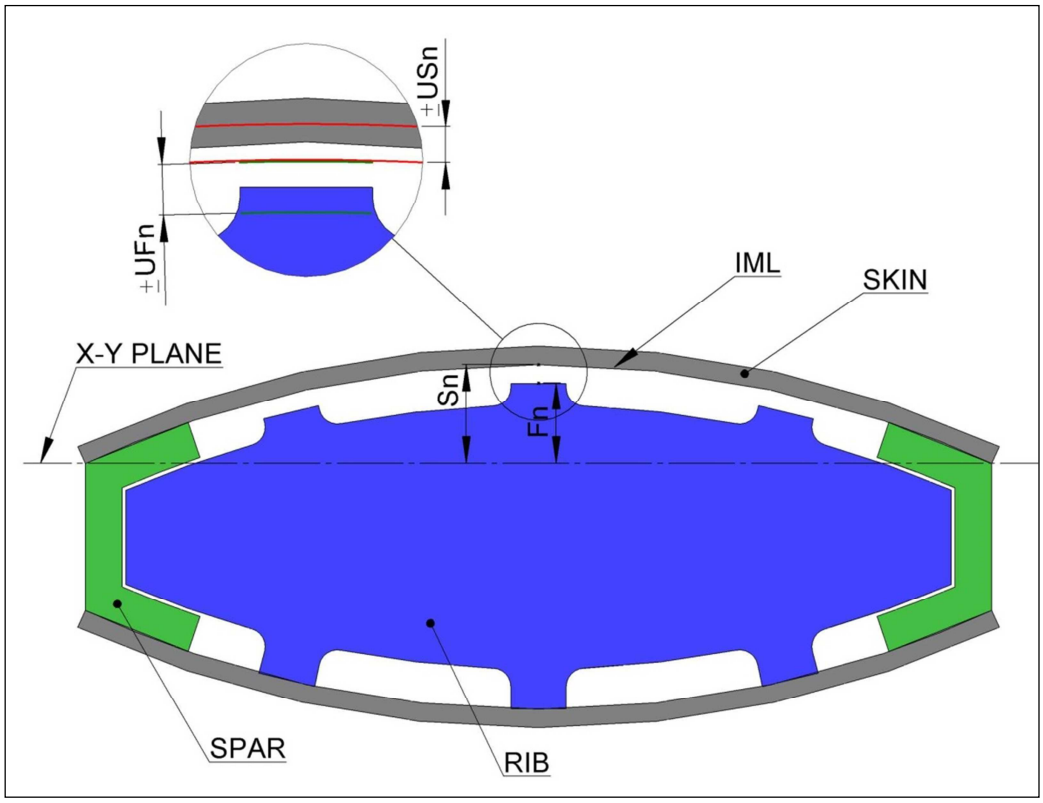

Figure 65 : Cross-section diagram of Wing Box Assembly highlighting the rib feet-wing skin interface

A simple Monte Carlo simulation has been created in MatLab in order to demonstrate how gap or clash prediction can be carried out. This models the uncertainty in the wing box skin to rib foot interface in two dimensions. Three processes are modelled:

- Scanning of IML (50μm standard uncertainty)
- Fettling of rib from scanned data (100μm standard uncertainty)
- Assembly of wing skin to rib (250μm standard uncertainty)

The simulation process is illustrated in Figure 66. Figure 67 and Figure 68 show the simulation results for the wing skin of a single random Monte Carlo trial.

A smooth quadratic formula was used to represent the nominal interface profile. Random errors are first added to simulate the variability in the real surface as compared to the nominal profile. Random errors were then used to simulate the measurement uncertainty in the measurement of the real surface (Figure 67). Further errors are added to the wing IML profile to create the rib profile, representing the uncertainties of robotic fettling.

The two profiles are then combined in an assembly simulation which includes uncertainties in locating the parts in the jig. The gaps between the two profiles are then computed and recorded (Figure 68).

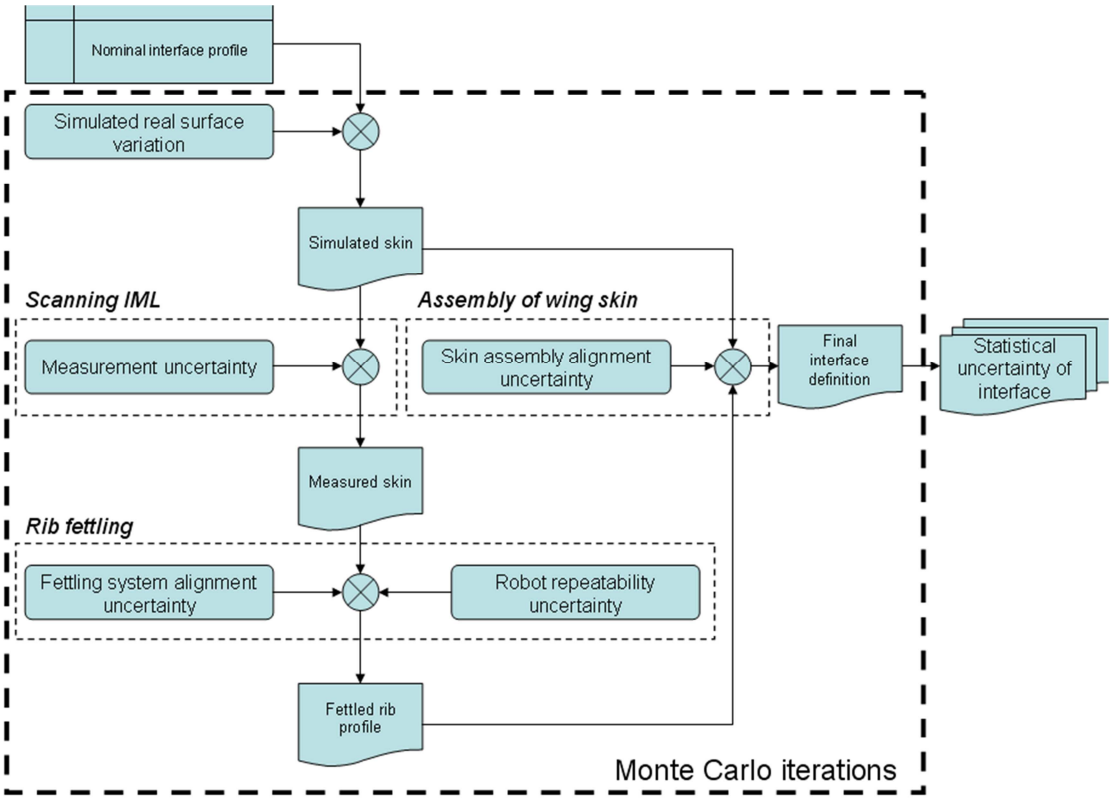

Figure 66 : Monte Carlo Simulation of Interface Management Process

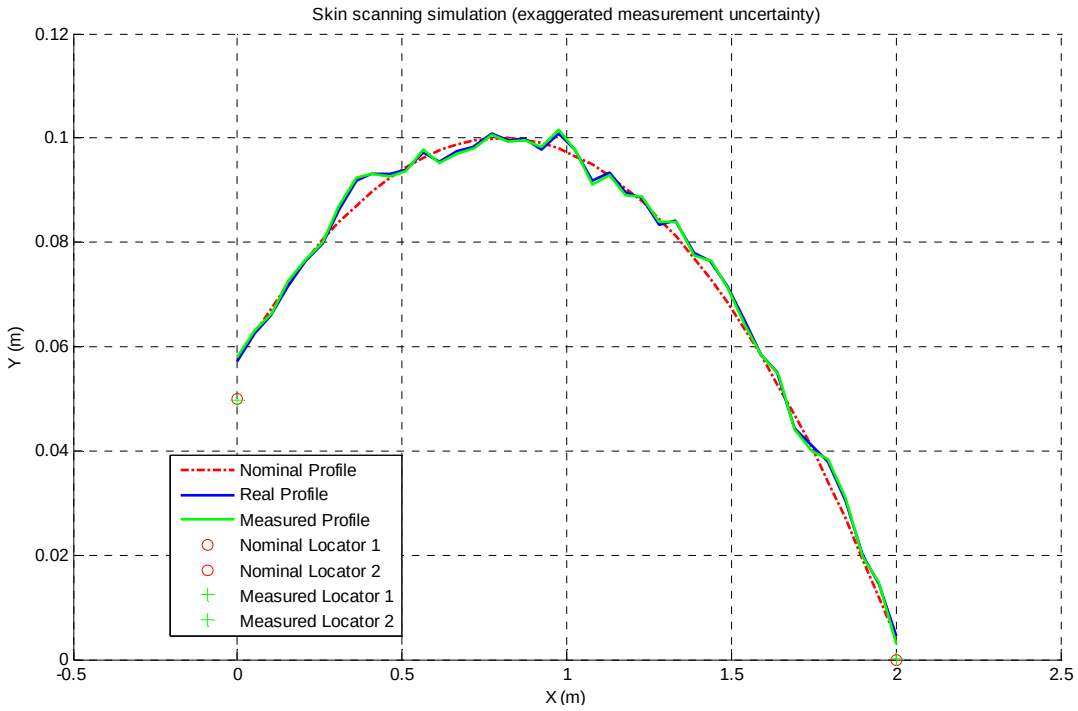

Figure 67 : Simulation of Wing Skin Surface Variability and Measurement Uncertainty

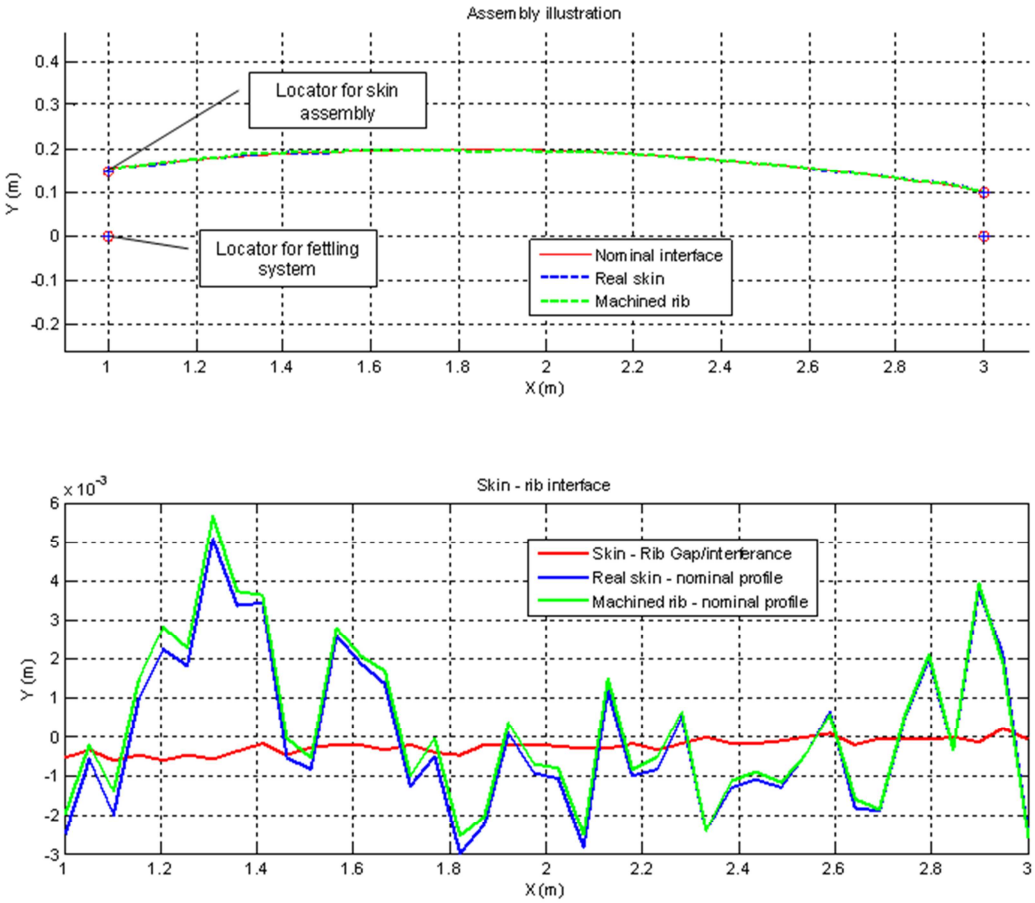

Figure 68 - Assembly analysis of a single trial

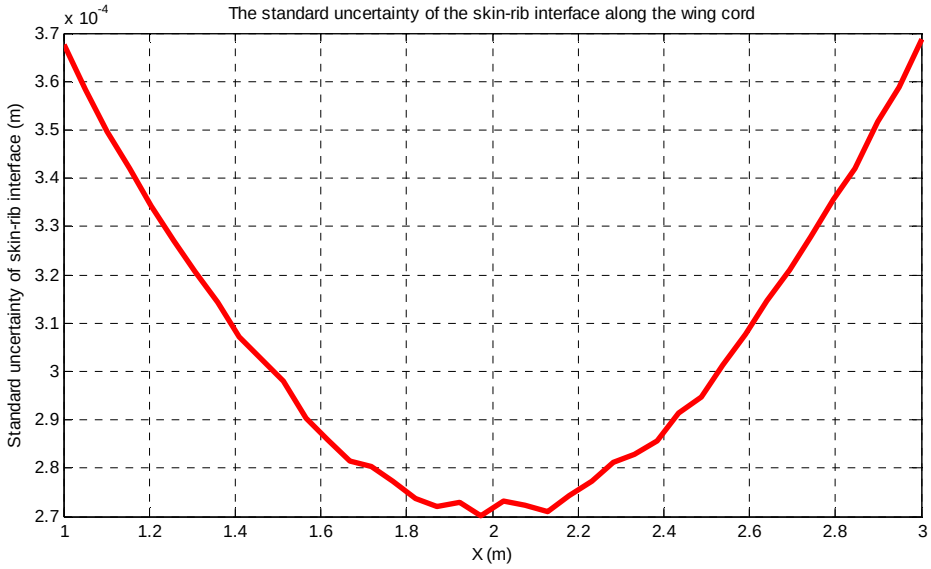

Figure 69 : Results of simulation after 10000 trials

Figure 69 shows the final simulation results after 10000 trials of fitting the real skin profile to the wing box assembly with the fettled rib profiles, representing the predicted uncertainty of the interface alone the wing cord.

It predicts that the gaps will be largest towards the spars and lowest in the middle of the rib.

The approach described here allows variability due to measurement uncertainty, fixture location and forming process to be readily combined. It is therefore a suitable technique for modelling interface management operations. Specialist knowledge and software is however required to create the algorithms and careful consideration of the problem is required to determine what exactly must be modelled. In addition to the obvious expense involved in this there is also a considerable potential for human error. For routine use in production planning generic simulations which have been fully validated and which can be rapidly reconfigured to a specific problem would be preferable.

4.3.2. IntEq Flap Track Assembly

4.3.2.1. Introduction

In some cases it is possible to inject measurement data directly into the assembly model such that it can be used during production to ensure that the assembly is accurate and optimal. This represents a transformation of assembly modelling from strictly a planning tool to an essential part of the assembly process. An example of this is the proposed IntEq project solution developed for Airbus.

The Airbus IntEq (Integrated Equipping) project focuses on integrating metrology into the wing equipping processes. One of the processes studied is the metrology assisted flap track assembly process.

In the current process the aerodynamic profile is referenced using hard tooling which has a physical pointer where the trailing edge of the flap should be in cruise configuration. Another piece of hard tooling, the ‘shark fin’ is located on the flap beam which also has a physical pointer where the trailing edge of the flap should be. The position of the flap track is adjusted by inserting packers until the two pointers are aligned. The ‘shark fin’ remains in position and will be used to align the flap during the flap rigging process. This is currently a tedious manual process that involves trial and error fitting of the flap track which involves multiple assembly and disassembly steps until the flap is at the correct position.

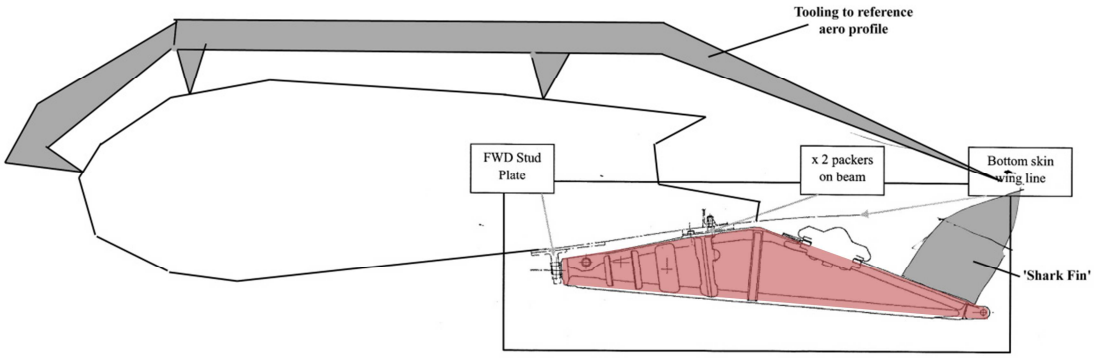

Figure 70: Current flap track (shaded red) Rigging Process

In the proposed process the aerodynamic profile and brackets for the flap track on the wing box would be measured during the initial metrology scan and datum targets would also be located within the same reference frame. Similarly the flap track would be measured by the supplier and datum targets would also be located at this stage. By comparing the measurements of the wing box with those of the flap track it would then be possible to calculate the correct packers before assembling the flap track to achieve a one-way assembly.

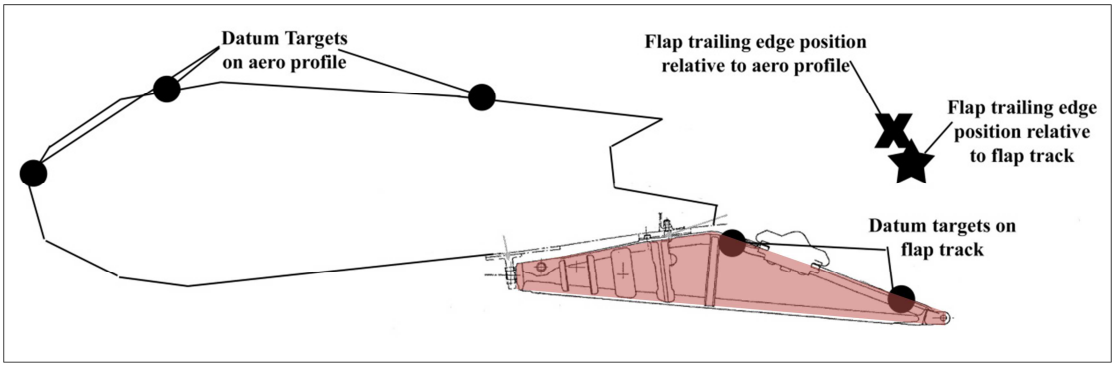

Figure 71: Proposed flap track (shaded red) Rigging Process

Algorithms based on transformation matrices can be used to predict the shims required and facilitate a one-way right-first-time assembly of the flap beam with no in-assembly rigging required. The following data obtained in the initial wing box and component metrology stations will be used:

- Flap beam brackets on underside of the wing box datumed to the upper aerodynamic profile and hinge-line brackets
- Bracket pick-ups for the wing box and flap located on the flap beam

Since the algorithms used to predict the shim thicknesses use measurements made at the previous measurement stations no measurement or automation would be required at this stage. A simple manual process could therefore be used to locate the flap beam as a determinate assembly. Verification could be carried out after assembly by comparing the flap trailing edge position calculated from the datum targets on the aero profile with the trailing edge

position calculated from the flap track, this is exactly equivalent to the comparison of two pointers on hard tooling carried out in the current process. This could however take place before the rigging of flaps is started and make use of the same cameras used for flap rigging.

The assembled position of the flap beam can be verified by measuring coded targets using the overhead photogrammetry in a subsequent rigging station before any further assembly is carried out.

A small scale demonstrator (Figure 72) was constructed at Bath in order to verify the proposed processes. A simulation of the flap track assembly process was developed in MatLab, and used to calculate the required shim sizes from photogrammetry measurement of the aerodynamic profile and CMM measurements of the flap track.

Figure 72 – Level adjusted photo of IntEq demonstrator from photogrammetry measurements

4.3.2.2. Geometry Abstraction

The flap track fitting algorithm abstracts the CAD geometry into the key characteristic points that are required to compute the shim sizes, as shown in Figure 73.

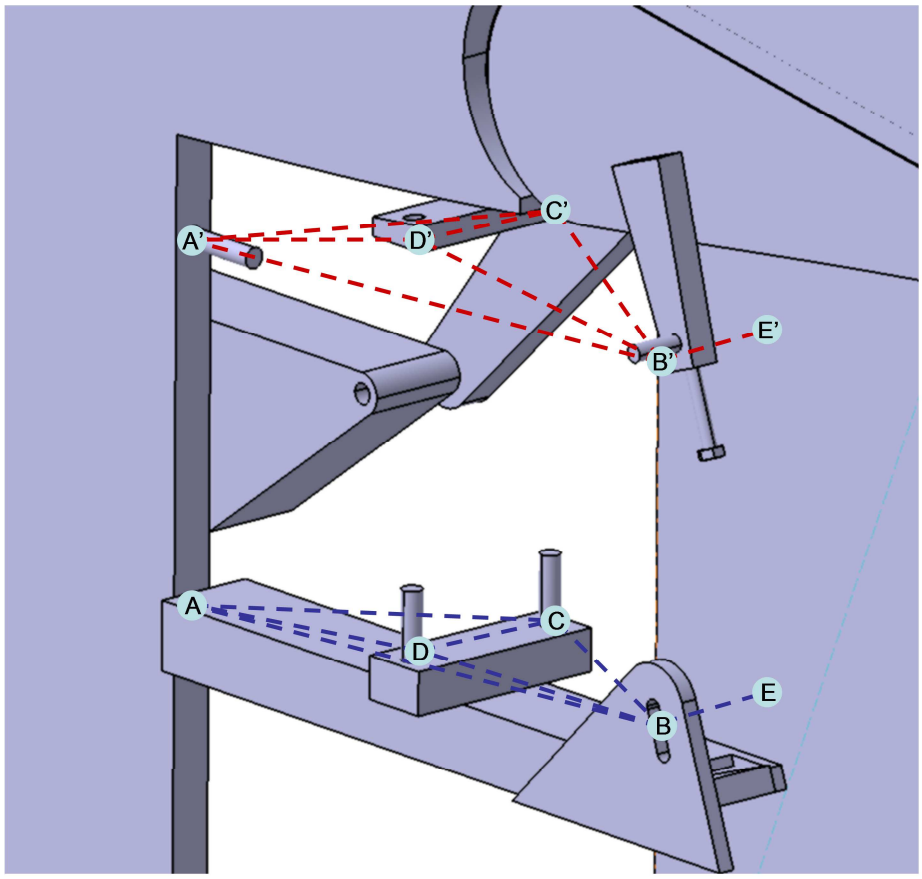

Figure 73 – Abstraction of CAD geometry

The points A, B, C, and D represent the measured KC positions on the flap track, and vector $\overrightarrow{BE}$ represents the flap hinge axis vector, which is generated from the known nominal relationship between point E and the rest of the points.

The points A', C', and D' represent the flap mounting points on the wing, which are measured before assembly using photogrammetry. The optimal B' position is determined from the scanning of the wing and flap aerodynamic profile. The $\overrightarrow{B'E'}$ vector then represents the optimal flap hinge axis.

4.3.2.3. The Flap Fitting Algorithm Process Steps

A simulated flap fitting process using test data will be used to illustrate the steps the algorithm goes through to calculate the required shim sizes.

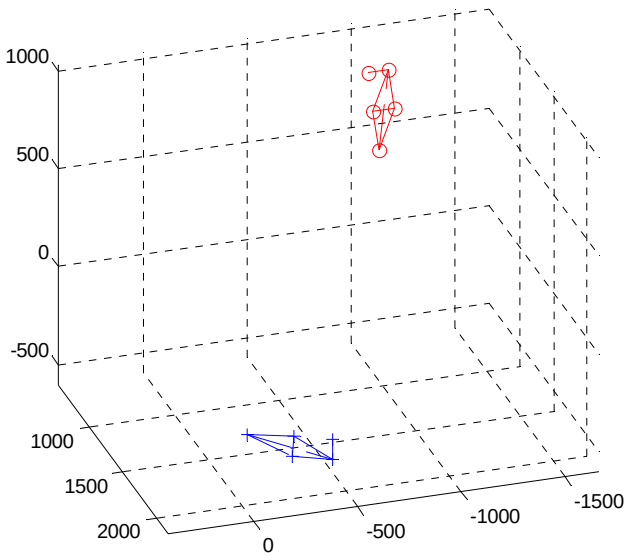

Figure 74 - Generated flap track KCs and wing fitting position

As shown in Figure 74, at the start of the process, the flap track is at a random position and orientation with respect to the wing points.

4.3.2.3.1. Locating to flap hinge point

The first step of the process is to simply locate the flap track hinge point B to the optimal hinge point position B', as shown in Figure 75.

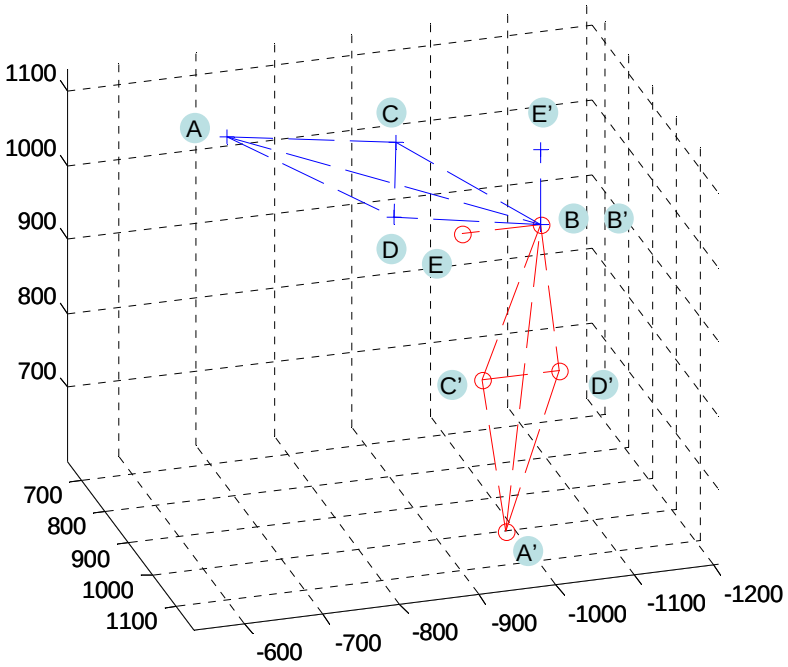

Figure 75 - Locate B to B'

This is a simple translation of the flap track by the difference vector between points B and B'. This step ensures that any errors caused by the

geometric deviations from nominal of the flap track KCs and their corresponding points will not affect the correct positioning of the flap.

4.3.2.3.2. Rotation about hinge point to line up $\overrightarrow{AB}$ with $\overrightarrow{A'B'}$

The second step is to rotate the flap track about the point B' or B so that the vector $\overrightarrow{AB}$ is coincident with $\overrightarrow{A'B'}$. This is accomplished by first determining the angle between the two vectors, and then performing a rotation about the axis formed by the cross product of $\overrightarrow{AB}$ and $\overrightarrow{A'B'}$ passing through point B', as shown in Figure 76.

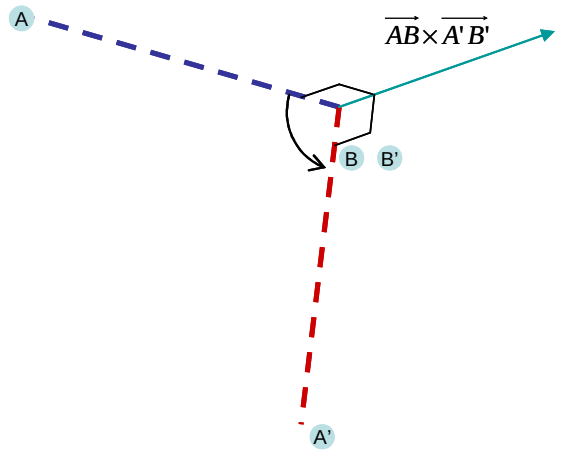

Figure 76 - Rotation of $\overrightarrow{AB}$ to coincide with $\overrightarrow{A'B'}$

The result of this step is shown in Figure 77.

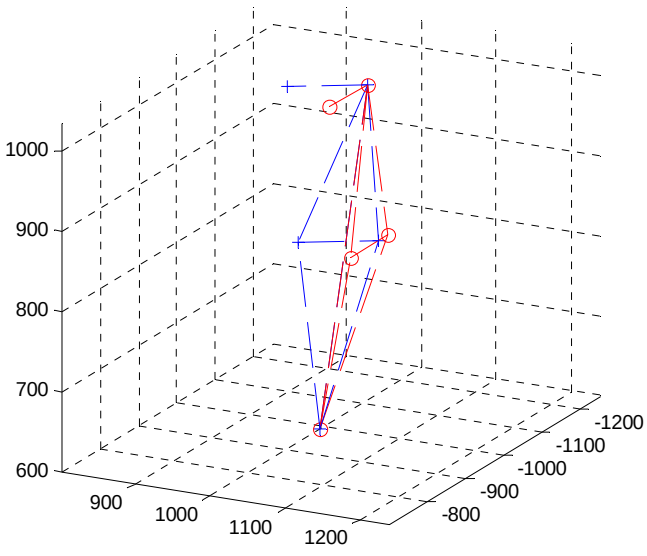

Figure 77 - After the rotation

4.3.2.3.3. Rotation about $\overrightarrow{A'B'}$ to line up the hinge axes

The next step is to line up the flap hinge axes $\overrightarrow{EB}$ and $\overrightarrow{E'B'}$ by rotating the flap track about the vector $\overrightarrow{A'B'}$. In order to do this, we must first find the angle between $\overrightarrow{EB}$ and $\overrightarrow{E'B'}$ in the plane of rotation. Since the rotation is about $\overrightarrow{A'B'}$, the plane of rotation has the $\overrightarrow{A'B'}$ as its normal vector.

Using $\overrightarrow{A'B'}$ as the normal vector, we can create a pair of orthogonal basis vectors $\overrightarrow{a_1}$ and $\overrightarrow{a_2}$ in the rotation plane, using which the vector projection of $\overrightarrow{EB}$ and $\overrightarrow{E'B'}$ in the rotation plane can be found. The rotation angle is now simply the angle between the projected vectors (Figure 78).

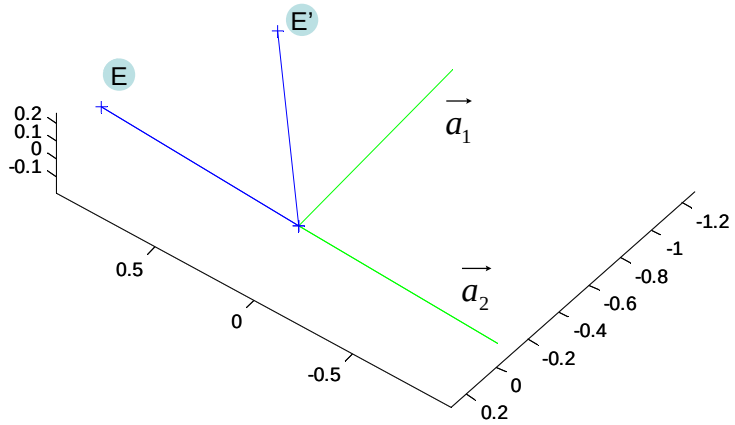

Figure 78 - Projection of $\overrightarrow{EB}$ and $\overrightarrow{E'B'}$ in the rotation plane

After this rotation, the flap track is at the correct position and orientation to calculate the required sizes of the shims. The result of this step is shown in Figure 79.

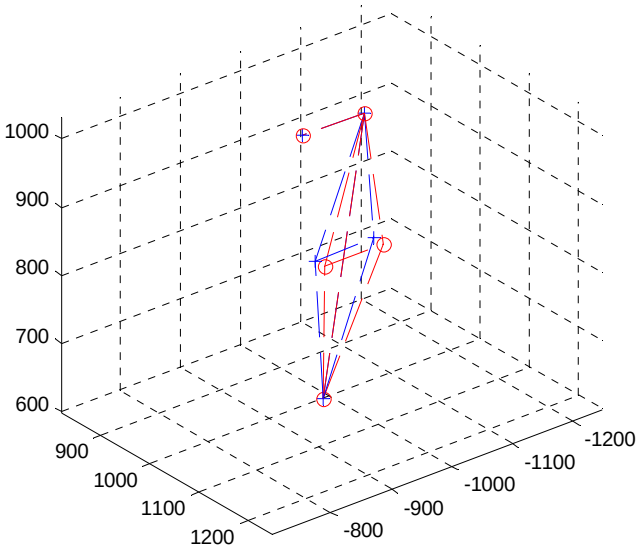

Figure 79 - After the rotation

4.3.2.4. Determining the shim sizes

The shim sizes are determined by the shortest distance from points C and D to the plane formed by the points C', D' and an arbitrary point at the same height as C' and D'.

4.3.2.5. Modelling of Shim Size Distributions

Using this fitting algorithm, it is possible to establish the most likely shim sizes, given part tolerances and measurement uncertainties. A simple test was conducted by injecting a 300μm standard uncertainty to the position of all of the points. A Monte Carlo simulation with 10000 trials was run, the results of which can be seen in Figure 80.

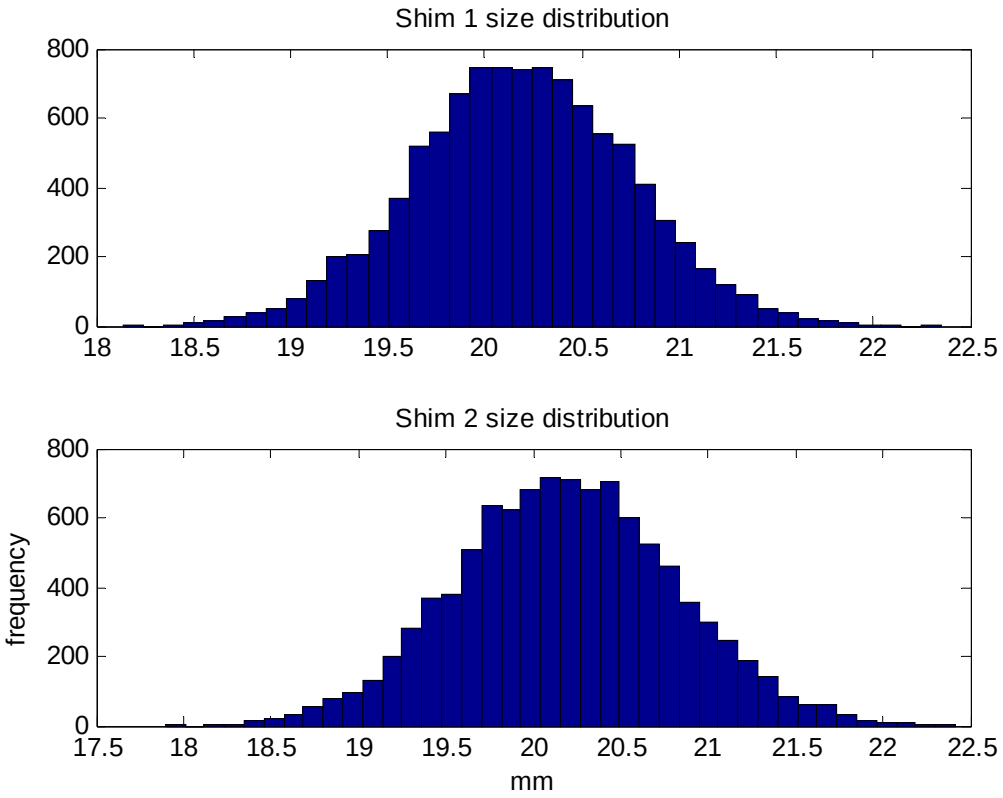

Figure 80 – Shim size distributions after 10000 runs.

The mean and standard deviations of the shim sizes are summarized in Table 7.

Table 7 – Summary of simulation results

	Shim 1 (C → C')	Shim 2 (D → D')
Mean size (mm)	20.1935	20.1879
Standard deviation (mm)	0.5475	0.6204

4.3.2.6. IntEq Conclusions

The IntEq process was fully demonstrated using an AICON photogrammetry system on the small scale demonstrator at Bath, from the initial photogrammetry survey to feeding measurement data to the assembly model to selecting the correct shim sizes and outputting necessary adjustment for the flap and spoiler. The assembly model was used successfully as an essential part of the assembly process, as well as a planning tool.

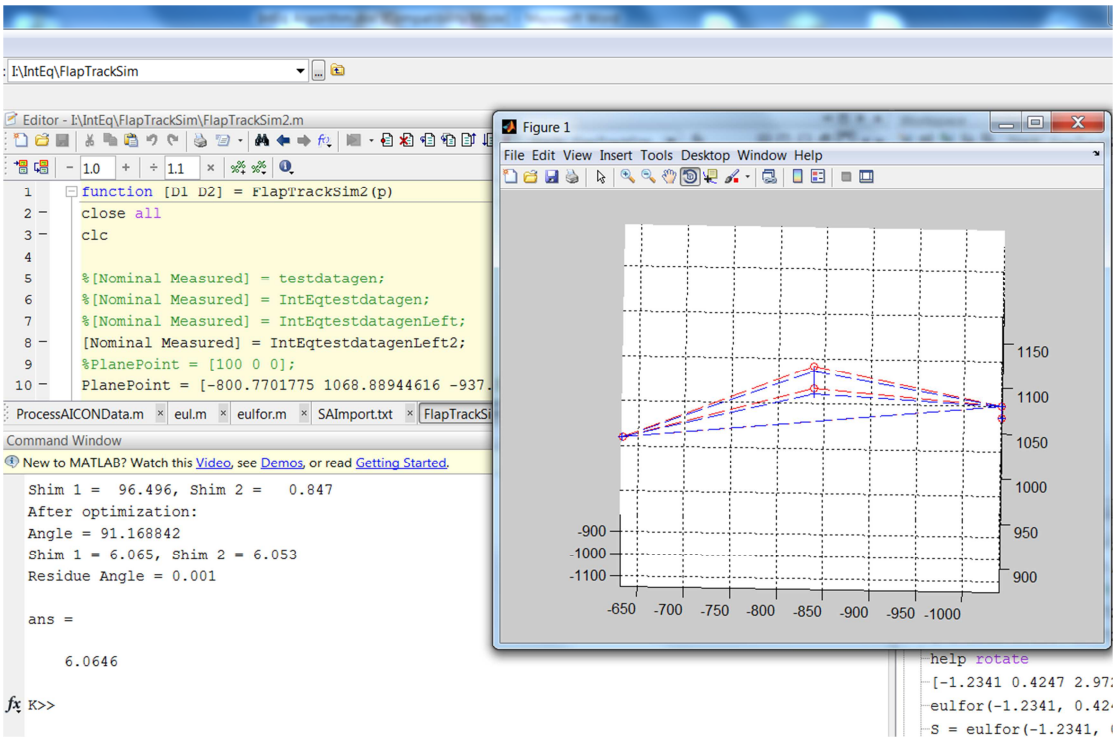

Figure 81 - Screenshot of the MatLab script generating required shim sizes from photogrammetry measurements.

In the final demonstration, the wing mock-up is measured using photogrammetry to establish the relationship between the wing profile and wing mounting points. The mock-up flap track is measured using a Faro coordinate measuring arm to determine its dimensions. The two sets of data are imported into the MatLab assembly model to compute the predicted optimal shim sizes required (Figure 81).

The flap track is then assembled using a stack of shims of the correct size, and its position is re-measured and compared to the predicted nominal position in relation to the wind profile in SpatialAnalyzer (Figure 82). The process was repeated ten times, and the flap track was placed within 100µm of the predicted position everytime.

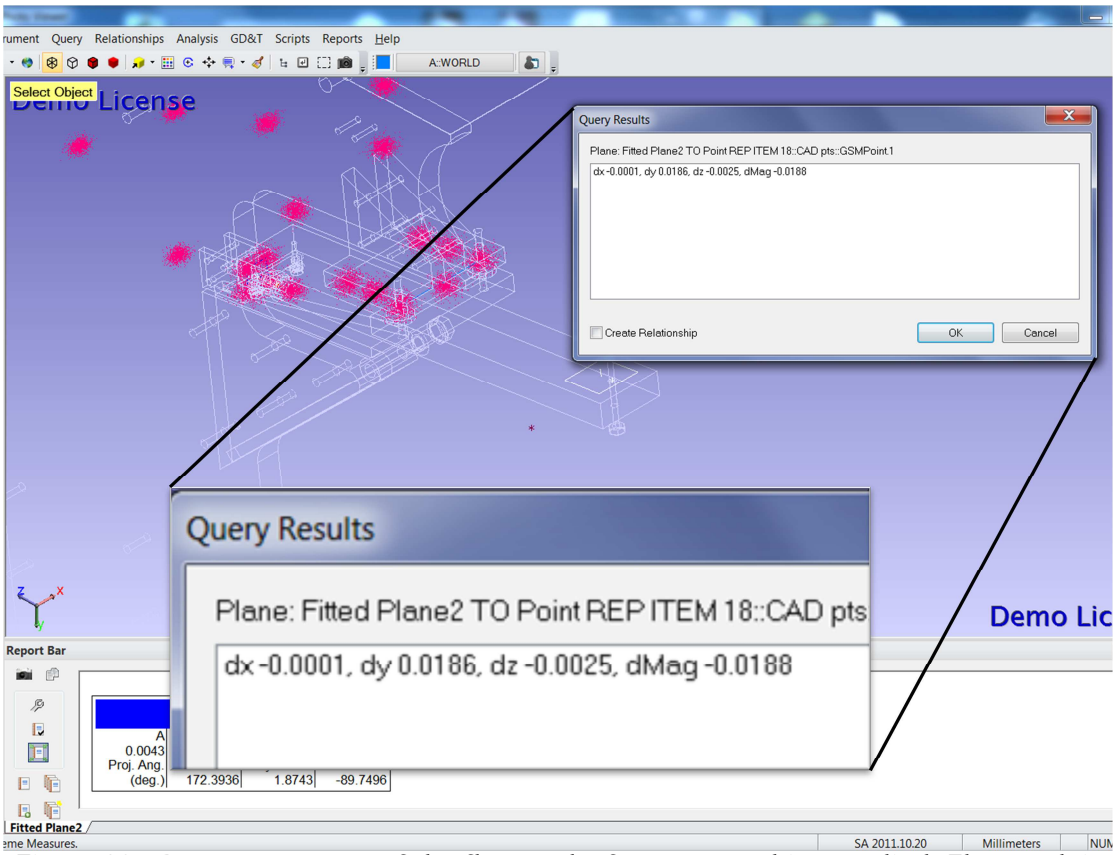

Figure 82 – Re-measurement of the flap track after correct shims applied. Flap track is within 20µm of the predicted position.

4.3.3. Vestas Modular Blade Assembly Interface Modelling

4.3.3.1. Introduction

Vestas have traditionally built entire wind turbine blades in large full length moulds. As the diameter of wind turbines have grown from 60 to more than 100 metres, the traditional methods of manufacturing could potentially become unsustainable. Vestas research and technology UK has therefore been studying the possibility of building blades from components made using smaller moulds.

The goal of this analysis is to reveal the impact of part and assembly tolerances of a multi-component blade on its final assembled geometry, hence its aerodynamic and structural performance. Further, the analysis is used to determine whether the use of an integrated metrology assisted production system can be used to improve the quality of the final component, and reduce tooling cost.

The following blade assembly scenarios are analysed:

- Without integrated metrology

    - Without additional LE (Leading Edge)/TE (Trailing Edge) twist tooling
    - With additional LE/TE twist tooling
- With integrated metrology
    - Without additional LE/TE twist tooling
    - With additional LE/TE twist tooling

4.3.3.2. Problem Definition

4.3.3.2.1. Geometry Description

A CAD drawing of the Vestas blade assembly test prototype is shown in Figure 83 and Figure 9. It is approximately 12 metres long, and has a chord of 2.4 metres at its widest end. The prototype will be assembled in a test assembly jig, to study the feasibility of automated assembly of a 36 metre long blade from 12 metre sections.

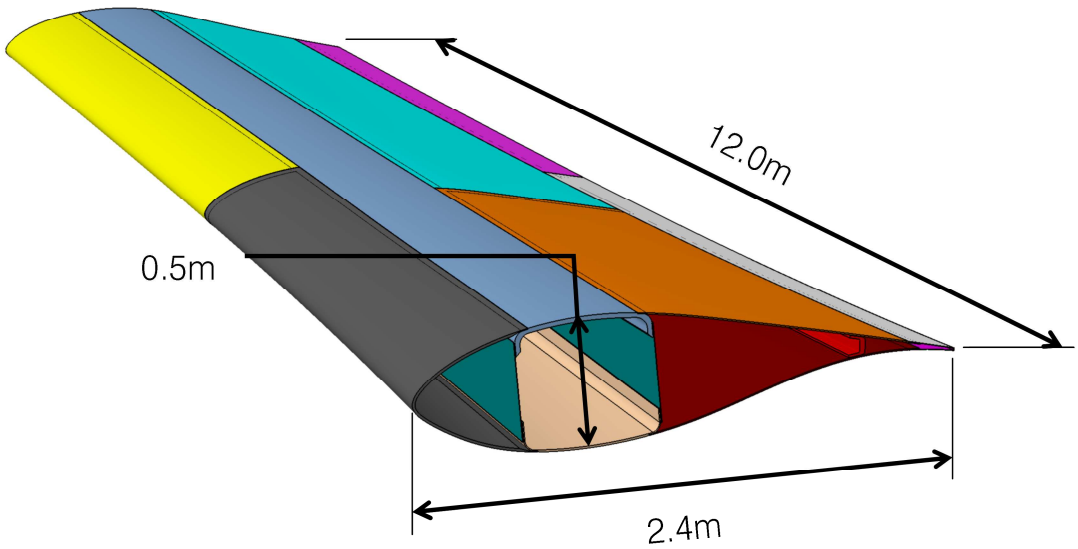

Figure 83 - The test assembly blade section and approximate dimensions

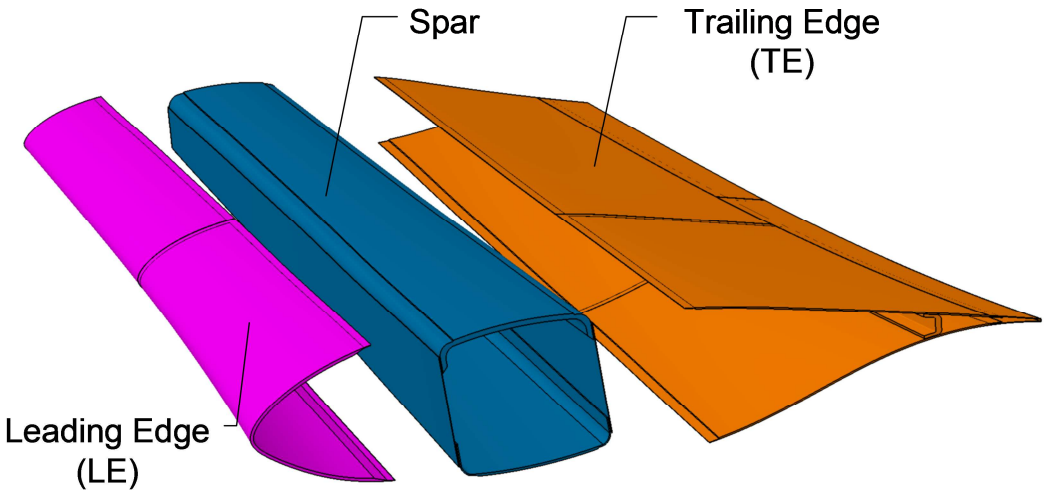

Figure 84 - Parts to be assembled in the assembly jig

In this analysis, the leading edge and trailing edge components are assumed to be single one-piece parts (Figure 84), since the gap between the LE TE and the spar are of more interest than the gap between the separate LE and TE pieces. Specifically, through modelling of the interactions of the leading edge (LE) and trailing edge (TE) components with the spar, a prediction of the expected gap size can be produced. Using the gap information, the LE and TE position and twist uncertainties, as well as their impact on the airfoil profile can also be calculated. The areas of particular interest are illustrated in Figure 85.

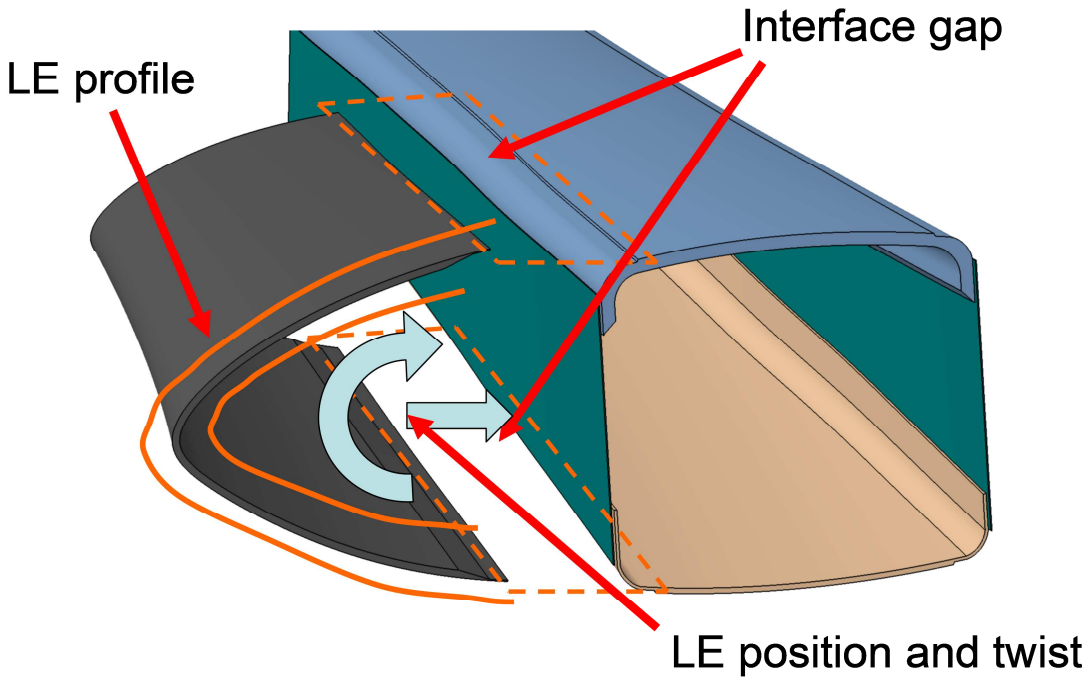

Figure 85 - Areas of interest analysed

A detailed view of the joint between the spar with LE and TE is shown in Figure 86. During the assembly process the complete spar is first fixed to the jig, and is held in place by suction pads on attached to the lower spar cap. The LE and TE are then assembled to the spar. The LE and TE have extensions that fit into recesses in the top and bottom spar caps, and are fixed in place using adhesive.

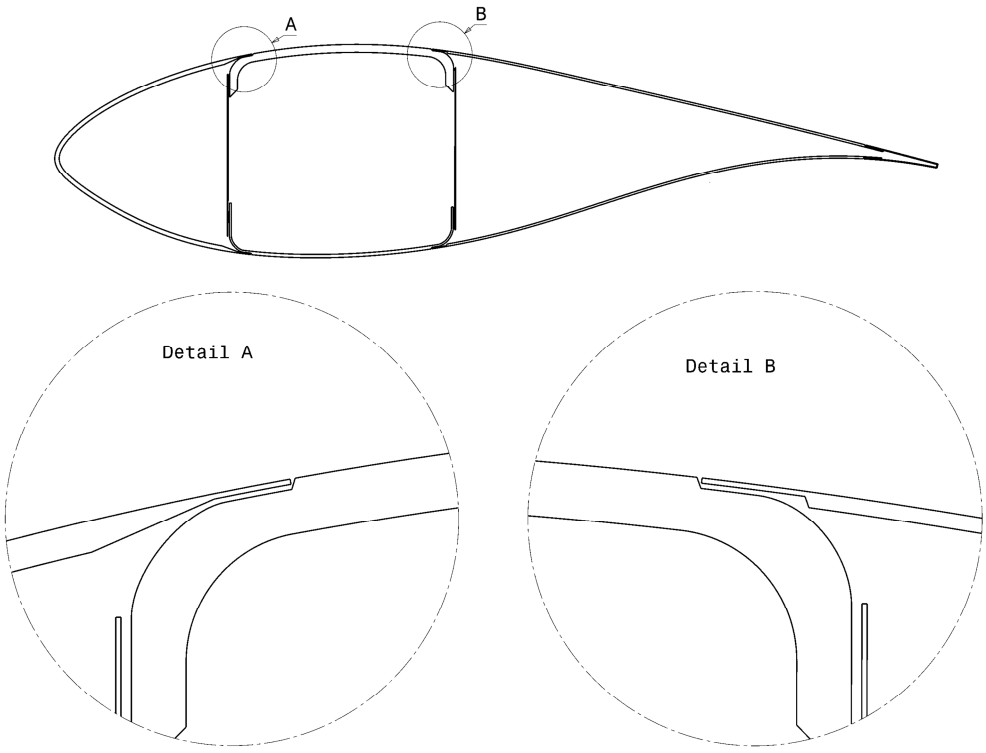

Figure 86 - Cross-section view of the component interfaces

The gap and flush conditions of the interface between the LE and TE extension and the spar cap recess are critical to the aerodynamic and structural performance of the blade. The interface gap must be minimized, and any step conditions must be avoided completely. In the "Build to nominal" scenario, both the spar recesses and the TE and LE extensions may need to be built to very tight tolerances. The tooling required for this scenario may end up being prohibitively expensive. Therefore it was proposed to use a large volume metrology system to measure the spar as it is positioned in the jig, and machining the LE and TE extensions to the measured data, thereby sidestepping a large part of the tooling tolerance requirements.

Another significant factor affecting the gap sizes is whether the LE and TE components are allowed to twist along the axis of the blade, the advantages and disadvantages of allowing twist are:

Advantages:

- Optimal for controlling gap uncertainty
- Flexibility in tooling for design changes

Disadvantages:

- Increases airfoil profile camber uncertainty which can have an effect on performance
- Potentially more expensive tooling

The decision to use or not to use tooling with built-in twist capability should be based on whether the uncertainty in the airfoil profile or the uncertainty in the gap size will have the most impact on the performance of the blade, and whether flexibility is more important than cost. The simulation described in here will attempt to produce more scientific answers to how much geometric uncertainty is to be expected under the various scenarios.

4.3.3.2.2. Simplified Geometry for Simulation

For the ease of simulation, the fairly complex 3D geometry is reduced to simpler 2D approximations. First, the nominal interface profile is assumed to be a straight line, and the interface problem is reduced to 2D (Figure 87). This is a valid approximation because the interface is basically a straight line, and the parts have the same degrees of freedom as a 2D simulation, due to the way they are held in place in the assembly jig.

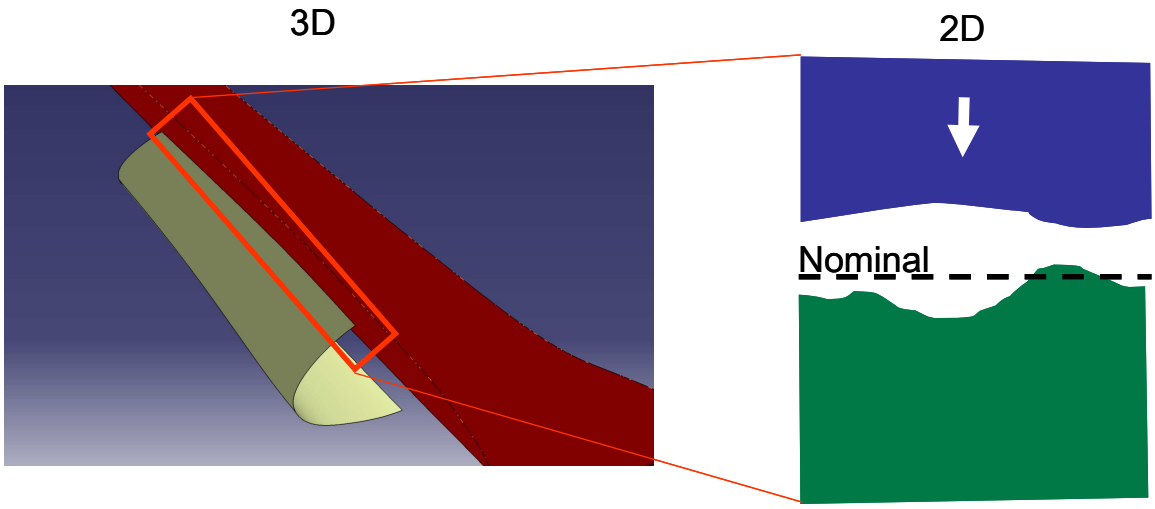

Figure 87- Simplification of 3D interface problem to 2D

In order to simulate the effect of the interface gap uncertainties, a simplified model of the blade is constructed, as shown in Figure 88. The leading edge of the blade is approximated by a quadratic equation, and the trailing edge is represented by a slender isosceles triangle. These representations can be easily substituted with real geometry if required in the future. The profile of the spar is not modelled, since it is outside the scope of this project.

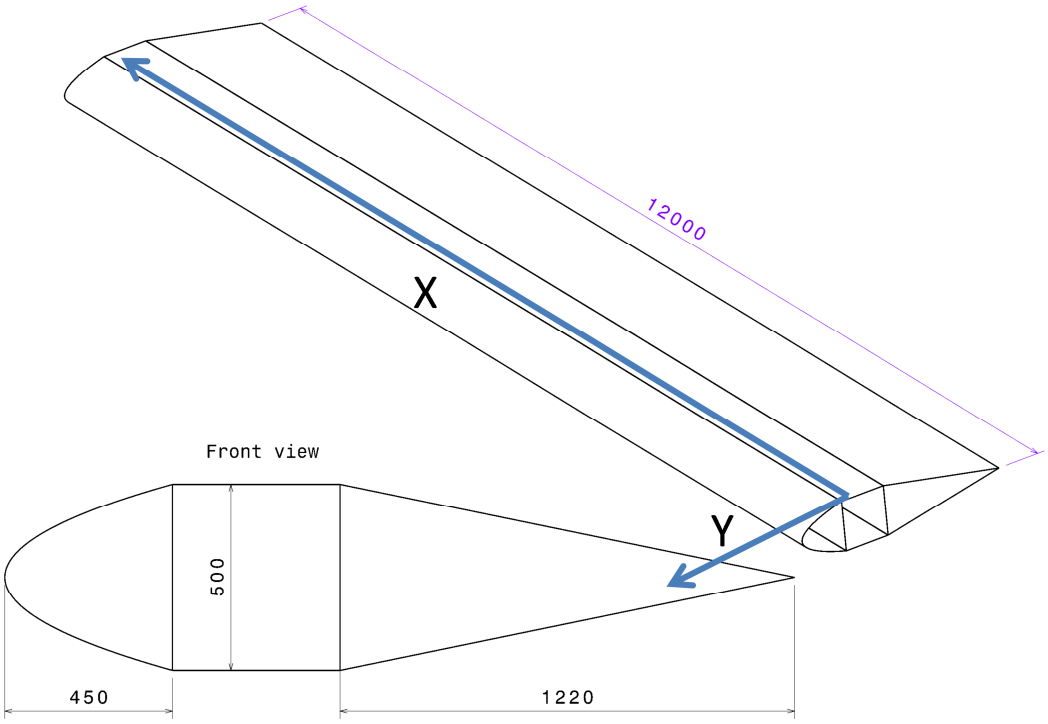

Figure 88 - Simplified blade geometry for airfoil profile uncertainty calculation (All units are in mm). The X axis of measurement coordinate system is aligned with the blade axis and the Y axis is tangent to the blade surface.

It is assumed that the blade has the same airfoil profile along its entire 12 metre length, and all parts are rigid. While the parts are large and flexible, since the parameter of interest is the gap between the LE/TE with the spar, the parts should have reasonable rigidity in the Y direction. Therefore the profile uncertainties should be the same everywhere along the blade.

4.3.3.3. Simulation Strategy

The overall strategy of the assembly uncertainty simulation is to solve the spar → LE (or TE) interface problem using Monte Carlo method. One of the Monte Carlo loops is illustrated in Figure 89.

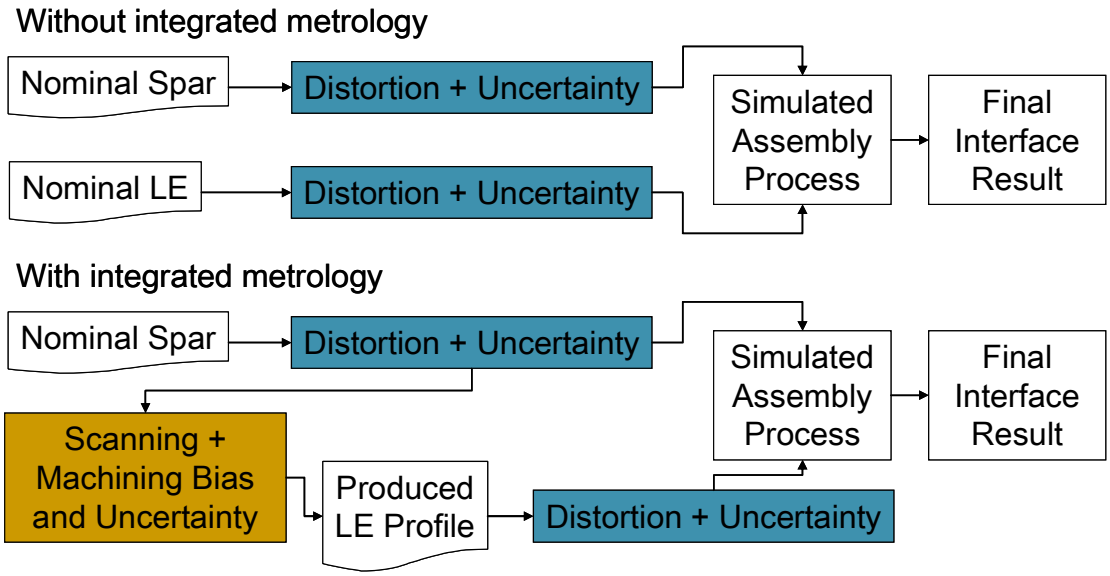

Figure 89 – High level uncertainty model flow chart for scenarios with and without metrology assisted trimming of leading edge

In the no integrated metrology scenario, distortions and noise are added to the nominal spar and LE (or TE) profiles. The generated parts then go through a simulated assembly process, in which a collision model is used to move the LE (or TE) interface profile towards the spar. The gap between the spar and LE can then be measured.

In the "with integrated metrology" scenario, the spar profile generation and assembly modelling is treated in exactly the same as the no metrology scenario, but the LE interface profile is generated from the spar profile by simulating a measurement of the spar, and a machining process from the measurement data. The resulting profile is then distorted and assembled to the spar.

The assembly process provides information on how much the LE interface is offset from the nominal position. Knowing this information for the top and bottom spar interfaces, the LE twist and or offset can also be calculated.

4.3.3.3.1. Interface model

Three sources of uncertainties are modelled when a spar or LE profile is generated:

1. Sinusoidal distortion with normally distributed amplitude
2. Normally distributed profile noise
3. Normally distributed disturbances in the locating the spar or LE in the jig

A graphical illustration of the effect of the three sources of uncertainty is shown in Figure 90.

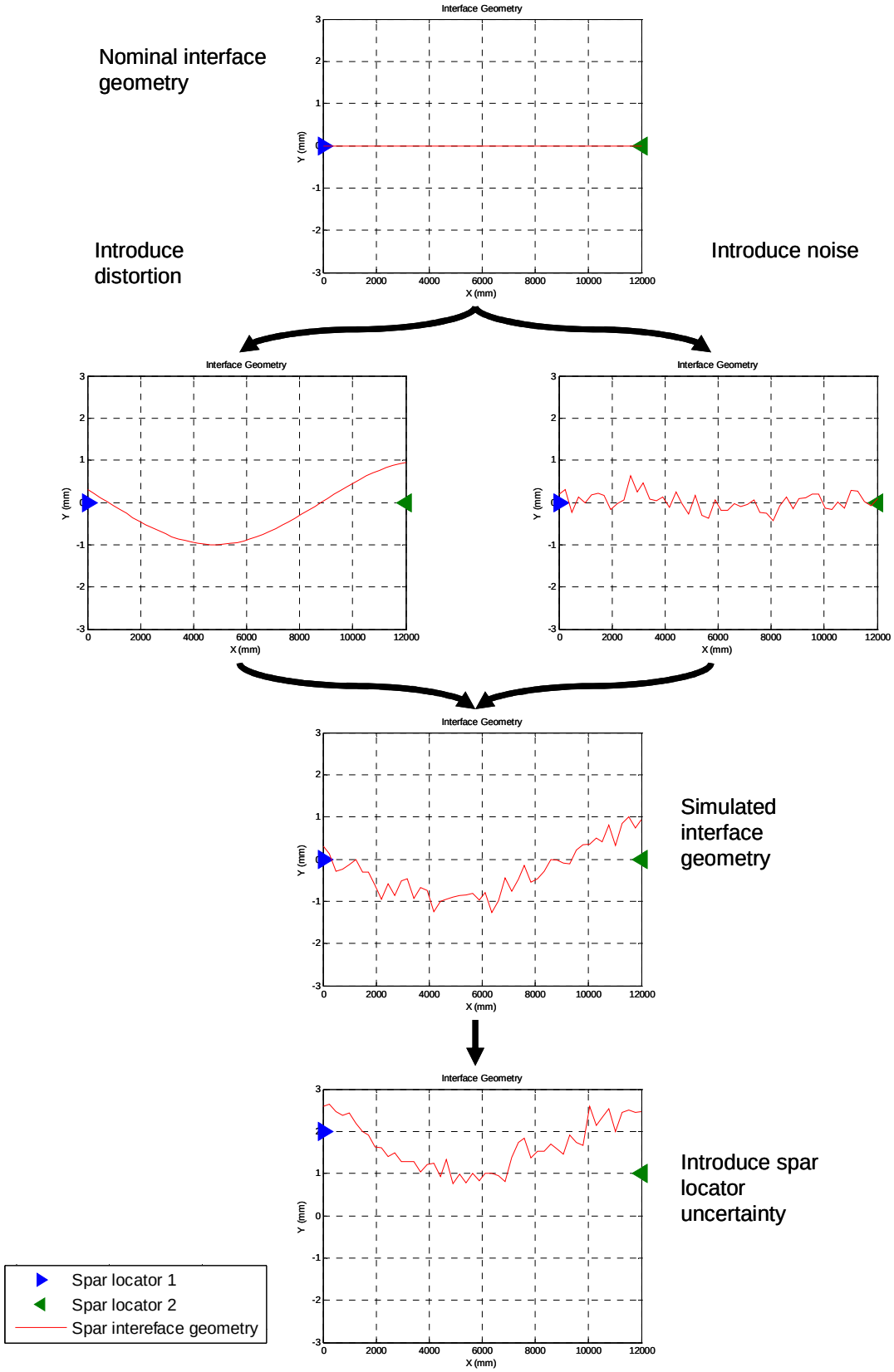

Figure 90 - A breakdown of uncertainty sources in the spar interface geometry model

4.3.3.3.2. Assembly modelling

The assembly model translates the LE profile in 2D until a collision with the spar profile is detected, as shown in Figure 91. The LE is not allowed to rotate in the 2D plane.

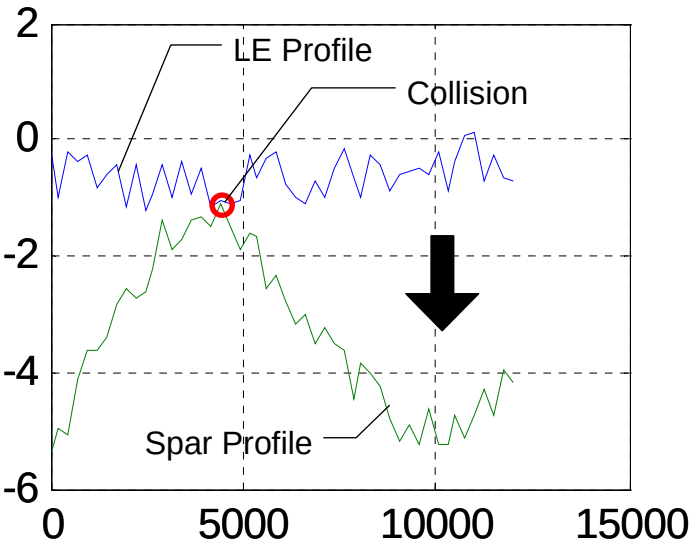

Figure 91 - Spar - LE collision in assembly modelling

The difference between the simulated translation of the LE and the nominal LE translation for the top and bottom interfaces is used to calculate the LE twist (see Figure 92). Or in the scenario in which LE twist is not allowed, the difference between the top and bottom offset is added to the smaller one in order to simulate a larger at one of the interfaces.

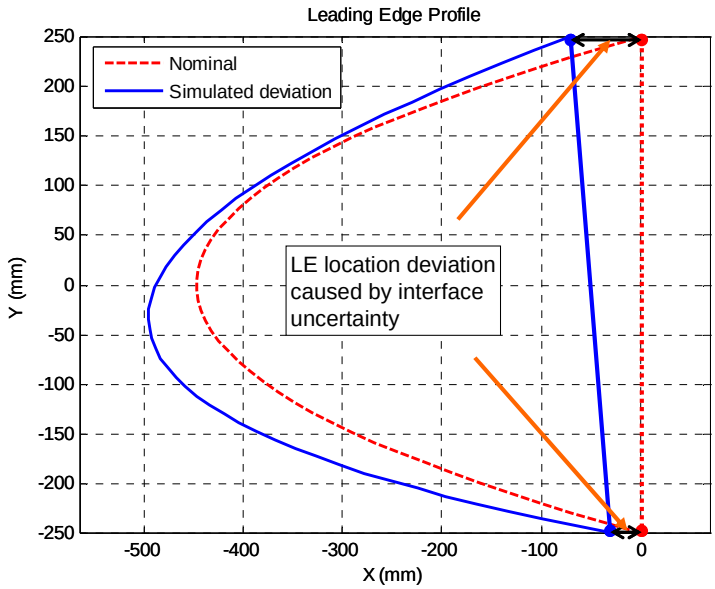

Figure 92 - Leading edge profile deviation as a result of the LE-spar interface uncertainties, the trailing edge is modelled similarly

4.3.3.3.3. Integrated metrology model

In the integrated metrology model, a simulated measurement and trimming operation is performed by introducing additional uncertainties to the spar profile to create the LE profile, instead of generating the LE profile independently.

There are a total of three sources of uncertainties that are simulated in the integrated metrology model:

1. Normally distributed combined metrology instrument and machining uncertainty
2. Normally distributed combined metrology instrument and machining registration/locator bias
3. Sinusoidal distortion with normally distributed amplitude to simulated distortions after the trimming process

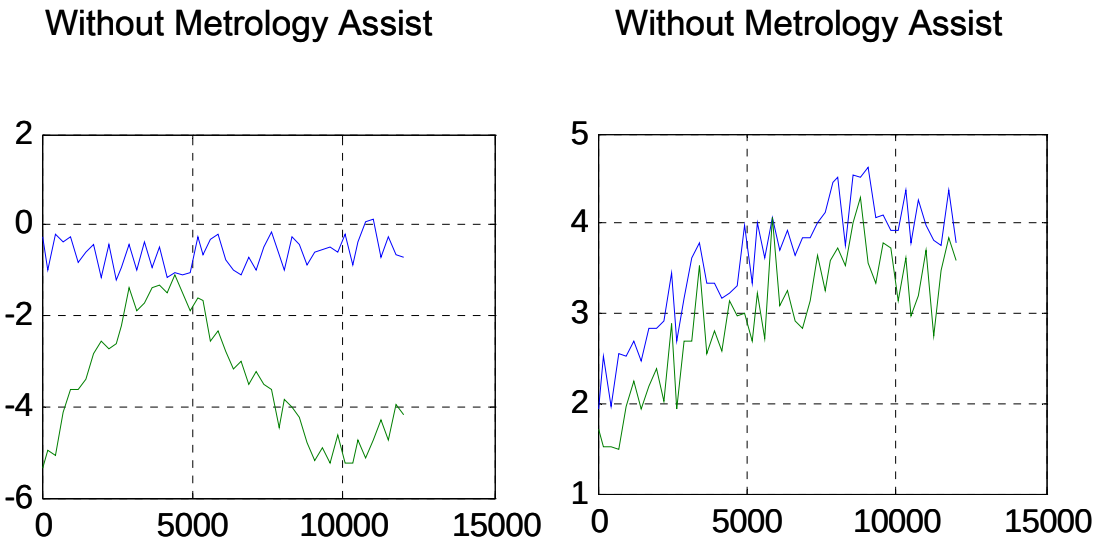

Figure 93 - Typical generated interface assembly solutions

A comparison of typical interface assembly simulations with and without integrated metrology is shown in Figure 93. Since the LE is produced from the spar data, it generally matches the spar profile better, even though it has more parameters of uncertainty associated with it.

4.3.3.3.4. Model inputs, assumptions and limitations

All of the input values for the various component uncertainties are summarized in Table 8.

Table 8 - Summary of simulation input variables

Without integrated metrology			With integrated metrology		
Variable	**Value**	**Description**	**Variable**	**Value**	**Description**
Spar interface noise	0.2 mm	1 sigma, normally distributed	Spar interface noise	0.2 mm	1 sigma, normally distributed

Spar interface distortion amplitude	1.0 mm	1 sigma, normally distributed	Spar interface distortion amplitude	1.0 mm	1 sigma, normally distributed
Spar distortion wavelength	6000-36000 mm	Discrete uniform distribution	Spar distortion wavelength	6000-36000 mm	Discrete uniform distribution
Spar locator uncertainty	1.0 mm	1 sigma, normally distributed	Spar locator uncertainty	1.0 mm	1 sigma, normally distributed
LE interface noise	0.2 mm	1 sigma, normally distributed	LE combined metrology instrument and machining uncertainty	0.25 mm	1 sigma, normally distributed
LE interface distortion amplitude	1.0 mm	1 sigma, normally distributed	LE post trimming distortion amplitude	0.5 mm	1 sigma, normally distributed
LE distortion wavelength	6000-36000 mm	Discrete uniform distribution	LE post trimming distortion wavelength	6000-36000 mm	Discrete uniform distribution
LE locator uncertainty	1.0 mm	1 sigma, normally distributed	LE combined metrology instrument and machining registration and locator bias	0.5 mm	1 sigma, normally distributed

Model assumptions and limitations

- All parts are assumed to be rigid
- All the nominal interface profiles are assumed to be 2D straight lines.
- The LE and TE is not allowed to rotate (about the turbine axial direction) during assembly
- Simple 2D geometries are used to represent LE and TE profiles
- The airfoil profile is assumed to be the same along the length of the blade

4.3.3.4. Analysis Results and Conclusions

4.3.3.4.1. Interface gap results

The overall shape of the distribution of gap sizes along the interface is plotted in Figure 94. The gap sizes appear to follow a one-sided Rayleigh distribution, and they are less spread out in the with integrated metrology scenario than the without integrated metrology scenario.

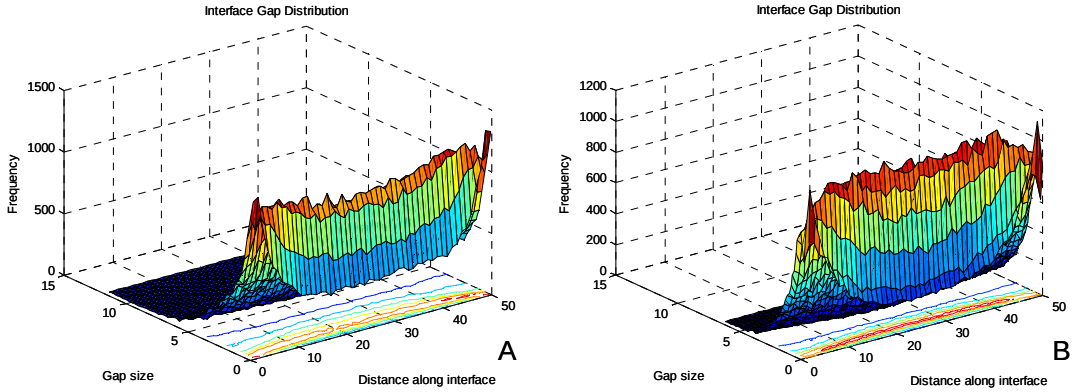

Figure 94 - Plot of the distribution of gap sizes along the interface. A) Without integrated metrology, B) With integrated metrology.

The differences between with and without metrology case can be seen more clearly in Figure 95.

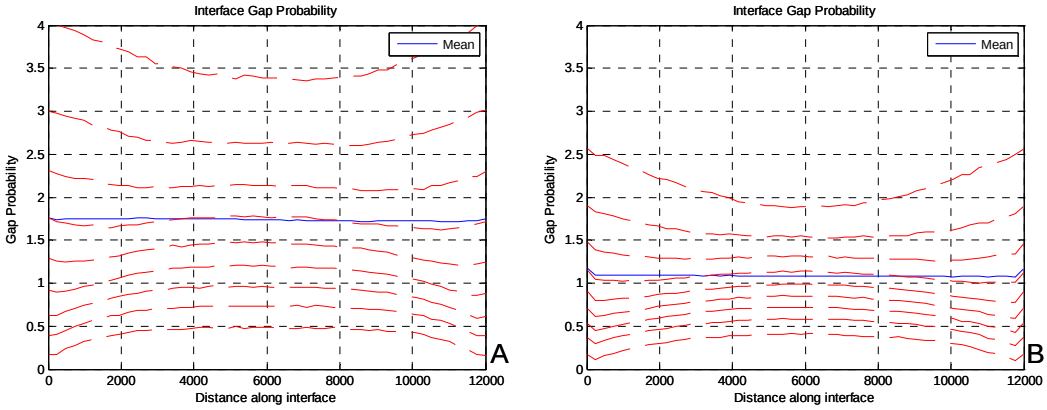

Figure 95 - Gap probability distribution along the length of the interface. Each red dashed line represents 10% of all results. A) Without integrated metrology, B) With integrated metrology.

90% of the gaps in the with metrology scenario are below 2.5 – 2 mm, while 90% of the gaps in the without metrology scenario are blow 4 – 3.5 mm. Therefore if 2mm was the upper specification limit, the integration of metrology will result in approximately 10% of rejects, compared to more than 30% in the no metrology scenario. Therefore the integration of metrology produces significantly better results in gap size control.

If the LE and TE are not allow to twist, then typically only one side of the LE or TE extensions will contact the spar recess (the “interfering side”), and result in a larger gap on the side that is not contacting the spar (the “non-

interfering side"). The difference in the gap size distributions of the interfering and non-interfering side are plotted in Figure 96.

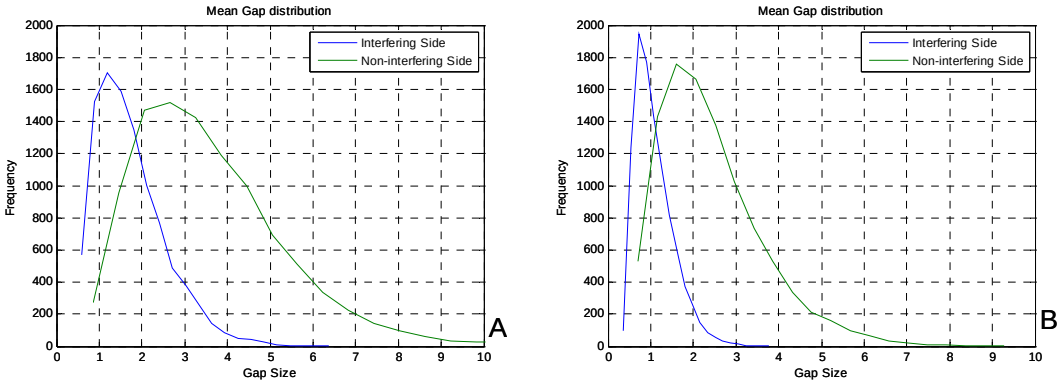

Figure 96 - Mean gap sizes of the interfering and non-interfering interfaces. A) Without integrated metrology, B) With integrated metrology.

Again, the benefits of integrated metrology assisted trimming are clear. In fact, at 3 sigma, the non-interfering side gaps for the with metrology scenario are within 7.7mm, compared to 11.6mm for the without metrology scenario.

4.3.3.4.2. Leading edge and trailing edge profile results

If the leading edge and trailing edge are allowed to twist to reduce the gap size, their twist distributions will look like Figure 97.

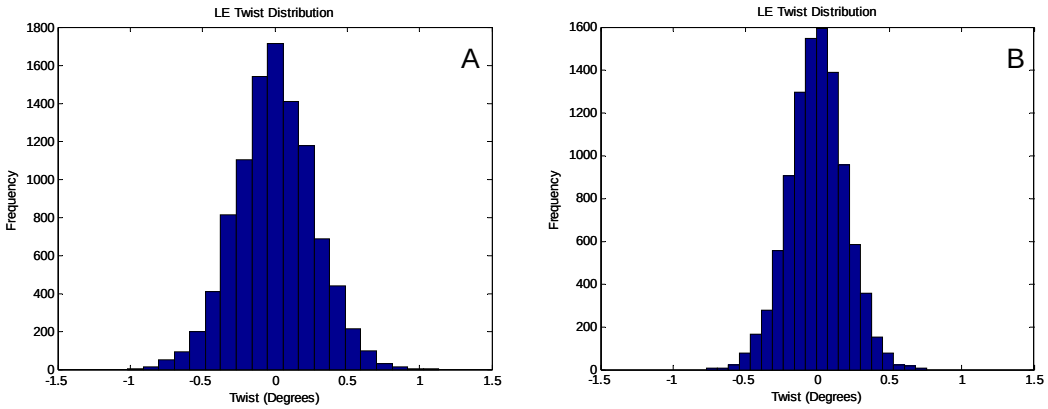

Figure 97 – Twist distributions as a result of top and bottom interface uncertainties. A) Without integrated metrology, B) With integrated metrology.

As a result of the reduced gap sizes, the twist distribution is also better for the integrated metrology case.

The leading edge and trailing edge profile 3-sigma uncertainties are plotted in figures Figure 98 and Figure 99 respectively. Note that in general, twisting the LE and TE causes the profile uncertainty to increase in the up and down direction, where as not allowing twist increases the uncertainty at the tips of the LE and TE. As in the previous results, the profile uncertainties are significantly reduced in the with integrated metrology scenario.

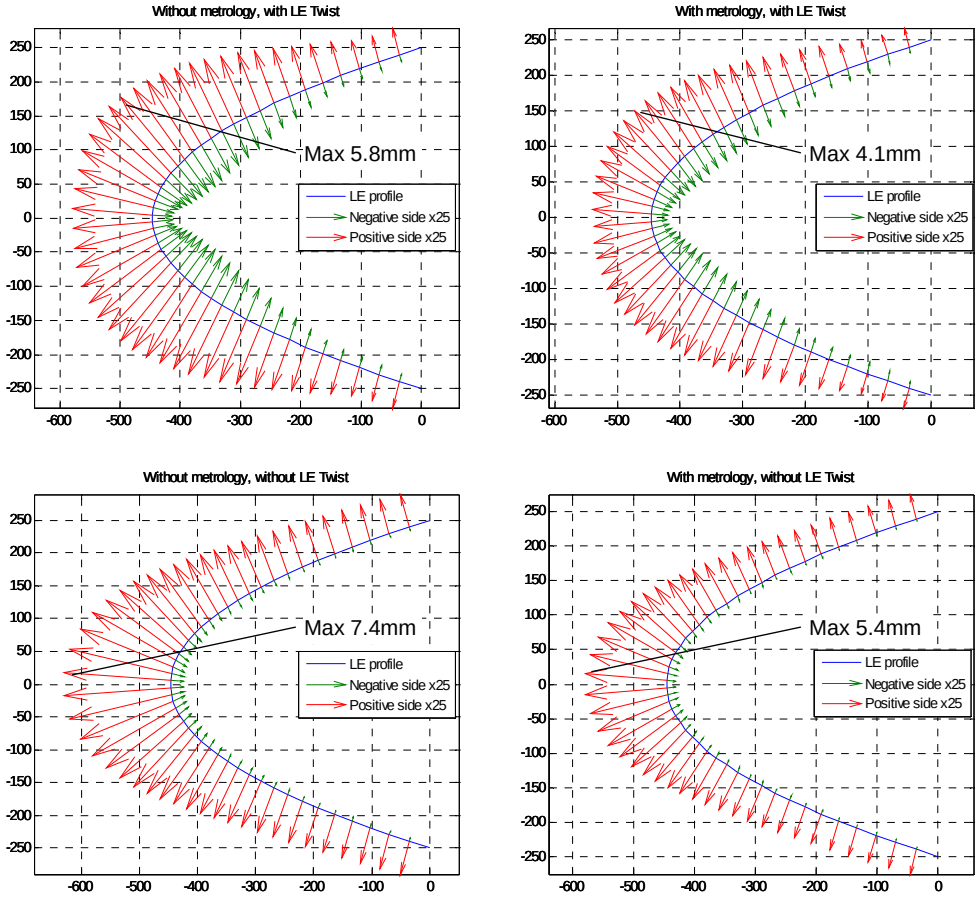

Figure 98 – 3 sigma leading edge profile uncertainties for the four scenarios.

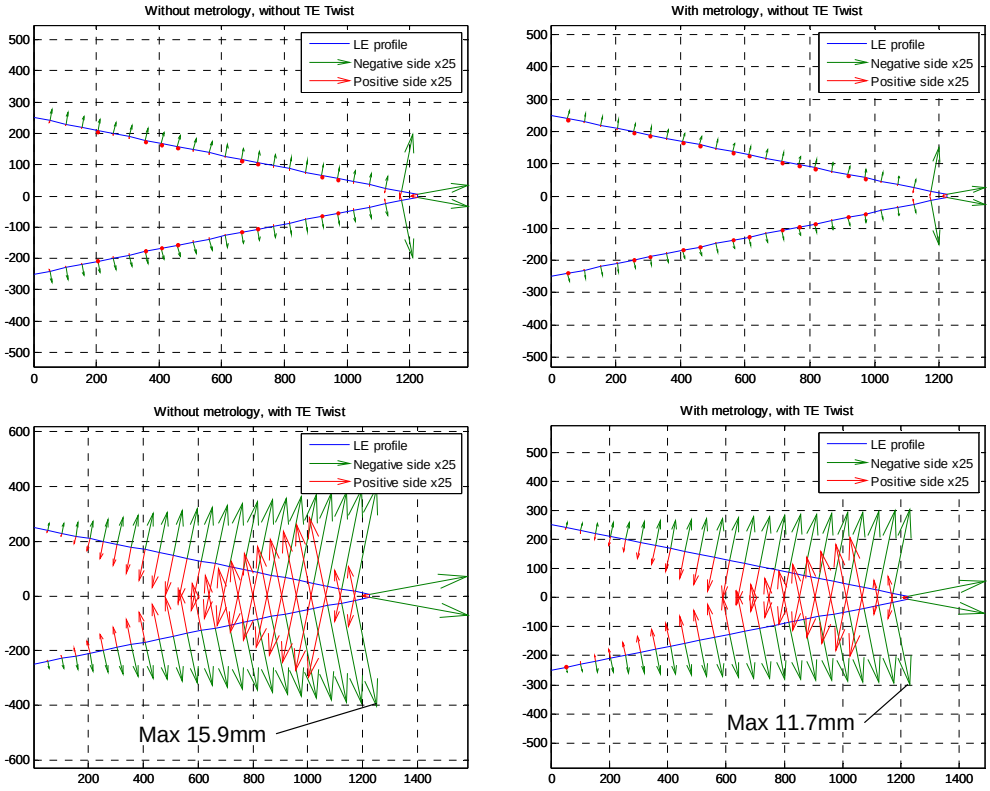

Figure 99 – 3 sigma trailing edge profile uncertainties for the four scenarios.

Using these results, the aerodynamics and structures design teams can make a more educated decision on whether twisting of the leading edge and trailing edge should be allowed in the assembly system.

4.4. Summary and Discussions

In this chapter, digital simulations of metrology assisted assembly using the Monte Carlo method are explored. Three case studies showing in detail the applications of the simulations are described. This demonstrates that the stream of variations approach used to analyse assembly variability can be adopted to take into account of integrated metrology systems along with fixture and part variations.

These simulations provide the decision makers predictions of the process capability before committing to the physical construction. They enable the production engineers to experiment with “what if” scenarios, such as in the case of Vestas modular blade assembly, comparing the difference in the final product quality with or without the integration of metrology.

In the IntEq case study, it was demonstrated that is it possible to inject measurement data directly into the assembly model such that it can be used during production to ensure that the assembly is accurate and optimal. This represents a transformation of assembly modelling from strictly a planning tool to an essential part of the assembly process.

5. New Large Volume Technologies for Measurement Assisted Assembly

5.1. Introduction

In chapter 4, methods and case studies of mathematical simulations of metrology assisted assembly are presented. In this chapter, practical methods of implementing such systems will be studied.

Since the aim of this research project is to study real-time metrology integration, this chapter will specifically focus on methods and demonstrations of interfacing with metrology instruments in real-time, and using the real-time data for control.

The difference between real-time integration and the more traditional off-line integration as described in chapter 3 is that the former can detect any errors during production processes and correct them while the process is underway. This can potentially guarantee the product quality, and therefore eliminate rejects which can be very costly to rework.

Being able to track the errors *during* production necessitates the *dynamic* measurements of tools and/or parts that are moving. The dynamic capability of LVM instruments is one area that has not been explored very extensively, without existing international standards on its assessment or even definition. Therefore instrument dynamic capabilities need to be better understood before using them for real-time control.

Efforts in attempting to determine the dynamic performance of laser tracker and indoor GPS systems will be presented in the first part of this chapter, following which the initial development of real-time metrology driven automation will be described. Lastly, the development and characterization of a novel MAA technology demonstrator concept will be presented in the final section of this chapter.

The dynamic performance study was conducted at the University of Bath in collaboration with Luka Mastrogiacomo of Politecnico di Torino.

5.2. Dynamic Performance of iGPS and Laser Tracker

5.2.1. Introduction

LVM instruments are traditionally used for static measurements, and their accuracy specifications are typically given by the instrument manufacturers for static measurements. There is little to no information on the dynamic tracking performance of most of the instruments.

The accurate tracking of moving objects is a complex problem. It has wide applications in industry, including robot guidance, motion analysis and machine tool calibration. Dynamic tracking measurements are typically conducted using laser trackers or photogrammetry [39, 37, 27, 28 and 40]. While these systems have excellent performance, they are usually restricted by the number of points that can be measured simultaneously (laser tracker), and their volume of measurement (laser tracker and photogrammetry). Additional systems must be purchased in order to increase the coverage in volume and/or number of points, at very high cost.

The indoor GPS system was proposed as a potential solution to provide cost effective dynamic 6 degree of freedom measurements, possibly replacing the traditional laser trackers.

The experiments described in this section attempts to study and analyze the dynamic repeatability [54] measurement capabilities of the iGPS, comparing them with the performances of a laser tracker under the same experimental conditions.

5.2.2. Equipment Description

5.2.2.1. iGPS

The iGPS can be used to perform either static or dynamic measurements. However, due to the positioning method used, it is believed that degradation in accuracy will occur under dynamic conditions. The transmitters' sampling rate depends on the angular speed of their rotating heads. As explained above, the spinning speed is also the unique 'ID' for each transmitter. Given that the rotation speed is around 3000 rpm, each transmitter will be able to communicate with sensors at approximately 50Hz. Even though differences in the transmitters sampling rate are small, it is impossible to receive concurrent data from all transmitters. The inevitable difference in data streaming is in the range of a few hundredths of a second. This effect does not create any problem for static measurements, but it will affect dynamic measurement. Figure 100 shows

such a scenario, in which a sensor is moving in time (t). The position of the moving sensor is calculated by triangulating data collected in quick succession, but while the receiver is moving.

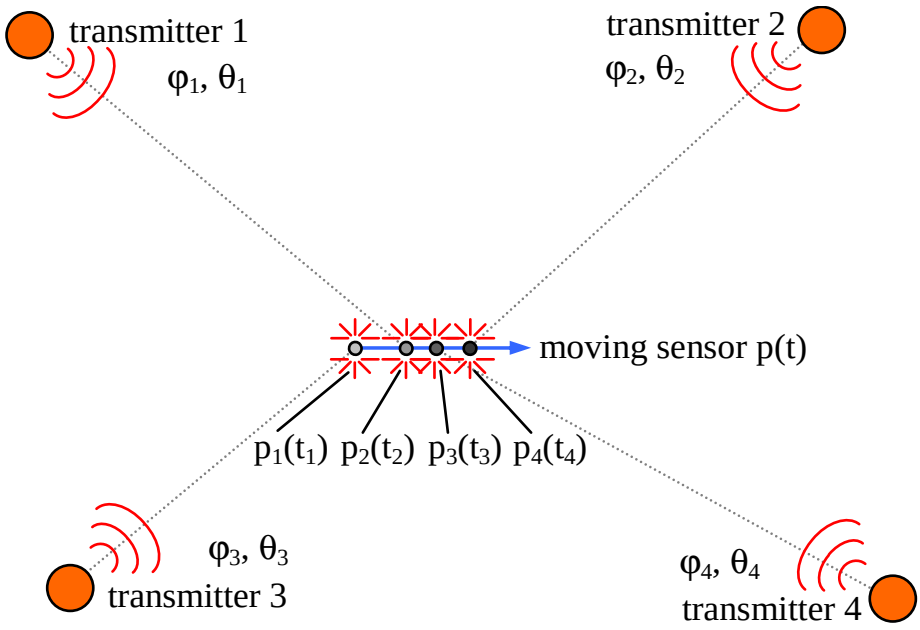

Figure 100 - If the sensor is moving, pulses from transmitters are received in different instances in time and space.

It can be assumed for the purpose of discussion that the data collection occurs by sensing information received firstly by transmitter-1, secondly by transmitter-2, thirdly by transmitter-3 and finally by transmitter-4. At time t_1, a moving sensor's angles to the corresponding transmitter are read when it is located in position p_1, at time t_2, when it is in position p_2 and so on. Even if the difference consists of a few hundredths of a second, because the angles no longer resolve to correct position, location errors are produced. It is hypothesised that the faster the sensor moves, the larger this dynamic error likely will be.

5.2.2.2. Laser Tracker

The FARO Tracker SI using in this experiment has a single point angular accuracy (2 sigma) of 18μm + 3μm/m, and distance accuracy (2 sigma) of 20μm + 1.1μm/m in ADM mode. [21]

5.2.2.3. Industrial Robot

An industrial articulated robot in the laboratory was used to generate the trajectories for the experiment. The robot offered a fast and simple way of generating a number of test trajectories, and the speed of the movement can also be easily altered.

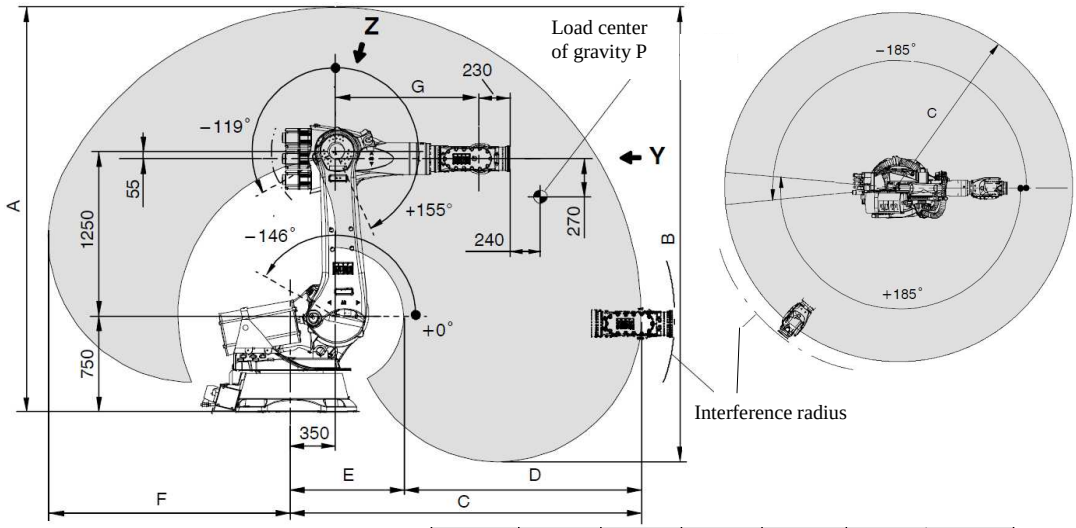

A	B	C	D	E	F	G	
3100	3450	2700	1875	825	1788	1100	[mm]

Figure 101 - Drawing of the working envelope of the KR240-2. [55]

The KUKA KR240-2 (Figure 101) robot used in this experiment has a static point repeatability of ±0.12mm, and maximum movement speed of 2m/s. A two hour static repeatability test conducted on the robot before the experiment using a grid of 30 points in the robot working volume confirmed that the repeatability of the robot is within the manufacturer's specifications [56]. The details of this test are described in section 3.2.

5.2.3. Equipment Setup and Experiment Procedure

5.2.3.1. Equipment Layout

The measurement instruments are arranged as shown in Figure 102. The laser tracker is placed approximately 4 metres from the robot base. The iGPS transmitters are arranged in a 'C' shaped network approximately 6-7 metres from the robot base. The lengths of the robot trajectories are approximately 1m, 1.7m and 0.75m for X, Y and Z respectively (see Figure 102).

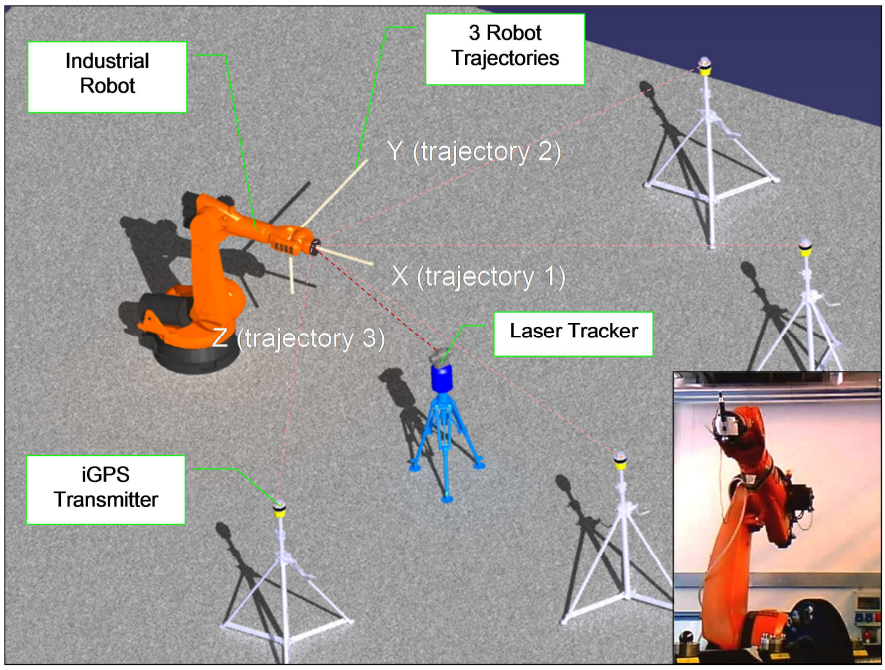

Figure 102 - Approximate experiment layout illustration, and picture of the robot carrying the iGPS vector bar

The iGPS transmitters' positions in the network were calculate through a bundling, procedure. For this experiment, 8 points in the working volume are measured using the vector bar, which provided enough angular and scale information for the software to solve for the transmitter positions. A more accurate scale bar was then setup using a two metres carbon fibre artefact from the National Physical Laboratory, which was measured using the laser tracker in interferometry mode. The measurement of the scale bar obtained using the iGPS was compare to that from the tracker, the ratio of the two measurements was used to rescale the iGPS network.

A 1.5 inch laser tracker SMR nest was attached to the end of the robot arm. The location of this nest is measured using a 1.5 inch SMR with the laser tracker, and the iGPS vector bar with a 1.5 inch tip probe (see Figure 102). The centre of the SMR was defined as the Tool Centre Point (TCP) of the robot.

Within the measurement range in the experiment, the laser tracker is expected to have a single point measurement uncertainty of 30-40μm (2 sigma) according to the manufacturer's specifications [21], and for similar sized network setups, the iGPS has been demonstrated to be capable of single point static uncertainties of 500-1000μm (2 sigma) [52]. While the static repeatability of the robot has been shown to be less than 110μm [56], its dynamic performance is unclear. Since it is expected that the iGPS dynamic error should be many times greater than that of the robot, the robot error should only contribute to a small portion of the final measured error.

5.2.3.2. Experiment Procedure

The industrial robot was programmed to repeatedly run through three mutually orthogonal linear trajectories (see Figure 102). Measurement data were collected at six robot movement speeds ranging from 1cm/s to 1m/s. In every program loop, each of the three trajectories was run twice, once forwards and once backwards. The program is looped 4-6 times at each robot speed. Reference data sets for each instrument were constructed from the slowest speed trials, which is then used as a basis for comparison with higher speed trials, such that the two instruments are not directly compared with each other, but to the reference data constructed by their own slowest runs.

A total of 64 sets of data were collected from the two instruments at six different speeds (1%, 10%, 30%, 50%, 75% and 100% of 1m/s) in three axis and two directions. The Z trajectory data was not available for 75% and 100% speeds, due to robot joint speed limitations.

5.2.4. Analysis and Results

5.2.4.1. iGPS Dynamic Bias

Recorded data from one of the linear robot trajectories (Y direction) at 1m/s speed, showing the effect of movement on the position of the Vector Bar as perceived by the iGPS software compared to the laser tracker data is shown in Figure 103. At the end points of the trajectory, speed is zero, the iGPS measurements are very close to that of the laser tracker. However, as the robot accelerates to the specified trajectory speed, clear biases are introduced into the iGPS readings. The direction of the biases appears to depend on the direction of the robot movement.

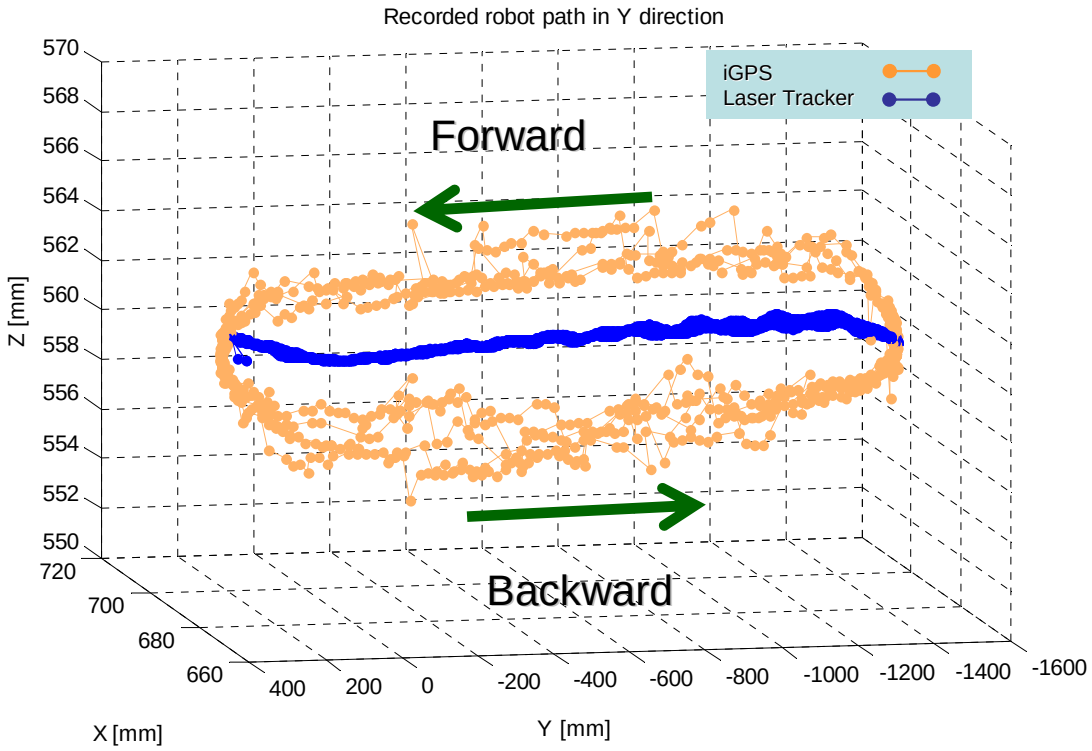

Figure 103 - Difference between iGPS and laser tracker measurements at 1m/s.

Please note Figure 103 is only included to illustrate the iGPS bias generated as a result of movement, not to make any statement about the relative accuracies of the iGPS compared with the tracker. Comparisons of accuracies require more rigorous methods of fitting to convert one instrument's coordinate system into the other. A simple linear least squares method using trajectory end points was used to create Figure 103.

5.2.4.2. Reference Line Generation

In order to generate a reference data set to enable the comparison between data recorded at different speeds, a line in 3D space is fitted to the data collected over 4-6 runs at the slowest speed (1cm/s) for each robot trajectory. The Robust Least Squares (RLS) fitting method was used to reduce the influence of outlier points on the fitting result [57].

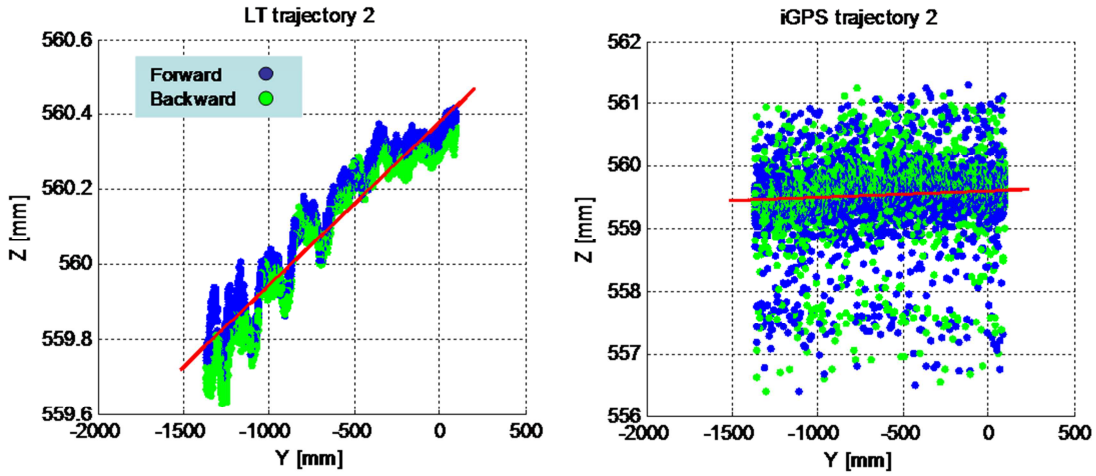

Figure 104 - Robust Least Squares (RLS) fitting of reference line. The first and last 150mm of data from each trajectory are deleted.

Figure 104 shows the result of the fitting for the Y trajectory. Since the robot took 100mm to accelerate to a constant linear speed at the TCP, the first and last 150mm of the trajectory were deleted before the data is further processed. This ensures that only the constant speed portions of the trajectories were compared to each other.

5.2.4.3. Reference Line Normal Projection

Due to the difficulties in quantitatively and qualitatively comparing large amounts of 3D point cloud data, a method is developed to visualise the differences in the recorded data.

Using the 3D reference line generated in 4.2 as the normal vector of a plane, it is possible to project the trajectory measurements on this plane. The coordinate system of the trajectory data is transformed into that of the reference line. The resulting 2D plot represents a view of the data down the reference line, as shown in Figure 105. Also included in the figure are standard deviation ellipses to aid visualization of the grouping of data for different speeds and directions of travel. In this figure, the forward movements along each trajectory are coloured from light green to cyan, and the backward movements are coloured from orange to pink. The colours differentiate the direction of travel and movement speed.

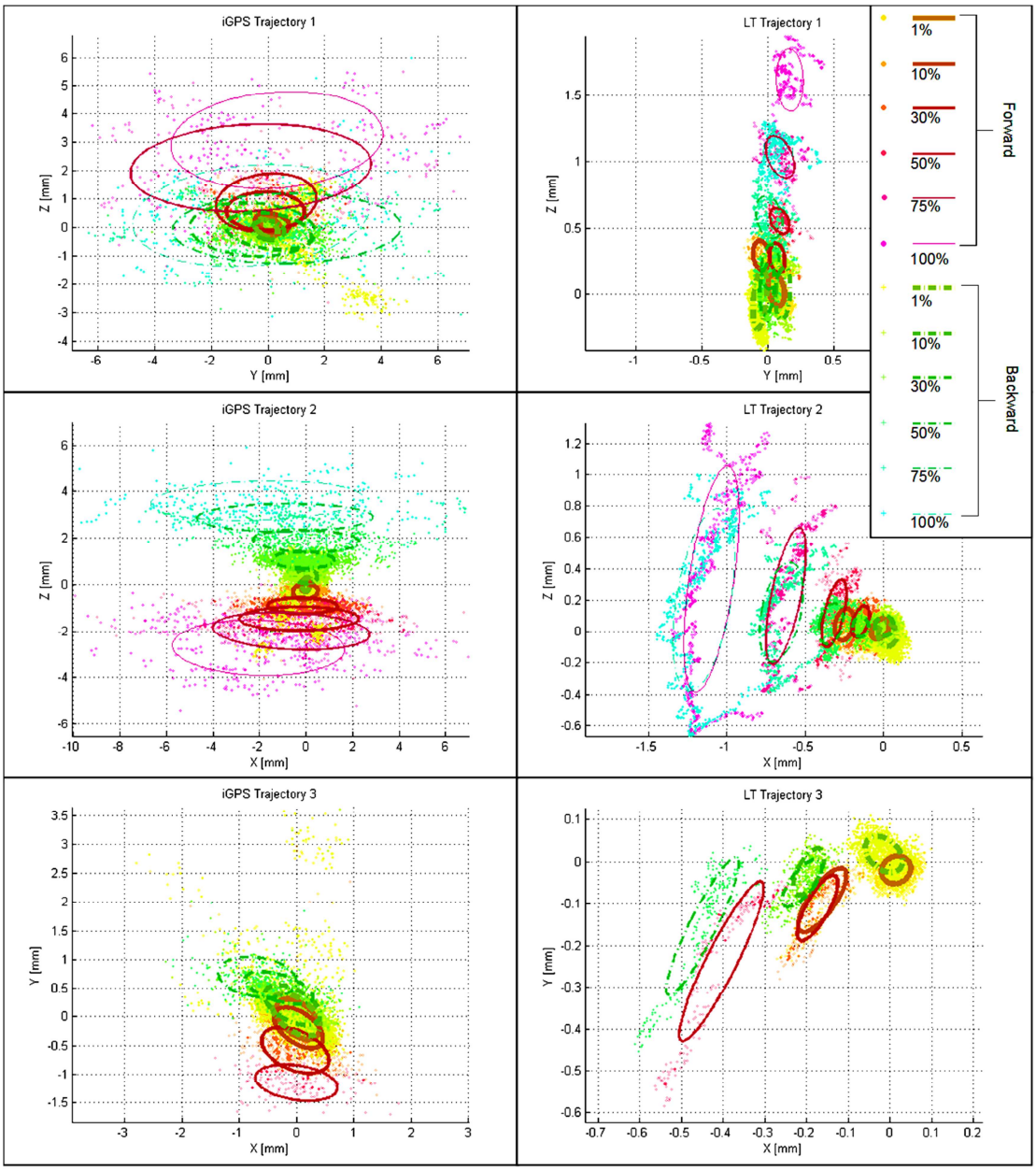

Figure 105 - Projected three trajectory measurements by the iGPS and laser tracker, including standard deviation ellipses. Percentages shown in the legend are robot speeds as a percentage of 1m/s.

A clear difference between the robot trajectory as measured by the laser tracker and the iGPS is the overall scatter of the data points. The distribution of the iGPS data is much wider than the laser tracker, with more outliers. It can also be seen that the iGPS appears to develop somewhat symmetrical biases about the reference line for opposite directions of travel. This effect is much less visible in the laser tracker data, in which the robot movement error is the predominant source of error, which increases with robot speed, but is fairly repeatable irrespective of the directions of travel.

The distribution of the distance of each measured point to the reference line at different robot speeds can be studied quantitatively by plotting their mean and distribution against speed, as shown in Figure 106.

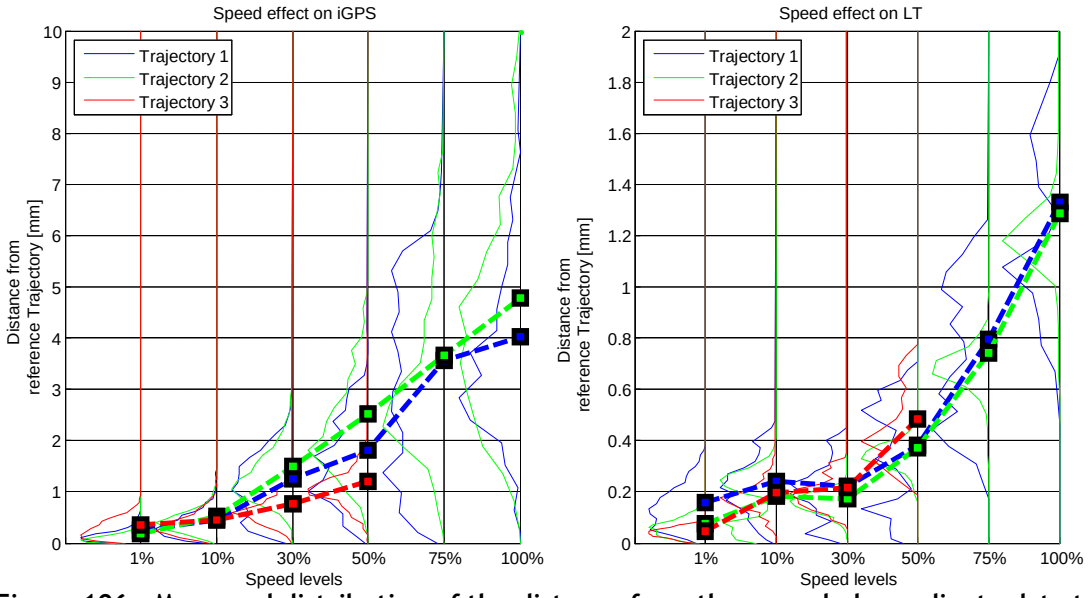

Figure 106 - Mean and distribution of the distance from the recorded coordinate data to the theoretical linear trajectories for iGPS and laser tracker. Percentages shown are robot speeds as a percentage of 1m/s.

As speed is increased, the accuracy of the robot, iGPS and laser tracker are degraded. It appears that at least up to 10cm/s, the iGPS is capable of providing tracking data affected by reasonably low variability and small bias. The iGPS is clearly more affected by higher robot speed, with distances from the reference trajectory up to 4-5mm at 1m/s compared to the 1.2-1.4mm of the laser tracker. The reason of this bias can be attributed to both the tracking instruments and robot movement inaccuracy.

If the robot paths are assumed to be repeatable between the laser tracker and iGPS trials, the amount of bias error introduced when the iGPS sensor is moving at 1m/s is expected to be at least 3-4mm on average.

On the contrary it is difficult to state something about laser tracker performances in dynamic conditions since we do not have any reference for a comparison, but given that the tracker accuracy is estimated to be in the range of 30-40μm [21], the tracker bias shown in Figure 106 is likely dominated by the error of the robot.

Considering the distribution of the distances from the reference trajectory, for both the laser tracker and the iGPS it is possible to notice a bimodal distribution due to the forward/ backward effect of robot movement discussed above. It is also evident how the data variance increases as the speed grows.

Although in general the repeatability of the measurements degrades as speed is increased, it can be said that iGPS and laser tracker have comparable repeatability performances up to speeds of 10cm/s. Then while the laser tracker keeps performing with a bias smaller than 1mm until 75cm/s, the iGPS performances quickly reach relatively high level of bias.

5.2.5. Summary and Conclusions

In this section, the experimental results of the dynamic performance tests of the iGPS metrology system is presented, and compared to the results of the same experiments conducted on a laser tracker. As expected the experiments showed that, a bias error is introduced to an iGPS sensor while it is moving at speed. The direction and magnitude of this bias appears to depend on the movement direction and speed. Further, it was determined that for speeds below 10cm/s, the iGPS is capable of producing relatively repeatable tracking data. However, as speed is increased, the tracking accuracy degrades. At 1m/s, the mean tracking error can be on the order of 3-4mm.

Even if laser tracker static and dynamic accuracies are generally better, the iGPS can be more convenient than laser tracker depending on the function and the speed of the points to be tracked. Furthermore the developers of the iGPS have informed the author that a new software system is being developed that may reduce some of the dynamic bias errors.

5.3. Interfacing with Metrology Instruments in Real-time

After studying the dynamic performances of iGPS and laser tracker, in this section software interfaces for retrieving the real-time data from the two instruments will be described.

Almost all LVM instruments are designed to work in Microsoft Windows PCs, using special software such as SpatialAnalyzer, PolyWorks, and Metrolog. There are two different paths that can be taken when developing software to interface with LVM instrument: establish communication through existing software such as SA (Figure 107), or communicate directly with the instruments using manufacturer supplied software development kit (SDK) (Figure 108).

There are two ways to communicate with the instruments through SpatialAnalyzer. One is using the SA SDK, which allows an external program to access the majority of the functionality of SA, including commanding the instruments. This approach is more powerful and flexible, it is also more difficult to use and requires more processing power, especially when measuring at a high sample rate. The second option is to use UDP (User Datagram Protocol) stream offered by SA, which is more lightweight, but also less flexible. This option is more useful for a real-time system.

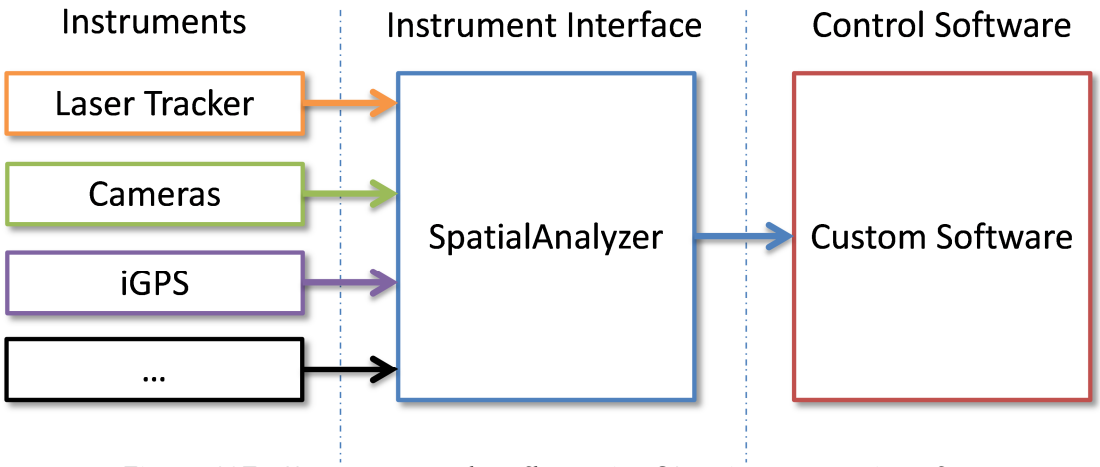

Figure 107 - Measurement data flow using SA as instrument interface

SA however, does not guarantee the real-time delivery of the UDP stream, and there maybe processing delays between SA receiving the data from the instrument and sending out the UDP. Therefore the developers of SA do not recommend using the UDP for real-time control.

Despite the limitations, because SA can communicate with a large number of instruments, it allows the instrument to be interchanged without having to rewrite the interface code, thereby saving considerable development time. It may be the preferred solution where data latency is not a critical consideration.

However, if minimal data latency *is* critical, the other option is to develop custom instrument interfaces using SDKs provided by each instrument manufacturer.

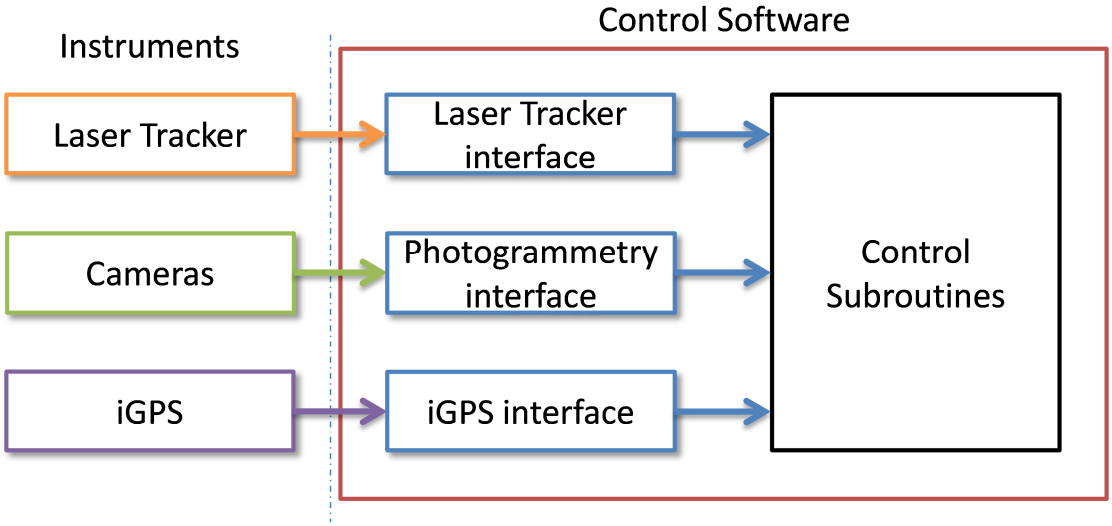

Figure 108 - Measurement data flow using custom instrument interfaces

Custom interfaces have the benefit of being able to directly access the instrument data, therefore reducing possible latency. They also allow greater control over the instrument functionality. Screenshots of the Faro

Laser Tracker and Nikon iGPS interface C# software developed for this research study are shown in Figure 109 and Figure 110.

The laser tracker interface is a C# program that sends basic control commands to the laser tracker, and receives position data through an Ethernet TCP/IP connection using the FARO laser tracker SDK.

The software has an option to log the measurement data, and to send the real-time data to the control software. The iGPS interface is very similar to the laser tracker interface, passing the coordinate and orientation data from the Surveyor software to the controller, using the iGPS Surveyor SDK provided by Nikon.

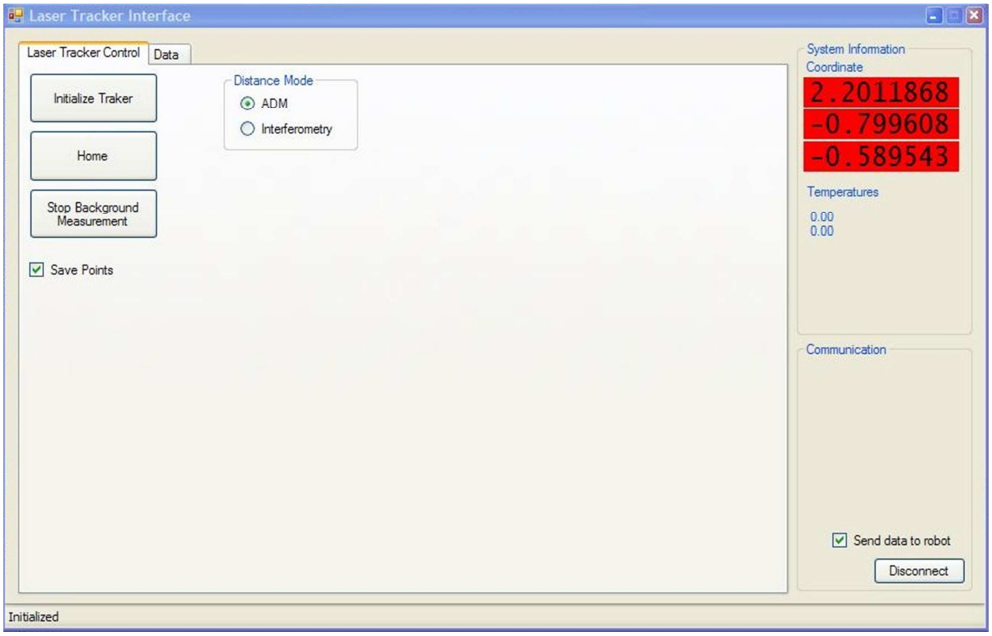

Figure 109 - Faro Laser Tracker interface software

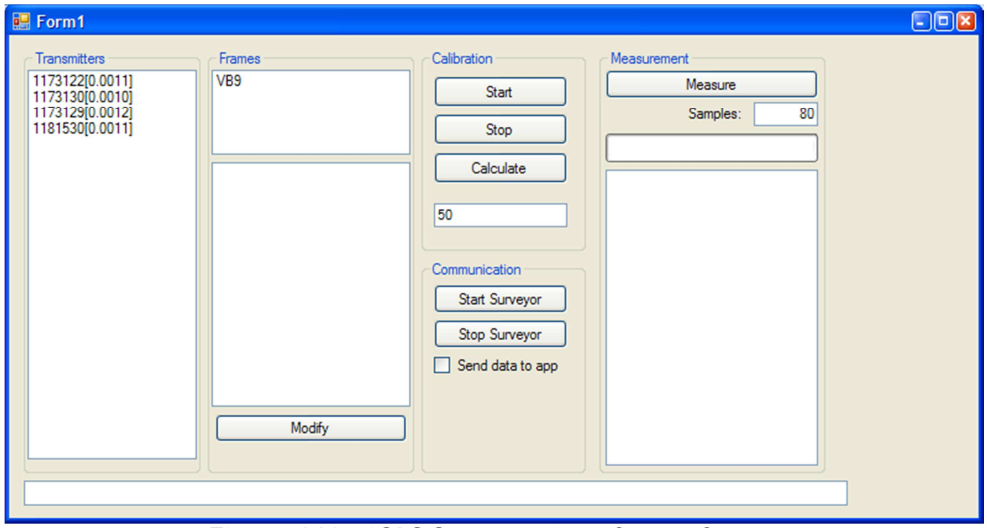

Figure 110 - iGPS Surveyor interface software

While the custom instrument interface software minimizes processing overheads, and provide greater control over the instruments, they are

considerably more time consuming to develop, since each instrument requires a completely different interface. The instrument manufacturer may require additional training before supplying the SDK, and the SDK may be written in a programming language the interface creator may not be familiar with.

5.4. Demonstration of Real-time Metrology Feedback using a Mobile Robot

5.4.1. Introduction

Having studied the dynamic performances of iGPS and laser tracker, and methods of interfacing with the instruments in real-time, a demonstration of real-time metrology feedback using the software described in the previous section is presented here. The real-time measurement data is used to provide navigation information to a mobile robot.

One of the most difficult problems in mobile robot navigation is the accurate estimation of the robot's position and orientation. A large variety of mobile robot navigation methods ranging from dead reckoning using odometry or inertial navigation systems, to beacon type systems, to the more complex multi-sensor map-based systems have been developed by a number of research groups [63, 60, 61, and 59]. However, most of the proposed methods are not accurate or reliable enough to be used to guide Automated Guided Vehicles (AGV) in manufacturing processes such as assembly, machining, or inspection. Many of the navigation methods also require significant computing power, which is usually at a premium on small low power mobile robots.

In this section, a proof of concept automated mobile robot surface form inspection system using a Laser Tracker as both the measurement instrument and robot position feedback is described. As a demonstration of the system's capability, a section of a wind turbine blade was scanned and digitized, the result of which is presented here. Further, indoor GPS (iGPS) guidance of a small KUKA omni-directional robot has been demonstrated, and a full scale prototype system is being developed in cooperation with KUKA Robotics UK.

5.4.2. Motivations for More Centralized Localization Methods for Industrial Automated Guided Vehicles

Traditionally AGVs used in the manufacturing industry run on fixed paths, guided by induction wires buried under the floor or optical/magnetic tapes

[65, 62] stuck on the floor. While they are adequate for the typical material handling operations, the increased demands for greater flexibility, positional accuracy and autonomy has led to the development a number of different new robot types and guidance methods, allowing the AGV to drive to arbitrary positions on command, and react to its local environment.

The vast majority of the research efforts are focused on the distributed side of localization methods, i.e. AGVs carrying complex sensors such as laser scanners [67, 66] and processing capabilities themselves to determine their own locations. There are very few examples of centralised processing for the localization and guidance in the literature, such as the work of Beliveau et al. [58], where external systems provide the localization information to a central computer that sends commands to the relatively simple AGVs. While there has been extensive research into mobile robot and virtual reality system localization using external systems (typically vision or photogrammetry based such as work done by Liang et al. [64]) in lab conditions, these systems do not offer nearly enough range for typical AGV operation, and they are not robust enough to work in the very varied lighting conditions that are found on the factory floor.

As more and more manufacturers integrate metrology systems such as laser tracker, photogrammetry and iGPS into their production facilities, opportunities for using metrology instruments to provide AGV position information emerge. Since providing reliable measurements of 3 DOF – 6 DOF coordinates with very low uncertainties is indeed what metrology instruments are designed to do, utilizing metrology systems to localize AGVs side steps perhaps the most difficult problem in AGV navigation, reducing the complexity and cost of on-board systems.

Typical metrology instruments have absolute coordinate uncertainties much less than 1mm (<50μm for typical laser tracker and photogrammetry, 250-1000μm for indoor GPS), and offer very high update rates for real-time control (> 1000Hz for laser trackers, 40Hz for iGPS). Even though their dynamic performances are not as good as their static performances, as presented in section 5.2, their level of accuracy is at least an order of magnitude better than most distributed localization methods, opening the door to a number of interesting applications that are not previously possible. An example application of using the AGV directly as an automated inspection tool is described in this chapter. Perhaps in the future part carrying AGVs may be able to directly replace fixed tooling, as a part of an automated reconfigurable tooling solution.

5.4.3. System Description

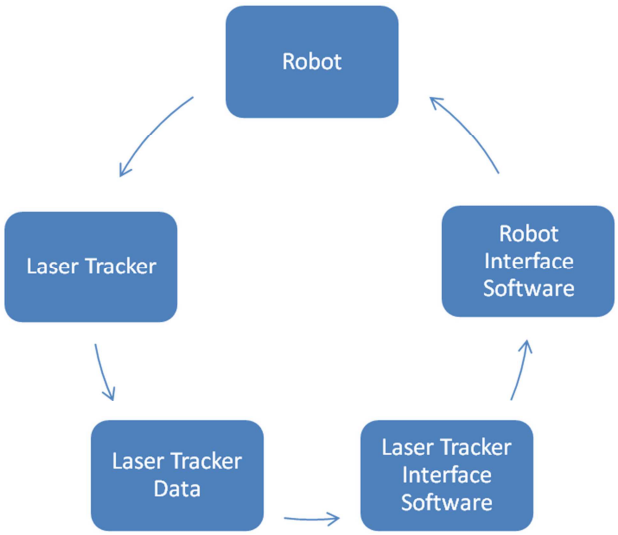

Figure 111 - System overview

The overall control loop of the system is shown in Figure 111.The robot's position is recorded using an external LVM instrument such as a laser tracker, which sends the position to an instrument interface software on a PC which then passes the information to the robot control software that uses the current robot position and the desired position to compute the speed and steering correction commands. The commands are sent to the robot wirelessly. Details of the software and control method are discussed in sections 5.4.3.2 and 5.4.3.3.

5.4.3.1. Mobile Robot

The mobile robot, shown in Figure 112 and Figure 113 used in this proof of concept experiment is a low cost LEGO MINDSTORM NXT system, with a 32bit processor, USB and Bluetooth support.

A simple firmware program on the robot processes the speed and steering commands sent from the computer via Bluetooth, and converts them into skid steering motor commands, and sends them to the two drive servo motors.

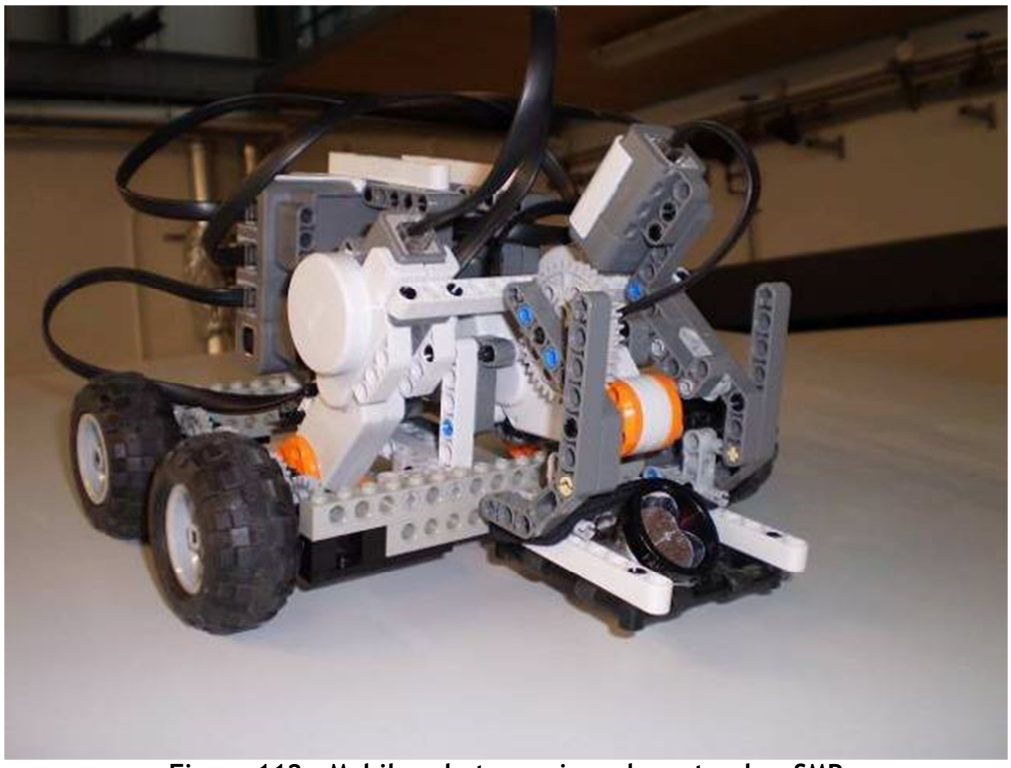

Figure 112 – Mobile robot carrying a laser tracker SMR

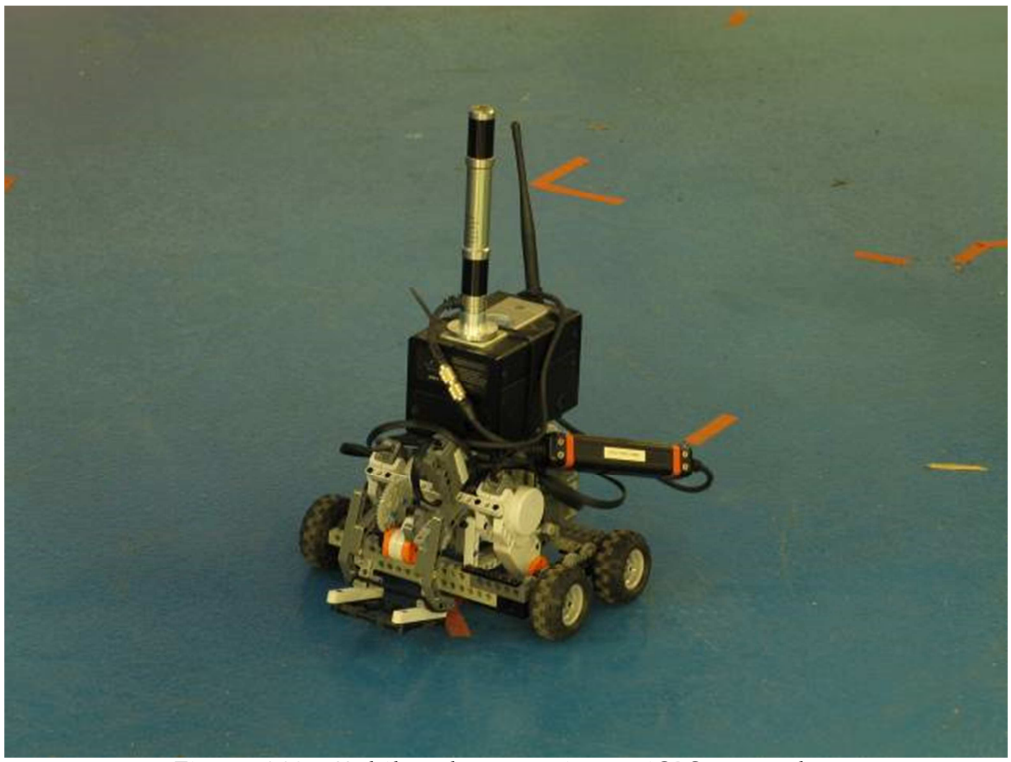

Figure 113 - Mobile robot carrying an iGPS vector bar

In surface scanning operations, the SMR is held in place using rubber mounts, which ensures that it is always in contact with the measuring

surface. Additionally, the robot has the ability to raise the SMR off the surface on command, if for example, it need to move over a rough surface that may damage the SMR.

An iGPS vector bar and wireless transmitter can also be mounted on top of the robot for iGPS guidance (Figure 113).

5.4.3.2. Command and Control Software

The command and control software runs on a normal Windows XP personal computer. It consists of instrument interface software and robot control software, as shown in Figure 114. Since the Software Development Kit (SDK) from the instrument vendors often require different programming languages, the separation of the instrument interface and the robot control blocks allows the software to be developed independently from each other.

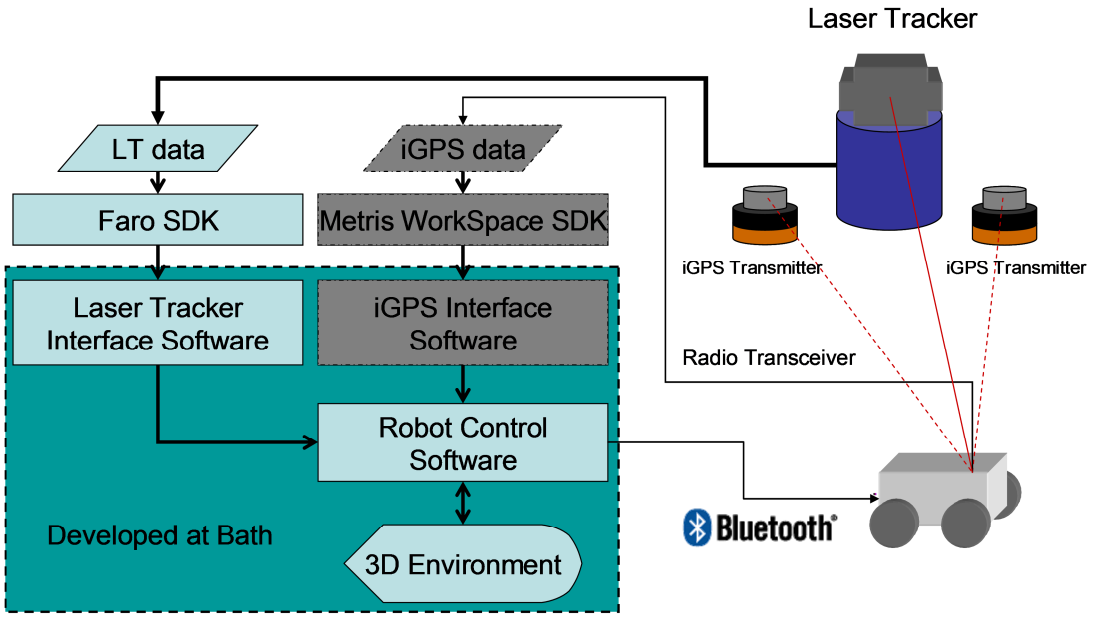

Figure 114 - Software system

The communication between the software is facilitated using a Windows API. This modular design also allows the position data sent to the robot control software to be easily switched between different instruments such as the laser tracker or iGPS.

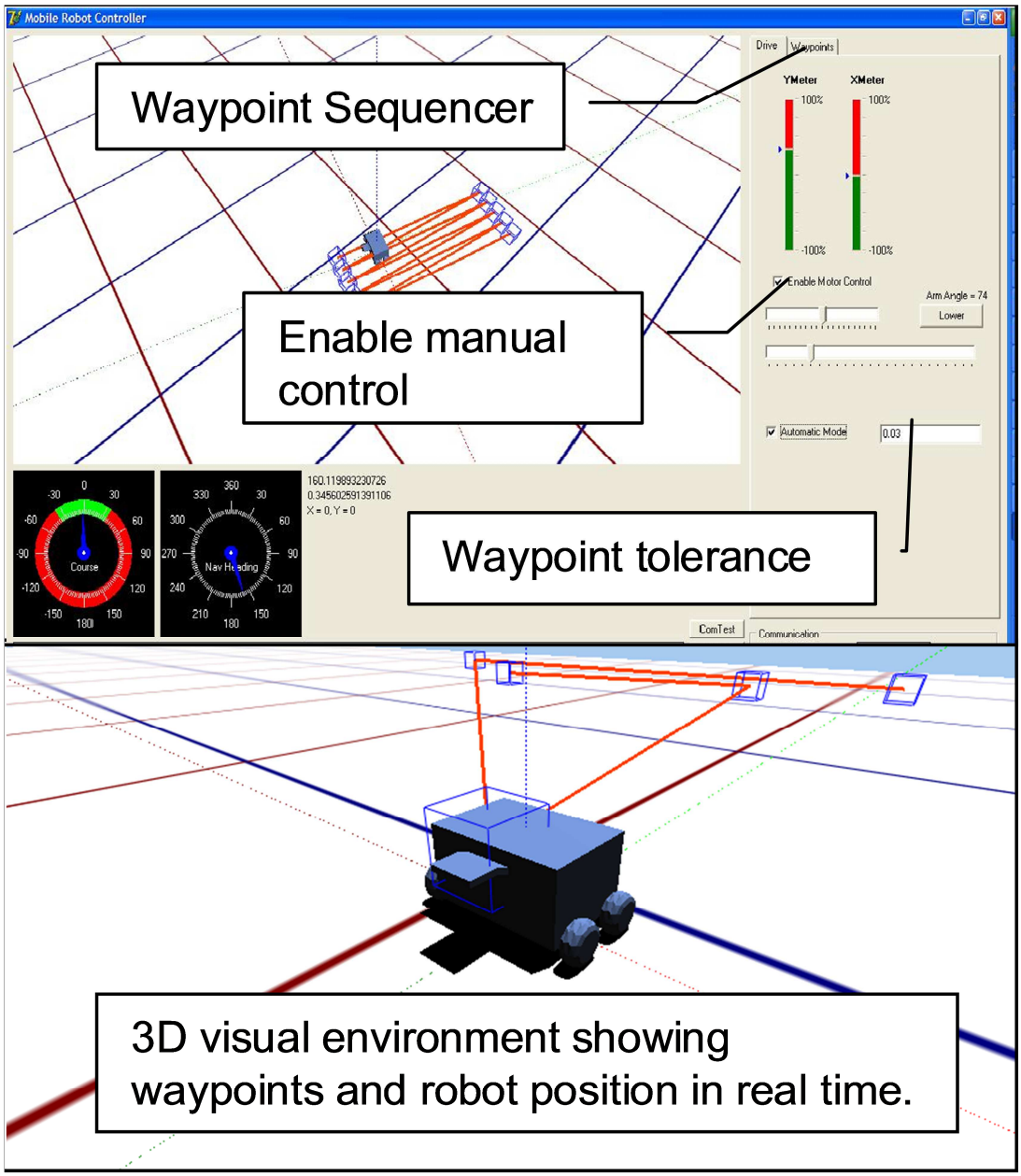

Figure 115 – Robot control software

The robot control software Figure 115 is written in Delphi 7, and communicates with the robot through a Bluetooth serial connection. The software includes a 3D environment showing the relative positions of the robot and the waypoints. The robot waypoints are entered into the waypoint sequencer in plain text format. The software also allows manual remote control of the robot through a PC joystick or gamepad.

When in waypoint mode, the robot control software receives the real-time robot position from the laser tracker interface software, generates a correction command and sends the correction to the robot through the Bluetooth link.

To simplify the process of waypoint creation for operations requiring driving in a grid pattern, a MatLab script was written. The script generates a series

of waypoints (shown in Figure 115 top) from three manually input coordinates.

5.4.3.3. Navigation Method

Since the precise position of the robot is known at all times, the navigation algorithm is exceedingly straightforward. There are only two simple control loops, one for speed and one for course.

The robot speed is in open loop control at a set speed when the robot is more than 40cm from the target waypoint. When the robot is less than 40cm from the target waypoint, speed is decreased linearly, until the robot is within a tolerance distance to the waypoint, at which point speed reduces to zero.

The heading of the robot cannot be measured directly, but its course can be easily calculated from two consecutive positions. In order to reduce measurement noise from the robot vibrations, the minimum distance between the consecutive measurements is set at 5mm. Knowing the course of travel and the course to the target waypoint, a proportional control loop is used to send turning corrections to the robot.

There are a few complications due to the limited angle of view of the SMR. This means that the robot cannot turn more than 30 degrees from the laser tracker, or the line of sight to the SMR will be lost. To overcome this problem, care needs to be taken when generating the waypoints, such that the robot travels forwards towards the tracker and backwards away from the tracker, rather than turning around 180 degrees.

5.4.4. Experiment Results

5.4.4.1. Robot Repeatability

An experiment was conducted to assess the repeatability of the robot. The robot was commanded to repeatedly travel between two points approximately 1.5m apart 20 times using different waypoint tolerances.

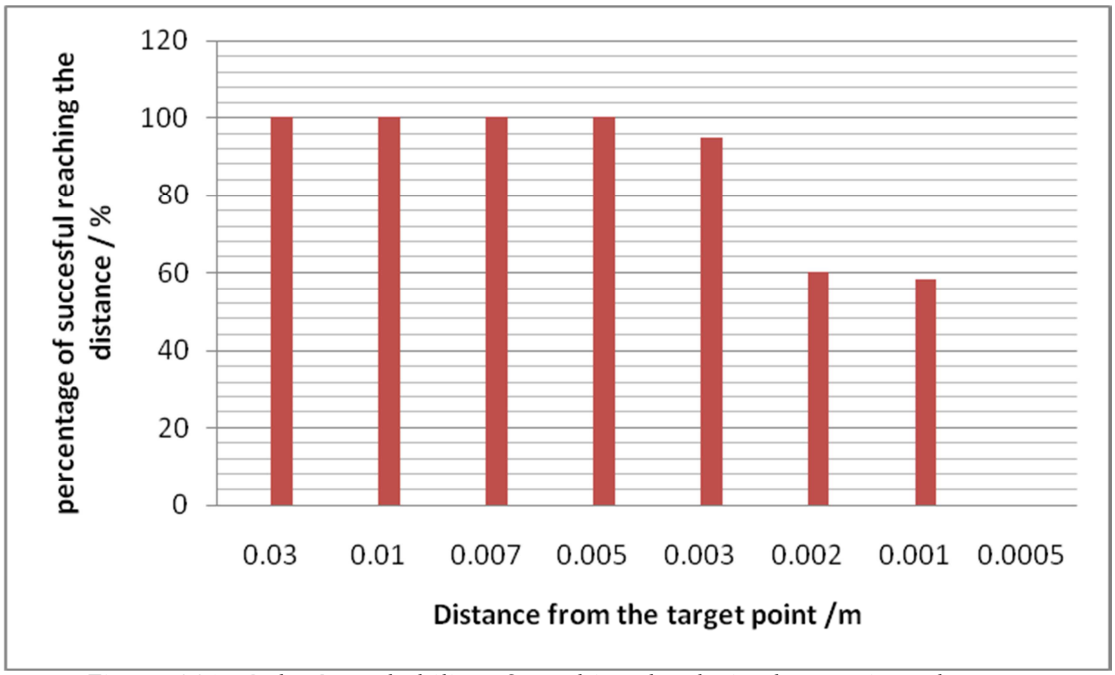

Figure 116 - Robot's probability of reaching the desired waypoint tolerance

Figure 116 shows that the robot is capable of moving to within tolerance of 5mm or higher from the target point with 100% success. This repeatability value should be put in the context that the range of the Faro laser tracker used in this experiment is 30 metres, thus the robot is capable of reaching any point in the 30m radius circle with a repeatability of 5mm.

The 5mm result is likely to be caused by the course angle measurement distance set for this experiment, as described in the section 2.4. When the waypoint tolerance is less than 5mm, the robot cannot receive any direction updates since it cannot record the next position to compute its course angle. As a result of this, if the robot was turning left when it reaches the distance of 5mm to the target point, it would keep turning left until it travelled more than 5mm. This causes the robot to never reach the waypoint tolerance if it is less than 5mm.

However, Figure 116 also shows that the repeatability is still reasonably good when the desired tolerance is about 1 or 2mm. In these cases, the robot was able to approach the waypoint in a straight line. Therefore no turning correction was needed.

The repeatability is also very much dependent on the robot course angle measurement distance setting. The closer between the records of coordinates when calculating the heading angle, the more accurately the robot could get to the target point.

There are many opportunities for better tuning the control algorithms, since it is rather crude and most gains and constants used in this experiment were chosen somewhat arbitrarily.

5.4.4.2. Demonstration of Surface Scanning of a Wind Turbine Blade Section

The purpose of this experiment is to estimate the shape of a curved surface (a Vestas wind turbine blade section, Figure 117) using the mobile robot as an automated measurement tool, controlled using real-time laser tracker position feedback.

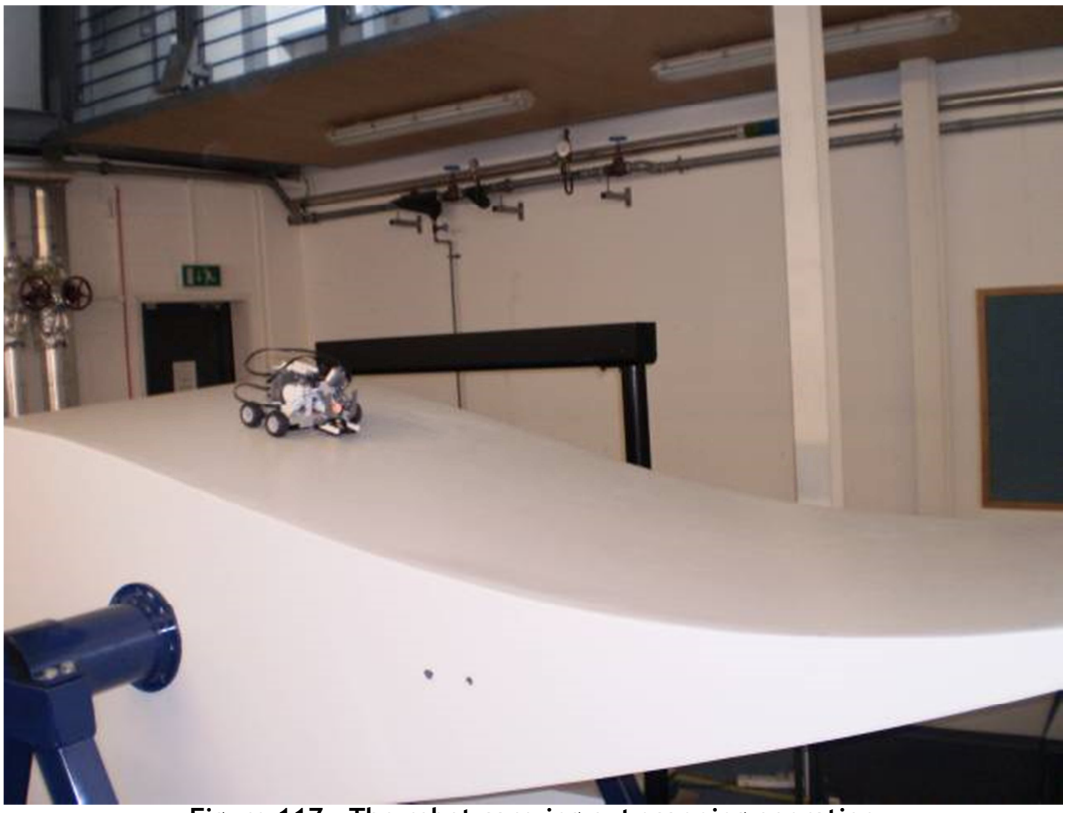

Figure 117 - The robot carrying out scanning operation

The measurement process involves the robot driving in a zigzag pattern, while carrying the SMR in lower position such that it is in contact with the surface.

These types of scans are typically carried out manually in industry, which is not only time consuming, but also difficult for large parts that the operator cannot easily reach.

A MatLab script was used to create the 10 waypoint grid for the robot. The position of the SMR is measured every 1mm the robot travels. The raw data from two trials are plotted in Figure 118. The robot took slightly different paths in the two trials, especially in the beginning, because the robot starting positions were different.

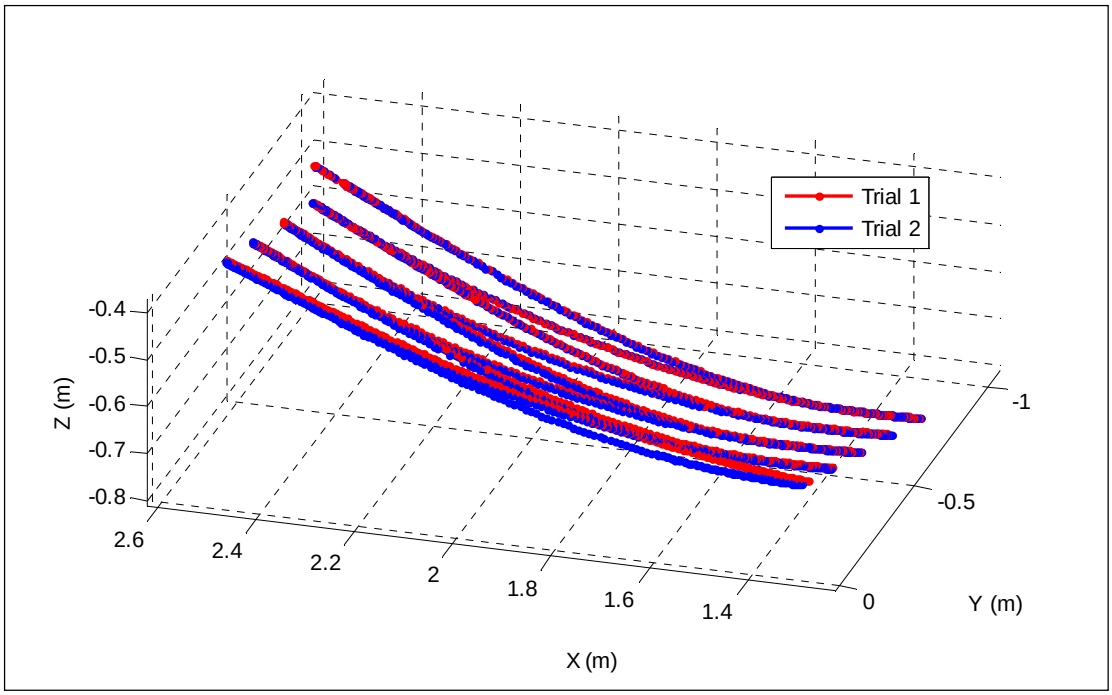

Figure 118 - Scanned data points

The scanned data can then be imported into CAD software, such as Catia V5, as shown in Figure 119, in which a surface can be fitted to the data cloud. The fitted surface is then offset in the surface normal direction, by a distance equal to the radius of the SMR, to take into account that the measurement data corresponds to the centre of the SMR, not the surface measured.

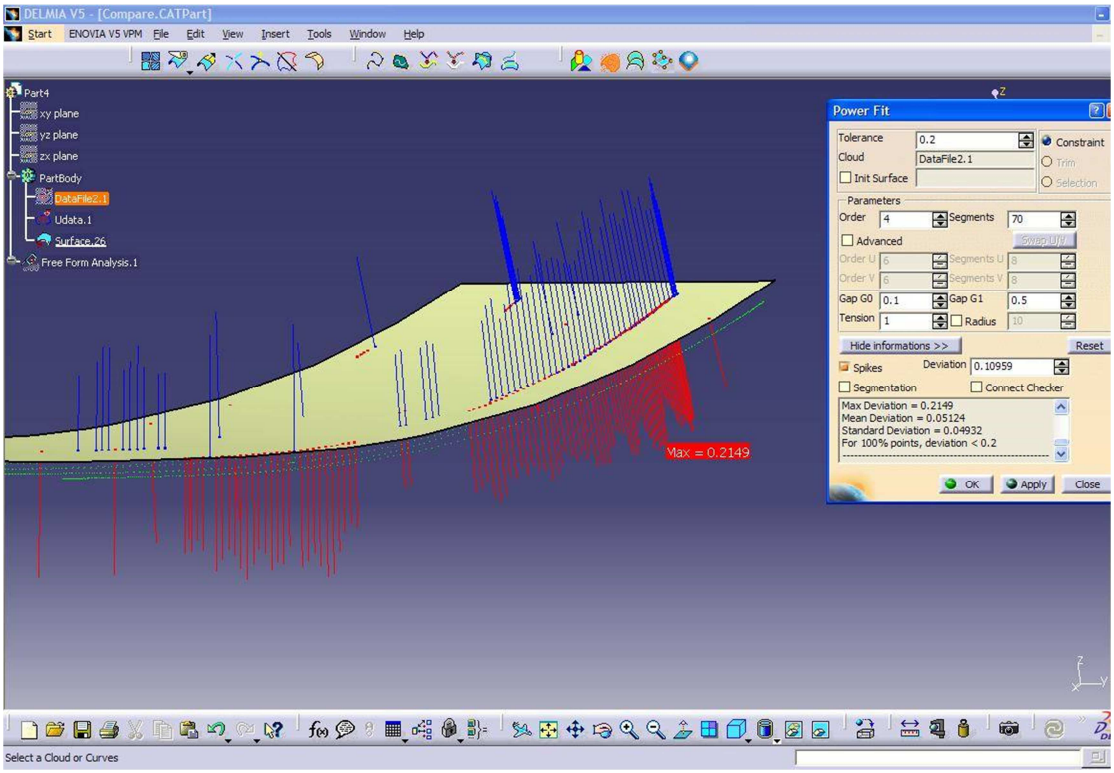

Figure 119 - Best fitting a NURBS surface to the scanned data in CATIA V5

Since the data is acquired at laser tracker accuracies (20-30μm), it can be used for operations such as reverse engineering, metrology assisted assembly or quality control.

5.4.5. Further Work on the iGPS Guidance of the KUKA omniMove

The KUKA omniMove platform is a scalable omni-directional vehicle that is designed primarily for material handling, replacing lift trucks, trolleys and overhead cranes. The omni-directional drive mechanism allows the vehicle to travel in any direction and orientation. The omniMove platforms come in sizes ranging from less than half a metre long and a few kilograms capacity to over tens of meters long and over tens of tons of load capacity.

All current omniMove vehicles are driven manually by a trained operator. KUKA Robotics UK is interested in developing the omniMove into an Automated Guided Vehicle (AGV), to increase production line automation.

Preliminary trials showed that the iGPS is a very suitable system for providing the position and orientation data to drive an omniMove type AGV. Only a small amount of additional work was needed to adapt the Lego robot control software to control an omnidirectional vehicle.

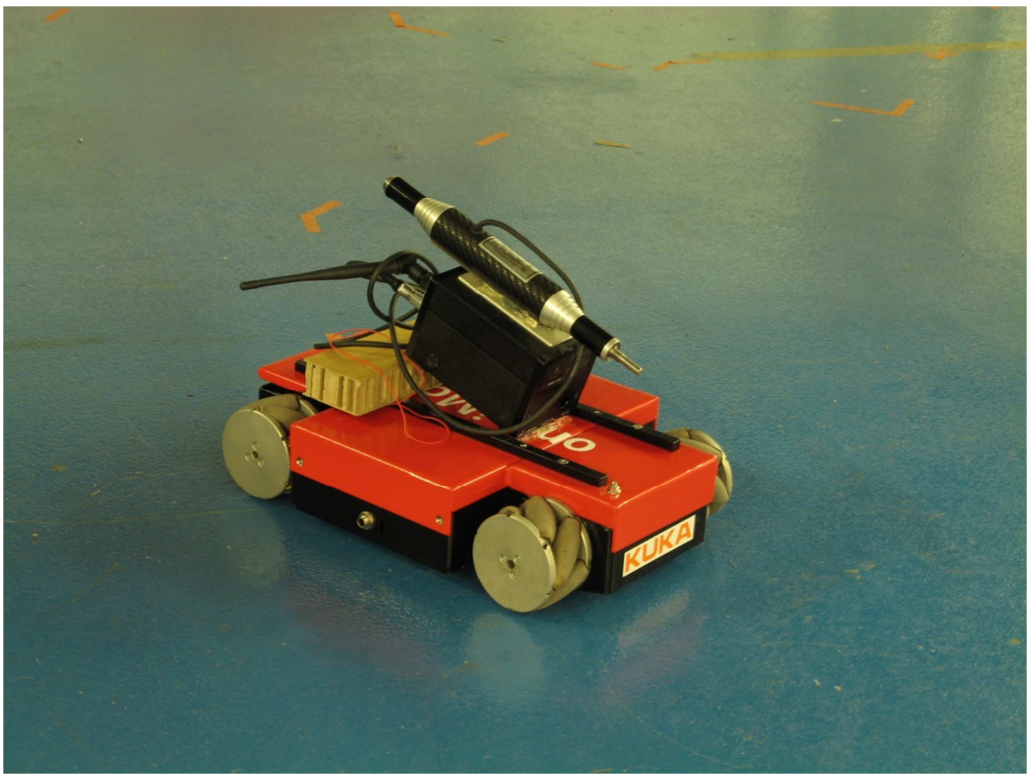

Figure 120 - Mini omniMove carrying an iGPS vector bar

Figure 121 – Mini omniMove control station

The working mini omniMove (Figure 120 and Figure 121) was demonstrated at Airbus ALCAS (Advanced Low Cost Aircraft Structures) open day in 20th-22nd October, 2009. Work is currently being carried out to trial the system on a full size omniMove (Figure 122), in a simulated production environment.

Figure 122 – Full-scale omniMove moving to waypoint under iGPS guidance

5.4.6. Conclusions

In this section, the possibility of using an external Large Volume Metrology (LVM) instrument such as the laser tracker to provide real-time feedback for mobile robot navigation was investigated. The repeatability of the robot was experimentally determined to be 5mm, and there exists room for improvement in the robot navigation algorithm.

A surface scanning of a wind turbine blade section was also demonstrated, illustrating possible applications of the method for manufacturing processes.

Metrology guidance simplifies many of the most difficult problems in mobile robot navigation, and the accurate metrology information allows the robot to perform tasks such as measuring the shape of an irregular surface, which would have been very difficult to automate.

A number of improvements can be made in the robot hardware and navigation algorithm. For example, a proper digital filter maybe used to calculate better estimates of the robot course at any given time, rather than the 5mm distance limit used in the experiments described here. Other on-board sensors such as an inertial navigation system may also be used in conjunction with the laser tracker, to improve navigation and achieve 6 DOF measurements.

Given reliability and accuracy of the LVM position data and reduced complexity in integration, the methods described in this project are currently being applied to develop an industrial AGV prototype.

5.5. Metrology Assisted Assembly Technology Demonstrator

5.5.1. Introduction

The dynamic performance of the iGPS and laser tracker, as well as developed methods and demonstrations of software interfaces with large volume metrology instruments were examined in the previous sections. The final part of the research study focuses on the development and performance assessment of a real-time metrology compensated machine tool using the software tools developed in section 5.3.

It was determined that best demonstration of the research methodology of integrating metrology into production is to develop a machine tool that is completely dependent on a metrology system for its accuracy in real-time. This is a demanding task that has very wide applications, and is a novel approach to the traditional machine tool compensation methods.

It is worth noting that the system describe here is not simply a new machine tool compensation technique, it has greater implications. In such a system, the machine tool accuracy is controlled by a traceable instrument, so that the parts/features produced are in a sense already verified. Since the machine tool gets its absolute position from the metrology system, it can be moved with respect to the part without having to re-datum before starting a new process.

5.5.2. Traditional Machine Tool Compensation

The field of machine tool error compensation arises from the fact that no matter how much time and effort is spent on the design, it is physically impossible to construct “the perfect machine tool”.

Error compensation and accuracy enhancement of machine tools has become a very heavily researched area, due to the increasing demand on the performance of machine tools for precision manufacturing. There are two major categories of error compensation: one approach is to attempt to “calibrate” or measure the error map of the machine before or after machine operations, which is then applied during the operations; the other approach is to monitor the error during the machine operations, which is then used to alter the machining process while the machine is operating, this is commonly referred to as “real-time compensation”. The advantage the latter approach is that it is more accurate, and allows a lower cost, lower performance machine to be used in operations that demand high accuracy [70].

The majority of the body of work on real-time error compensation focuses on minimizing or compensating for the intrinsic and environmental sources of error for each component of the machine tool [68, 70, 71, 72, 73, 74, and 75]. Using these traditional methods, in order to achieve complete compensation of all the possible sources of error, all of the individual contributors such as geometric (21 errors for a 3-axis machine), kinematic, thermal, and cutting forces must be painstakingly modelled, and a large array of sensors such as temperature sensors, load cells, and laser interferometers must be installed to monitor the status of the machine. The complexity of this method means that it is time consuming to setup, and is sensitive to the performance and position of the sensors [72, 74].

In this chapter, a simpler and more straightforward real-time method of using an external metrology instrument to directly measure the 3D position of the tool is proposed as an alternative to the traditional real-time machine tool error compensation methods.

5.5.3. Development of the System

The metrology assisted positioning system described in this chapter is a part of a larger undertaking in the Metrology Assisted Assembly (MAA) project at the University of Bath. The MAA project aims to develop a flexible, scalable and low cost assembly cell to demonstrate the integration of metrology systems directly into the manufacturing processes of large aerospace components. The integration of metrology instruments has the potential of reducing the cost of the tooling, and because the parts are measured while they are being manufactured, inspection time can be reduced if not eliminated, and the probability of reject parts is also reduced.

The MAA cell will attempt to use metrology instruments and reconfigurable tooling rather than the traditional heavy and expensive jigs and fixtures to solve the problem of locating the part and the tool. This chapter will be focused on the development and verification of the system that is designed to perform the tool locating task.

5.5.3.1. System Design Goals

The system design is primarily driven by the requirements from the aerospace industry, to be used in manufacturing processes such as wing assembly, where high accuracy must be maintained over a large working volume. Therefore the system needs to be able to meet the following requirements:

- Large volume 6 DOF positioning
- 50-100μm coordinate accuracy
- Real-time metrology control
- Scalable
- Flexible multi-process
- Off-the-shelf hardware
- Low cost

5.5.3.2. Proposed Solution

While originally the design focused on using metrology instruments to guide an industrial robot, it soon became clear that real-time control required access to the low level control system of the robot, to which most industrial robot manufacturers are not willing to grant access, because of the sensitivity of the IP.

Therefore the decision was made to build a simple and small 3-axis actuator using off-the-shelf components, which meant complete control over every aspect of the software and hardware design. Early design concept mock-ups can be seen in Figure 123.

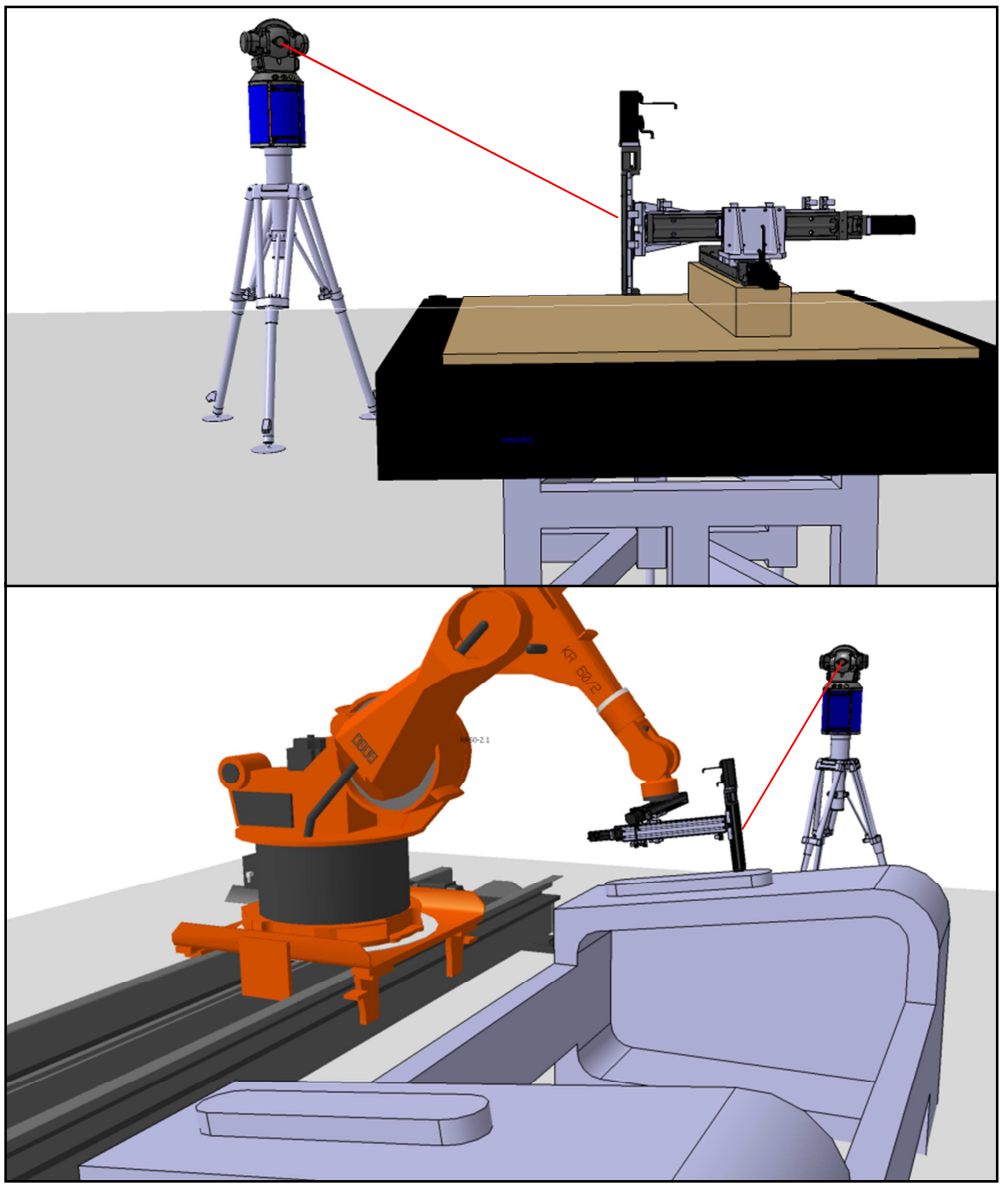

Figure 123 – Concept mock-ups envisioning the MAA 3-axis actuator on static mount and as the end effector of an industrial serial robot, monitored by a laser tracker

The main design philosophy of the system is to use a laser tracker to provide an absolution position reference to the actuator, such that despite of its inherently low working volume and lack of rigidity, the 3-axis system can be moved around a large assembly either manually or by a serial robot, and perform tasks that typically can only be carried out with very large machine tools. Since the position error of the device is compensated at all times by the laser tracker, high feature to feature accuracy can be achieved.

Although a full 6 DOF solution would have been more preferable, a simpler 3-axis system dramatically reduces the complexity and cost of the system, allowing the actuator to be fully compensated using a single laser tracker. The lack of 6 DOF ability can be somewhat mitigated if a serial robot is used to position the 3-axis actuator in different orientations as shown in Figure 123.

5.5.3.3. Final System Design

This section describes the major components of the final system. Since the proposed solution calls for the construction of a custom machine tool, all of the software and hardware needed to be designed and constructed by the researcher.

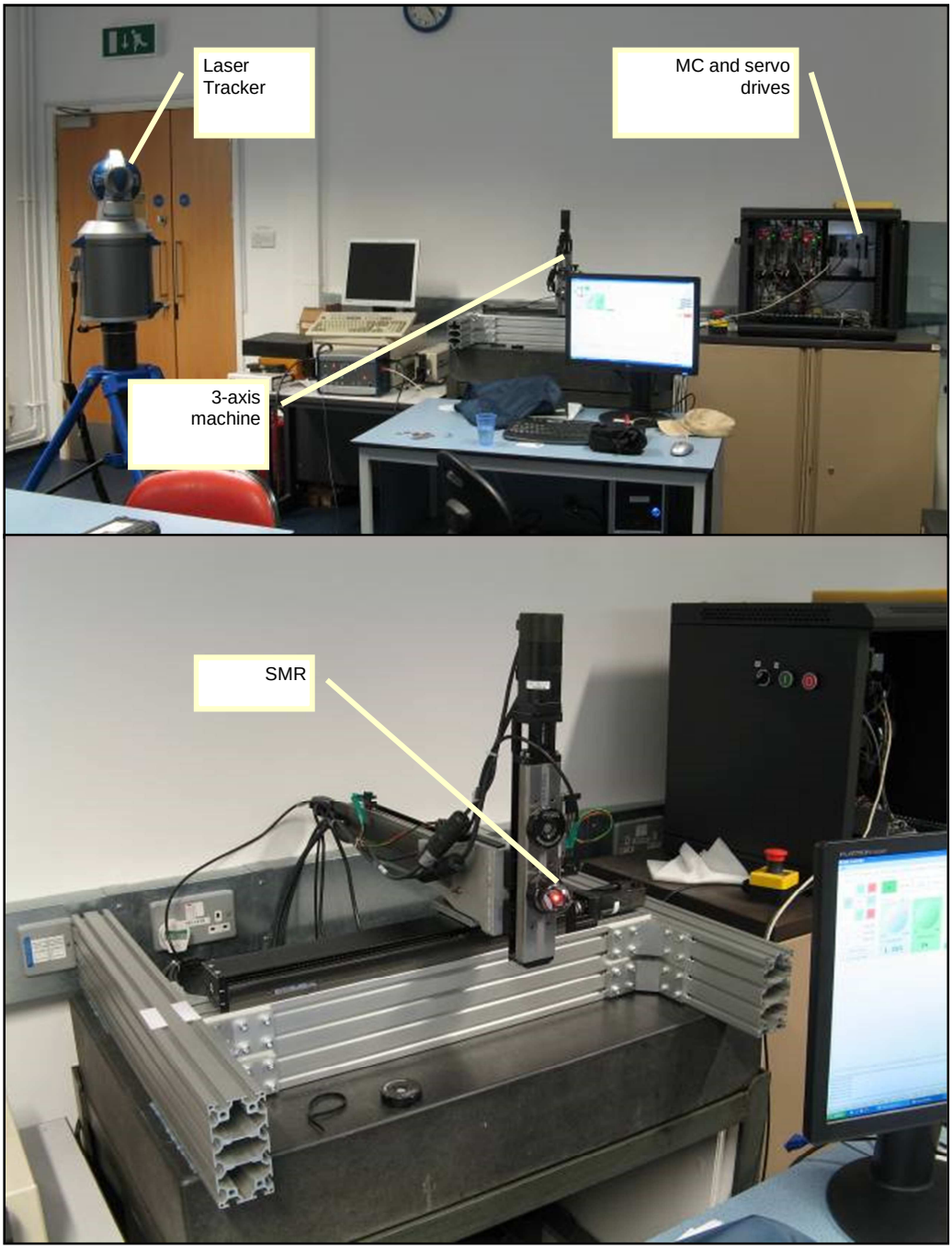

Figure 124 - Pictures of the prototype system

Pictures of the final prototype system can be seen in Figure 124. It consists of a PC, a 3-axis machine, a laser tracker and a box housing the motion controller and servo drives. The laser tracker tracks the position of a

Spherical Mirror Reflector (SMR) magnetically mounted on a SMR nest fixed to the Z axis of the machine.

5.5.3.4. Laser Tracker

The laser tracker used to compensate the 3-axis actuator is an ADM only FARO ION. It has a Maximum Permissible Error (MPE) [20] of 16µm + 0.8µm/m for distance measurements and 20µm + 5.0µm/m for angular measurements. Typical measurement uncertainties are less than half of the MPE. It has a maximum range of 40m when using normal 1.5 inch SMRs. [69]

5.5.3.5. Hardware Design and Construction

The 3-axis actuator was designed and analysed in Dassault Systemes Catia as a fully functional virtual machine tool with a kinematic model (Figure 125).

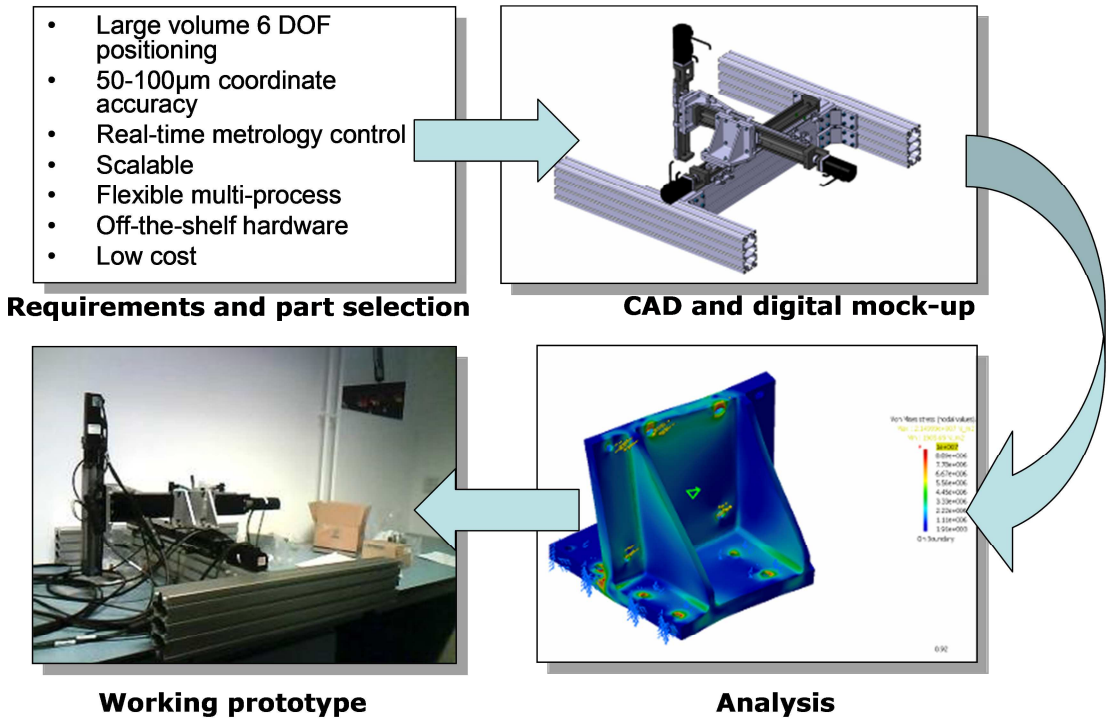

Figure 125 - Hardware design process

DS Catia NC simulation is used to verify the axis movements for clashes, simulate NC machining processes including material removal (Figure 126), and generate G-Codes.

The hardware system consists of 3 THK linear slides, with 20µm positioning repeatability, an extruded aluminium frame and custom parts for mounting the slides to each other.

While basic FEA analysis was performed on the parts connecting the axes to ensure the machine will be able to carry the specified payload weight, no

attempt was made to manufacture them with high accuracy. In fact, the parts are hand made from aluminium plates, and hand welded together. Measurements of the axes squareness using a laser tracker showed that the axes are misaligned by up to 0.4 degrees.

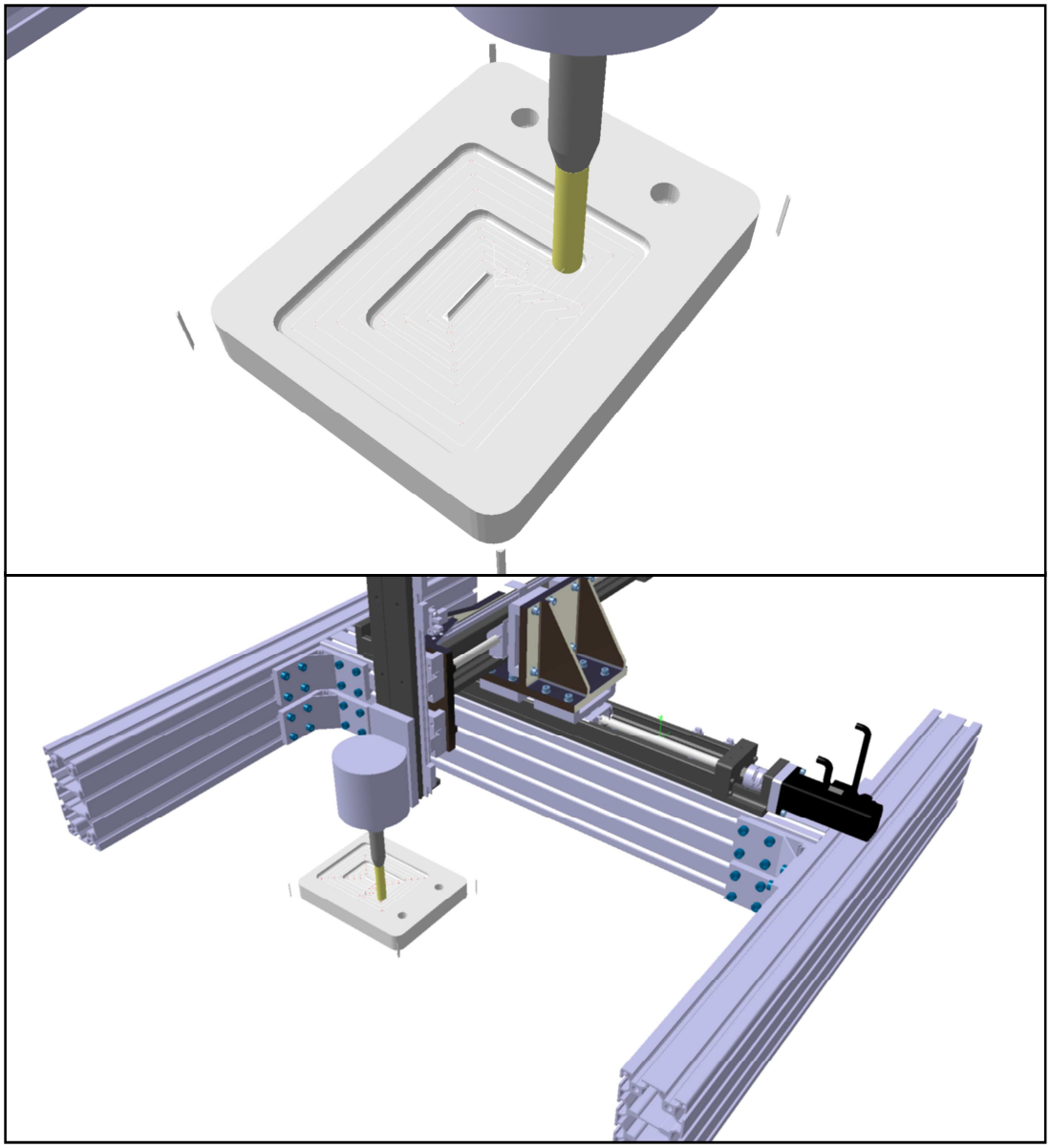

Figure 126 - Catia machine tool simulation with tool path G-Code generation

Overall specifications of the 3-axis actuator are listed below:

- Weight: 20kg (With frame)
- Working volume (mm):
- X = 300
- Y = 200
- Z = 80
- Payload: 5kg
- 3 × THK KR linear slides
- Servo motors and drives: OMRON SMGAH

- Motion controller: OMRON Trajexia

5.5.3.6. Software

The integration of the laser tracker and the machine is handled by the main control software. The main control software runs on a Windows XP PC, and is written in C# (Figure 127). Communication with the motion controller is achieved using the serial port, and communications with the laser tracker is handled through the laser tracker SDK provided by Faro. The main control software also provides an easy to use user interface to control the machine manually, plot position information of the machine and the tracker, loading and executing G-Code files, enable or disable compensation and record and save measurement results.

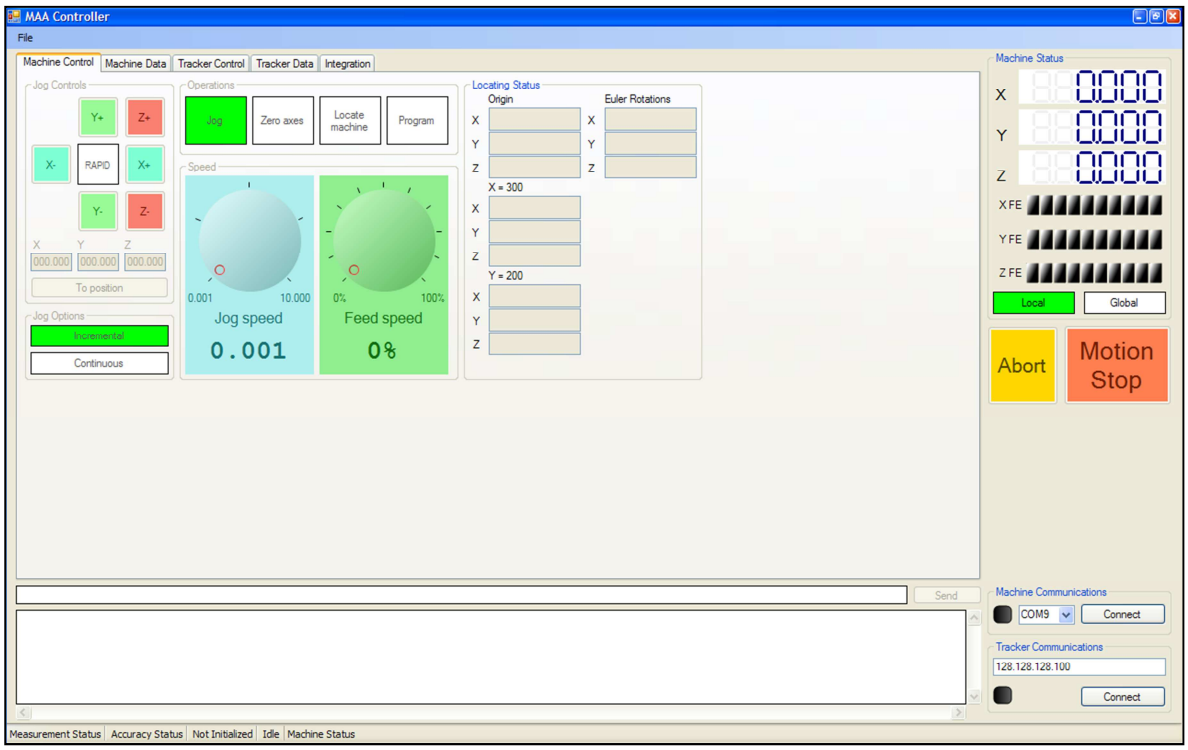

Figure 127 - Main control software run on PC written in C#

Two concurrently running programs written in OMRON BASIC run on the OMRON Trajexia motion controller (Figure 128). One of the programs provides machine status feedback to the PC, the other processes commands sent from the PC and converts them into servo motion commands.

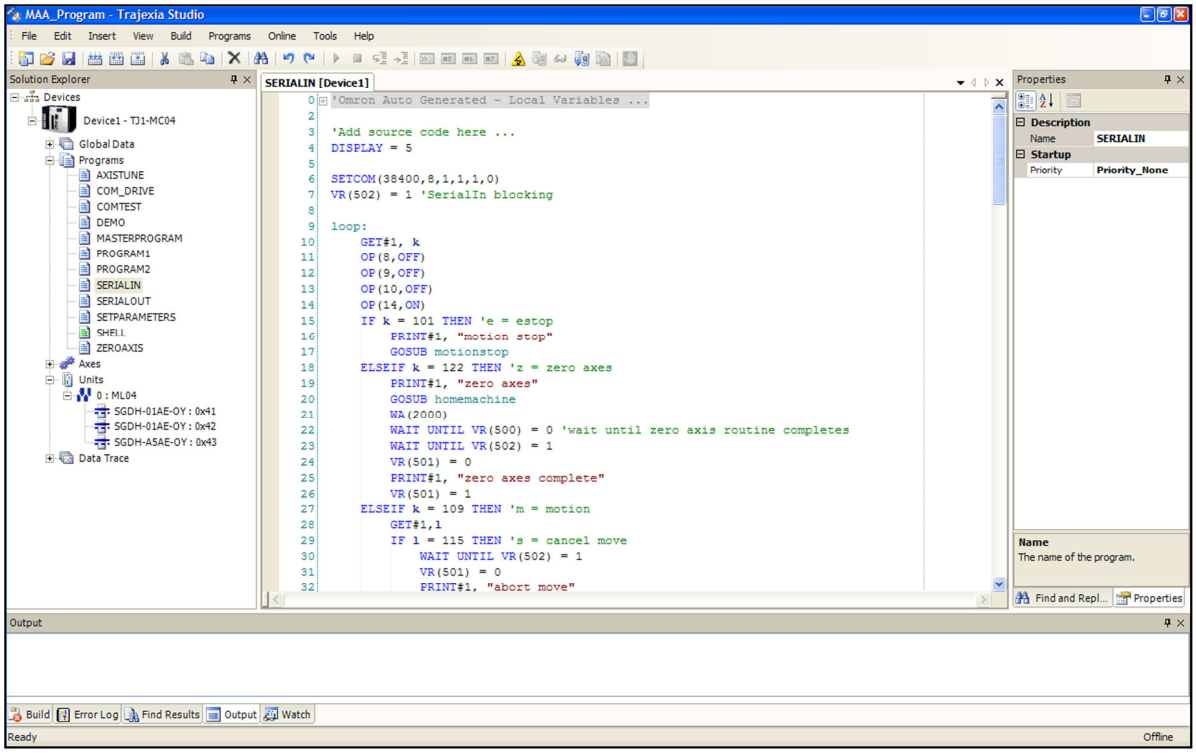

Figure 128 - Motion controller is programmed in OMRON BASIC

5.5.3.7. Controls and Communications

The overall layout of the connections and data flows is illustrated in Figure 129. The laser tracker is connected to the PC via 100Mpbs Ethernet, and the PC is connected to the motion controller through a 38400 Baud RS232 serial connection. The Motion controller drives the servos through the proprietary OMRON Mechatronlink-II connection.

A simplified overview of the control software, including those running on the motion controller is shown in Figure 130. The first step before the real-time compensation can start is to locate the 6DOF position of the 3-axis machine in the laser tracker coordinate system. This is accomplished by pressing a button on the main controller software, which moves the machine through a series of three points, the positions of which are measured by the laser tracker. This provides enough information to compute an Euler rotation matrix and an offset vector to convert the machine coordinate system into the tracker coordinate system and vice-versa.

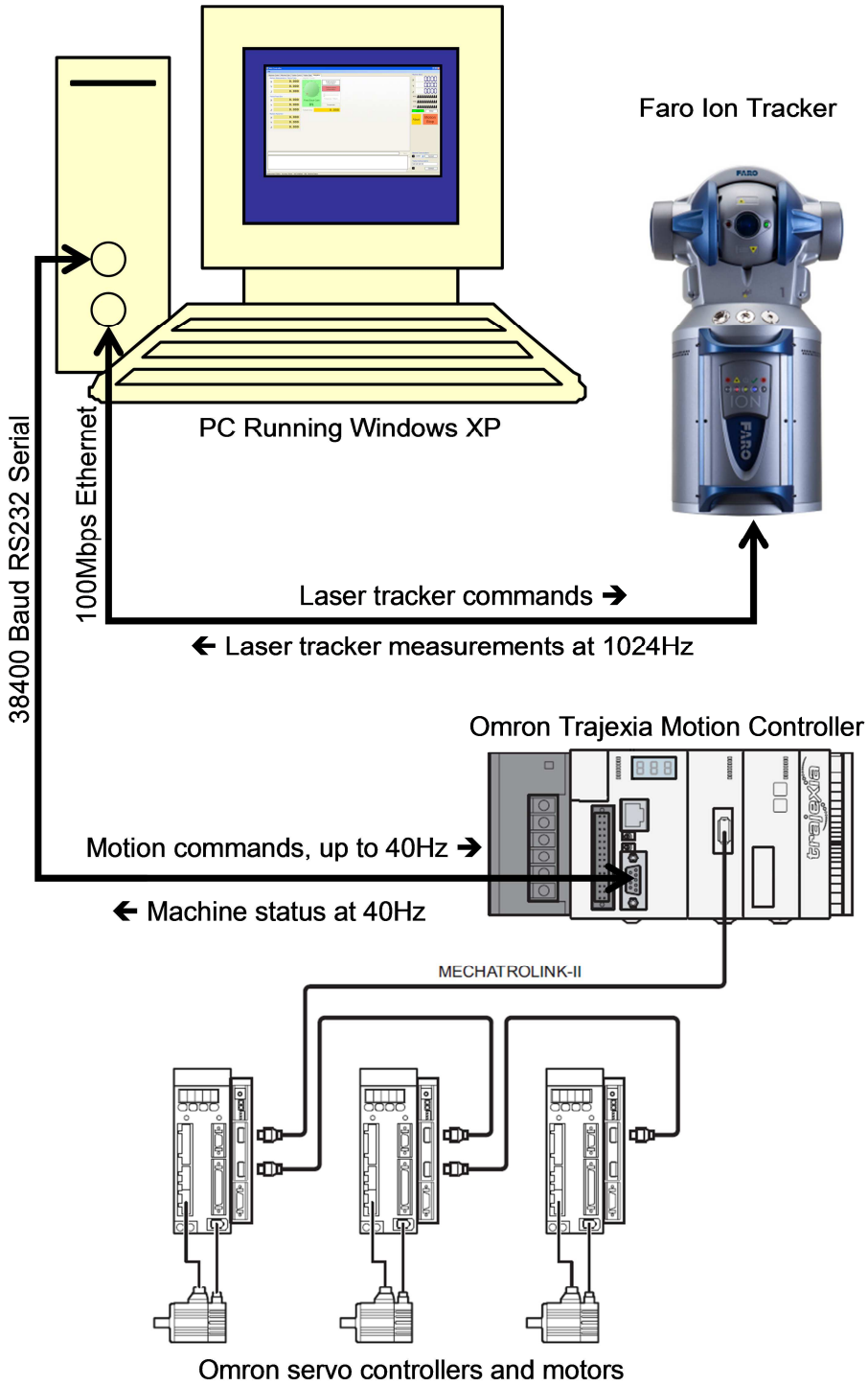

Figure 129 - Layout of physically connections and data flow

Then a G-Code command is read from the input file. The G-Code command is sent to the G-Code interpreter, which converts the G-Code command into a simpler machine command that is subsequently sent to the motion controller through the RS232 serial link. Currently the G-Code interpreter only supports a small subset of the G commands. A motion controller program then receives, parses, processes and executes the command sent from the PC.

If the error compensation loop is disabled, the motion controller will wait until the motion is complete, and then sends a “motion buffer empty” command to the PC, which triggers the main control software to load the next line of G-Code.

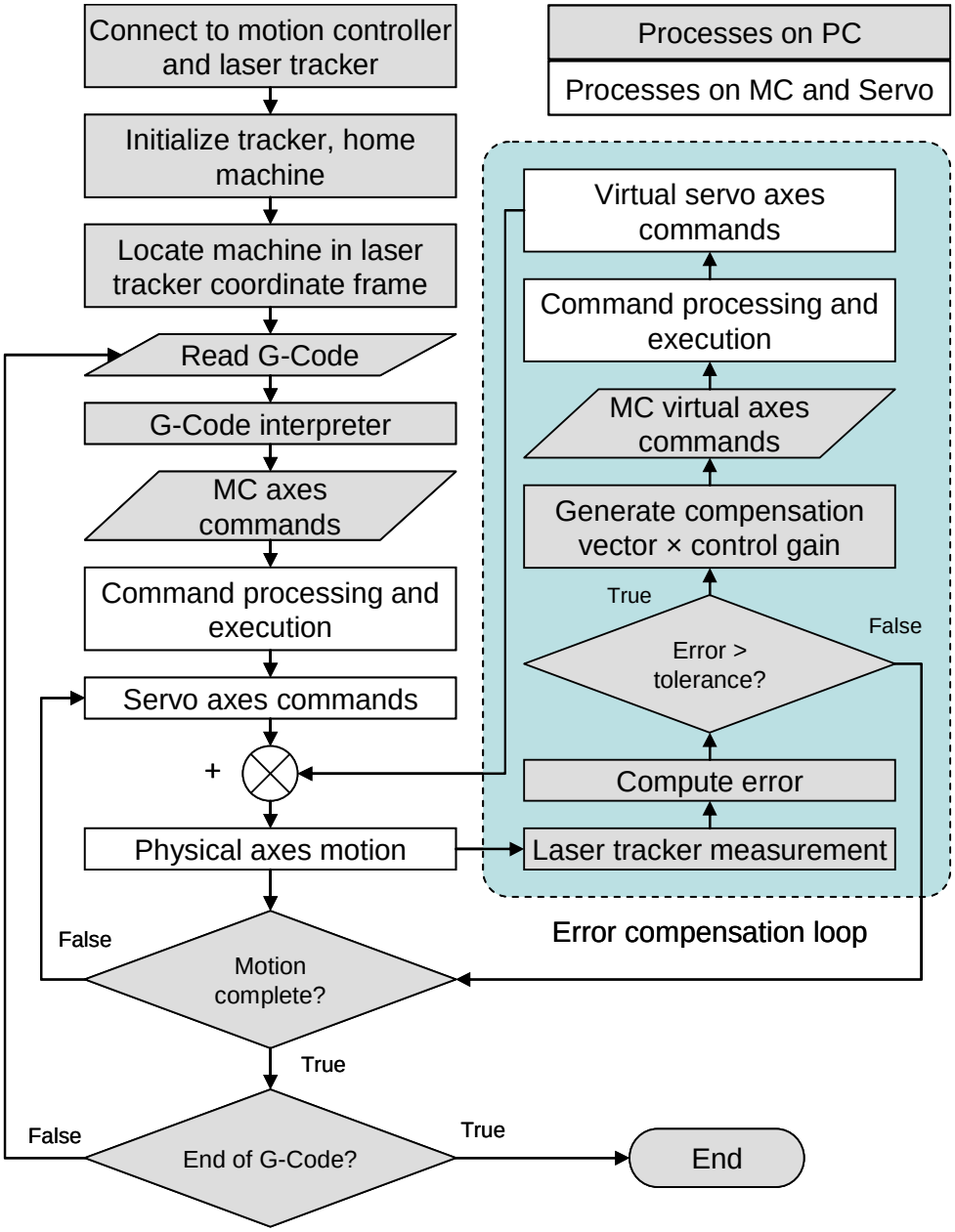

Figure 130 - Overview of the control software

If error compensation is enabled, a compensation vector is sent to the motion controller, which then performs a synchronized 3-axis move command on 3 “virtual axes” using the compensation vector. The movement of the virtual axes are then added to the physical axes. On the OMRON MC, a “virtual axis” is implemented exactly like a physical axis, and includes all the properties a real axis would have, such as movement speed and acceleration. It is essentially a virtual simulation of a physical axis. By superimposing virtual axes moves on top of the physical axes moves, the end point of a currently executing move can be seamlessly modified, without

having to abort the current move and starting a new one, causing the machine to briefly stop all motion.

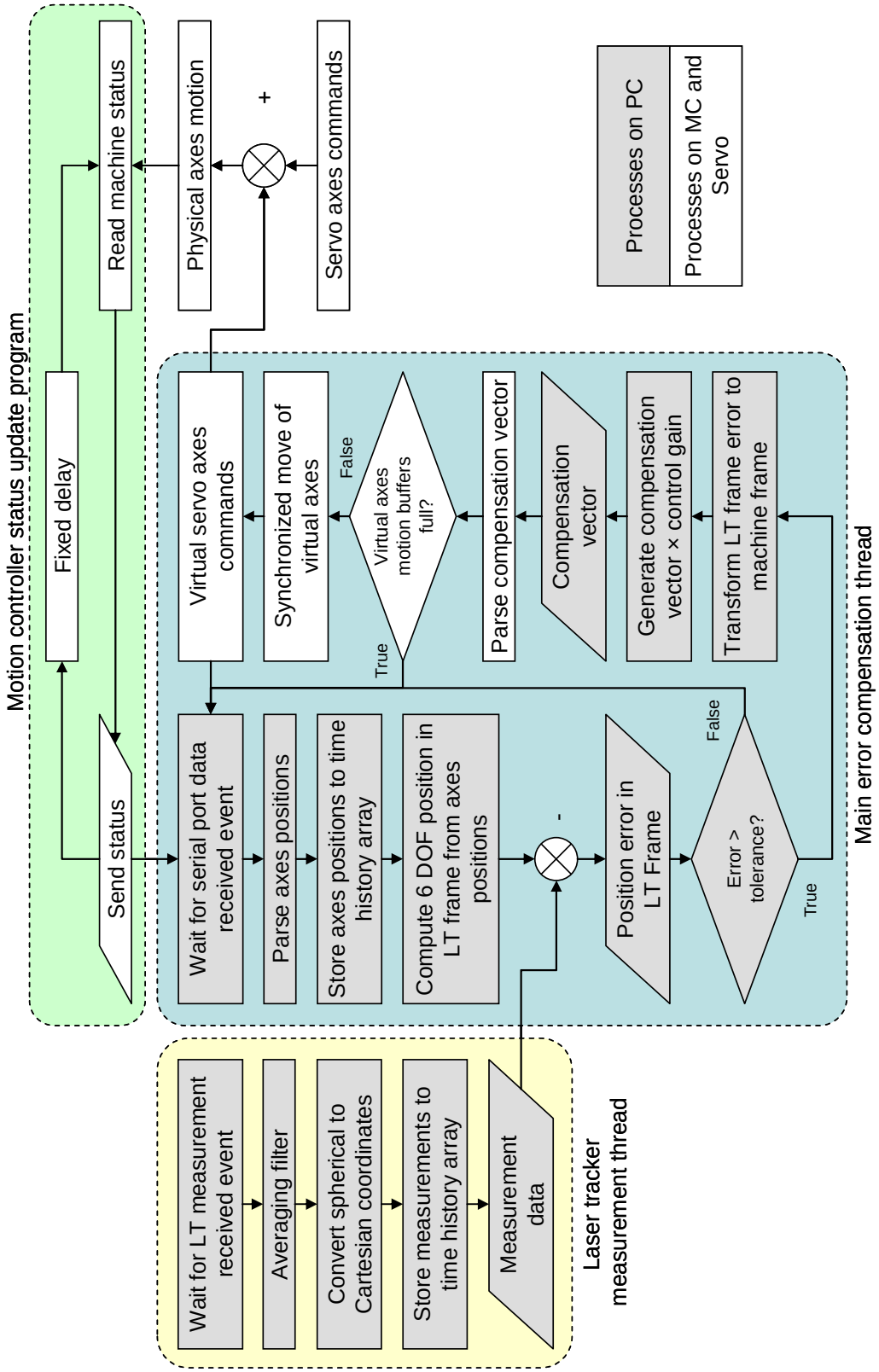

Figure 131 - Detailed flow chart of the error compensation loop showing the three concurrent threads

A detailed flowchart of the compensation loop and its relationship with the other two concurrently running threads is illustrated in Figure 131.

The laser tracker thread is an always running background thread that continuously takes measurements from the laser tracker at 1024Hz. The motion controller status update program is a program that runs on the motion controller. It sends the key statuses of the machine including axis positions and motion buffer state to the PC through the serial connection. Since the compensation loop depends on the data sent back from the motion controller, the frequency of the feedback loop depends directly on the frequency of the update program. The status update is set at approximately 40Hz.

When the main control software receives an axis position update from the motion controller, the positions of the axes are transformed into the laser tracker coordinate system, this coordinate represents the position the machine "thinks" it is at. This position is then compared with the actual measurement from the tracker. If the error between the predicted position and the measured position is greater than the pre-set tolerance, a compensation vector is generated, multiplied by a gain value and sent back to the motion controller. The gain value is used to fine tune the feedback response and prevent oscillations. This is a purely proportional control loop, thus the gain value is the proportional loop gain.

5.5.4. Evaluation of Static Positioning Performance

An experiment was carried out to assess the static positioning performance of the machine with and without real-time compensation from the laser tracker.

5.5.4.1. Experiment Design

A G-Code tool path of a 3D grid of 30 points was generated covering the entire working volume of the machine. The grid consists of 2 planar grids of 15 points, separated by 60mm in the machine Z axis, as shown in Figure 132 and Figure 133. Each planar grid is traversed twice, in both the forward and reverse directions, in order to identify backlash errors, which are not compensated in the servo controller. The complete tool path is repeated 10 times; therefore each point is reached 20 times, 10 in the forward and 10 in the reverse directions, taking approximately 1.5 hours.

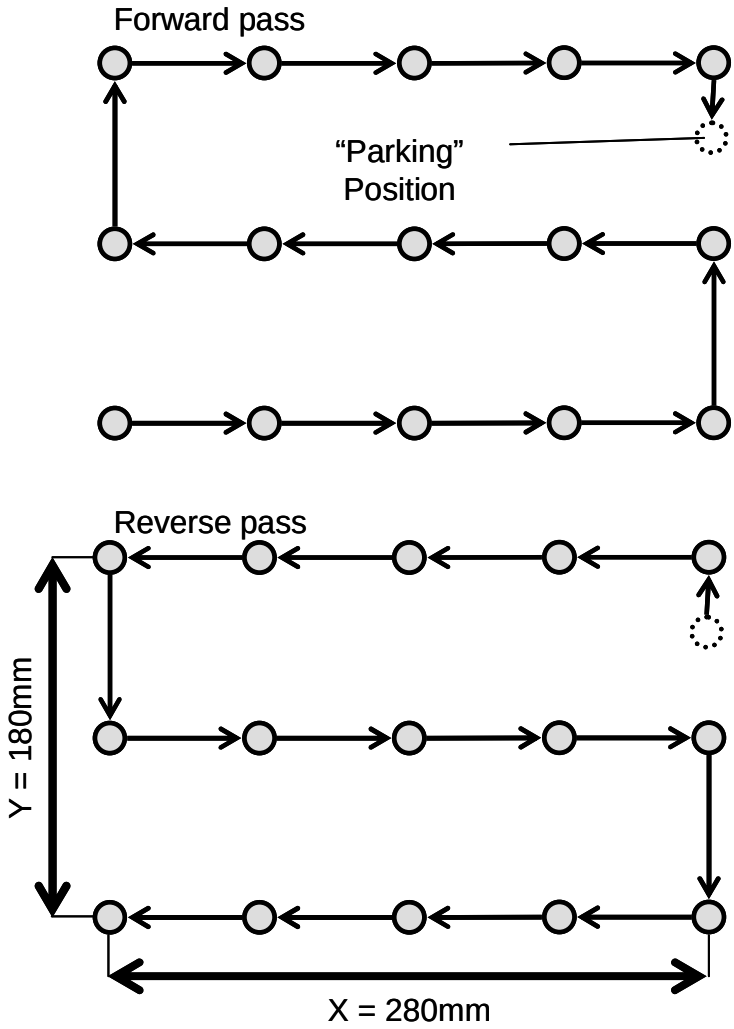

Figure 132 - Tool path for each planar grid of 15 points

At each grid point, the machine dwells for 3 seconds, during which a 2 second laser tracker measurement is taken, after allowing the machine to stabilize for 1 second.
During the experiment with laser tracker feedback, the error tolerance was set at 10μm, and gain was set at 50%.

5.5.4.2. Analysis of Results

5.5.4.2.1. Repeatability Results

Since each point is repeated 20 times, the drift over time of the subsequent measurements compared to the first measurement can be plotted to demonstrate the repeatability of the system. The positioning drift over time for both the forward and backward passes is plotted in Figure 133, providing a qualitative visual representation of repeatability.

It is clear that significant drift and backlash errors are present in the 3-axis machine, especially in the Y and Z axes. When real-time compensation is enabled, drift is considerably reduced.

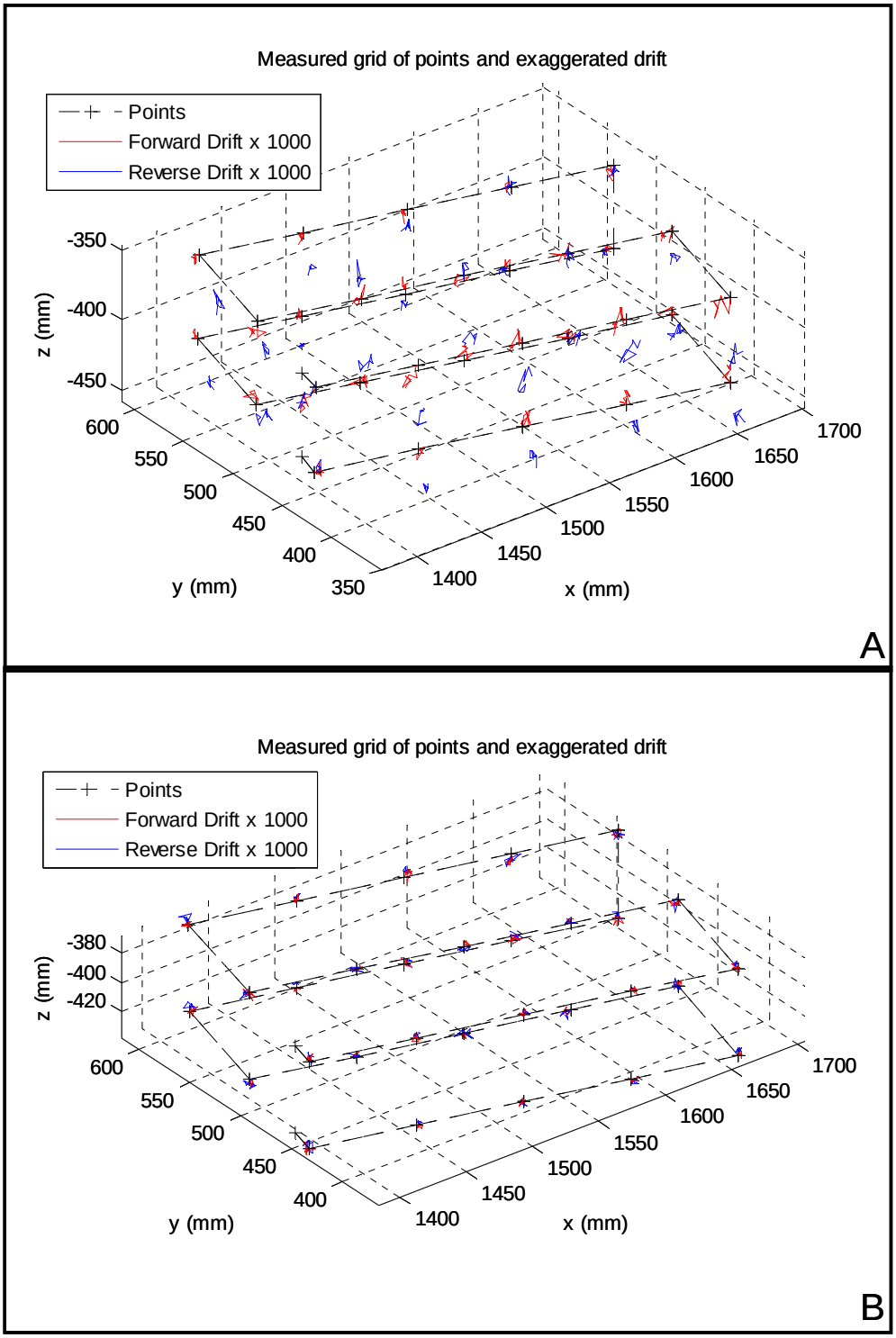

Figure 133 - Plot of programmed tool path and exaggerated drift for runs with (B) and without (A) real-time compensation

The increase in repeatability can be seen more quantitatively in Figure 134. The saw tooth shaped plots for the Y and Z axes of the uncompensated

experiment show the differences between the forward and reverse passes, illustrating the effect of backlash on these axes.

Although the results of the uncompensated case shows that the machine has reasonable repeatability, on the order of 20 - 30µm, when compensation is enabled, backlash error is almost completely eliminated, and repeatability errors are at least halved.

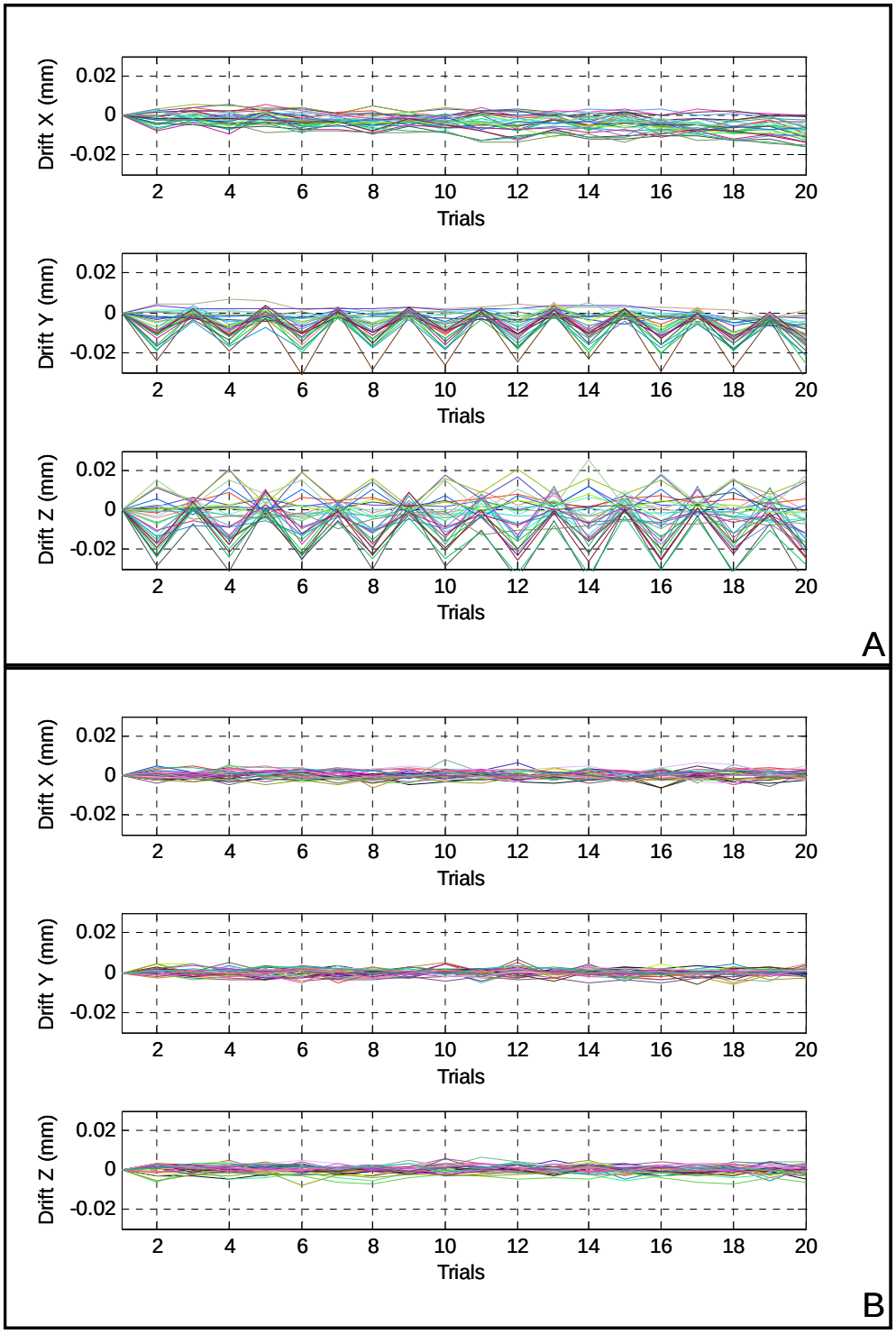

Figure 134 - Run chart of drift for runs with (B) and without (A) real-time compensation

5.5.4.2.2. Inter-point Distance Comparison

While repeatability is an important measure of machine performance, the absolute volume metric accuracy of positioning is a more meaningful assessment of the machine.

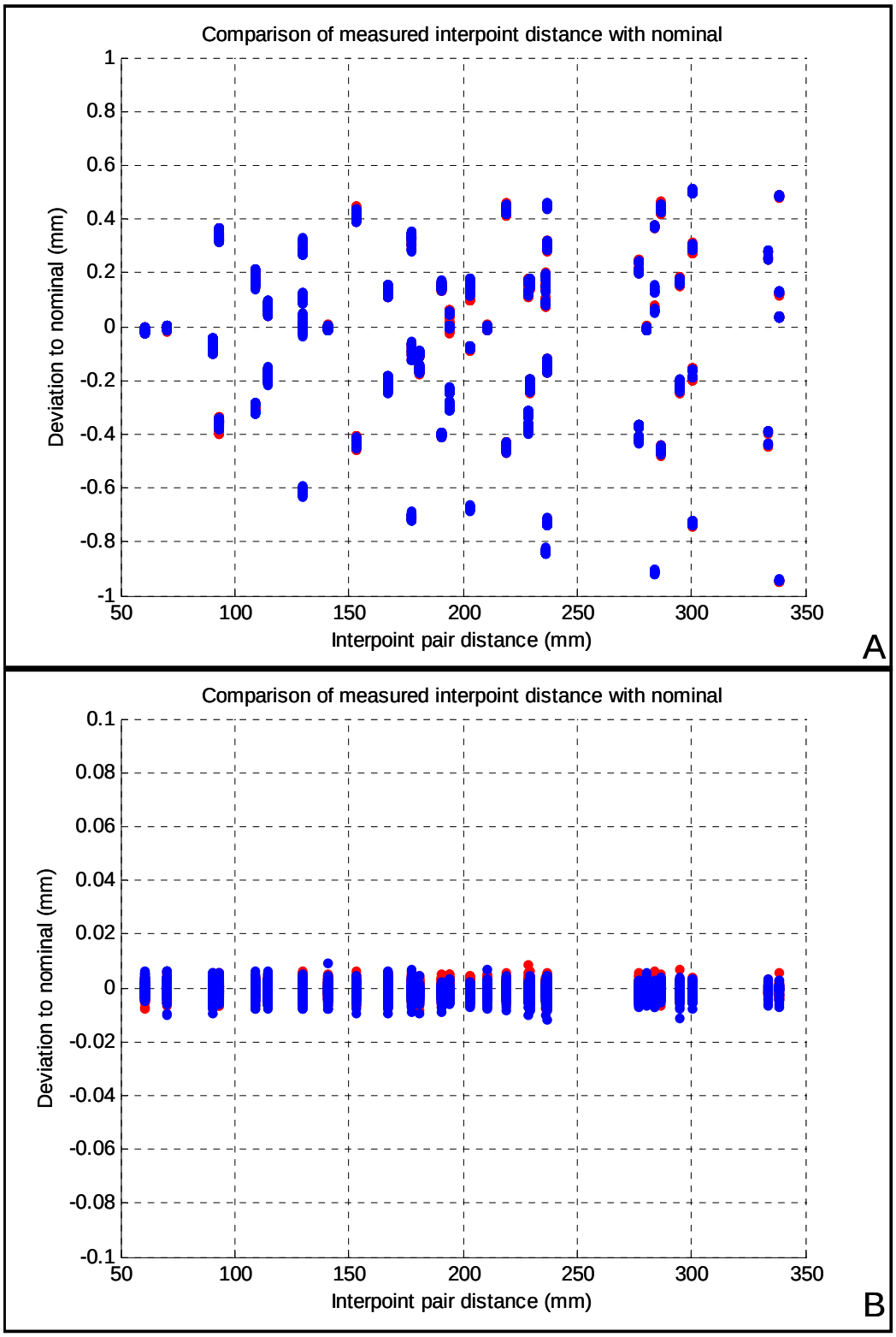

Figure 135 - Inter-point distance error vs. inter-point distance for runs with (B) and without (A) real-time compensation, note the change in y axis scale

The volumetric accuracy of the machine is evaluated by comparing the measured inter-point distances (IPD) to the nominal distances. That is, a list of the distances between all of the measured points for each pass is compared to the list of nominal distances. Looking at the accuracy this way instead of comparing the coordinates of the points directly avoids the possible errors introduced in the least squares point fitting and coordinate transformation process which is required for direct coordinate comparisons.

Figure 135 shows the IPD error plotted against corresponding IPD, note the 10 × difference in Y axis scale. Without compensation, the IPD error is very large, and increases with IPD, reaching almost 1mm for the longest distances. This means that the machine by itself has very poor volumetric accuracy, which is not surprising, considering that no attempt was made to align the axis, or compensate for any errors such as backlash.

When real-time compensation is enabled however, IPD error is reduced dramatically to well below 15µm for all IPDs.

This large reduction in error is shown more clearly in histogram form in Figure 136. The reduction in the parts per million (PPM) errors is approximately 100 fold.

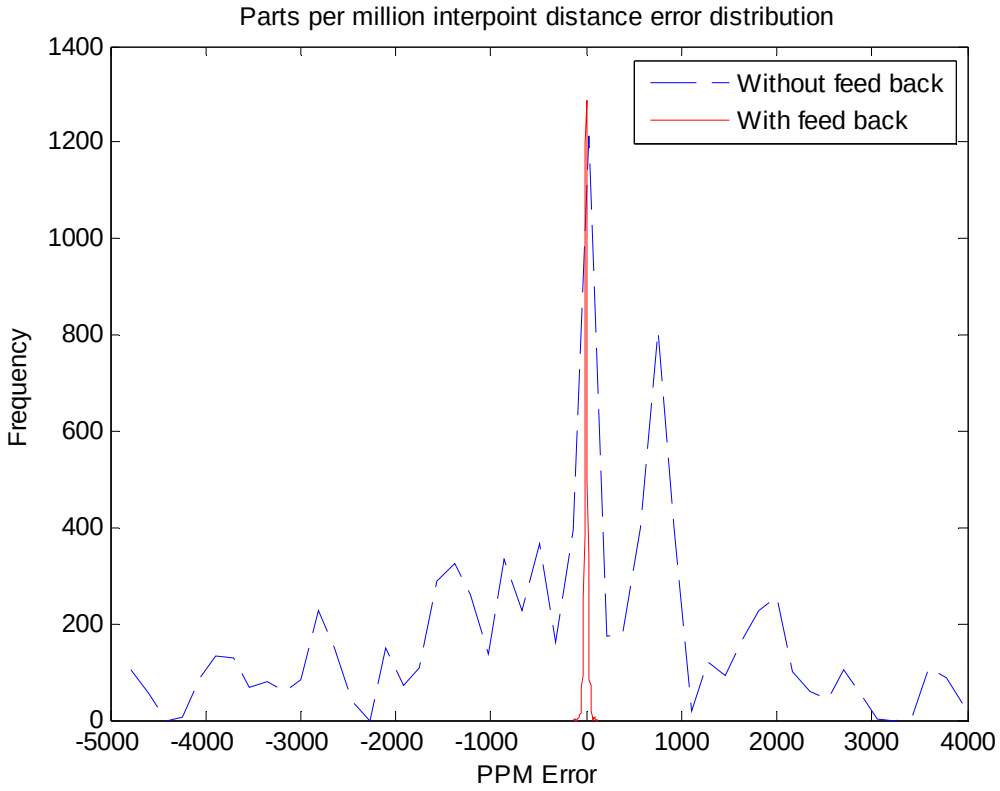

Figure 136 - Inter-point distance PPM error comparison

The reduction of IPD error vs. IPD is plotted Figure 137, showing a remarkable 40 to 140 times reduction in error when real-time compensation is enabled.

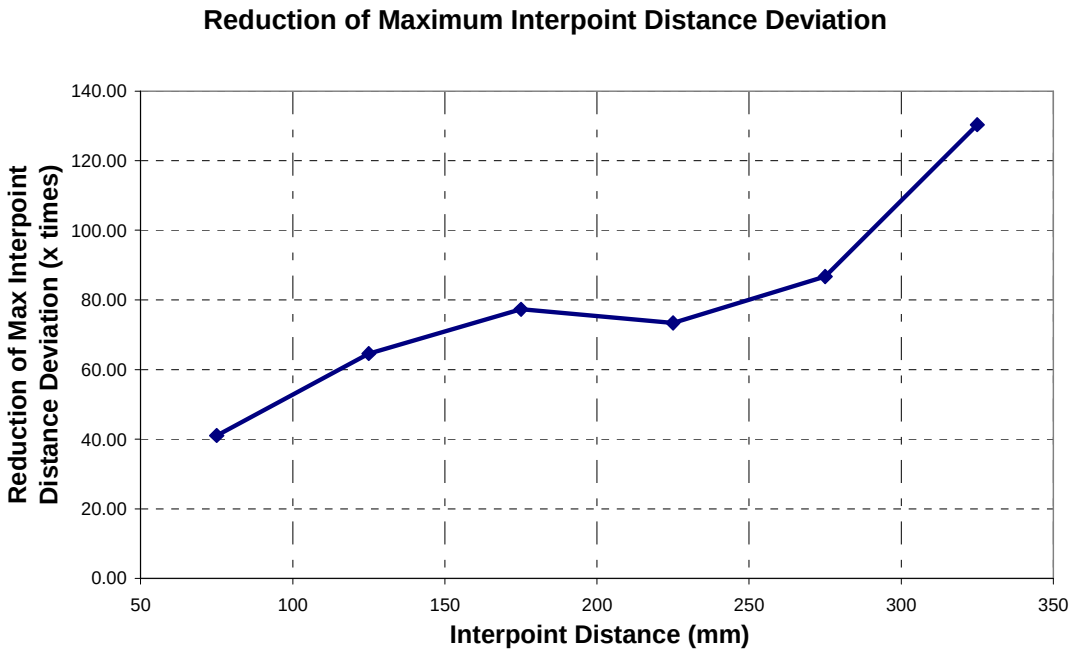

Figure 137 - Reduction of IPD error vs. IPD when compensation is enabled

Considering that the laser tracker is approximately 1.5m away from the machine during the test, the tracker's measurement uncertainty would be better than 30μm. Therefore the total positioning accuracy of the machine would be below 45μm, and is likely to be considerably less since IPD error is the combination of 2 positioning errors. What is more, the positioning accuracy of the machine is very much limited by the performance of the laser tracker.

5.6. Summary and Discussions

The dynamic performance of indoor GPS and laser tracker LVM systems are experimentally examined in this chapter, in an attempt to fill gaps in existing literature, and provide confidence for using these instruments in real-time metrology assisted assembly.

Various methods of interfacing with LVM instruments in real-time are examined, and custom software interfaces for iGPS and laser tracker are developed.

A proof of concept metrology guided mobile robot using the interface software is also presented, showing that LVM instruments can be used to provide reliable and accurate real-time navigation feedback to guide AGVs.

This chapter has also described the development, working principles, and performance assessment of a prototype 3-axis machine with real-time laser tracker error compensation. The static positioning experiments have shown very encouraging results, demonstrating that the laser tracker real-time compensation produced improvements in both volumetric positioning repeatability and accuracy.

The inter-point distance results show that the machine is able to consistently reach positioning accuracies of better than 45μm. While 45μm static accuracy may not be particularly impressive for a small sized 3-axis CNC, because the system is designed to be mobile and flexible, it can be moved to a different position when required while still maintaining positioning accuracy close to that of the laser tracker.

This implies that since the laser tracker's measurement uncertainties are typically below 100μm at distances up to 10 metres, the system described in here is effectively capable of meeting typical aerospace positioning accuracy within a spherical volume 20m in diameter, achieving what usually requires a much larger and more expensive machine.

Although only the static performance is studied in the chapter, because the compensation is real-time, there will also be dynamic performance improvements. The dynamic performance of the machine, more advanced control algorithms and more optimal methods of filtering and combining the data from both the servo encoders and the laser tracker will be explored in future work. A milling spindle attachment is also being designed, so that the real machining performance of the system can be evaluated as well.

6. Assessment of Work, Conclusions and Recommendations for Future Work

6.1. Introduction

This chapter presents an assessment of the results from the work completed in this research project, reviewing the quality and effectiveness of the methods, processes and systems developed to meet the research aims and objectives of metrology integration.

The research aim is realised first through a thorough understanding of the metrology systems and the manufacturing processes. The current LVM measurement and data processing automation demands of aero-structure manufacturers are explored in chapter 3.

Secondly, methods of mathematically simulating metrology assisted assembly systems are outlined, and a number of application case studies using the assembly simulation are presented in chapter 4.

The practical implementations of real-time integration are then addressed in chapter 5, and software methods of interfacing directly with a number of the instruments in real-time are developed and demonstrated. Finally the research aim is met by developing, demonstrating and assessing the capabilities of a real-time metrology integration demonstrator. The benefits and weaknesses of the methodology of real-time integration of metrology systems will be reviewed.

The conclusions of the research described in this thesis are also presented in this chapter. The aim and objectives of the research defined in chapter 1 are reviewed, and their achievement is assessed. Possible areas for future work are also suggested.

6.2. Large Volume Metrology Data Processing Evaluation and Automation in Manufacturing

While the methodology of this research study is to move towards having metrology systems fully integrated into the aero-structure manufacturing systems, such a system is complex and often has to be designed from the conception of the product, which does not solve many of the existing issues manufacturers have with metrology integration that have been highlighted during onsite visits. It is clear that what the manufacturers are currently demanding are integrated and automated metrology solutions that can be applied to existing production processes.

The case studies presented in chapter 3 demonstrates that the current generation of metrology systems have the capabilities to meet the demands of the manufacturers, and that the main challenges lie in system integration, data processing and automation. While these are not very complex challenges, they do require insights into the LVM systems and software development, which typical manufacturers do not possess.

This gap in knowledge potentially represents a gap in the market for groups/organizations/companies that are able to provide solutions to LVM automation problems from instrument selection to the implementation of the system.

Since large volume measurement tasks vary greatly, LVM must be able to adapt to be effective. In the past, this “adaptation” is embodied by bespoke hardware hard tooling, and product specific measurement tools. In a future flexible production environment with reduced reliance on capital intensive large jigs and hard tooling, where the jigs and measurement instruments are more or less standardized off-the-shelf components, it is the software that must adapt.

6.3. Digital Modelling and Simulation of Metrology Assisted Assembly (MAA) Technology

Developing metrology automation solutions meets the near and medium term demands of the manufacturers. However, the ultimate goal of the Metrology Assisted Assembly methodology is to demonstrate the complete integration of LVM systems in aero-structure production.

To better understand and quantify the capabilities and benefits of a hypothetical MAA system, it is necessary to show that the direct integration of LVM in the assembly process for future products can be simulated mathematically. This allows the LVM integrated assembly process to be evaluated and optimized prior to construction. The assembly simulations

can also provide a sound theoretical basis illustrating potential gains from an integrated LVM system.

In chapter 4, digital simulations of metrology assisted assembly using the Monte Carlo method are explored. Three case studies showing in detail the applications of the simulations are described. By taking account of the measurement process and instrument uncertainty, the stream of variations approach used to analyse assembly variability can be adopted to take into account of integrated metrology systems along with fixture and part variations.

It was demonstrated that is it possible to inject measurement data directly into the assembly model such that it can be used during production to ensure that the assembly is accurate and optimal. This represents a transformation of assembly modelling from strictly a planning tool to an essential part of the assembly process.

These simulations provide the decision makers predictions of the process capability before committing to the physical construction. They enable the production engineers to experiment with "what if" scenarios, such as in the case of Vestas modular blade assembly, comparing the differences in the final product quality with or without the integration of metrology.

There are however still many limitations to the approach described here. The most significant one is that it is very time consuming to correctly model the transformations, requiring specialist knowledge. It is currently also very difficult to model flexible components, without resorting to time consuming FEA analysis. Additionally, due to its low volume nature, it can be very difficult to statistically validate assembly models in aero-structure manufacturing compared to automotive manufacturing.

Despite these limitations, digital simulations can be a very useful tool as shown in the case studies.

6.4. New Large Volume Technologies for Measurement Assisted Assembly

Having studied the theoretical simulations of MAA in chapter 4, the practical implementation of such systems is examined in chapter 5.

It was soon realised that a real-time MAA system will require the LVM instruments to measure dynamically, while they are traditionally used for static measurements. Their performance specifications are typically given by the instrument manufacturers for static measurements. There is little to no information on the dynamic tracking performance of most instruments. Therefore an experimental study of two types of LVM instruments (iGPS and laser tracker) was carried out, filling gaps in existing knowledge.

Currently, research in what can be referred to as “Dynamic Metrology” is almost completely non-existent, without any standards on how dynamic performances can be evaluated or even expressed. The understanding of dynamic metrology will likely to become increasingly important as more and more research into real-time MAA is conducted.

Methods of getting access to the real-time data stream from iGPS and laser tracker are also explored in chapter 5, and the applications of the data stream are demonstrated on a number of mobile robotic platforms, paving the way to integrating these instruments into a real-time MAA system.

Apart from being integration demonstrators, using a LVM instrument to provide navigation information to mobile robots, and using mobile robots to perform metrology measurements can have very novel and practical future applications, an example of which is shown in Figure 138.

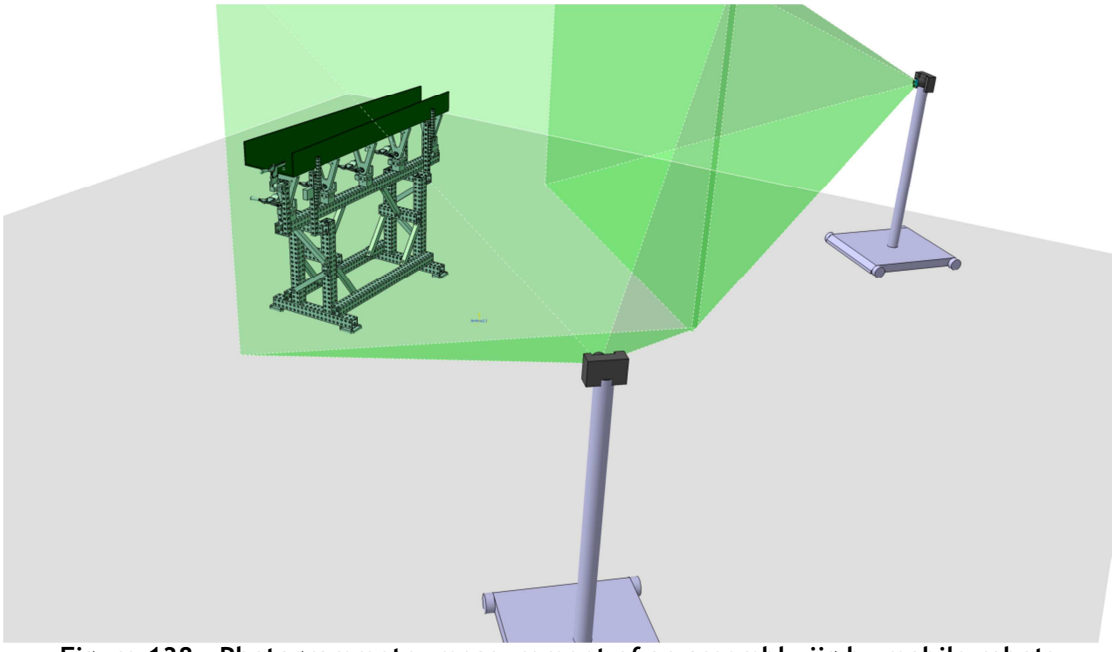

Figure 138 - Photogrammetry measurement of an assembly jig by mobile robots

Using the demonstrator system developed in chapter 5, it is possible to use metrology guided (photogrammetry or iGPS) mobile robots to replace human operators in the photogrammetry measurements of a jig and/or product. This can increase the speed and consistency of measurements, and allow the camera positions to be optimized for maximum accuracy.

6.5. MAA Demonstrator

The final phase of the research realises the research aim by demonstrating what is possible through complete real-time metrology integration, providing a glimpse of a future production process where real-time

metrology feedback can be used directly to improve the quality of the product.

The development of the MAA demonstrator described in section 5.5 combines the knowledge gained from the dynamic capability study of iGPS and laser tracker, as well as the interface and control software for mobile robots presented earlier in chapter 5.

In order to demonstrate the potentials of real-time MAA for manufacturing processes such as milling and drilling, a simple 3-axis machine was constructed using low cost off-the-shelf components. Using a laser tracker to provide real-time error correction, it was possible to double the repeatability of the machine, and reduce positioning errors by 40 to 140 times.

While this method can be applied as a novel machine tool on-line compensation technique, it has much deeper implications. It shows that in a future production environment the quality of the product can be decoupled from the quality of the machine tools used to produce it. In such a production environment, the machine tools and positioning systems only need to be stiff enough to perform their operations while having little inherent accuracy, while depending on external dedicated measurement systems for their capabilities. The benefits of a MAA system include:

- **Reduced machine tool cost**
  The reduction in (or the lack thereof) accuracy requirement can dramatically reduce the cost of machine tools and positioning systems, many of which are made bespoke for the production of a specific aero-structure. This allows the machine tools and jigs to use off the shelf components such as industrial robots.

- **Achieve high feature to feature accuracy over large volumes**
  It is more cost effective to use a LVM system to ensure accuracy over large distances than relying on the inherent stability and accuracy of a jig or machine tool.

- **Scalable and flexible**
  Depending on the size and accuracy required, a LVM system can be chosen from the large selection of different systems to suit a particular MAA task. They can also be interchanged if the requirement changes. Although the additional costs of metrology systems have to be considered, they can be reused for other tasks after decommissioning.

Real-time MAA systems however, also have a number of draw backs:

- **Dynamic capabilities of many LVM systems are unknown**
  Real-time MAA requires dynamic measurements, while most LVM systems are only rated to static measurements.

- **Reliabilities of many LVM systems are unknown**
  If the machine tools and positioning systems derive their accuracy from LVM systems, the LVM systems must be highly reliable over an extended period. It is unclear how reliable the current LVM systems are when operated in such a manner.

- **Line-of-sight challenge**
  As the majority of LVM system are optical, line-of-sight access is required for measurements, which may be difficult/impossible to guarantee in a cramped manufacturing jig.

6.6. Conclusions

The aim of this research project was:

- To develop and demonstrate novel integrated and automated metrology systems in aero-structure production.

To achieve the research aim, a number of objectives were set that realise the research aim and fill in the gaps in the existing knowledge. The research objectives are listed in this section, together with the results obtained as a result of the research.

- **Demonstrate the value of integrated and automated metrology in solving immediate issues in production. (Chapter 3)**
  - Software was developed to demonstrate automated measurement and analysis of robotic positioning repeatability. It allowed the point repeatability of any robot or positioning system to be quickly analysed.
  - Software algorithms were developed to semi automatically process the Vestas prototype wind turbine blade scan data and convert them into plots of flushness against distance along the glue joint.
  - Development of rapid automatic fixture health-check of the Airbus ALCAS jig. Many different hardware and software processes were proposed, developed, and demonstrated to facilitate the project. This work showed that an automated fixture health-check system can potentially complete a health-check within 13 minutes.

- **Develop mathematical simulations of Metrology Assisted Assembly. (Chapter 4)**
  - Methods of mathematically simulating metrology assisted assembly systems are developed using the Monte Carlo method.

    - Three of application case studies using the assembly simulation were carried out.
    - It was demonstrated that is it possible to inject measurement data directly into the assembly model such that it can be used during production to ensure that the assembly is accurate and optimal. This represents a transformation of assembly modelling from strictly a planning tool to an essential part of the assembly process.

- **Develop and demonstrate direct software/hardware integration with LVM instruments. (Chapter 5)**
    - The dynamic performance of indoor GPS and laser tracker LVM systems were experimentally examined, filling gaps in existing knowledge.
    - Various methods of interfacing with LVM instruments in real-time were examined, and custom software interfaces for iGPS and laser tracker were developed.
    - A proof of concept metrology guided mobile robot using the interface software was also developed and demonstrated, showing that LVM instruments can be used to provide reliable and accurate real-time navigation feedback to guide AGVs.

- **Demonstrate direct real-time control of typical production system. (Chapter 5)**
    - A real-time laser tracker compensated prototype 3-axis was developed and its static positioning experiments have shown very encouraging results.
    - The inter-point distance results showed that the machine is able to consistently reach positioning accuracies of better than 45µm.

6.7. Recommendations for Future Work

As much of the research is new and on-going, there are still large gaps in the knowledge, and potentials for innovative solutions. A number of research areas and projects recommended for future work are listed below.

- **Robot - MAA Demonstrator Integration**
  It was shown that the MAA demonstrator performs in situ. However, the original design was to have the 3-axis system mounted as a robot end-effector, to demonstrate its full potential.

- **OmniMove Automatic Photogrammetry**
  Using the demonstrator system developed in chapter 5, it is possible to use metrology guided (photogrammetry or iGPS) mobile robots to replace human operators in the photogrammetry measurements of a jig and/or product. This can increase the speed and consistency of

measurements, and allow the camera positions to be optimized for maximum accuracy

- **Dynamic Instrument Capability**
  The dynamic performances of LVM instruments are currently a poorly understood area. The dynamic capability assessment and standardization will be very important to the future of MAA systems.

- **Dynamic Metrology Sensor Fusion**
  It should be possible to optimally fuse the positioning information from the machine tool with the LVM instrument measurements using a digital filter. This can improve the overall performance and reliability of a MAA system. Such a system will be capable of handling metrology instruments with a large range of measurement uncertainties, latencies and update rates.

- **RAG with Confidence**
  The Airbus RAG project described in chapter 3 informs the jig operator about the health of the jig in terms of a red, amber and green light system based on the interaction between the measurement, uncertainty and tolerance. It may be better to use a more mathematically correct probability based system for the decision algorithm.

References

1. U.S. Department of Energy - Energy Efficiency and Renewable Energy Wind and Hydropower Technologies Program. *"History of Wind Energy"*, http://www1.eere.energy.gov/windandhydro/printable_versions/wind_history.html (2005) (retrieved 2008).
2. Linda M. Kamp, Ruud E.H.M. Smits, Cornelis D. Andriesse. *"Notions on learning applied to wind turbine development in the Netherlands and Denmark"*, Energy Policy 32 pp. 1625–1637 (2004).
3. Matthias Heymann. *"Signs of Hubris: The Shaping of Wind Technology Styles in Germany, Denmark, and the United States, 1940-1990"*. Technology and Culture, Vol. 39, No. 4, pp. 641-670, The Johns Hopkins University Press (1998).
4. Angelika Pullen. *"Record year for wind energy: Global wind power market increased by 40.5% in 2005"*, Global Wind Energy Council Press Release (2006).
5. Vestas. *"Capacity expansion: Investment in the future"*, Vestas Win[d] No.09 2007. Vestas Wind Systems A/S (2007).
6. Airbus. *"Airbus Global Market Forecast 2010-2029"*, http://www.airbus.com/fileadmin/media_gallery/files/brochures_publications/Global_Market_Forecast/Airbus_Global_Market_Forecast_-_2010-2029.pdf (2009) (Retrieved 2011)
7. Puttock, M. J., *"Large-Scale Metrology"*, Annuals of CIRP, 27/1: 351-6 (1978).
8. BSI. *"Geometric Product Specifications (GPS) - Geometrical features"*, BS EN ISO 14660-1:2000 (2000).
9. Per Bennich and Henrik Nielsen. *"An Overview of GPS - A Cost Saving Tool 1st edition"*, Institute for Geometric Product Specifications (2005).
10. BSI. *"Geometrical Product Specifications(GPS) - Geometrical tolerancing - Tolerances of form, orientation, location and run-out"*, BS EN ISO 1101:2005 (2004).
11. David Flack and John Hannaford. *"Measurement Good Practice Guide No. 80: Fundamental Good Practice in Dimensional Metrology, Chapter 3"*, National Physical Laboratory (2005).
12. Jody Muelaner. *"Metrology Instrument Reviews RE Wing Build"*, Internal report, University of Bath (2008).
13. BSI. *"Inspection by measurement of workpieces and measuring equipment. Part 1: Decision rules for proving conformance or non-conformance with specifications"*, BS EN ISO 14253-1:1999 (1999).
14. DD CEN ISO/TS 17450-1, *"Geometrical product specifications (GPS) — General concepts — Part 1: Model for geometrical specification and verification"*, (2007)
15. DD CEN ISO/TS 12780-2, *"Geometrical product Specifications (GPS) — Straightness — Part 2: Specification operators"*, (2007)
16. DD CEN ISO/TS 12181-2, *"Geometrical product Specifications (GPS) — Flatness — Part 2: Specification operators"*, (2007)

17. DD CEN ISO/TS 12180-2, *"Geometrical product Specifications (GPS) — Cylindricity — Part 2: Specification operators"*, (2007)
18. DD CEN ISO/TS 12181-2, *"Geometrical product Specifications (GPS) — Roundness — Part 2: Specification operators"*, (2007)
19. Estler WT, Edmundson KL, Peggs GN and Parker DH, "*Large Scale Metrology-An Update*", CIRP Annals, NIST Technipubs (2002)
20. ASME B89.4.19. "Performance Evaluation of Laser-Based Spherical Coordinate Measurement Systems", (2006)
21. FARO EUROPE GmbH & Co. KG. "*New Faro Laser Tracker SI. 2: Tougher with Exclusive Features*", Faro UK technical specification sheet (2004)
22. Joint Committee for Guides in Metrology Work Group 1. *Evaluation of measurement data - "Guide to the expression of uncertainty in measurement"*, JCGM 100:2008 (2008)
23. John Michael Hammersley, David Christopher Handscomb. "*Monte Carlo methods - Methuen's monographs on applied probability and statistics*", Taylor & Francis, (1964).
24. William Kimberley. "*The drive for quality*", Automotive Engineer, vol:29 iss:9 pg:40 -42 (2004).
25. Wen-Han Qian, Liang-Han Hsieh, Giinther Seliger. "*On the optimization of automobile panel fitting*", Proceedings - IEEE International Conference on Robotics and Automation, vol:2 pg:1268 - 1274 (1996).
26. *"First sale of novel robot goes to Boeing"*, The Engineer, 15 January 2000. http://www.theengineer.co.uk/Articles/288194/First+sale+of+novel+robot+goes+to+Boeing.htm. (Retrieved 2008).
27. S J Eastwood, P Webb, and C Mckeown. *"The use of the Tl^2 manufacturing system on a double-curvature aerospace panel"*, Proceedings of Institute of Mechanical Engineers Vol. 217, Part B: J. Engineering Manufacture, page 849, (2003).
28. P Webb, S J Eastwood. *"An evaluation of the Tl^2 manufacturing system for the machining of airframe subassemblies"*, Proceedings of Institute of Mechanical Engineers Vol. 218 Part B: J. Engineering Manufacture, page 819, (2004).
29. Kihlman H. *"Affordable Automation for Airframe Assembly - Development of Key Enabling Technologies"*, Dissertation Thesis No. 953, ISBN: 91-85299-59-6, Department of Mechanical Engineering, Linköpings universitet (2005).
30. Henrik Kihlman, Raimund Loser, Andrew Cooke, Albin Sunnanbo, Konrad von Arb. *"Metrology-integrated Industrial Robots - Calibration, Implementation and Testing"*, Proceedings of the 35th International Symposium on Robotics (2004).
31. Henrik Kihlman, Magnus Engström. *"Affordable Reconfigurable Tooling"*, Society of Automotive Engineers (2001).
32. Henrik Kihlman, Magnus Engström, John Anderson. *"Low-cost Automation for Aircraft Assembly"*, Society of Automotive Engineers (2004).
33. Jonas Herbertsson, Henrik Kihlman, Magnus Engström. *"Reconfigurable Aircraft Assembly - Using industrial robots and new*

tooling to meet future production scenarios", Proceedings of the 33rd ISR (International Symposium on Robotics), (2002)
34. N. Jayaweera, P. Webb. *"Metrology Assisted Robotic Processing of Aero-Structure Components"*, Proceedings of DET 2007, 4th International Conference on Digital Enterprise Technology, pages 410-417 (2007).
35. N. Jayaweera, P. Webb. *"Adaptive robotic assembly of compliant aero-structure components"*, Robotics and Computer-Integrated Manufacturing Vol 23, Issue 2, Page 180–194 (2007).
36. N. Jayaweera, P. Webb. *"Automated assembly of fuselage skin panels"*. Assembly Automation 27/4 page 343–355 (2007).
37. Brian Rooks. *"Automatic wing box assembly developments"*, Industrial Robot, Volume 28, Number 4, Pages 297–301 (2001).
38. Jafar Jamshidi. *"Metrology Report on A350 Demo Box"*, Large Volume Metrology Group internal report, University of Bath (2007).
39. Amir Kayani, Jafar Jamshidi. *"Measurement Assisted Assembly for Large Volume Aircraft Wing Structures",* Proceedings of DET2007, 4th International Conference on Digital Enterprise Technology, Bath, (2007).
40. Maropoulos PG, Bramall DG, McKay KR. *"Assessing the Manufacturability of Early Product Designs Using Aggregate Process Models"*. Proceedings of the IMechE Part B Journal of Engineering Manufacture 217:1203–1214 (2003).
41. Baxter D, Gao J, Case K, Harding J, Young B, Cochrane S, Dani S. *"An Engineering Design Knowledge Reuse Methodology Using Process Modeling"*. Research in Engineering Design 18(1):37–48 (2007).
42. Reinhart G, Cuiper R. *"Assembly Process and Assembly Control Development—A holistic and Consistent Approach"*. Annals of the CIRP 48(1):25–28 (1999).
43. Wang H, Ceglarek D. *"Quality-driven Sequence Planning and Line Configuration Selection for Compliant Structure Assemblies"*. Annals of the CIRP54(1):31–35 (2005).
44. Kru¨ ger J, Bernhardt R, Surdilovic D. *"Intelligent Assist Systems for Flexible Assembly"*. Annals of the CIRP 55(1):29–32 (2006).
45. Chouvion, B., Popov, A., Ratchev, S., Mason, C. et al., *"Interface Management in Wing-Box Assembly"* SAE Technical Paper 2011-01-2640, doi:10.4271/2011-01-2640 (2011).
46. Giirsel Alici, Bijan Shirinzadeh. *"Laser Interferometry Based Robot Position Error Modelling for Kinematic Calibration",* Proceedings of the 2003 IEEE/RSJ, Intl. Conference on Intelligent Robots and Systems, Las Vegas, Nevada October (2003)
47. N. Romman. *"Measurement of Connecting Rods in A380 Wing Boc TR2"*, Presentation at Large Volume Metrology Conference, Liverpool (2007).
48. *ARCSecond, "Indoor GPS technology for Metrology", White Paper 071502, Dulles, Virginia: ARCSecond, (2002)*
49. *Maisano DA, Jamshidi J, Franceschini F, Maropoulos PG, Mastrogiacomo L, Mileham AR, Owen GW, 2008, "Indoor GPS: System Functionality and Initial Performance Evaluation",* International Journal of Manufacturing Research

50. Maisano Domenico; Jafar Jamshidi; Fiorenzo Franceschini; Paul G Maropoulos; Luca Mastrogiacomo; Antony R Mileham; Geraint W Owen, *"Indoor GPS: System Functionality And Initial Performance Evaluation, International Journal Of Manufacturing Research"*, pp. 335-349, 2008, Vol. 3, n. 3 (2008)
51. J. E. Muelaner, Z. Wang, J. Jamshidi, P. G. Maropoulos, A R Mileham, E. B. Hughes, and A. B. Forbes. "*iGPS - An Initial Assessment of Technical And Deployment Capability*", Proceedings of the 3rd International Conference on Manufacturing Engineering (ICMEN), Chalkidiki, Greece (2008).
52. Z. Wang, J. Jamshidi, P. Maropoulos, G. Owen, and T. Mileham. "*Experimental Deployment of the Indoor GPS Large Volume Metrology System in a Large Scale Production Facility*", Proceedings of the 3rd International Conference on Manufacturing Engineering (ICMEN), Chalkidiki, Greece (2008).
53. Jody Muelaner, Ben Hughes, Alistair Forbes, Paul Maropoulos, Jafar Jamshidi, Zheng Wang, and Wenjuan Sun. "*iGPS capability assessment*", Large Volume Metrology Conference, Liverpool (2008)
54. VIM "*International Vocabulary of Basic and General Terms in Metrology, Third Edition*", ISO/DG 99999 (Geneva, Switzerland: International Organization for Standardization) (2004).
55. KUKA Roboter GmbH, Germany. "*KR 240-2 – KR 240 L210-2 – KR 240 L180-2 (Serie 2000) Technical Data*", KWM--Nr. 841612--86/D+E/3/04.05 (2002)
56. Zheng Wang. "*KUKA KR240 Robot Repeatability Study*", Airbus ALCAS internal report (2008)
57. Street, J. O., R. J. Carroll, and D. Ruppert. "*A Note on Computing Robust Regression Estimates via Iteratively Reweighted Least Squares*." The American Statistician. Vol. 42, 1988, pp. 152–154.
58. Beliveau, Y.J., Fithian, J.E., and Deisenroth, M.P. 1996. *"Autonomous vehicle navigation with real-time 3D laser based positioning for construction"*. Automation in Construction 5, 261-272.
59. Chong, K.S. and Kleeman, L. 1997. *"Accurate Odometry and Error Modelling for a Mobile Robot"*, IEEE International Conference on Robotics and Automation, Albuquerque USA, pp. 2783-2788.
60. Desouza, G.N. and Kak A.C., 2002. *"Vision for Mobile Robot Navigation: A Survey"*, IEEE Transactions on Pattern Analysis and Machine Intelligence, Volume 24, Issue 2, pp 237 – 267.
61. Dixon, J. and Henlich, O., 1997. *"Mobile Robot Navigation"*, Imperial College. Available from: http://www.doc.ic.ac.uk/~nd/surprise_97/journal/vol4/jmd/ (Retrieved 11 November, 2009).
62. Hashimoto, J., Kawabata, N. and Nakanishi K., 1996. *"Development and Introduction of Automatically Guided Vehicle for Steel Product Distribution"*, Nippon Steel Technical Report No. 68.Norifusa Kawabata and Keiji Nakanishi, Jan 1996.
63. Krotkov, E., *et al.*, 1995. *"Stereo Perception and Dead Reckoning for a Prototype Lunar Rover"*, Autonomous Robots, Vol 2, pp 313-331.
64. Liang X., *et al.*, 2008. *"Multiple Robots Localization Using Large Planar Camera Array For Automated Guided Vehicle System"*,

Proceedings of the 2008 IEEE International Conference on Information and Automation, June 20 -23, Zhangjiajie, China.
65. Martínez-Barberá, H. and Herrero-Pérez, D., 2010. *"Autonomous navigation of anautomate dguided vehiclein industrial environments",* Robotics and Computer-Integrated Manufacturing 26, 296–311.
66. Moore P., *et al.*, 1999. "*Intelligent semi-autonomous vehicles in materials handling*", Mechatronics 9, 881-892.
67. Surmann, H., *et al.*, 2001. *"A 3D laser range finder for autonomous mobile robots",* Proceedings of the 32nd ISR (International Symposium on Robotics), pp. 153 - 158, 19-21.
68. Chih-Hao Lo, Jingxia Yuan, and Jun Ni, "*An Application of Real-Time Error Compensation on a Turning Center*" International Journal of Machine Tools & Manufacture, Vol 35, No. 12, 1995, pp 1669–1682.
69. FARO EUROPE GmbH & Co. KG. *"Faro Laser Tracker Ion",* Faro UK technical specification sheet, 2010
70. J. Ni, *"Study on Online Identification and Forecasting compensatory control of volumetric Errors for Multiple Axis Machine Tools"*, PhD Dissertation, University of Wisconsin-Madison, 1987.
71. Jingxia Yuan and Jun Ni, *"The Real-Time Error Compensation Technique for CNC Machining Systems",* Mechatronics, Vol 8, 1998, pp 359-380.
72. R. Ramesh, M.A. Mannan, and A.N. Poo, *"Error compensation in machine tools — a review Part I: geometric, cutting-force induced and fixture-dependent errors"*, International Journal of Machine Tools & Manufacture, Vol 40, 2000, pp 1235–1256.
73. R. Ramesh, M.A. Mannan, and A.N. Poo, *"Error compensation in machine tools — a review Part II: thermal errors",* International Journal of Machine Tools & Manufacture, Vol 40, 2000, pp 1257–1284.
74. S. Yang, J. Yang, and J. Ni, *"The Improvement of Thermal Error Modelling and Compensation on a Turning Centre*", International Journal of Machine Tools & Manufacture, Vol 37, No. 11, 1996, pp 527–537.
75. W.T. Lei and Y.Y. Hsu, *"Accuracy Enhancement of Five-Axis CNC Machines through Real-Time Error Compensation"*, International Journal of Machine Tools & Manufacture, Vol 43, 2003, pp 871–877.